SEYFERT GALAXIES AS X-RAY SOURCES

thesis submitted by

Martin Elvis

for the degree of Doctor of Philosophy, February, 1978.

X-ray Astronomy Group,
Department of Physics,
University of Leicester.

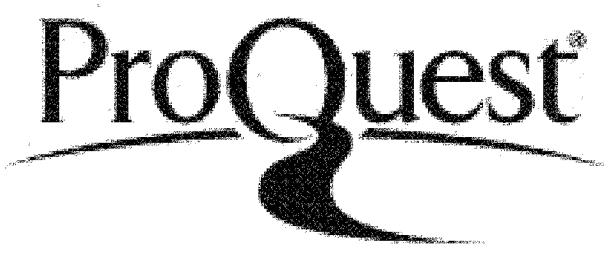

ProQuest LLC
789 East Eisenhower Parkway
P.O. Box 1346
Ann Arbor, MI 48106-1346

DECLARATION

I hereby declare that no part of this thesis has been previously submitted to this or any other University as part of the requirements for a higher degree. The work described here was conducted by the undersigned except for the contributions from colleagues, listed in the Preface and in the publications in the following Note, or indicated in the text.

Martin Elvis

Martin Elvis,

February, 1978.

NOTE

Most of the work reported in this thesis has been published elsewhere, as follows:

chapter 2: Cooke B.A., Ricketts M.J., Maccacaro T., Pye J.P., Elvis M., Watson M.G., Griffiths R.E., Pounds K.A., McHardy I., Maccagni D., Seward F.D., Page C.G., Turner M.J.L., 1978, MNRAS, 182, 489.

chapter 3: Cooke B.A., Elvis M., Maccacaro T., Ward M.J., Fosbury R.A.E., Penston M.V., 1976, MNRAS, 177, 121p.

Ward M.J., Wilson A.S., Disney M.J., Elvis M., Maccacaro T., 1977, Astr. & Ap., 59, L19.

Elvis M., Maccacaro T., Wilson A.S., Ward M.J., Penston M.V., Fosbury R.A.E., Perola G.C., 1978, MNRAS, 182, .

chapter 4: Elvis et al., 1978.

chapter 5: Elvis et al., 1978.

chapter 6: Elvis M., 1976, MNRAS, 177, 7p.

Lawrence A., Pye J.P., Elvis M., 1977, MNRAS, 181, 93p.

chapter 7: Ward M.J., Wilson A.S., Penston M.V., Elvis M., Maccacaro T., Tritton K.P., 1978, Ap.J., submitted.

CONTENTS

ABSTRACT

Using data from the Leicester University Ariel V Sky Survey Instrument (SSI) the work reported in this thesis establishes that Seyfert galaxies form a class of extragalactic x-ray source.

The properties of Seyfert galaxies are reviewed and it is shown how standard arguments lead to a model of the structure of Seyfert galaxy nuclei containing three regions characterised by three types of emission: forbidden line, permitted line and 'non-thermal' continuum. Radio, infrared and optical parameters believed to derive from these three regions are then compared with x-ray flux densities from the SSI in an attempt to locate the source of x-ray emission. It is found that x-ray flux density correlates only with parameters describing the permitted line and continuum regions. Standard arguments presented earlier show that these regions are very small ($\approx$0.01 - 1pc diameter). Observable x-ray variability is thus possible and is indeed seen. The variability of x-ray emission from x-ray active galaxies is described using, in the main, SSI observations. Some suggestive similarities in their light curves are noted.

An x-ray luminosity function for Seyfert galaxies is constructed by two methods whose results agree well. Using this luminosity function the Seyfert galaxies are found to contribute $\approx$ 6% to the diffuse x-ray background, without evolution. They can account for the entire background if only moderate evolution is allowed.

Finally, recent developments in the field are noted: the discovery of more Seyfert galaxies as x-ray sources, variability, and some first x-ray spectra are reviewed. An extension to the class of 'x-ray active galaxies' in the form of high excitation

emission line galaxies is reported. The great possibilities for future research in the area of x-ray active galaxies provided by new x-ray observatories in flight or under construction are explored briefly. It is clear that this is a subject just begun.

ABBREVIATIONS as used in the text

2A	refers to the "Ariel V (SSI) catalogue of high galactic latitude ($\|b\| > 10^{o}$) x-ray sources" (Cooke et al. 1978, Appendix A). X-ray sources in this catalogue have the prefix '2A'.
3U	refers to the "Third UHURU catalogue of x-ray sources" (Giacconi et al., 1974). X-ray sources in this catalogue have the prefix '3U'.
4U	refers to the "Fourth UHURU catalogue of x-ray sources" (Forman et al., 1978). X-ray sources in this catalogue have the prefix '4U'.
Akn	Arakelian, referring to a galaxy from his list (1975), see chapter 1-2.
Ariel V UK-5	refer to the Ariel V (UK-5 before launch) x-ray astronomy satellite, see chapter 2-1.
Ariel V (SSI) ct s^{-1} SSI ct s^{-1}	Count rate from SSI on Ariel V. see chapter 2-2, 1 SSI ct $s^{-1} \approx 5.1 \times 10^{-11}$ erg $cm^{-2}s^{-1}$.
F	Flux density
Fx	2-10 keV x-ray flux density
FWHM	Full width at half maximum.
FWZI	Full width at zero intensity.
H_o	Hubble's constant-taken as 50 km s^{-1} Mpc^{-1} throughout.
hexelg	high excitation emission line galaxy. see chapter 7-1,
IP	Ionisation potential.
L	Luminosity (erg s^{-1}).
L_x	2-10 keV x-ray luminosity (erg s^{-1}).
LOP	line-of-position. The $\approx 20^{o} \times \approx \frac{1}{2}^{o}$ rectangle characterising the best estimate of the position of an x-ray source in celestial co-ordinates from a single sighting with the SSI. see chapter 2-4.

Mkn	Markarian, referring to a galaxy from the lists of Markarian and Markarian and Lipovetzky. see chapter 1-2.
n_e	electron density (cm^{-3}).
PST	Point Summation Technique. see chapter 2-4, and Appendix A, § 8.
SSI	Leicester University Sky Survey Instrument on board Ariel V. see chapter 2-2.
XLF	X-ray Luminosity Function. see chapters 4-2, 4-3.
z	redshift, $z = \frac{\lambda - \lambda_o}{\lambda_o}$. λ = observed wavelength, λ_o = emitted wavelength.
cz	redshift x velocity of light . (km s^{-1})

PREFACE

On arriving in the Leicester University X-ray Astronomy group at the beginning of October 1974 I heard that some members of the group were in Kenya preparing for the launch of a satellite called UK-5. It was not then obvious, to me, that this satellite would produce several major advances in x-ray astronomy and my main feeling was one of disappointment at not arriving early enough to go on safari courtesy of the SRC. I have subsequently learnt that even at this late point much work had to be done and that this was only the last stage of some five years of effort by a large number of people in building this satellite - a satellite which I have never seen and have merely used. To all those who built and tested the satellite and the Leicester Sky Survey Instrument I must extend my thanks and appreciation. I do not know everyone who was involved but without my supervisor, Ken Pounds, and Brin Cooke the Sky Survey would surely not have been possible.

My part in operating the satellite and in making the messages it returned intelligible also begins at a late stage in the programme. The staff of the Ariel V Operations Control Centre at the Appleton Laboratory have been efficient and helpful throughout the lifetime of the satellite. At Leicester the observing programme and most of the initial stages of data analysis were tackled by Martin Turner, Russell Silk, Tony Peacock, Gavin Eadie and Clive Page. Other important contribuions to the software were made by Mike Watson, Martin Ricketts and John Pye. I am grateful to them all.

The work in this thesis was broadened and improved greatly by an intense collaboration with Mike Penston, Martin Ward and Andrew Wilson. My astrophysical knowledge has benefitted from innumerable conversations with these astronomers as it has from conversations with Richard Griffiths and Andrew King.

Finally without the help of Mrs. V.H. Elvis this thesis would not have been finished so presentably, or on time.

chapter 1. SEYFERT GALAXIES

1-1 Definitions

There is a class of galaxies, first described by Carl Seyfert (1943) whose members possess

(1) A bright, unresolved, nucleus. ('bright' here implies a luminosity a significant fraction of that of the body of the galaxy);

(2) Broad emission lines in the optical spectrum of the nucleus. ('broad' implies greater than that which might arise from normal galactic rotation - upwards from 500 km s^{-1} to, at least, 22,000 km s^{-1}).§

These properties make the 'Seyfert' galaxies a major sub-set of the 'active' galaxies: radio galaxies, N-galaxies, narrow emission line galaxies, and possibly (or probably) quasars and BL Lac objects.

In order to qualify as a Seyfert galaxy an object should have a clearly visible galaxy surrounding it. This then prevents any argument over the nature of the Seyfert redshifts. At distances conventionally implied by redshifts greater than $z \approx 0.2$ ($cz \approx 60{,}000$ km s^{-1}) an underlying galaxy can no longer be detected. Thus Seyfert galaxies are restricted, by definition, to being a relatively nearby, bright ($m_v \approx 13 - 16$), set of objects. They can therefore be studied in much greater detail than quasars by optical astronomers.

Galaxies which qualify as Seyferts on the above criteria are often found to have other common properties

(3) Variability on timescales at least as short as 1 month and by at least as much as a factor 1.6 in optical, broad-band colours (Penston et al., 1974, and fig. 1-1, Dibaiye, private communication). (Variability in both permitted emission (fig. 1-2, Tohline and

---

§ 10,000 km s^{-1} corresponds to $\Delta\lambda/\lambda_o = 0.033 = 162$ Å at Hβ (4861 Å)

Osterbrock, 1976) and in absorption (Anderson, 1974) lines is also seen on less than a 1 year timescale.

(4) 'power-law' or 'non-thermal' optical continua. The continuum radiation from Seyfert nuclei does not resemble the integrated emission from many stars and in many cases is well represented by a distribution of the form $F \propto \nu^{-\alpha}$ (Oke and Sargent, 1968). It is the continuum emission which provides the great luminosity of Seyfert nuclei.

(5) All Seyferts where a galaxy type can be unambiguously determined are spiral (Adams, 1977).

In this thesis it is also shown that they are, as a class, powerful x-ray emitters.

Variability on timescales which imply sizes small in terms of galactic distances are a feature common to Seyferts, nuclei of radio galaxies and quasars (see e.g. Liller and Liller, 1975). Power-law spectra are also normal in quasars (Strittmatter and Williams, 1976). Such hints at some kind of unity behind all the types of active galaxy stimulated a great deal of research into Seyfert galaxies in the years following the discovery of quasars. This increased interest in Seyferts, which has not abated, is reflected in the numbers discovered. There are now certainly more than 100 known and this number is growing rapidly.

Recent observations of Seyfert galaxies are reviewed by Weedman (1977). He covers observations, mainly optical, up to the time just prior to the work reported in this thesis. In the following sections of this chapter the main features of Seyfert galaxy research needed to put the results reported later into context are explained.

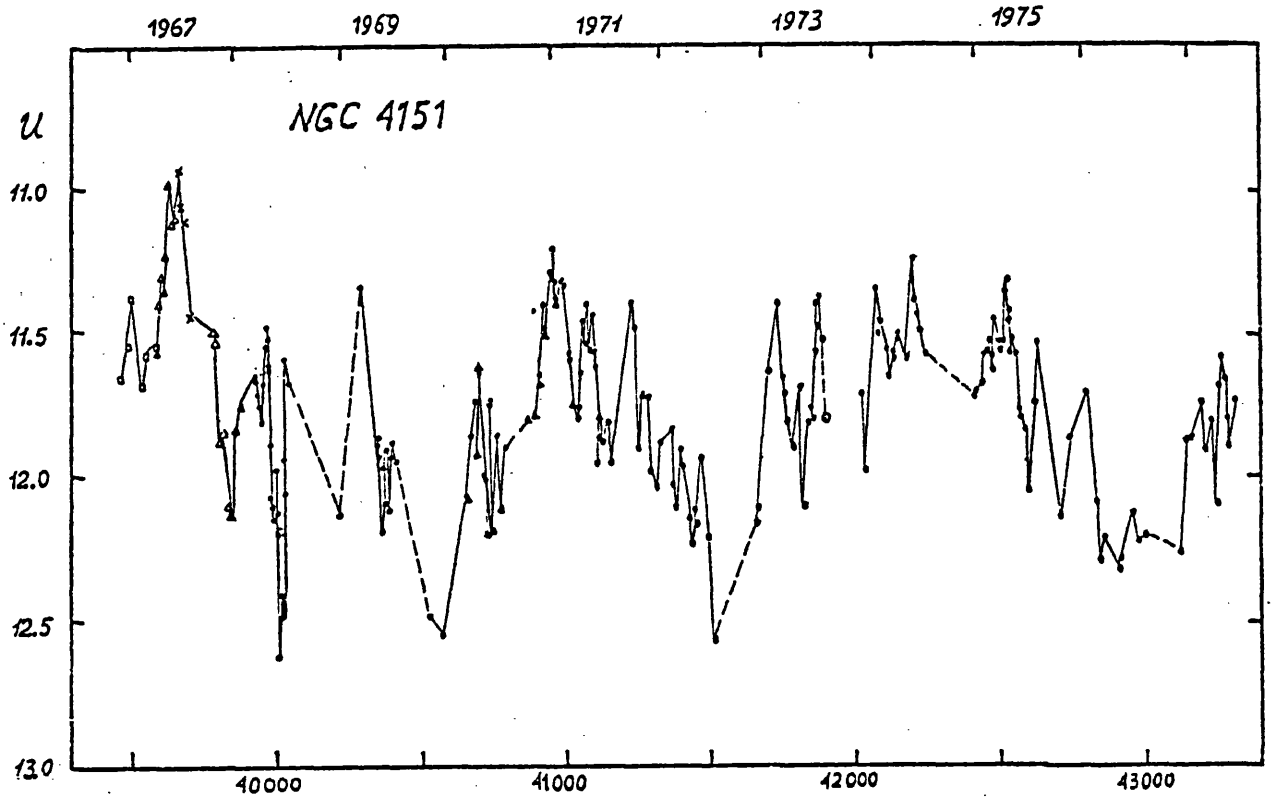

fig 1-1 U-BAND LIGHT CURVE OF NGC4151 (Dibaiye, private communication). Errors are smaller than the point marks.

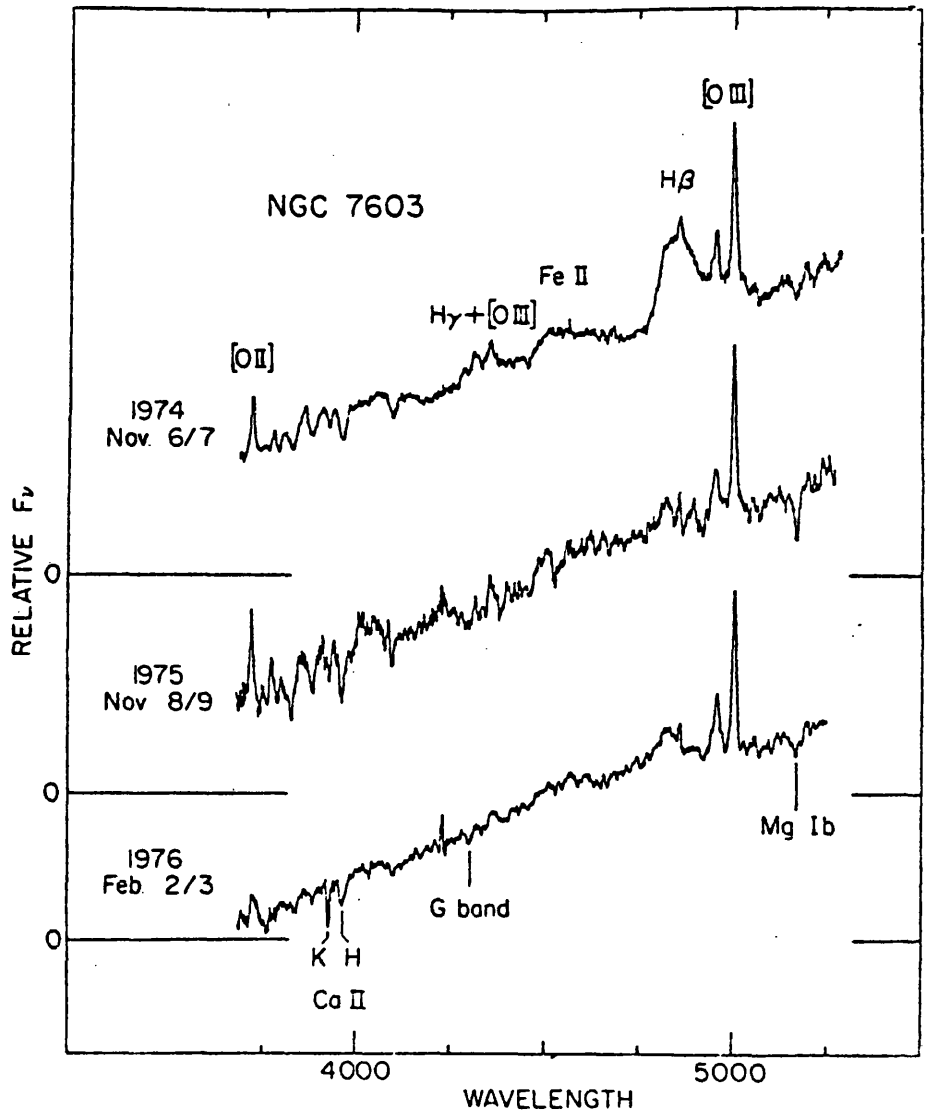

fig 1-2 VARIABILITY OF Hβ LINE IN NGC7603 (from Tohline and Osterbrock, 1976). Scans are normalised to the [OIII] flux density since absolute calibrations were not available.

1-2 Occurrence of Seyfert activity

How common is Seyfert activity amongst galaxies? To answer this question requires not just a comprehensive survey of galaxy spectra complete over some solid angle of the sky and out to a known distance. It also requires that our definition of 'Seyfert' activity can be made sufficiently distinct. If there are real links with other kinds of active galaxy this may well not be possible. For instance the 'N-galaxies' defined by Mathews, Morgan and Schmidt (1964) as "galaxies having brilliant, starlike nuclei...(with) a faint nebulous envelope of small visible extent", may, with improved photography, become clearly resolved galaxies and not just 'nebulosities'. In which case, if, as they often do, they show broad emission lines, they would be reclassified as Seyferts (the same point applies to Zwicky's (1964) 'compact galaxies'). N-galaxies which show broad emission lines are now normally classed as Seyfert galaxies. This practice may be misleading, however, since it has not been established that in all cases the nebulosity is an underlying galaxy.

SURVEYS There is not, as yet, any sample of Seyfert galaxies which can be considered complete in the sense mentioned above. Some surveys have come sufficiently close to being so to allow a first answer to the question of how often galaxies show Seyfert properties.

The search methods used to find Seyfert galaxies have been very diverse:

(1) "random" methods -

(i) spotting bright nuclei at the telescope.

(ii) finding emission lines during a redshift determination programme.

These are the means by which the "classical" (NGC) Seyferts were discovered.

(2) systematic methods -

(i) looking for compact blue nuclei in galaxies by either:

(a) comparing Palomar Sky Survey red and blue prints, or

(b) using a low dispersion (e.g. 2500 Åmm^{-1} at Hβ) survey with an objective prism, as first done by Markarian (1967,1969a,1969b,1973, and Markarian and Lipovetsky, 1971,1972,1973,1974). Markarian's surveys have been by far the most successful means of finding Seyfert galaxies. They have yielded over half of those so far discovered.

(ii) identifying radio sources. There a half dozen or so bright compact radio sources discovered to be Seyferts but, in general, this is an inefficient means of finding these objects. It also produces an untypical sample of Seyferts exactly because such a small proportion of Seyferts are radio-bright (Osterbrock, 1977a). The opposite procedure of searching for (weak) radio sources in optically selected Seyferts is more successful (de Bruyn and Wilson, 1976).

(iii) searching for high surface brightness galaxies.

(a) Zwicky searched the Palomar Sky Survey for objects only just discernable from stars (c.f. N-galaxies) (at a time before quasars had been discovered). Zwicky's lists of 'compact galaxies' (unpublished) have not been thoroughly searched spectroscopically but have, nevertheless, supplied about 10% of known Seyferts. (Sargent, 1970).

(b) Arakelian has recently noted a simple way of finding high surface brightness galaxies from already published data. He has compared the apparent diameters of galaxies given in Vorontsov-Velyaminov's 'Morphological Catalogue of Galaxies' (1962) with the apparent magnitudes given by Zwicky

and his collaborators in the 'Catalogue of Galaxies and Clusters of Galaxies' (Zwicky et al. 1961,1963,1965,1966, 1968,1968). He has published a list of galaxies which are abnormally bright for their size (Arakelian, 1975). His list has only begun to be searched spectroscopically but has already provided at least 6 Seyferts (Weedman, 1977).

(iv) emission lines. By using a higher dispersion objective prism (1740 Å mm^{-1} at Hβ) M. G. Smith (1975) has been able to search directly for strong emission line galaxies. Again this is a new method but it promises to be the most efficient way of obtaining an optically complete sample of Seyfert galaxies.

As a result of the work reported in this thesis it is likely that another survey technique, perhaps more easily made complete, has been found in the detection of Seyfert galaxies in x-ray source error boxes (see chapters 4 and 6).

SPACE DENSITY

From these surveys the problem is to estimate the number of Seyfert galaxies per unit volume of space. Clearly this can only be achieved down to some absolute luminosity - nothing can be known about galaxies fainter than the detectors will reach. The space density must be determined as a function of absolute magnitude. This function is the 'luminosity function' for a class of objects.

Huchra and Sargent (1973) have used the first four of Markarian's lists to determine the space density of Markarian Seyferts. There may be a problem here in that two classical Seyferts appear in the part of the sky covered by these lists but do not appear in the lists. Markarian's survey may thus be more incomplete at low luminosities than it appears. Huchra and Sargent make corrections for incompleteness based on Schmidt's (1968)

V/V_{max} estimator. Their results are shown in fig. 1-3.

Galaxies listed by Markarian form around 5-10% of field galaxies except at the higher luminosity end where their frequency increases. Of Markarian galaxies around 5-10% are Seyferts. This proportion increases too at brighter magnitudes until at $M_v \approx -23$ it appears that most galaxies are Markarian and that most of these are Seyferts. (Typical quasars have $-23 > M_v > -25$; Allen, 1975).

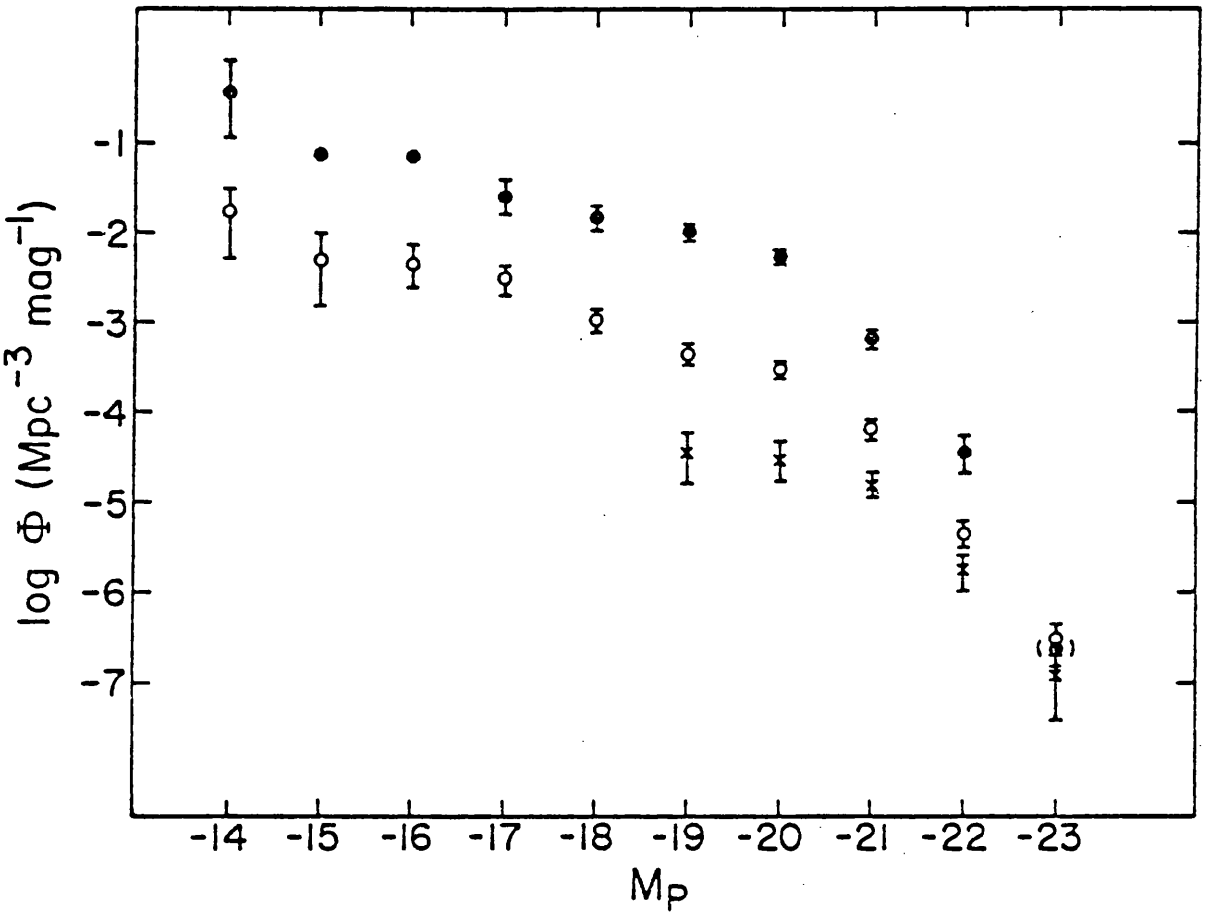

fig 1-3 LUMINOSITY FUNCTION (LOG SPACE DENSITY VERSUS ABSOLUTE MAGNITUDE) FOR FIELD GALAXIES (•), MARKARIAN GALAXIES (o), AND MARKARIAN SEYFERTS (x). Error bars represent the square root of the number of galaxies in each internal. The point representing the space density of field galaxies at M_p = -23 (in parentheses) has no error bar. (from Huchra and Sargent, 1973).

1-3 Classification

Although all Seyfert galaxies have 'broad' emission lines $\approx$500-1500 km s^{-1} wide, a sub-set have 'wings' on some of their emission lines that reach out to 5000-20,000 km s^{-1}. These wings (fig. 1-4, Osterbrock,1977b) are found only on the lines belonging to permitted transitions, notably the Balmer series of Hydrogen: Hα, Hβ and Hγ. The lines resulting from forbidden transitions never have these broad wings. They have only the widths of the 'cores' of the lines (500-1500 km s^{-1}, fig. 1-4). The presence or absence of the broad wings on the Balmer lines is the basis of a useful classification scheme for Seyferts introduced by Khachikian and Weedman (1974).

Many other features are found to correlate with this division into type 1 : broad wings present and type 2 : no broad wings. Table 1-1 lists the best established of these and figs. 1-5 to 1-7 illustrate them. This type 1 / type 2 division is remarkably clean for such a simple empirical criterion. There do, however, exist uncertain cases, as pointed out by Osterbrock and Koski (1976, fig. 1-8). In Weedman's (1977) review there are 70 type 1 and 17 type 2 Seyferts listed.

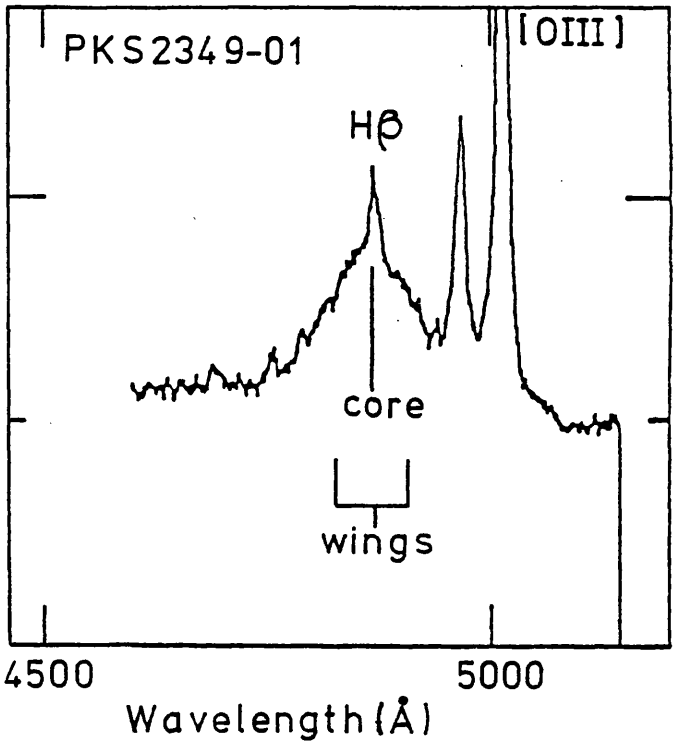

fig 1-4 THE Hβ TO [OIII] SPECTRUM OF PKS2349-01 (from Osterbrock, 1977b). This illustrates the different profiles of permitted and forbidden lines in type 1 Seyfert galaxies. Note core and wings components in Hβ and asymmetry in Hβ wings.

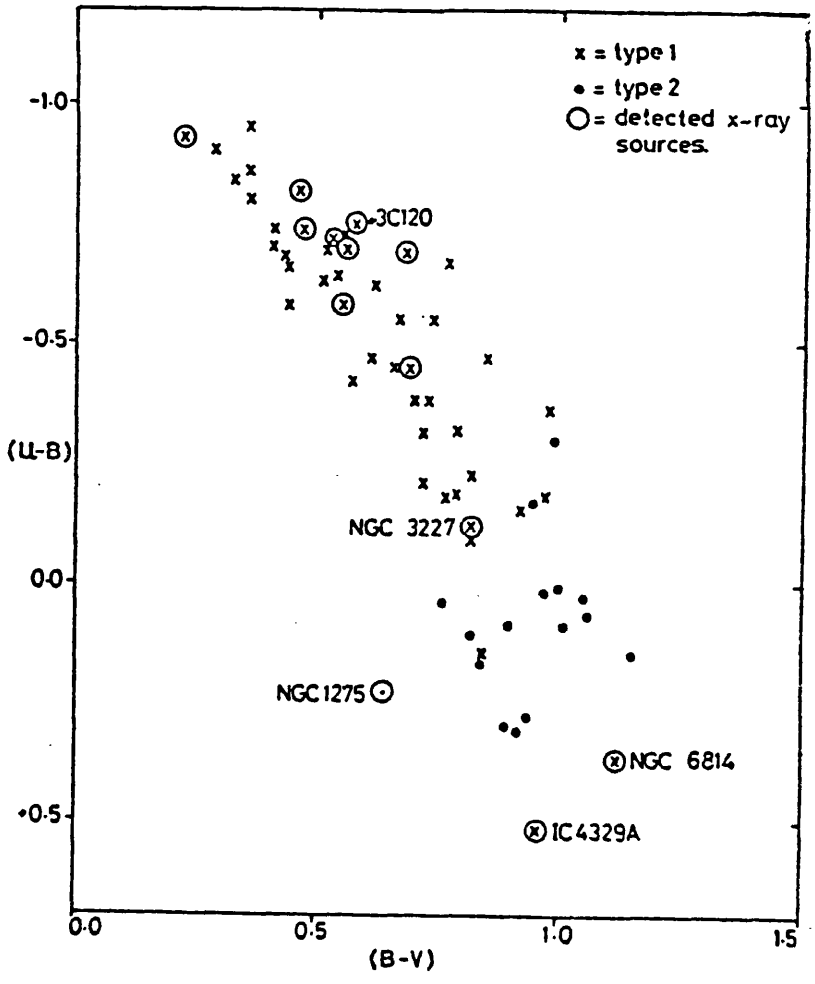

fig 1-5 (U-B) versus (B-V) PLOT FOR TYPE 1 AND TYPE 2 SEYFERT GALAXIES. Type 1 galaxies are, on average bluer than type 2. The preponderence of type 1 Seyferts amongst detected x-ray emitters is clear (see chapter 5-2).

Table 1-1 Distinctions between type 1 and type 2 Seyfert galaxies.

type 1	type 2
DEFINITION: Broad wings on Hydrogen Balmer lines. i.e. Permitted lines much broader than Forbidden. Typically 5000-20000 km s^{-1} for permitted and 500-1500 km s^{-1} for forbidden lines.	No broad wings. Permitted and forbidden lines have the same widths: 500-1500 km s^{-1} (see figs. 1-4) (Osterbrock, 1977b)
ALSO CORRELATES: Colours - $(U-B) \geq 0.2$ $(B-V) \leq 0.6$ i.e. top left of fig. 1-5	 $(U-B) \leq 0.2$ $(B-V) \geq 0.6$ i.e. bottom right of fig. 1-5
Continuum shape - often 'power-law', $F \propto \nu^{-\alpha}$ with $1 < \alpha < 2$ usually.	 rarely 'power-law'
Hβ : [OIII] λ5007 intensity ratio - ≈ 1	 ≈ 0.1 (see fig. 1-6) (Adams and Weedman 1975)
Balmer decrement - (Hα : Hβ) steeper than pure recombination (at 10^4 K) value of 2.87	 steeper than type 1 (more reddening ?) (see fig. 1-6)
Radio emission - maximum | luminosity $\approx 10^{23}$ W Hz^{-1} sr^{-1} mean | luminosity $\leq 10^{21}$ W Hz^{-1} sr^{-1} (see fig. 1-7) (de Bruyn and Wilson, 1978)	 same maximum | luminosity mean | luminosity $\approx 10^{21-22}$ W Hz^{-1} sr^{-1}. Higher mean value.
Polarization - either $\leq \frac{1}{2}\%$ or $\approx 4\%$ (Angel R. 1977)	 $< 2\%$

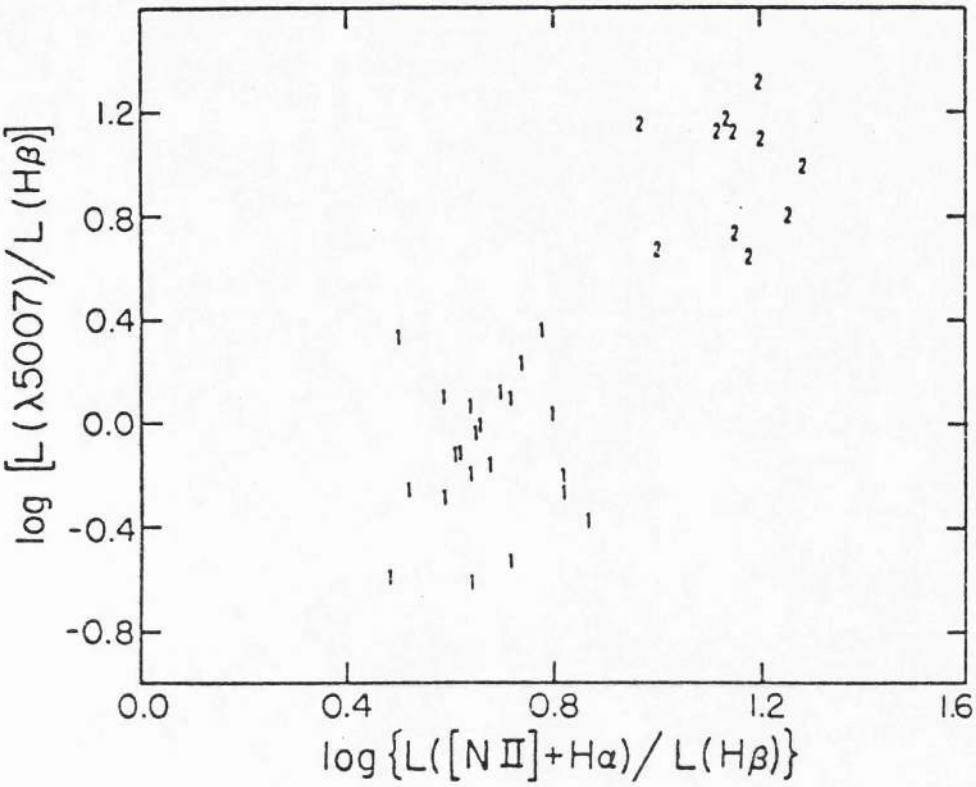

fig 1-6 [OIII] : Hβ POWER VERSUS BALMER DECREMENT (Hα :Hβ) FOR TYPE 1 AND TYPE 2 SEYFERT GALAXIES. The separation of the two types is clearcut. (L([NII] + Hα) is used as Hα is blended with [NII].

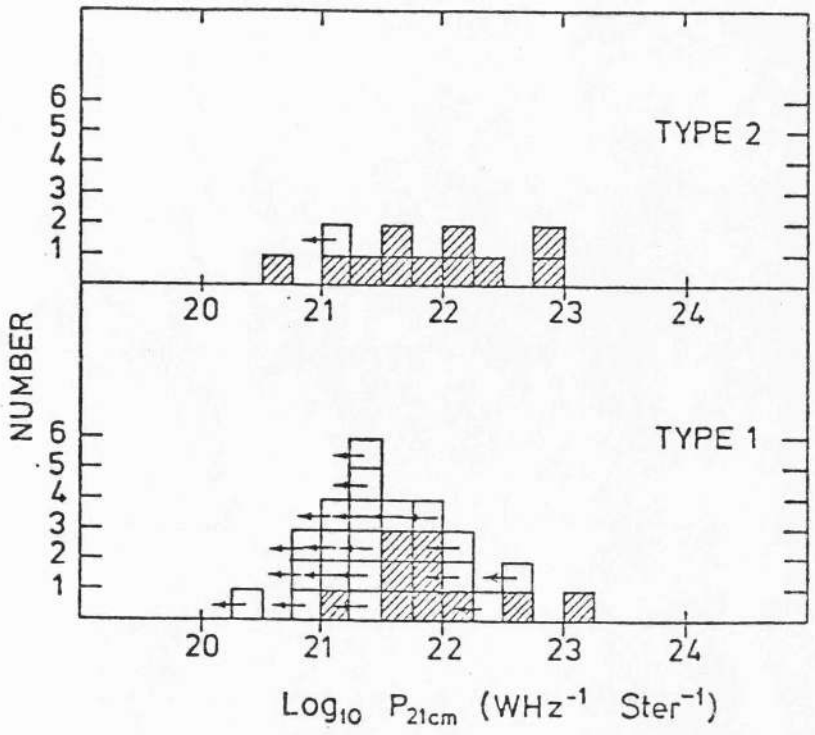

fig 1-7 HISTOGRAMS OF THE NUMBER OF TYPE 1 AND TYPE 2 SEYFERT'S EMITTING AS A FUNCTION OF POWER IN THE RADIO (1400 MHz). The maximum powers are the same for the two types byt the mean power for type 2's is higher.

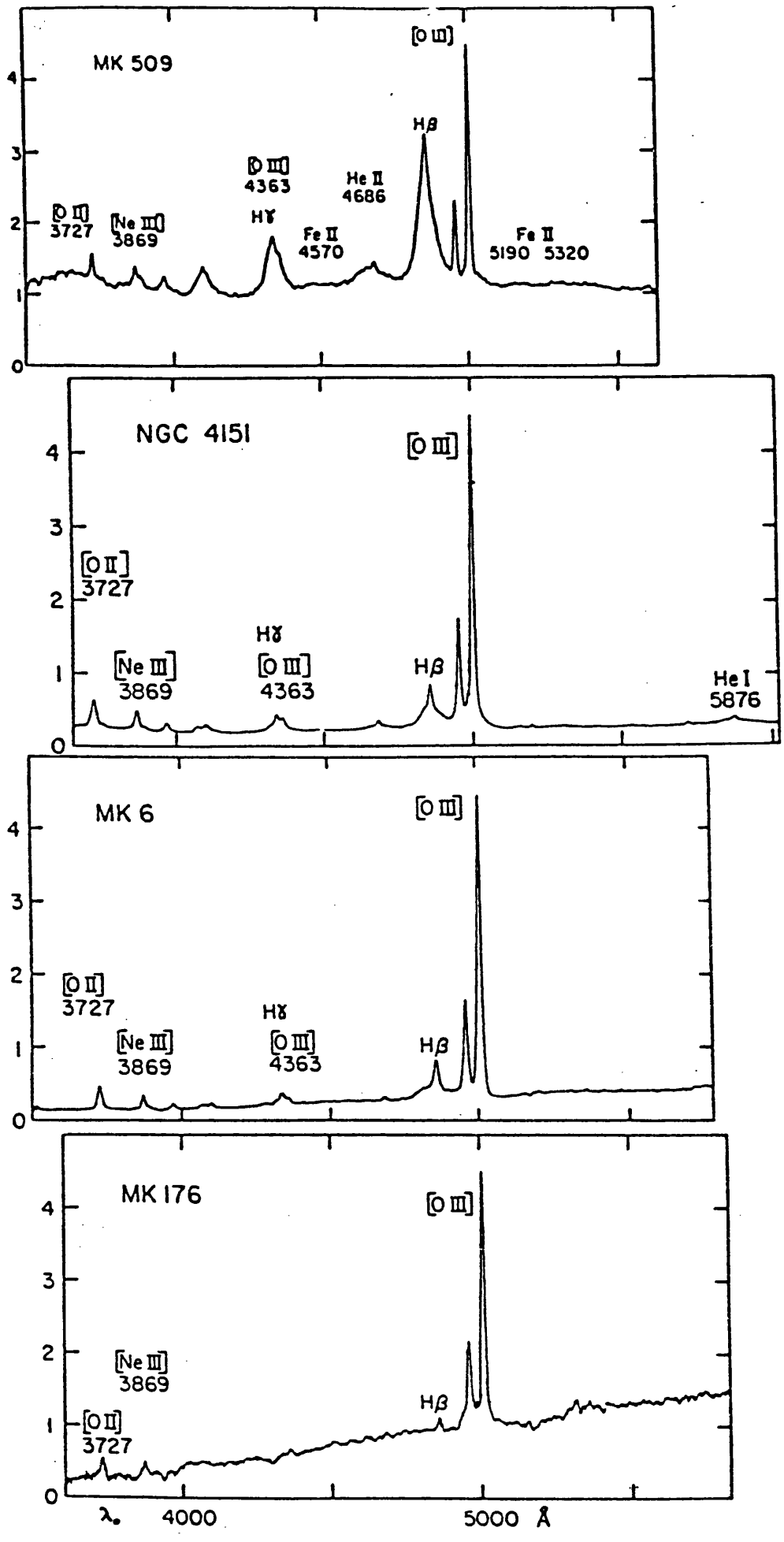

fig 1-8 TYPICAL SEYFERT SPECTRA GRADED FROM PURE TYPE 1 (at the top; Mkn509) TO PURE TYPE 2 (at the bottom; Mkn176). Clearly intermediate types do exist. (from Osterbrock and Koski, 1976).

1-4 Physical Conditions

Consideration of the optical spectra of Seyfert galaxy nuclei has led to a 'standard' model of their structure, but not of the energy mechanism which drives them. In this section the reasoning which leads to this standard model is described.

The nucleus is believed to be constructed from three distinct regions (see fig. 1-9):

(1) A central ionising continuum source < 0.01 pc diameter.

(2) A dense ($n_e > 10^{8.5} cm^{-3}$) permitted line 'wings' emitting region $\approx 0.1 - 1$ pc diameter.

(3) A rare ($n_e \approx 10^4 cm^{-3}$) forbidden line emitting region $\approx$ 100-1000pc diameter.

All three regions are present in type 1 Seyferts but region (2) is missing in type 2's. Regions (1) and (2) may be effectively identical on some models. The hypothesised initial energy source is assumed to lie somewhere in region (1). The continuum from (1) then causes photoionisation in the rest of the nucleus. Since ionisation levels up to [Fe VII] and now [Fe X] (see chapter 3-1) have been reported, the continuum must extend up to energies greater than their ionisation potentials of 0.10 and 0.19 keV respectively, i.e. at least into the soft x-ray region.

The sizes and densities of these regions are derived from the properties of the observed emission lines and variability observations:

BROAD PERMITTED LINE EMITTING REGION (2)

The broad wings of the permitted lines in type 1 Seyferts are never found in the forbidden lines. It seems then that the wings arise in a region where the forbidden transitions are suppressed through collisional de-excitation. Densities of $n_e > 10^{8.5}$ cm^{-3} (Osterbrock, Koski and Phillips, 1975) are needed to suppress all the lines expected.

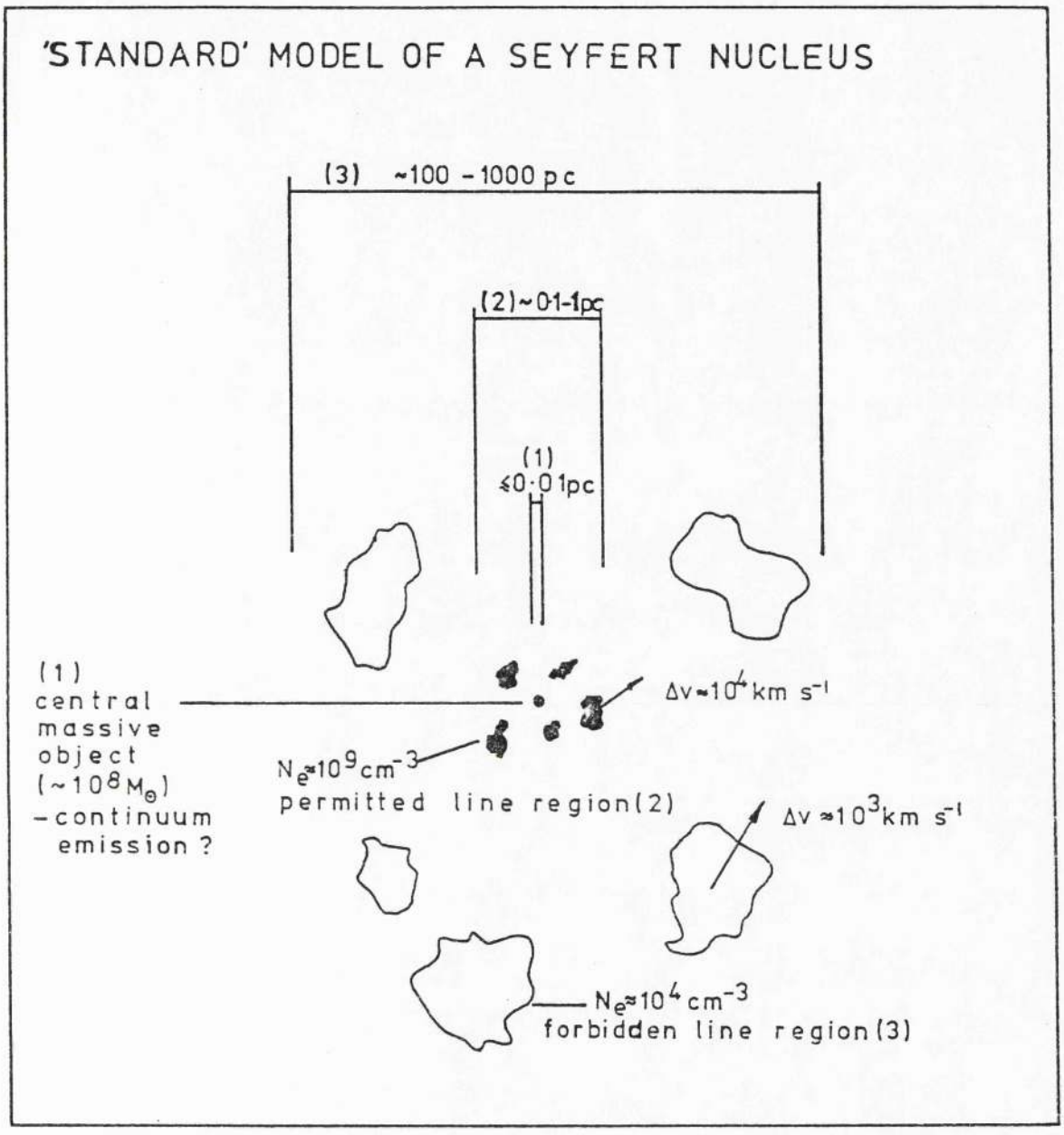

fig 1-9 SCHEMATIC ARRANGEMENT FOR THE "STANDARD MODEL" OF SEYFERT NUCLEI. Typical dimensions, electron densities (N_e) and 'random' velocites (Δv) are indicated.

These authors use this density limit, combined with the luminosity of the Hβ wings (L(Hβw)) and some assumptions, to give an estimate of the size, and thus the mass, of the broad line region (2), as follows:

The emissivity of Hβ, $j_{H\beta}$, can be assumed to have its recombination value for some temperature as a first approximation. A temperature, T, of 10^4K is usually used. Then -

$L(H\beta w) = 4\pi\, j_{H\beta} V$, V being the volume of emitting region.

$4\pi j_{H\beta} = 1.24\times10^{-25} n_e n_p$, erg $s^{-1}cm^{-3}$, n_e and n_p being the electron and proton densities.

and $V = {}^4/_3\pi\, r^3$

so, if $n = n_p \approx 10^9$ cm^{-3},

$L(H\beta w) = 5.19\times10^{-7}\, r^3$.

$L(H\beta w)$ is typically $\approx 10^{42}$ erg s^{-1} (see Table 5-1)

so $r \approx 1.3 \times 10^{16}$cm,

≈ 5 light days.

This, of course, is a minimum size. The probable size of the emitting region is much larger since the above assumes a uniform gas density. As pointed out below this is almost certainly not the case. From this size and density one can derive a mass for the broad line region gas of

$M = m_H n_p V$, m_H being the mass of a hydrogen atom,

$= 1.5 \times 10^{34}$g

$= 7.4\ M_\odot$, $M_\odot$ being one solar mass.

Osterbrock, Koski and Phillips find that values below 100 $M_\odot$ are normal for this mass. So at such high densities a surprisingly small mass is required to produce the dramatic broad line emission in Seyferts.

FORBIDDEN LINE EMITTING REGION (3)

For the forbidden line region (3), because the densities involved have to be much lower, the mass involved must be much larger. The ratio of the [O III] lines λ5007,λ4959 can be used to give a locus of possible combinations of (n_e, T). In favourable cases other line ratios can be used to give separate loci which, when they intersect, give the required values. (see e.g. Boksenberg et al., 1975). Different parts of this region could well have different values for n_e and T so that these loci do not always intersect at consistent values. However values of n_e between 10^3 and $10^5 cm^{-3}$ are normal. 10^4 cm^{-3} being a good canonical value. T is again around the value of 10^4 K. (Anderson (1970) gives (n_e, T) plots for 8 Seyferts).

The size of the forbidden line region is based on the case of NGC 1068 for which the forbidden line region has been measured directly to be $\approx$ 500 pc across. (Walker, 1968).

CLOUD STRUCTURE OF REGIONS (2) AND (3)

The permitted (2) and forbidden (3) line regions are believed to have a highly non-uniform distribution of the gas to contain a number of discrete clouds or filaments. The observed line widths can then be ascribed to the relative motions of the, fast-moving, clouds. In the case of the dense region (2) this view is based on the complex Balmer line profiles. The profiles are very often asymmetric (see Weedman (1977) Table 1-1, fig. 1-5) and both sides are far from gaussian. Multiple peaks (e.g. IC4329A, Disney, 1973) and 'shoulders' (Osterbrock, Koski and Phillips, 1976) are common. These profiles can be easily explained by invoking a, fairly small, number of discrete clouds moving at speed, but are difficult to explain with other broadening mechanisms (e.g. electron scattering).

Since region (2) is believed to be $\approx$ 1 pc across the crossing time for the clouds is $\approx$ 100 years. Clearly the gas must be replaced since even if all galaxies went through a Seyfert phase they would still

need to be active for 1% of their life, $\approx 10^{7-8}$ years. Alternatively the clouds could be gravitationally bound by invoking a large mass for region (1). This is mentioned in more detail below.

The profiles of the forbidden lines (region (3)) are less often complex but Mkn 509 shows double peaked structure, the peaks having a Doppler separation of 400 km s^{-1} (Ward, private communication). Walker (1968) resolved different parts of the nucleus of NGC 1068 and found them to have different forbidden line redshifts of the same order as for Mkn 509.

Thus the gross features of density, temperature, size and mass of regions (1) and (2) - the two line emitting regions - can be arrived at. The dimensions of these regions vary by factors of 10, depending on the author, and this could well be a property reflected in the objects themselves, as one goes from one to another.

"NON-THERMAL" CONTINUUM EMITTING REGION (1)

The continuum from a type 1 Seyfert nucleus generally follows a power-law distribution which does not at all resemble a composite stellar spectrum. By analogy with radio source spectra one might imagine that these power-laws were also due to synchrotron radiation but this is only an analogy and not at all necessary. The polarization data argue against such an interpretation (see Table 1-1) particularly as both continuum and line radiation are polarized to the same extent and at the same position angle (Angel, 1977). An upper limit to the size of the continuum region (1) can be found from variability arguments. Penston et al. (1974) found that the optical continuum in NGC 4151 varied by 0.5 mag in about 1 month. The diameter of the region must thus be less than $\approx 10^{17}$ cm. Anderson (1974) noted variability in the absorption line spectrum on a timescale of less than 1 year (possibly 30 days). Since these features probably arise from one of the clouds in the line emitting regions (2) and (3) as it crosses in front of the continuum source we can estimate the size of this source.

If we assume, following van den Bergh (1975), a transverse velocity of 1000 km s^{-1} then the source must be less than 3×10^{15} cm across, smaller than the minimum size for the permitted line region (2). This argument relies on uncertain assumptions so that models in which the continuum and permitted lines arise in the same region are still allowed.

The initial energy source for the Seyfert activity is assumed, on this 'standard' model, to lie within, or be coextensive with, the region (1). By assuming that the largest velocities, V, observed in the permitted line wings are of the order of the escape velocity for the clouds from the nucleus the mass of this central region can be estimated (Dibaiye, 1977). This assumption is clearly not required by the observations but does yield an order of magnitude estimate. The mass of the central region, M, is then

$$M \approx \frac{V^2 r}{2G} \quad , \quad r \text{ being the size of the region.}$$

If $V \approx 5000$ km s^{-1} and $r \approx 10^{16}$ cm then

$$M \approx 10^7 M_\odot \ .$$

The absorption line variability gives an upper limit to the central mass in NGC 4151 of $\approx 10^{10} M_\odot$ by comparing its size to the Schwarzschild radius of $3 \times 10^5 (M/M_\odot)$ cm (van den Bergh, 1975).

We are thus led to expect a massive central body at the core of the nucleus of a Seyfert galaxy. Most theories of such nuclei use gravitational infall on to such a body to provide the ultimate power source for Seyfert activity. Gravitational infall is invoked to some extent because it has proved to be an efficient source of energy on a smaller scale in the context of x-ray binaries. As yet there is no agreement on a satisfactory model for producing the power in the form observed from this assumed original source.

The great mass of high quality optical observations have cleared away the confusion of details arising in the outer regions of the Seyfert nuclei to a great extent. The central problem is one which can now be faced. The results reported in this thesis may, we believe, hold the potential for answering this question.

chapter 2. THE ARIEL V SKY SURVEY

The results reported in this thesis were obtained using the Leicester University X-ray Sky Survey Instrument (SSI) on board the Ariel V satellite. The observations were made mainly as contributions to the "Ariel V (SSI) Catalogue of High Galactic Latitude ($|b| > 10^{o}$) X-ray Sources". (The '2A' catalogue, Cooke et al., 1978). In this chapter the satellite and the Leicester instrument are described and it is shown how the 2A catalogue was produced from the data returned.

2-1 Ariel V

The Ariel V * (fig. 2-1) satellite has a payload of six x-ray astronomy experiments each with a specialized and complementary function (Table 2-2, fig 2-2, Smith and Courtier, 1976). The satellite was launched on 15th October 1974 with a planned minimum lifetime of one year. At the time of writing it has been operating for just over three years.

The main satellite parameters are given in Table 2-1. The low equatorial orbit is appropriate for x-ray astronomy as here the magnetic field of the Earth produces the greatest shielding from the primary cosmic rays and thus reduces the induced background in the detectors. The satellite is spin stabilised and this rotation provides a natural means of modulating the incoming signal. Most of the experiments make use of this ability, most notably the Rotation Modulation Collimator (expt. A, see Table 2-2).

Power for the satellite and its experiments is supplied by a set of solar panels which cover 7/8 of its outer surface (fig. 2-1, 2-2). When the spacecraft is passing through the earth's shadow an on-board Ni-Cd battery keeps the several key satellite systems functioning. Weight restrictions prevented the carrying of adequate battery capacity to allow

---

* The 'Ariel-' series of satellites are called 'UK-' before launch.

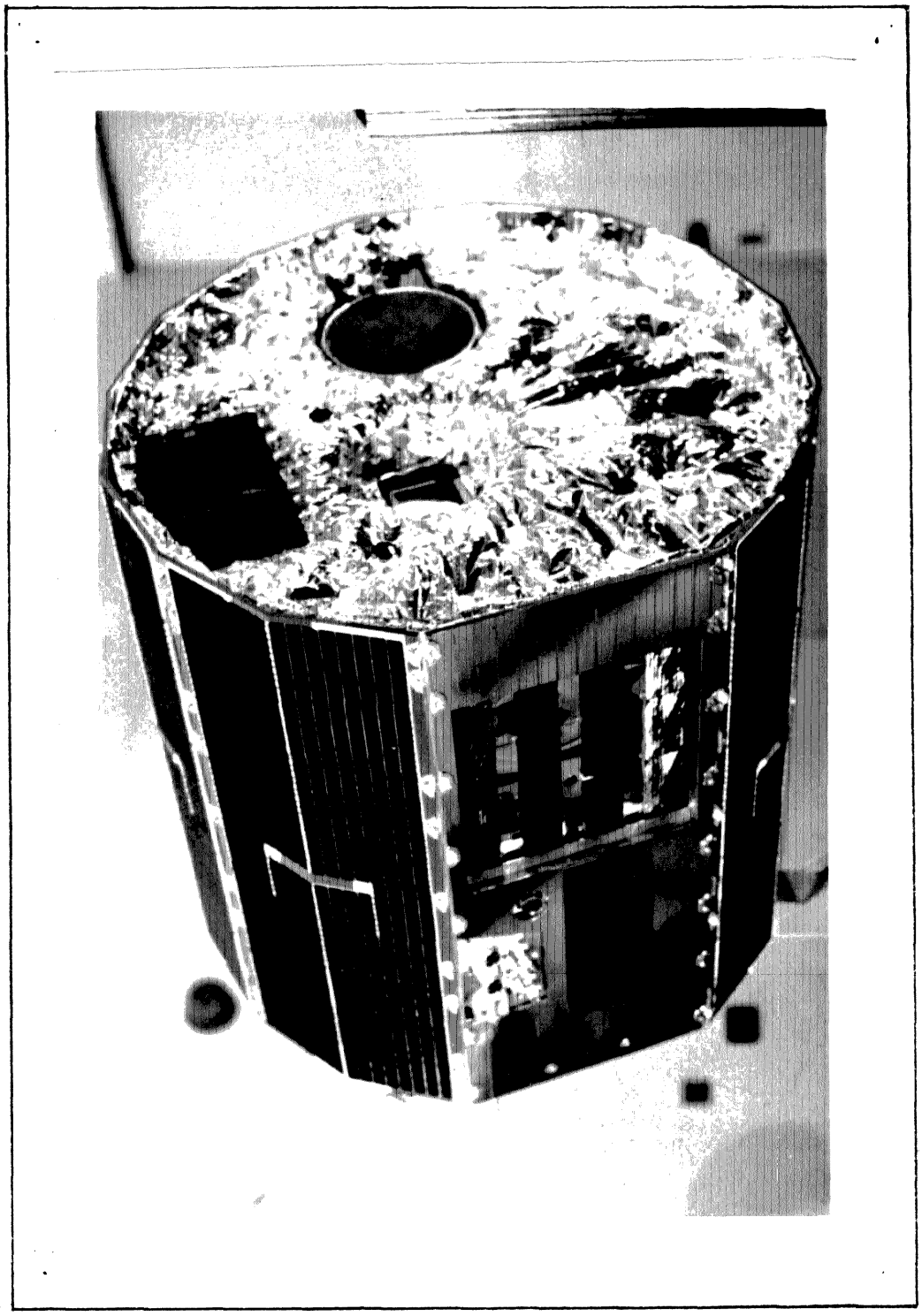

fig 2-1 THE ARIEL V SATELLITE SHOWING THE ARRANGEMENT OF THE INSTRUMENTS , as indicated in fig 2-2.

the experiments to remain switched on during this period of earth eclipse. This reduces the exposure time per orbit. The solar panels have to point at an angle of less than 45° to the sun otherwise they will generate too little power to keep the experiments operating. This imposes the major constraint on the parts of the sky available to the instruments and so affects the observing programme (see chapter 2-3 below).

The instruments other than the Leicester SSI are briefly described in Table 2-2. Four of these (A,C,D,F) have small field of view and point along the spacecraft spin axis (fig.2-3, Smith and Courtier, 1975). They perform detailed observations of individual sources. The fifth (G) is a scanning, low sensitivity monitor for transient events and for the long term behaviour of bright sources. It views about 90% of the sky at any one time.

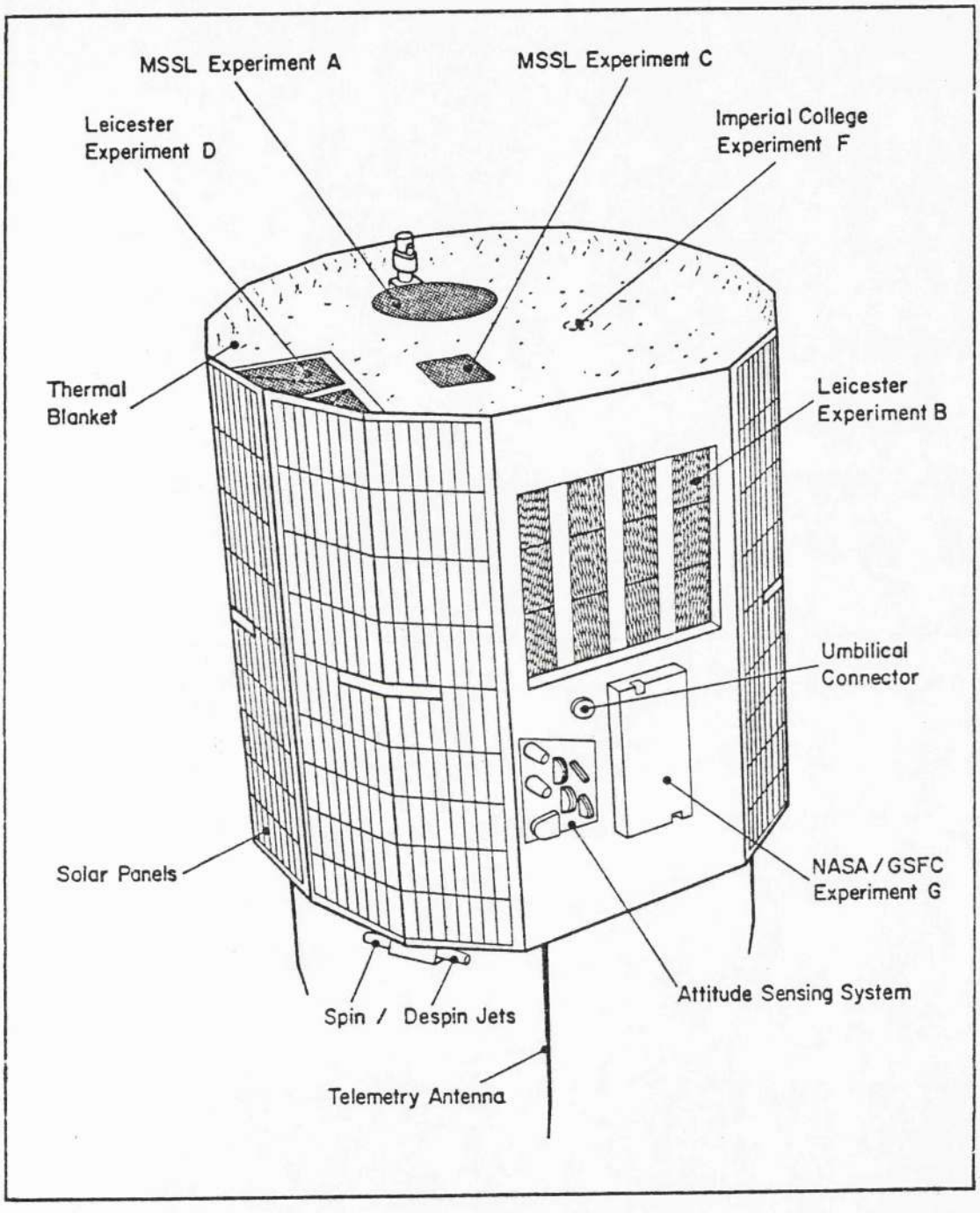

fig 2-2 DIAGRAM OF ARIEL V, showing how the four pointing instruments (A,C,D,F) look out of the top face and the two scanning instruments (B,G) look out of the side. (from Smith and Courtier, 1976)

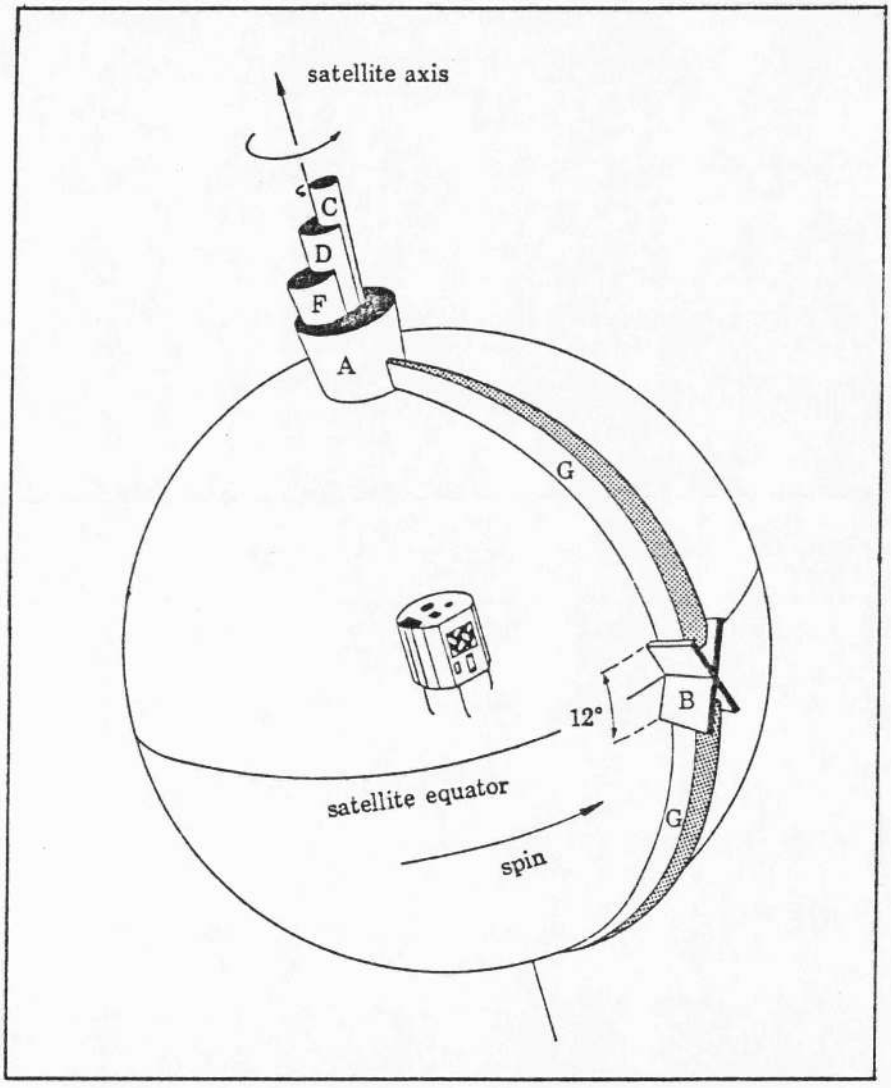

fig 2-3 THE FIELDS-OF-VIEW OF THE ARIEL V INSTRUMENTS in the satellite reference frame. Angular limits are drawn for the FWHM responses. (from Smith and Courtier, 1976)

Table 2-1 Ariel V Satellite parameters

(from: "The Scientific Payload for the UK5 Satellite", SRC (1973).)

Size:	diameter 95.9 cm ; height 86.4 cm (excluding telemetry aerials)
Weight:	131.6 kg.
Orbit:	≈circular and equatorial - apogee 556 km, perigee 512 km, inclination 2.°9
Launch vehicle:	4 stage NASA Scout
Attitude sensing:	2 sets of Sun and Earth-albedo sensors accurate to 10-30 arcmin (per orbit). Rate clock divides each rotation into 1024 equal angle azimuth sectors.
Attitude control:	-spin stabilised, accurate to 30-60 arcmin (per orbit) -propane gas jets (total 4000° manoeuvre) -controlled interaction of de-gaussing coil with earth's magnetic field.
Spin rate:	10 ± 2 rpm. controlled by: - gas jets - interaction of current from solar panels with the earth's magnetic field.
Power:	side mounted solar cells . battery when in earth's shadow. total power 11.3W. divided thus - data handling 5.92 W - tele-command 0.75 W - attitude control 0.85 W - experiments 3.75 W power division between experiments is roughly equal at ≈0.6 W each

Table 2-2 Ariel V Experiment Payload Summary

(see figs. 2-1 and 2-2)

Experiment	Research Group (Description ref.)	Experiment Definition	Field of View FWHM Degrees	Energy Range (keV)	Mission
A	Birmingham University/ Mullard Space Science Laboratory (Wilson,1977)	Rotation Modulation Collimator with Associated Star tracker	17	0.3 - 30	Positions bright x-ray sources to ≈30 arcsec
B (SSI)	Leicester University (Cooke et al.,1978, Villa et al.,1976)	Mechanically collimated scanning proportional counters	10.6 x 0.75	2.4 - 20	Sky Survey to $\approx 10^{-3}$ Crab flux density positions to ≈0.3 sq^{o}. 8 energy bins.
C	Mullard Space Science Laboratory (Sanford and Ives,1976)	Proportional Counter with 128 channels of Pulse height information	3.5 x 3.5	2 - 30	Detailed study of source spectra (32 or 128 energy bins). Time resolution down to ≈1s (or ≈ ms for a preset period, "pulsar" mode)
D	Leicester University (Griffiths et al., 1976)	Bragg Crystal Spectrometer/ Polarimeter	7.5	2 - 8	Emission line (1% resolution) and polarization (with Bragg angle at 45^{o}) studies of very bright sources.
F	Imperial College (Carpenter et al.,1976)	Caesium Iodide Scintillator with active Collimator	8.0	20 - 2000	High energy detection and Spectral Studies of bright sources (16 energy bins).
G	Goddard Space Flight Centre (Kaluzienski,1977)	Two Pin-hole Cameras	90% of celestial sphere	3 - 6	All Sky Monitor for bright sources and transient alert. 1 energy bin. Positions to 2^{o}

Table 2-3 The Sky Survey Instrument (SSI, Expt. B)

2 pairs of proportional counters - one pair High Energy (HE), - one pair Low Energy (LE).	
Area:	each counter 140 cm^2 effective (280 cm^2 each system)
Gas:	mixture Ar:Xe:CO_2 :: 76:16:8 pressure 900 mm Hg. depth 2 cm for LE pair 4 cm for HE pair
Window	Beryllium, thickness 0.0086 cm LE 0.0127 cm HE
Collimator:	stainless steel 1μm slats. angular constraints - 10.6 x 0.75 deg. FWHM, inclined at 25° to spin axis (see fig. 2-4). point response function - approx. triangular; see fig. 2-5.
Energy range:	LE 0.8 - 6 keV approx. HE 2.4 - 20 keV approx. obtained from pulse height analysis (PHA) energy gating
Spectral resolution:	PHA also divides counts into 8 energy channels spaced so that E(upper bound) : E(lower bound) :: 1.3 : 1 resolution ≈ 50% at 6 keV at launch.
Background rejection:	(1) anti-coincidence guard counters 1 cm deep on 2 sides and base of each counter. (2) Rise Time Discrimination (RTD) circuits reject pulses with risetimes greater than a critical value (≈200ns) Together (1) and (2) reject 96% of particle events. (3) data collection is inhibited by a 'sun diode veto' for the part of any satellite spin when the sun would shine directly into the collimators. (4) Instrument is switched off when the satellite passes through the South Atlantic Anomaly - triggered by background count rate in expt. C or D.
Background rates:	total ≈9 counts s^{-1} estimated proportions - particle ≈50% diffuse cosmic x-ray ≈50%

-continued-

Table 2-3 continued The Sky Survey Instrument

On-board data storage:	1024 16-bit words. Can be divided between azimuth and energy information. Width of azimuth bin stays constant ($0^{\circ}.35$) so proportion of scan plane covered is halved as number of energy bins is doubled. Normal Survey mode covers whole of scan plane in 1024 sectors with one energy channel.
Exposure time:	Instrument "on-time" is typically 60 min. per orbit, so exposure per azimuth sector ≈ 3 seconds per orbit.
Sensitivity:	to produce a 3σ peak, in HE system, (on-axis) - 1 orbit ≈ 4.5 SSI ct s^{-1} ≈ 15 UHURU ct s^{-1} ≈ 0.015 Crab 1 day ≈ 1.5 SSI ct s^{-1} ≈ 5 UHURU ct s^{-1} ≈ 0.004 Crab 1 SSI ≈ 0.7 SSI ct s^{-1} ≈2.5 UHURU ct s^{-1} ≈ 0.002 Crab observing slot (≈ 3 day)
Count rate conversion:	$\frac{1 \text{ SSI ct } s^{-1} \approx 5.1 \times 10^{-11} \text{ erg cm}^{-2} s^{-1} \text{ (2-10 keV)}}{\approx 2.7 \text{ UHURU ct } s^{-1}}$ Varies by $\lesssim 6\%$ for power law photon indices from 1 to 3 and thermal spectra with kT from 2 to 16 keV. It is more sensitive to low energy absorption cut-offs.

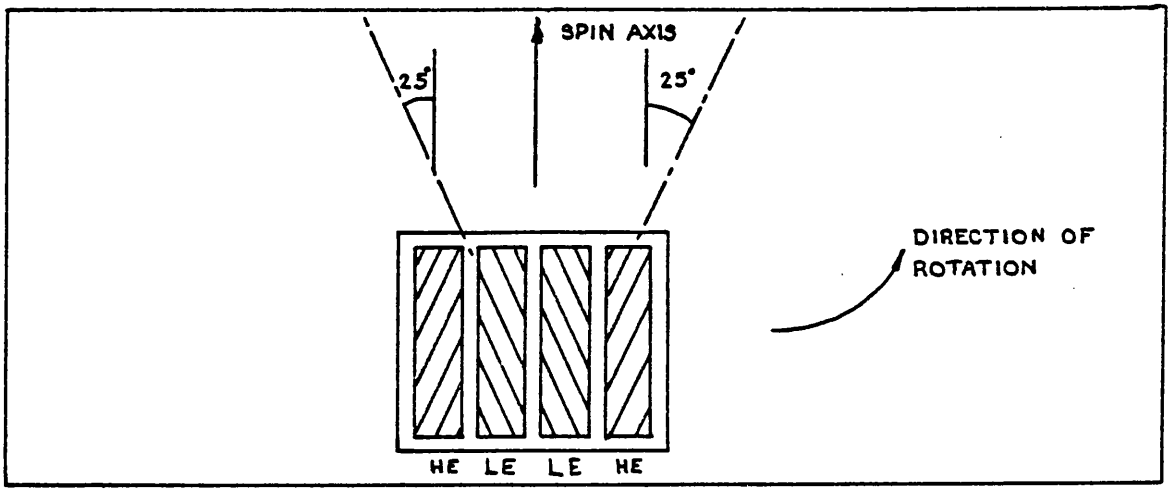

fig 2-4 SSI COLLIMATOR CONFIGURATION.

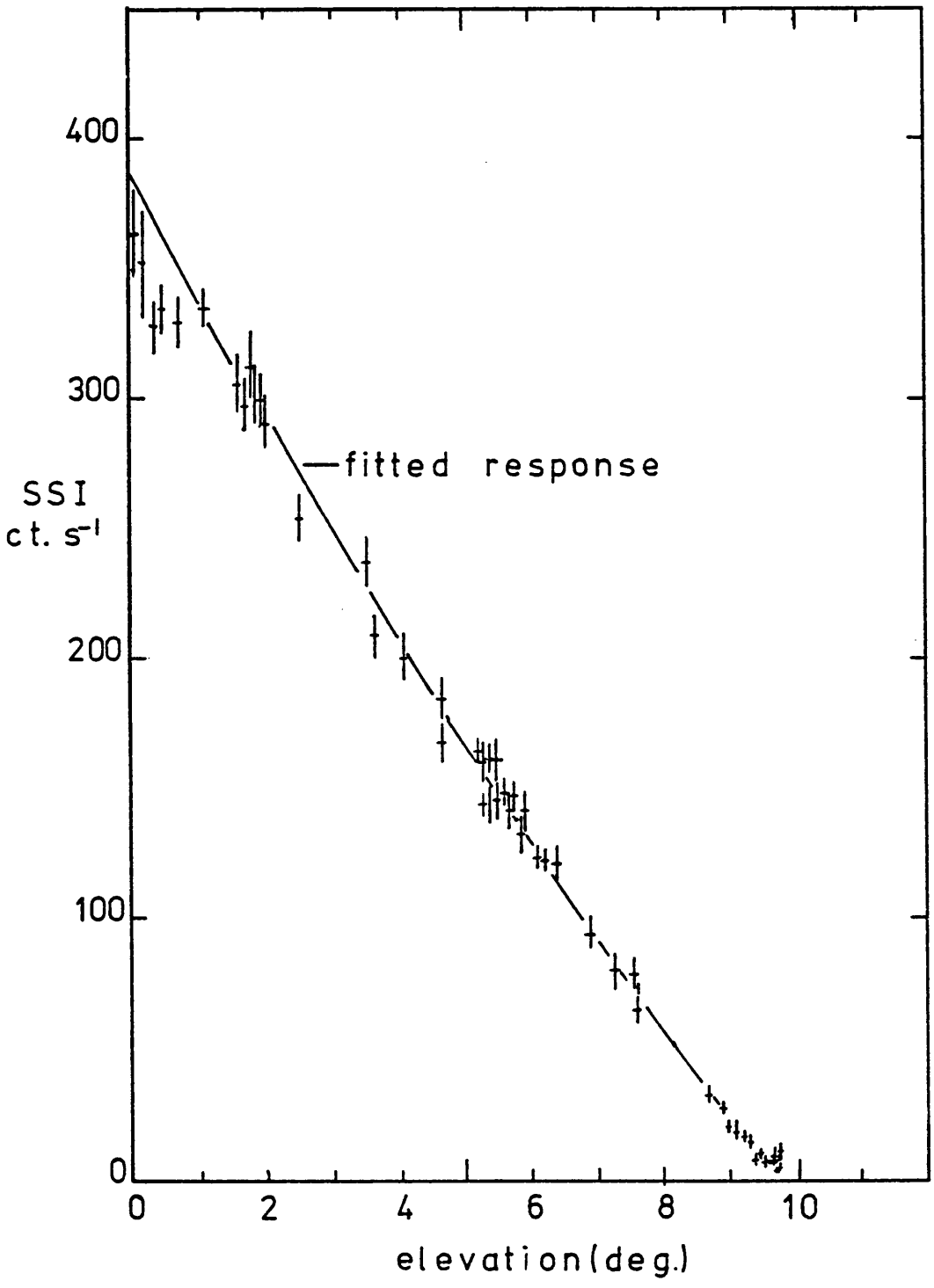

fig 2-5 POINT RESPONSE FUNCTION OF THE SSI, determined using the Crab Nebula as a calibration source. Crab observations are shown ($\frac{1}{4}$). (from Ricketts M.J., private communication)

2-2 The Sky Survey Instrument (SSI)

The SSI was designed to produce a whole sky survey in 2-20 keV x-rays down to around 10^{-3} of the Crab flux density (Tau X-1;3U0531+21) with sufficient positional accuracy ($\leq$ 0.5 sq deg.) to make identifications with reasonable certainty. It has many features in common with its only predecessor, the UHURU satellite (Giacconi et al., 1971).

The third UHURU catalogue of x-ray sources ('3U' , Giacconi et al., 1974) was around 50% complete over the sky down to 10 UHURU counts s^{-1} ($\approx 10^{-2}$ Crab) (Murray, 1978). Over 25% of its sources had positional uncertainties (error boxes) greater than 1 sq. deg. Since it is also now clear that x-ray sources are, in general, highly variable, a second whole sky survey using the SSI was clearly justified.

Table 2-3 lists the main technical details of the instrument. Other details are given in Villa et al. (1976). From the sensitivity figures it is clear that to reach the target depth of coverage observations which integrate data for 3 days or more at a fixed spacecraft attitude are called for. Each 3-day observation is called an 'Observing Slot'.

A major limitation on the SSI was the small size of the satellite core store data memory. This dramatically reduced the amount of spectral and temporal information which could be recorded. Data is dumped to a NASA ground station once per orbit (i.e. every 97 min.) and no finer time resolution than this is normally available. Only by sacrificing spatial coverage can any more than one spectral channel be made available. Clearly reducing the angular extent of a scan increases the time needed to complete a whole sky survey proportionately. Energy resolution was used in practice only for particular observations of sources, usually bright, galactic, sources.

The low energy system would have alleviated this problem somewhat by giving a "hardness ratio" (ratio of high energy to low energy count rates) for every source. Unfortunately the low energy system developed

leaks early in the mission (probably due to corrosion of the thin Beryllium window caused by the high humidity at the launch site) and had to be turned off. The survey was essentially performed using the high energy system only.

2-3 Sky Survey Observing Programme

Control of the attitude of the spacecraft is divided approximately equally in time between each of the experiments. Since experiment G views essentially the whole sky all the time it places no special demands on the attitude. Each remaining experiment has ≈20% of the time. The limited total angle of manoeuvre requires that all requests for positions be discussed well in advance to ensure that the control gas is used as slowly as possible. The power constraint of the satellite (Table 2-1) also restricts the available range of positions at each time in the year.

The strategy for the Sky Survey was to ensure that every part of the sky was covered to the nominal 3-day observing depth at least three times at position angles as widely spread as possible. This was achieved using the following scheme: (fig. 2-6).

(1) Points every 10° around $\frac{1}{2}$ of the galactic plane will cover the whole sky once. Many of these 18 points can be well approximated by directions determined by the four pointing experiments. Around the Galactic Poles these scans provide many cross-scans at well separated position angles.

(2) A series of 15 scans around $\frac{1}{2}$ a small circle with the spacecraft axis pointing at $\pm 30^\circ$ b will give cross-scans for $|b| \leq 60^\circ$. Crossing angles with respect to the scans of (1) above go from 90° at $b = \pm 60$ down to 30° at $b = 0^\circ$.

(3) North and South Galactic Pole pointing scans give coverage of the entire galactic plane at 90° to scans (1).

(4) To give good cross-scans at mid-galactic latitudes, where (1) and (2) cross at small angles, a series of 9 pointing positions around $\frac{1}{2}$ a small circle at $b = \pm 60^\circ$ were included.

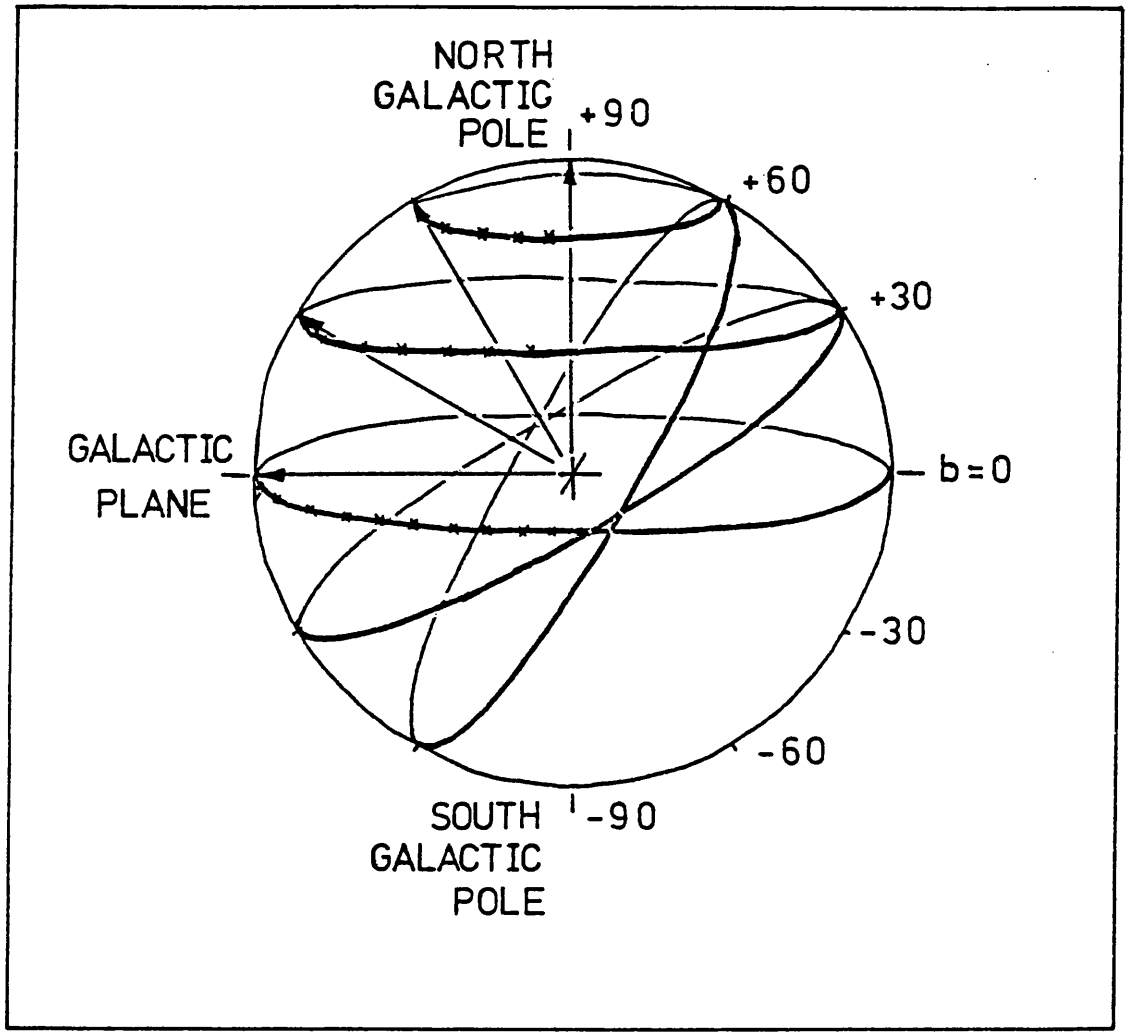

fig 2-6 SSI OBSERVING PROGRAM PLAN. The celestial sphere is shown in galactic co-ordinates. Positions of the satellite spin plane are shown for spin axis positions at b= 0 , 30 , 60 , 90 . The value of series of spin axis positions at b= 30 and 60 can be seen.

(5) "random" scans provided by the four pointing instruments' attitude requirements. These comprised some 80% of the spacecraft lifetime. Although not optimised for sky survey work the large number of these scans assured that essentially all the sky would be covered at some point.

(6) "fill in" scans to even out the coverage given by (5). The coverage was reviewed every six months or so to ensure this.

Thus two scans were systematically planned and third and subsequent scans of the sky were allowed to develop from the 80% of the time controlled by the other experiments. Anomalies were filled in by specific "one-off" SSI controlled positions.

Around 30 special SSI pointing positions were thus needed to complete the survey, each lasting 3 days. The SSI receives the necessary 90 days of satellite control in 15 months. Thus data up to at least the end of 1975 were needed to produce the catalogue.

2-4 Sky Survey - catalogue data analysis scheme

Initial problems in the analysis of SSI data were concerned with (a) the ability to locate peaks in the raw single orbit data and compute their strength reliably; (b) the ability to store the raw data in a quickly accessible manner; (c) the ability to sum all orbits in a given, 3 day, Observing Slot to produce the sensitivity needed for the survey.*

Only when all these problems had been satisfactorily resolved was it possible to consider the strategic problem of producing a catalogue of x-ray sources. A number of attempts at such a strategy were made.

Increasing experience, and, to some extent, available computer power, led to the following general scheme:

(1) Produce a computer file of all the raw data (fig. 2-7a) summed into Observing Slots. This gives the most sensitive available data base from which to search for sources (fig. 2-7b). Clearly the file will also need to store exposure information to calculate true flux densities and spacecraft attitude information to allow the positions of source sightings to be reconstructed in celestial co-ordinates.

(2) Use the file created in (1) to search automatically for peaks above some threshold significance (initially 2.5σ, later revised to 3σ). This process involves calculating a best fit background and subtracting it from the data. The resulting data is then cross-correlated with the collimator point response function (Table 2-3 and fig. 2-5) to find the significant peaks. The size in counts s^{-1} and the position of each peak is then stored on a second computer file. Where possible a peak is matched up with a catalogued x-ray source. In these cases the effect of reduced collimator transmission with elevation from the spin plane can be corrected for to give true flux

---

* These points are dealt with in detail by Eadie G.R.(PhD thesis, University of Leicester, 1978)

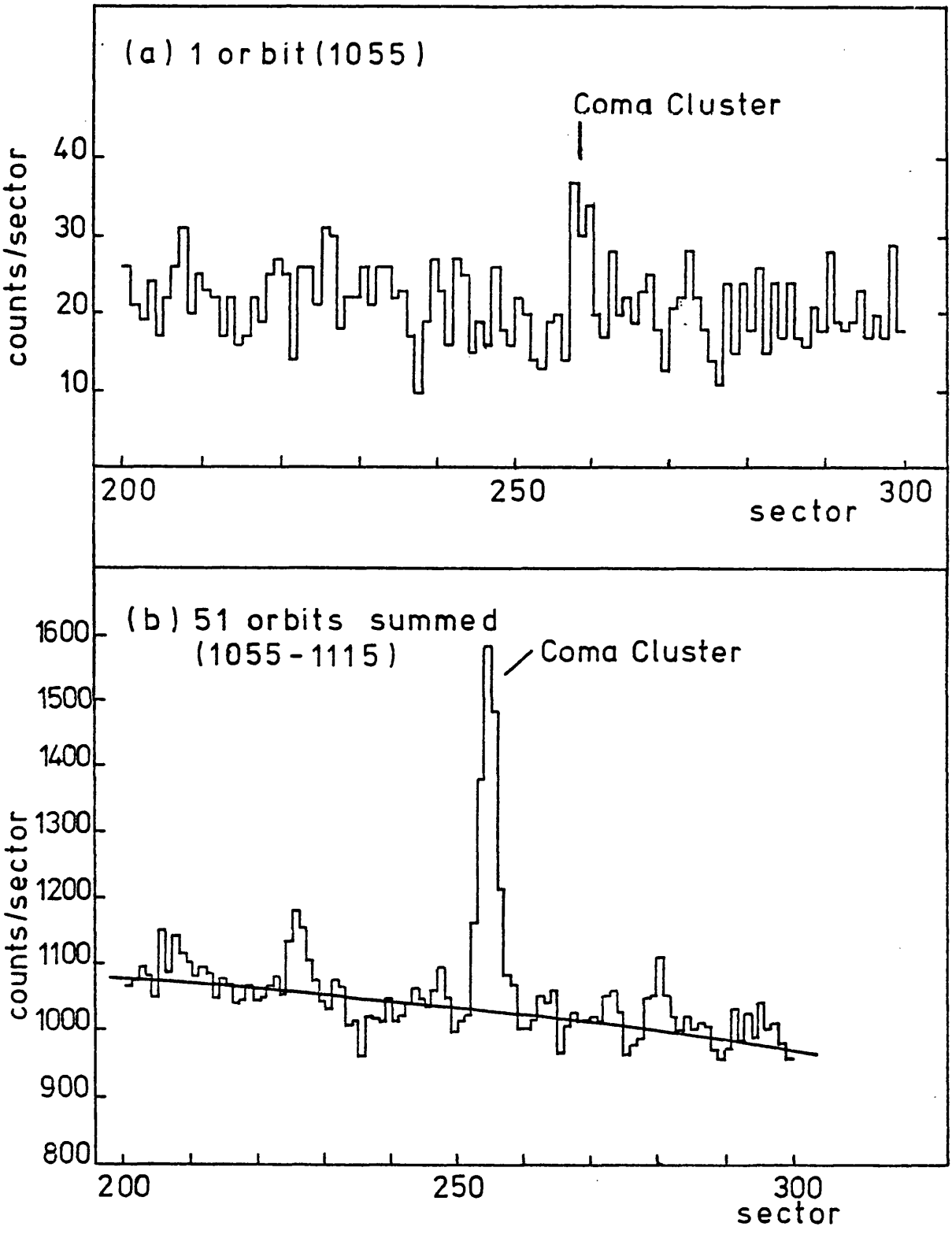

fig 2-7 TYPICAL DATA SETS FROM THE SSI SHOWING

(a) ONE ORBIT'S DATA. The Coma Cluster, one of the brightest extragalactic x-ray sources is just visible

(b) ONE OBSERVING SLOT'S DATA. (51 orbits in this case). This sum includes the data from (a) and shows the same strip of sky. With the increased exposure three more sources become visible.

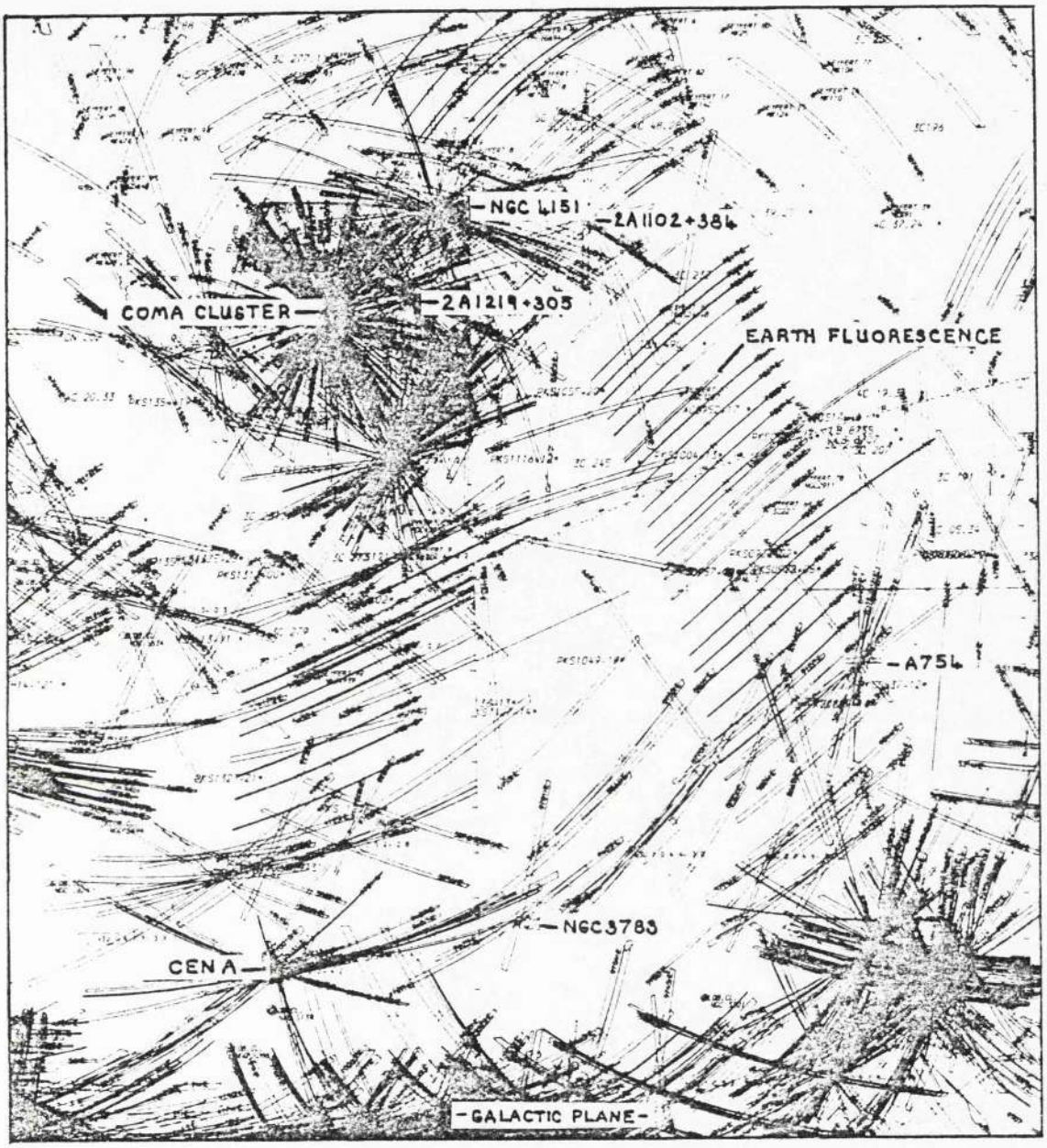

fig 2-8 A SECTION OF THE ALL SKY LINE-OF-POSITION MAP , from which new sources were noted. (first pass).

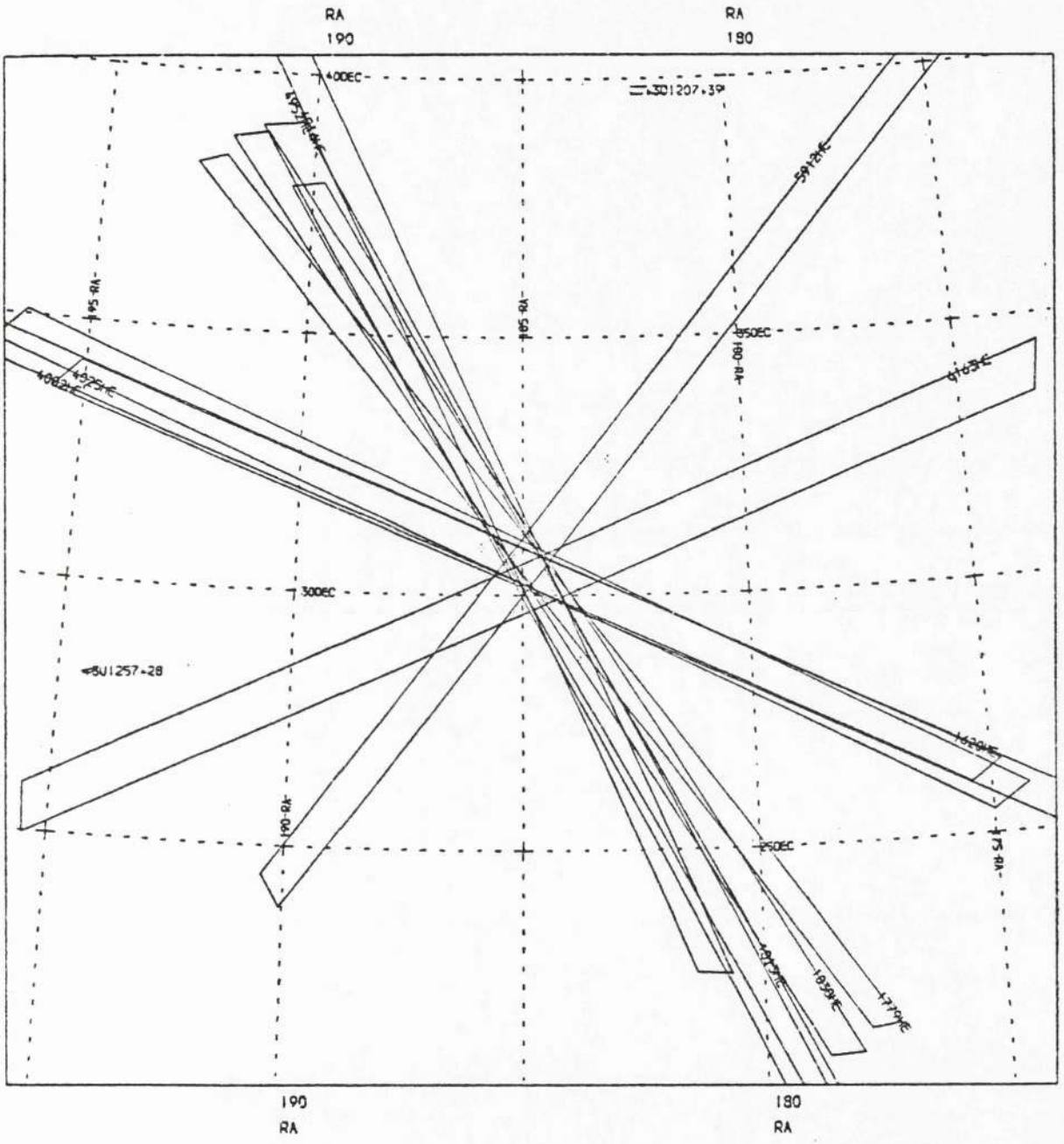

fig 2-9 THE BUNDLE OF LOP'S FOR A NEW SOURCE (number 3; later 2A1219+305).

densities for these sources. These flux densities are also stored on this second computer file.

(3) Taking the file created by (2) all the peaks can be located in celestial co-ordinates where they form collimator shaped lines (called "Lines-of-Position", LOP's). The width of a given LOP reflects the uncertainty with which the peak in the data histogram can be positioned on the sky. This is a function of the signal-to-noise ratio of the peak and of the errors in the solution of the spacecraft attitude. For a 5σ peak the 1 sigma full width of the line would be $0^{\circ}.44$. All these LOP's can be plotted on maps covering the whole sky (2-8). Wherever an x-ray source is located there should appear a bundle of intersecting LOP's (fig. 2-9). The map can also show the positions of all catalogued x-ray sources. This makes clear whether a catalogued source is seen by the Sky Survey or not and whether, if observed, its positional uncertainty (error box) is improved by the Sky Survey observations. It will also point up those Sky Survey sources which have not previously been seen at all.

(4) Each intersection of LOP's can then be examined to produce a Sky Survey error box. Each LOP must be checked for a good background fit and lack of confusion with other sources. The region of intersection of the LOP's can be made into an error box by converting each LOP into a positional probability distribution with a Gaussion shape perpendicular to the major axis of the LOP (fig. 2-10) and a standard deviation

$$= \sqrt{\frac{1}{3}\left(\frac{\mathrm{FWHM}}{\mathrm{S/N}}\right)^2 + \mathrm{A}^2}$$

(where FWHM is the full width at half maximum of the collimators, S/N is the signal-to-noise ratio of the peak and A is an angle, $0^{\circ}.07$ which allows for the error in the spacecraft attitude.) These distributions for each LOP can then be multiplied together in a matrix. The resulting joint probability distribution (fig. 2-11) can then be

contoured. One of the contours, traditionally that which gives a 90% chance of containing the source, is then chosen to be the error box (fig. 2-12). For simplicity this, approximately elliptical, contour is enclosed in the smallest fitting rectangle. This escribing rectangle is usually quoted as the error box.

(5) The mean count rate for each source could be calculated from the file of individual sighting intensities created in (2). The mean count rates were calculated from a carefully selected set of observations. All sightings at greater than 3σ were used plus some $< 3\sigma$ upper limits. This avoids a positive biasing of the flux densities (as encountered in the '4U' catalogue, Forman et al 1978, see Tananbaum et al, 1978 for an explanation). The upper limits were selected for each source by taking the largest count rate error on a $> 3\sigma$ sighting and rejecting all $< 3\sigma$ sightings with larger errors. In this way the criterion is matched to each source and so discards the least information. A χ^2 test is also performed to see whether a constant flux density is a reasonable fit to the data for the source.

This is the outline of the Sky Survey production process. In practice it is not possible to produce a final catalogue on a single pass through the data. The results from (4) will not be complete, but they can be fed back to make a larger catalogue to use for the matching of peaks with catalogued sources that takes place in (2). This second pass through the data allows a new set of maps of the sky to be plotted showing only the LOP's not used up in making sources produced from the first pass. Sources previously missed can then be picked up more easily. The second pass also allows true flux densities to be derived for the new sources. A third pass produces flux densities for sources picked up only on the second pass. The number of new sources goes down rapidly on each pass through the data base so that no fourth pass is necessary.

PLOTTING PROBABILITY CONTOURS : MAX PROB DENSITY = .882866E-01
SUM PROB ARRAY = .969005E+02

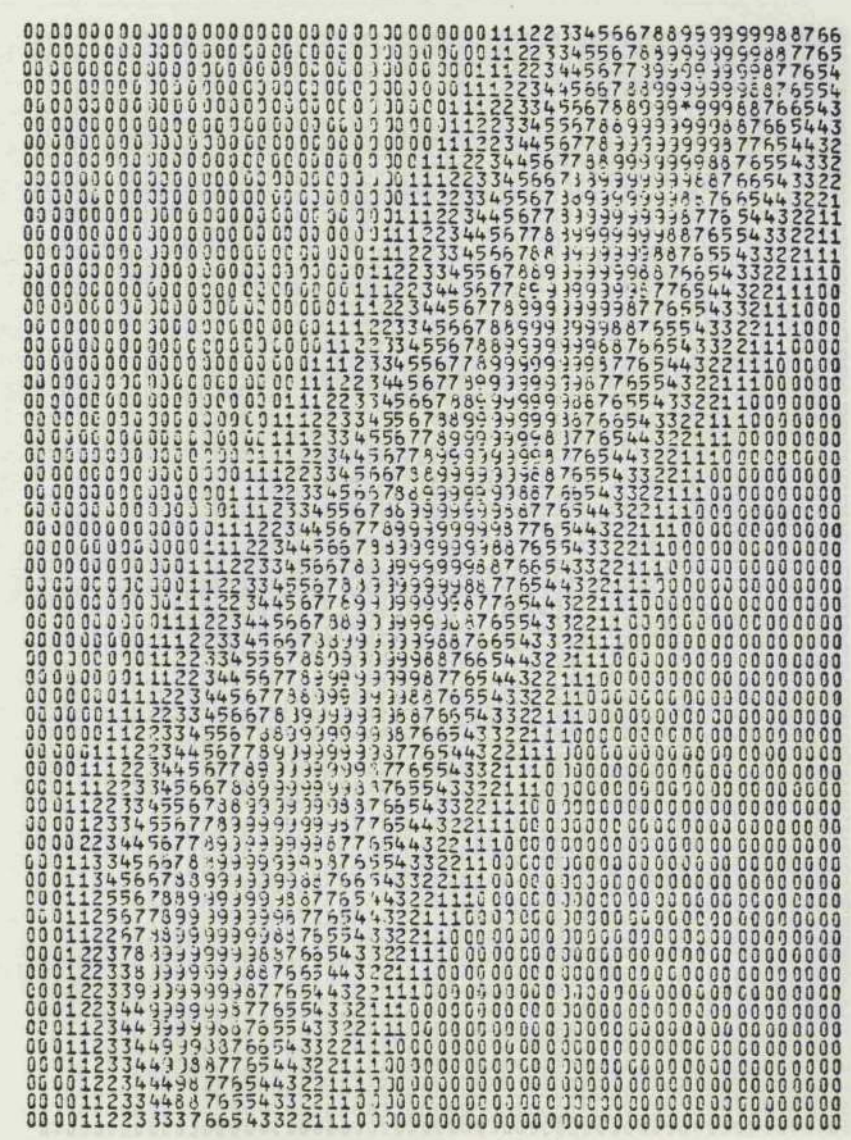

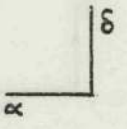

COORDS. OF MAX. PROB. DENSITY (DEG.,1950) RA = 179.6316
DEC = 36.1679

AREA INSIDE CONFIDENCE CONTOUR NO. 2 = .7275E+02 SQ.DEG.

IN GALACTIC COORDINATES : L2 = 170.5349
B2 = 76.1684

CORNERS OF RECTANGULAR ERROR BOX (DEG.)
R.A., DEC. (1950.0)

188.2146	175.4089	180.3327	192.8860
22.2249	35.7986	39.2857	25.2471

fig 2-10 A SINGLE LOP (for 2A1219+305) PRODUCES A ONE-DIMENSIONAL GAUSSIAN DISTRIBUTION OF POSITION PROBABILITY ON THE SKY.

PLOTTING PROBABILITY CONTOURS : MAX PROB DENSITY = .143003E-05
SUM PROB ARRAY = .319417E-03

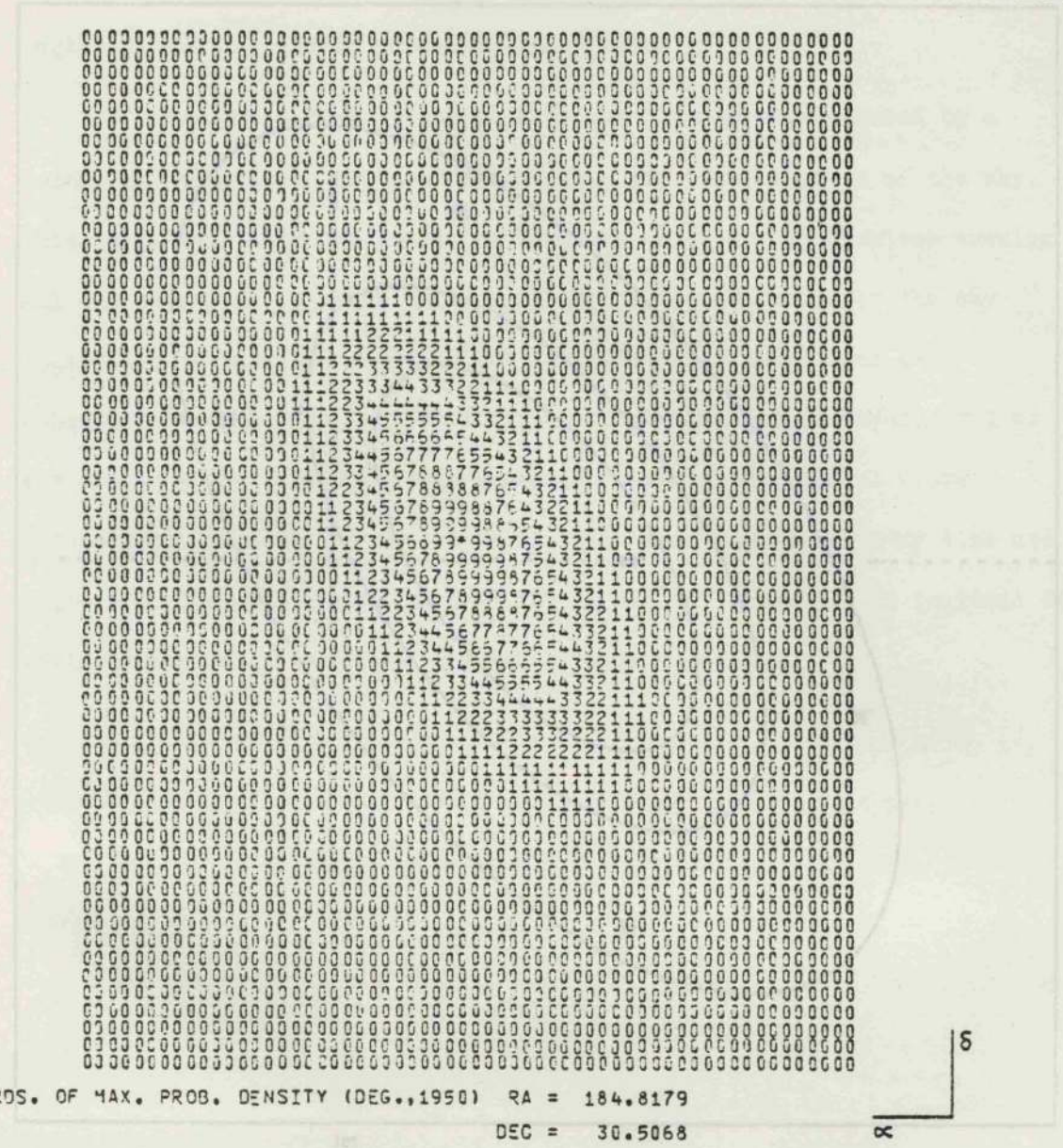

COORDS. OF MAX. PROB. DENSITY (DEG.,1950) RA = 184.8179
DEC = 30.5068

AREA INSIDE CONFIDENCE CONTOUR NO. 2 = .9469E-01 SQ.DEG.

IN GALACTIC COORDINATES : L2 = 185.6972
B2 = 82.7951

CORNERS OF RECTANGULAR ERROR BOX (DEG.)
R.A., DEC. (1950.0)

185.0955	184.7240	184.5094	184.8806
30.6096	30.2334	30.3903	30.7672

fig 2-11 THE ONE-DIMENSIONAL GAUSSIANS FROM ALL THE LOP'S FOR A SOURCE (2A1219+305) COMBINED TO GIVE A POSITIONAL PROBABILITY DISTRIBUTION.

2A1219+30 (N.S. 3) 6136 10 1 RUN

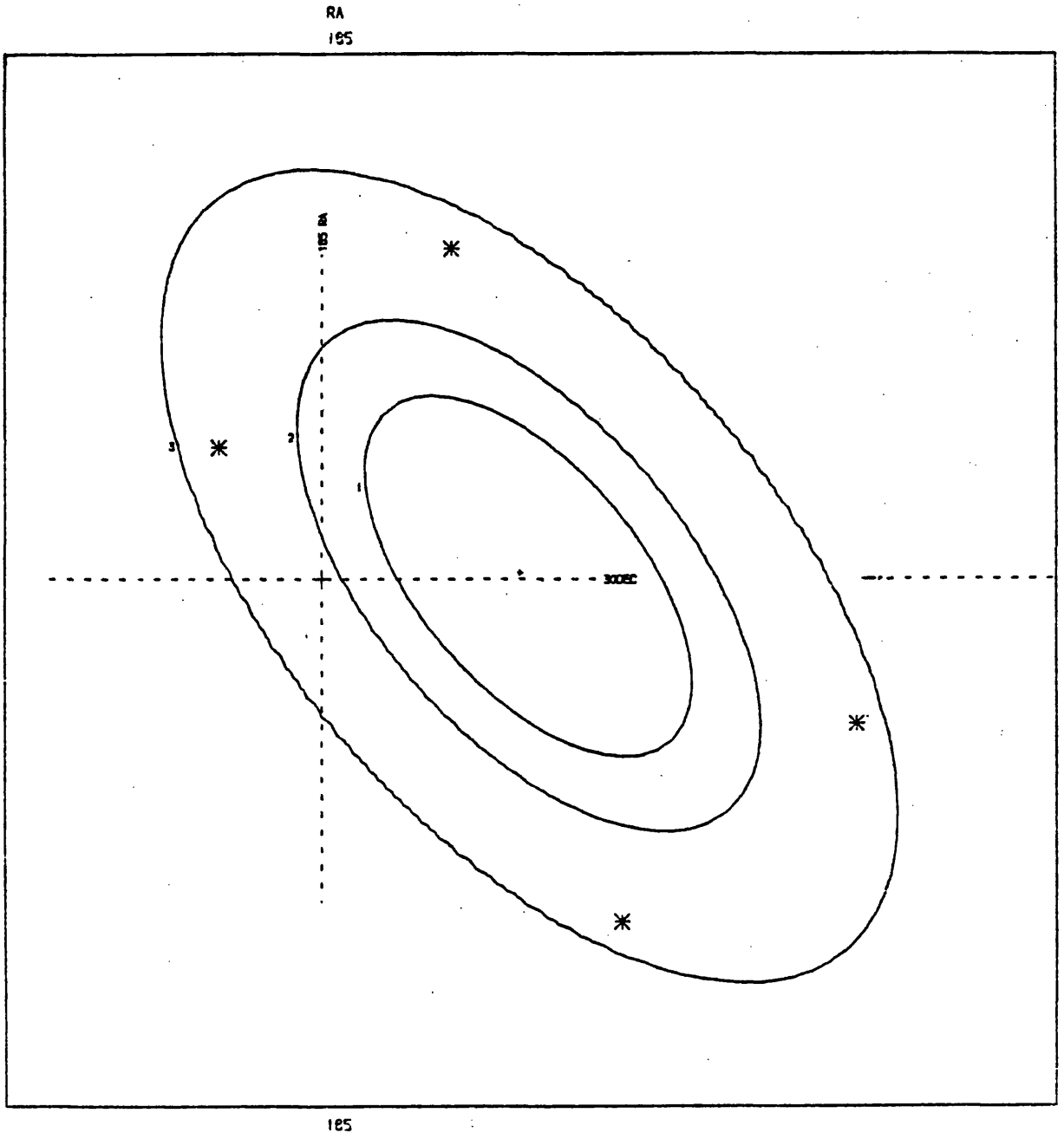

fig 2-12 THE POSITIONAL PROBABILITY DISTRIBUTION (for 2A1219+305) CONTOURED TO GIVE (in order of increasing area) the 1σ, 90%, and 2σ "error box" boudaries. The 90% contour is fitted by a escribing rectangle (whose corners are marked *). The numerical details of this error box are printed out in fig 2-11.

The author spent a large proportion of his time in helping to define this process, particularly in writing and operating the programs for parts (3) and (5) and in producing error boxes in part (4).

The LOP method of source detection can be supplemented by a technique which gives improved sensitivity for small regions of the sky. This is called the Point Summation Technique (PST). It involves summing all the data sets together which scan across a given point in the sky regardless of position angle. The counts at that point thus add coherently and provide increased exposure, at that point, beyond that of any single scan. Because this summation must be repeated at every independent point in the sky it is heavily demanding of computer time and could not, for this reason be used for an all-sky survey. It is ideal for making searches of candidate classes of x-ray emitters.

2-5 The 2A catalogue - a brief description

The results of this work at high galactic latitudes are embodied in the 2A catalogue (Cooke et al., 1978, Appendix A). The catalogue was compiled from the 10,000 orbits of data collected up until November 1976. It achieved 90% completeness of coverage over the high latitude sky down to 1.2 SSI counts s^{-1} ($\approx$ 3 UHURU counts s^{-1}) compared with UHURU's (3U) value of 52% down to 10 UHURU counts s^{-1} (fig. 2-13). The error box areas of the 2A catalogue are significantly smaller than those of the 3U catalogue (fig. 2-14). The lower limit on error box size ($\approx$ 0.01 sq.deg.) is imposed by the limitations of the satellite attitude sensing and control systems (Table 2-1).

Fig. 2-8 makes clear why the limit of greater than $\pm 10^{\circ}$ galactic latitude was imposed. Clearly the $10^{\circ}.6$ FWHM of the collimator produces a natural limitation in that the high density of sources in the glaactic plane produces a mass of LOP's out to $\approx \pm 10^{\circ}$ which present a very different analysis problem, being highly confused, from that at higher latitudes.

There are 98 LOP sources and 7 PST sources in the catalogue. When corrected for sky coverage they are fully consistent with an isotropic distribution in Euclidean space (Warwick and Pye, 1978 a). A fluctuations analysis of SSI background data (Warwick and Pye, 1978 b) shows that this distribution is followed down to $\approx$0.05 UHURU units. Subsequent work with the PST (chapters 4 and 6 ; Ricketts, 1978) has added to the number of sources, as have the new data collected since November, 1976.

The smaller error boxes of the 2A survey compared with the 3U survey have enabled much greater confidence in the identifications which could be proposed (e.g. Abell 478, Elvis et al. 1975; Abell 754, Pye et al. 1976). In the case of Abell clusters this allows many relationships which were only tentative to be made secure (Bahcall, 1977a,b, McHardy, 1978a)

and has also extended the class to include the 'cD groups' (Morgan, Kayser and White, 1975, McHardy 1978b).

A field in which the 2A results have had important consequences is that of Seyfert galaxies. The following chapters report this work.

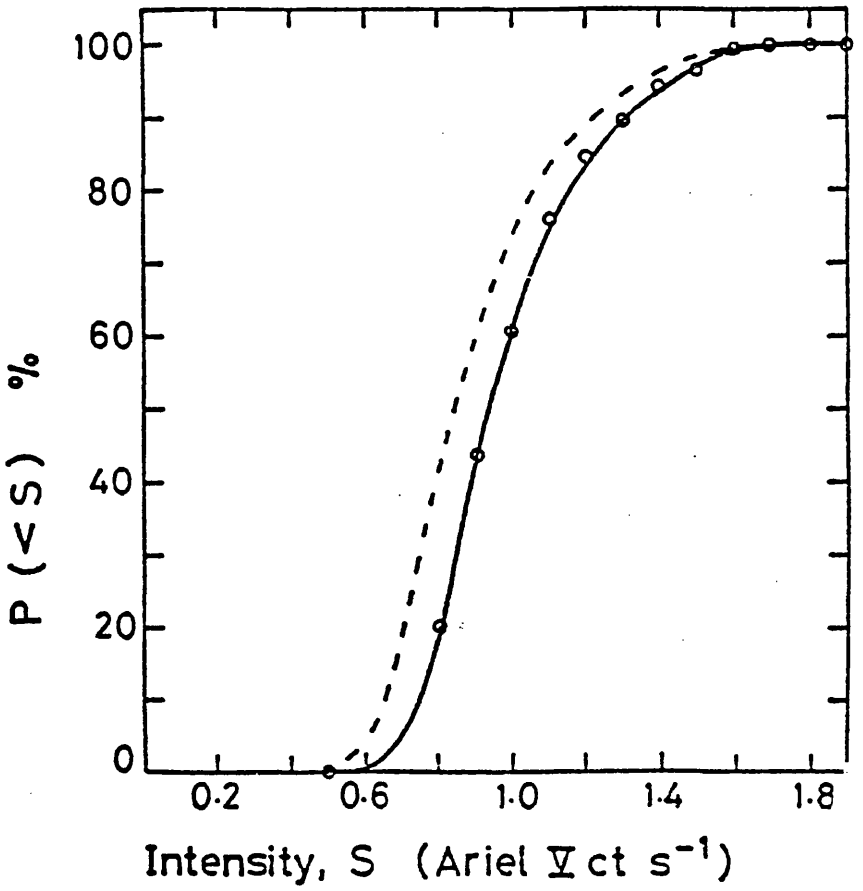

fig 2-13 SKY COVERAGE OF THE 2A CATALOGUE. Percentage of the high latitude sky ($|b|>10^{\circ}$) covered to a minimum detectable (3σ) intensity < S Ariel(SSI) ct s^{-1} for source discovery, according to the criteria of (a) the minimum detectable intensity on the 3rd most sensitive data set (solid line), and (b) the minimum detectable intensity for which the probable number of sightings, taking account of all useful data sets, is just 3 (dashed line).

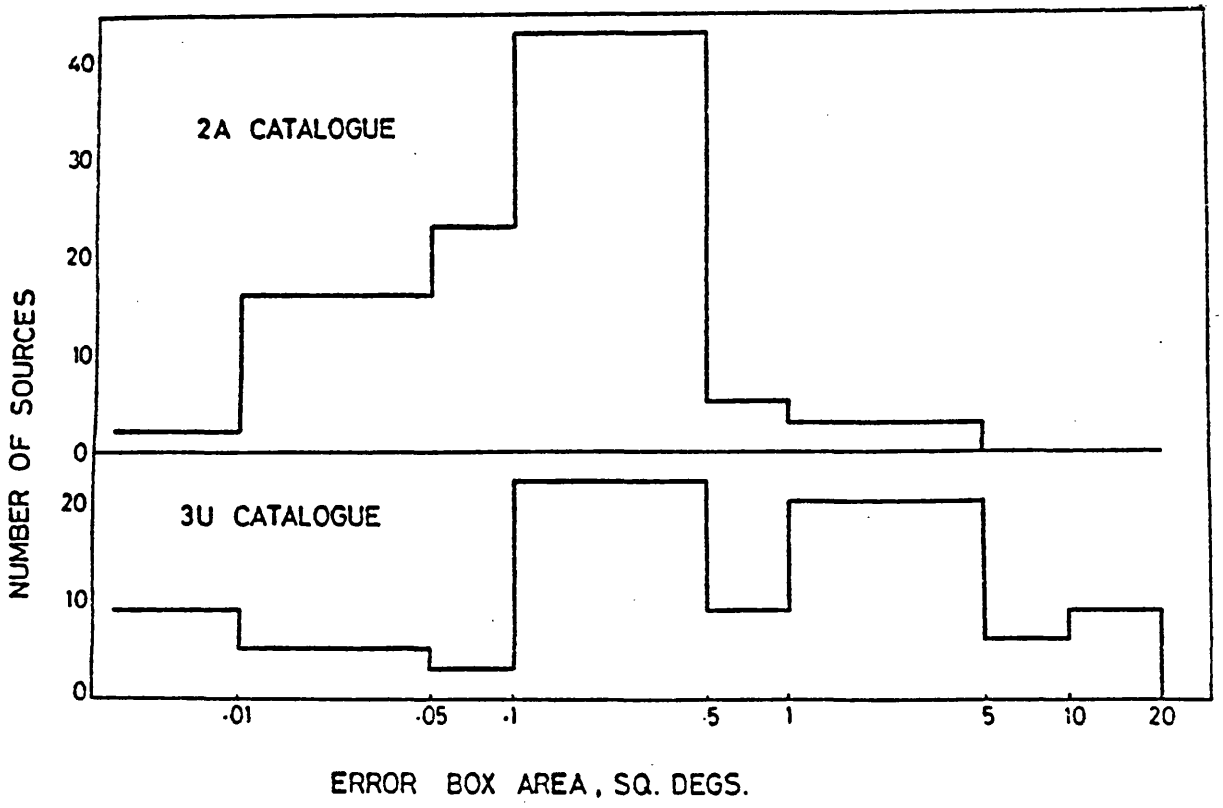

fig 2-14 FREQUENCY DISTRIBUTION OF ERROR BOX AREAS FOR THE 2A CATALOGUE (non-PST only) and the 3U catalogue.

chapter 3. DETECTION OF SEYFERT GALAXIES AS A CLASS OF X - RAY SOURCE

Introduction

The UHURU satellite and earlier surveys detected x-ray emission from a small number of active galaxies* but it has remained unclear whether these objects are typical or exceptional members of their class. (Kellogg et al., 1974, summarise these data). The early work has shown that a clarification of the x-ray properties of active galaxies is important for an understanding of the energetics and radiation processes in active galactic nuclei since, where x-ray emission has been seen, it accounts for an appreciable fraction of the total luminosity.

Also it has been suggested that these objects, in particular Seyfert galaxies, may contribute significantly to the isotropic background radiation (Schwartz and Gursky, 1974). An improved determination of this fraction is thus essential to test whether a genuinely diffuse component does, in fact, exist.

Of these active galaxies only NGC 4151 is a true Seyfert galaxy. NGC 1275 is neither clearly an x-ray source (it lies, unresolved, within the extended Perseus cluster x-ray source) nor a Seyfert galaxy. A survey of 5 Seyfert galaxies using a version of the "Point Summation Technique" (PST) on UHURU data (Ulmer and Murray, 1976) concluded that "In summary, neither BL Lac type objects nor Seyfert galaxies, on the average, are strong x-ray sources." In fact none of the Seyferts looked at in that study have been detected as LOP sources in the 2A survey.

The advent of the 2A survey with its substantial improvement in both completeness and sensitivity has radically altered this picture. Some 13 Seyferts lie in or near the 90% confidence contours of 2A source positions. Some of these were not previously known to be Seyfert galaxies

* viz. NGC 4151, Ives et al., 1976; NGC 1275, Fabian et al., 1974; 3C273 and Cen A, Giacconi et al., 1974.

and were discovered as a result of a 2A x-ray source being located in the vicinity. A joint programme of x-ray source identifications between Leicester and a group of optical astronomers centered around the Anglo-Australian Telescope (AAT) but based also at Sussex University and the Royal Greenwich Observatory, has greatly supported this area of research. Clearly, even with SSI sized error boxes, one hesitates to claim an identification, on positional grounds alone, of an individual x-ray source with an object belonging to a class not thought, at first, to be strong x-ray emitters. Evidence from optical spectra and x-ray variability can be used to support the claim. Two such examples follow, one previously known as a Seyfert galaxy and one newly discovered, for which the supporting evidence is strong.

3-1 2A1136-373 : NGC 3783

Among the new high latitude x-ray sources discovered with the SSI is 2A1136-373 which has an error box that includes the Seyfert galaxy NGC 3783. Nine observations of this region of the sky were made between April 1975 and June 1976 and on all but two occasions a $>3\sigma$ detection of an x-ray source was obtained. The lines of position from each detection have been combined to produce a 90% confidence contour which is shown superimposed on a UK Schmidt Telescope plate in fig. 3-1.

The Seyfert NGC 3783 lies well within the contour which includes no other unusual extragalactic objects, hot stars or variable stars (Kukarkin et al., 1969). The count rate of the x-ray source, 1.1 ± 0.1 Ariel (SSI) ct s^{-1}, is equivalent to an absolute luminosity of 1.9×10^{43} erg s^{-1} using the redshift of 2740 km s^{-1} given by Khachikian and Weedman (1974)*. This is 2.7 times the 2A luminosity (and ≈6 times the 3U luminosity, see chapter 6-2) of NGC 4151. The observations give little indication of variability. The reduced χ^2 for all of the 2A observations is 1.83 for 9 degrees of freedom. There is thus a 5% chance that a steady source would give such data points given our observing times.

Enlargements of a 3.9m AAT blue plate shows NGC 3783 to be a barred spiral with rather open, low surface brightness spiral arms attached to a prominent inner ring (fig. 3-2).

Spectrophotometric data have been obtained on the nucleus of this object using the image-dissector scanner on the AAT.

NGC 3783 is a bright (m_v(total)≈13.0) southern galaxy classified by Khachikian and Weedman (1974) as a class 1 Seyfert (see 1-3). The spectrum has previously been studied by Martin (1974) and Osmer et al. (1974) who found it to have a very blue continuum with broad Balmer lines and a narrow, high excitation forbidden line spectrum.

---

* Hubble's constant, H_o will be taken as 50 km s^{-1} Mpc^{-1} throughout this thesis

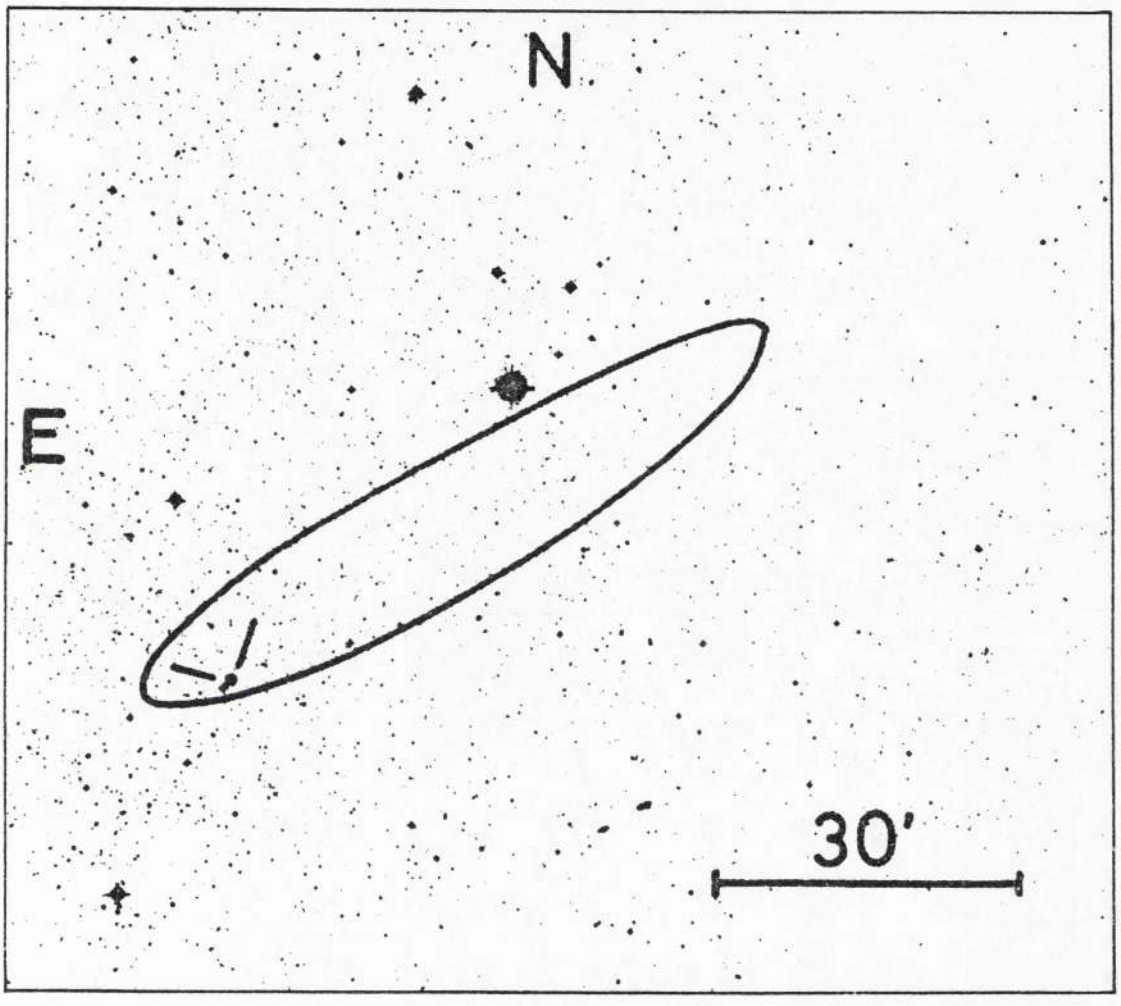

fig 3-1 90% ISOPROBABILITY CONTOUR FOR 2A1136-373, superimposed on a UK Schmidt Telescope plate. NGC3783 is indicated.

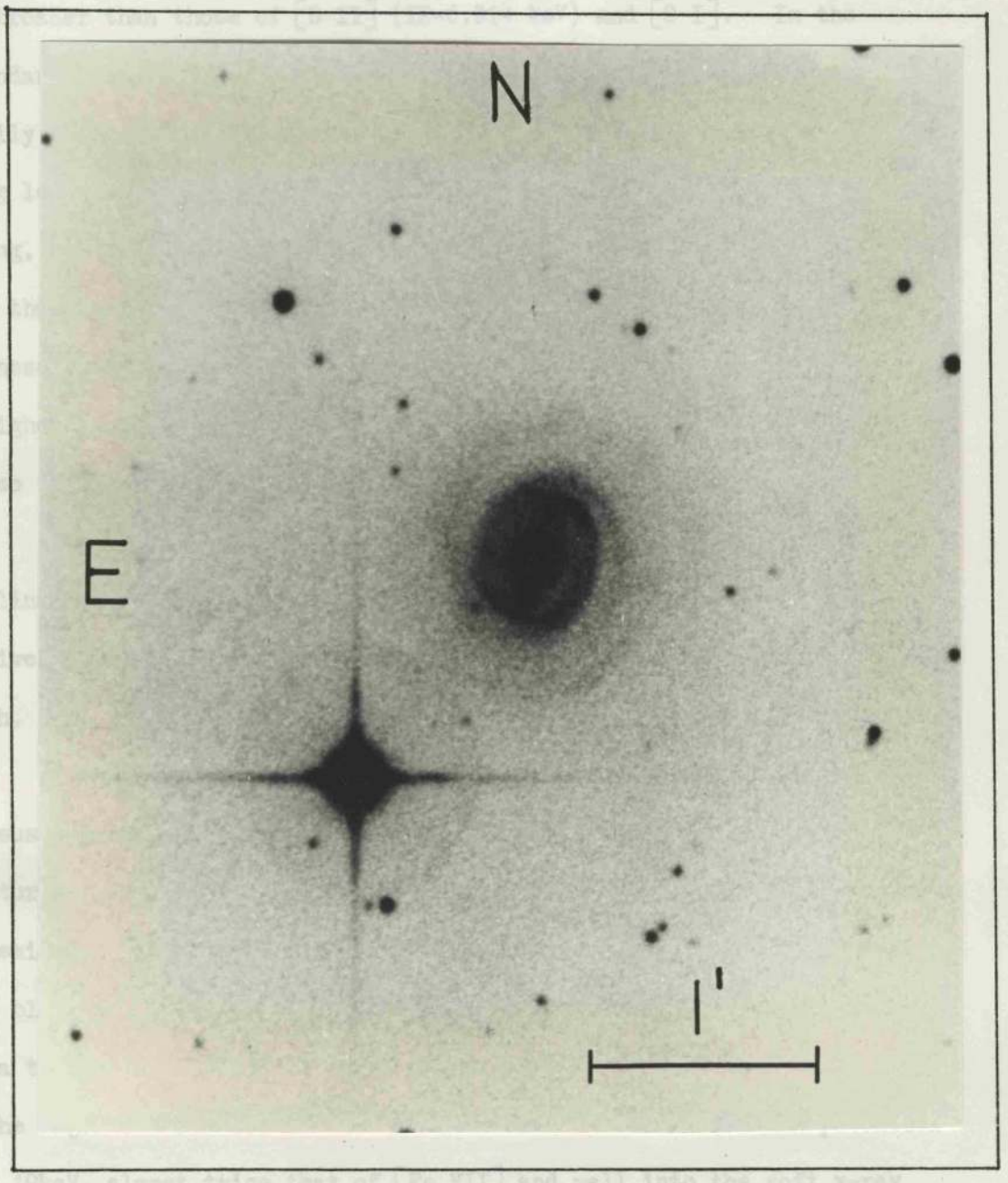

fig 3-2 REPRODUCTION FROM A BLUE AAT PLATE OF NGC3783.

The new data suggest that the forbidden lines from the high ionization species i.e. [Fe VII] (ionization potential, IP,=0.10 keV) are broader than those of [S II] (IP=0.014 keV) and [O I]. In the 'standard model' for Seyfert nuclei (see chapter 1-4) this effect can be readily interpreted. The clouds nearer to the central ionizing source, being lower in the potential well of the massive central body will be moving, on average, faster than those further out. The lines they emit will thus be Doppler broadened more than those of less central clouds. In these inner regions the lower ionization species will be depopulated to higher ionization species (see e.g. Tarter and Salpeter, 1969 a,b) and so their lines will not be seen.

Accepting this photoionization model for the forbidden lines the line requiring the greatest ionization potential should be looked for to give a lower limit to the energies to which the ionizing continuum must reach.

Fig. 3-3 shows sections of two image dissector scans of the nucleus around 6300 A : they were both made through a 2 x 4.5 arc sec aperture with spectral resolutions (FWHM) of 4 Å (upper) and 8 Å (lower). The emission feature at an observed wavelength of 6428 Å is identified as a blend of [O I]λ6363 and [Fe X]λ6374. The [O I] doublet λλ6300,6363 has a theoretical intensity ratio of 3:1 indicating that the [Fe X] line is the major contributor to the blend. This has an ionisation potential of 0.19keV, almost twice that of [Fe VII] and well into the soft x-ray region.

[Fe XI] (IP=0.26 keV) λ3990 may also be weakly present, however [Fe XIV] (IP=0.36 keV) λ5303 does not appear, the feature near to this wavelength being attributable to [Ca V] (IP=0.067 keV) λ5309. This lack of [Fe XIV] emission does not imply the absence of ionising continuum above 0.36 keV since this could easily be explained as an accident of the geometry of the 'clouds' in the nucleus.

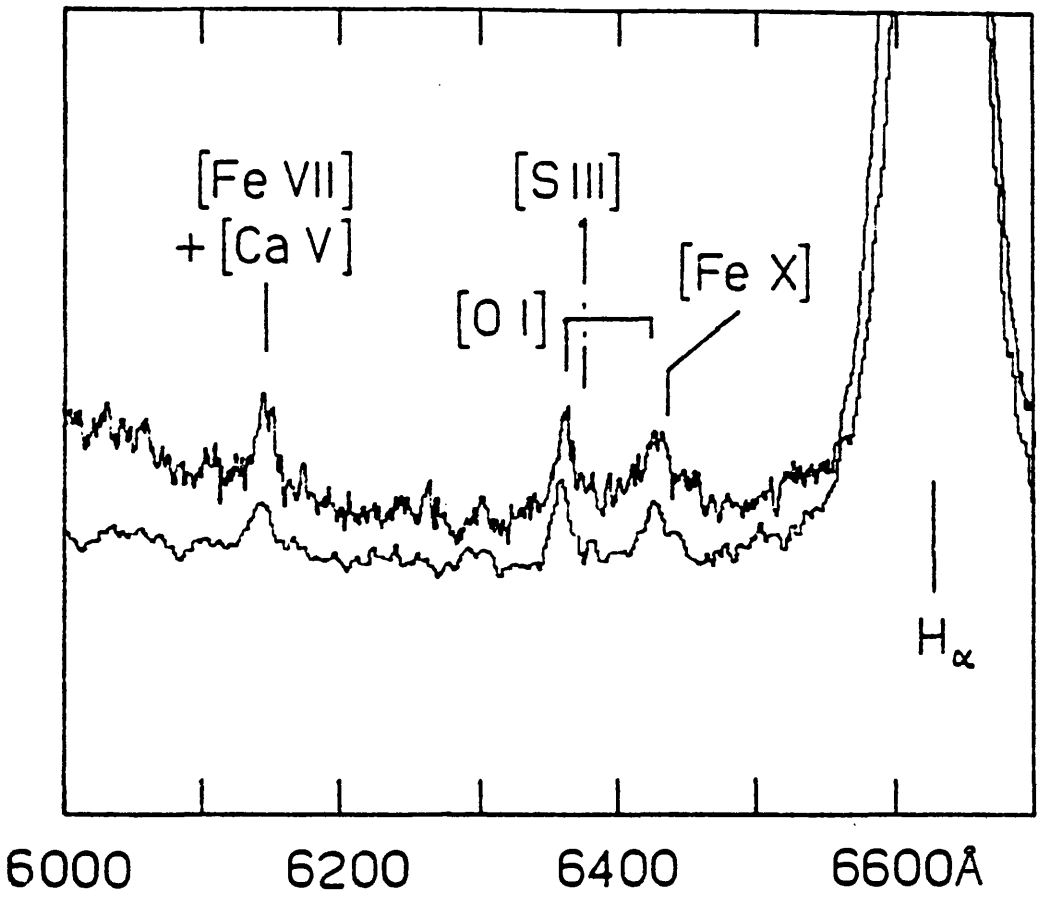

fig 3-3 SCANS OF THE NUCLEUS OF NGC3783 MADE WITH THE IMAGE-DISSECTOR SCANNER ON THE AAT. These are plotted on the observed wavelength scale. The spectral resolutions are 4 Å (upper) and 8 Å (lower). The two scans have the same zero level but otherwise the intensityscales are the arbitrary.

Another suggestive feature in the spectra is the emission near λλ 4640-50, on the wing of the broad He II λ4685 line. This is seen in several galactic x-ray sources (McClintock, Canizares and Tarter, 1975) and is thought to be N III which arises from Bowen fluorescence. This process involves O III which in turn is excited by the Lyman α line of He II, both of these being the result of the x-ray radiation field. Unfortunately the presence of the O III Bowen lines cannot be confirmed by the present data which does not extend shortward of 3800 Å.

Very broad (≈ 4500 km s^{-1}) He I λ5876 emission is seen with evidence for blue-shifted Na I D-line absorption on the blue wing. We do not detect absorption corresponding to the Mg b-lines or the G-band, but the calcium H and K lines are present in absorption at the emission line red-shift of 0.0086 ± 0.003 (the present data).

Physical conditions in the nucleus of the galaxy can be estimated. From the red [S II] doublet ratio, an electron density $n_e \approx 10^4$ cm^{-3} is found for the forbidden line region. Using this value of n_e, the [O III] line ratio λλ5006,4959 : λ4363 gives an electron temperature $T_e \approx 2 \times 10^4$ K. These are typical values for Seyfert nuclei (see chapter 1-4).

The [Fe X] line is also seen in 3C390.3 (Ward, Fosbury and Penston, unpublished), NGC 4151 (Oke and Sargent, 1968) and Cyg A (Minkowski and Wilson, 1956, Osterbrock and Miller, 1975), which show related emission line phenomena to NGC 3783 and are all x-ray sources. Thus the [Fe X] line, together with the possible Bowen fluorescence gives a fair degree of confidence in the identification.

This identification of the new x-ray source with NGC 3783 would be further strengthened if correlated variability were found during simultaneous x-ray and optical UBV photometry. Spectrophotometric data in the ultraviolet region is needed to see if the predicted Bowen [O III]

lines are present. If later x-ray data show a low energy cut-off above that expected from the path length in our galaxy, this will give an indication of the amount of self-absorbing gas intrinsic to the Seyfert as it does for NGC 4151 (Ives, Sanford and Penston, 1975).

Although the presence of [Fe X] in NGC 3783 suggests a similarity with NGC 4151 and 3C 390.3 (probably both variable in x-rays, Charles et al., 1975, Ives et al., 1975, and chapter 6) it is not clear which other parameters of Seyfert galaxies are related to x-ray emission from this work alone. The great variety of the optical classifications of the active galaxy x-ray sources found up to this point makes any detailed astrophysical considerations highly speculative. Further work with the SSI has enabled some advances to be made in this direction, as will be seen in chapter 3-3.

3-2 2A0551+466 : MCG 8-11-11

Of the many new x-ray sources produced by the SSI at high galactic latitude which have error boxes small enough to make plausible identifications, by no means all contain catalogued candidate objects. During a systematic search for likely identifications in the corresponding optical fields of these "empty" boxes, a galaxy with an intense, compact nucleus was noticed in the error box of the source 2A0551+466. Fig. 3-4 shows the error box superimposed on the Palomar Sky Survey (POSS) print. This 14^m galaxy has been listed in the Morphological Catalogue of Galaxies (Verontsov-Velyaminov and Krasnogorskaja, 1962) as MCG 8-11-11, in the Uppsala General Catalogue of Galaxies (Nilson, 1973) as UGC 3374 and in the Catalogue of Galaxies and Clusters of Galaxies (Zwicky and Herzog, 1966). Vorontsov-Velyaminov and Krasnogorskaja describe it as a face-on spiral of dimension 1.7 x 1.1 arc min., Nilson classifies it as SB, possessing a bright stellar nuclear region in a diffuse bar and of total extent 2.8 x 2.5 arc min. On the POSS faint filaments or spiral structure may be seen extending from its western edge. MCG 8-11-11 is by far the brightest extragalactic object within the error box of 2A0551+466, whose area is 0.093 sq. deg.

Several spectra of the nucleus of MCG 8-11-11 were taken on the 28th December 1976 with the Isaac Newton Telescope (2.5m) at the Royal Greenwich Observatory, Herstmonceux, England. The detector was an EMI tube attached to the Unit Spectrograph. Fig. 3-5 shows a tracing obtained with a Joyce-Loebel microdensitometer of one of these spectra, which has a dispersion of 210 Å mm^{-1}. It is clear from fig. 3-5 that MCG 8-11-11 is a type 1 Seyfert galaxy (i.e. Balmer lines much broader than the forbidden lines, see chapter 1-3) with hydrogen line widths $\approx$ 8000 km s^{-1} (Full Width Zero Intensity, FWZI). A higher dispersion (40 Å mm^{-1}) spectrum of the Hα region shows the possible presence of a component of H_α blue-shifted by 1100 km s^{-1} with respect to the forbidden line redshift $z = 0.0205 \pm 0.0004$.

Many Seyfert galaxies which are known to be sources of powerful x-ray emission, e.g. NGC 4151, NGC 3783 and probably 3C390.3, show lines

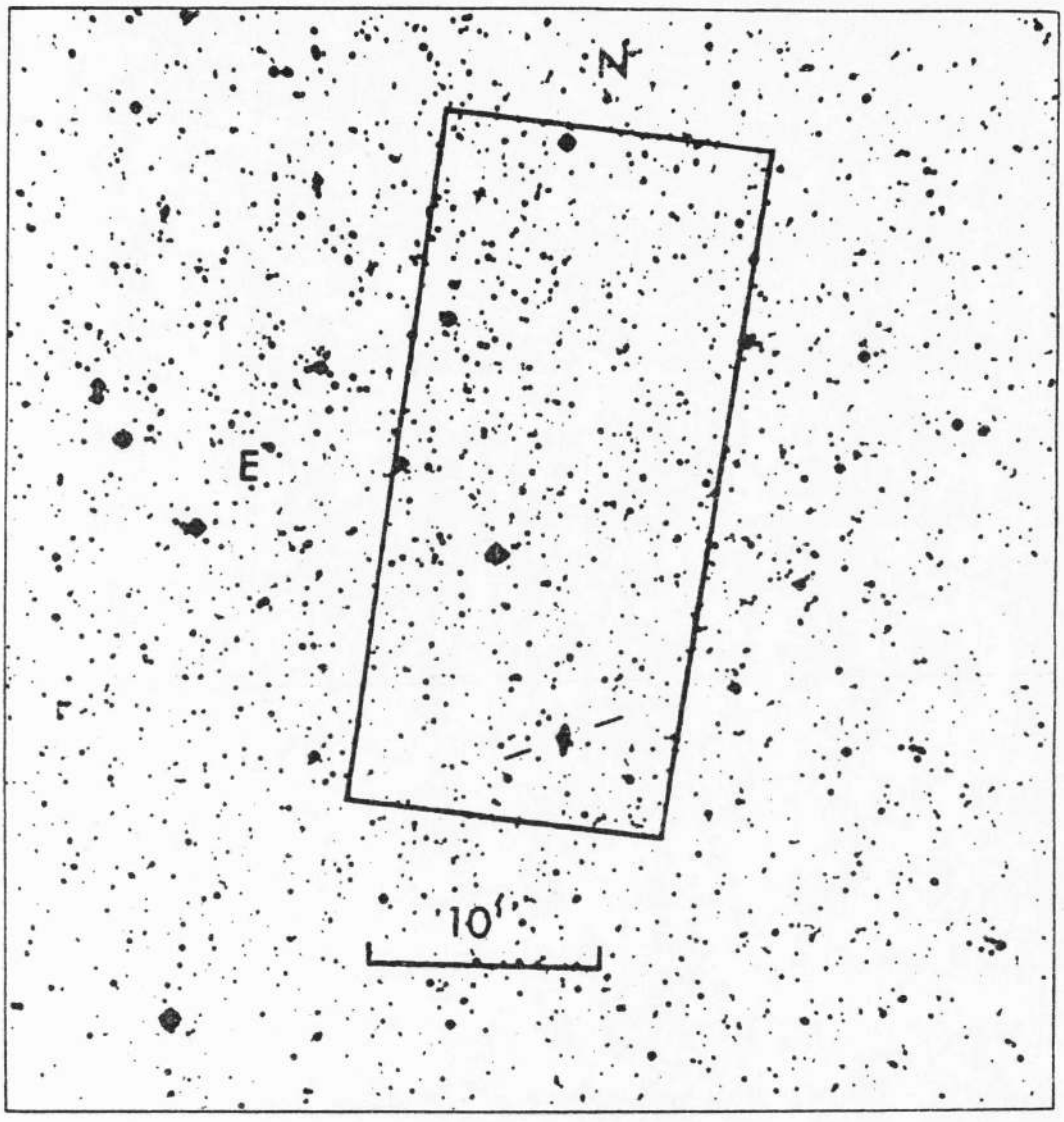

fig 3-4 SSI ERROR BOX FOR 2A0551+466 SUPERIMPOSED ON THE RED PRINT OF THE PALOMAR SKY SURVEY. THE SEYFERT GALAXY MCG 8-11-11 IS INDICATED.

from highly ionized species such as [Ne V] and [Fe VII]. In the cases of 3C390.3, NGC 3783 and possibly NGC 4151, [Fe X] is also seen. It may be that the presence of these lines, particularly [Fe X], is related to the x-ray emission. Our spectra of MCG 8-11-11 show lines of [Ne V] and [Fe VII] but higher signal to noise data are required to search for the much weaker [Fe X] line. Even so [Ne V] requires 0.097 keV photons to produce it so there is good evidence for a soft x-ray continuum source, as explained in the previous section.

Comparison with a spectrum of the Seyfert galaxy NGC 4151, obtained on the same night, shows MCG 8-11-11 to have a redder energy distribution, perhaps indicative of greater absorption. The object is of low galactic latitude ($b = 10^{\circ}.51$) so we expect an absorption due to our own galaxy of (Eggen, 1976)

$$A_V = 0.12 \text{ (cosec } b - 1) \text{ mag.}$$
$$= 0.54$$

In Table 3-1, which lists some of the salient properties of MCG 8-11-11 M_V, but not m_V, has been corrected for this absorption.

The existence of non-thermal activity in MCG 8-11-11 is also seen in the presence of a compact radio source of angular extent less than 3 arc secs, and coincident with the optical nucleus to better than 1 arc sec (J.J. Condon and L.L. Dressel, private communication). Condon and Dressel find flux densities of 141 and 53 mJy at 2695 and 8085 MHz respectively. The corresponding radio power, $P_{2695\text{MHz}} = 1.9 \times 10^{22}$ WHz^{-1} sr^{-1}, is higher than average for a type 1 Seyfert galaxy (de Bruyn and Wilson, 1976).

The proposed identification is supported by the fact that 2A0551+466 is one of the few ($\approx$10%) of the 2A catalogue sources which show evidence of variability, with x-ray flux density ranging from 0.0 ± 0.2 to 1.6 ± 0.2 Ariel (SSI) ct s^{-1} (errors are 1σ). The light

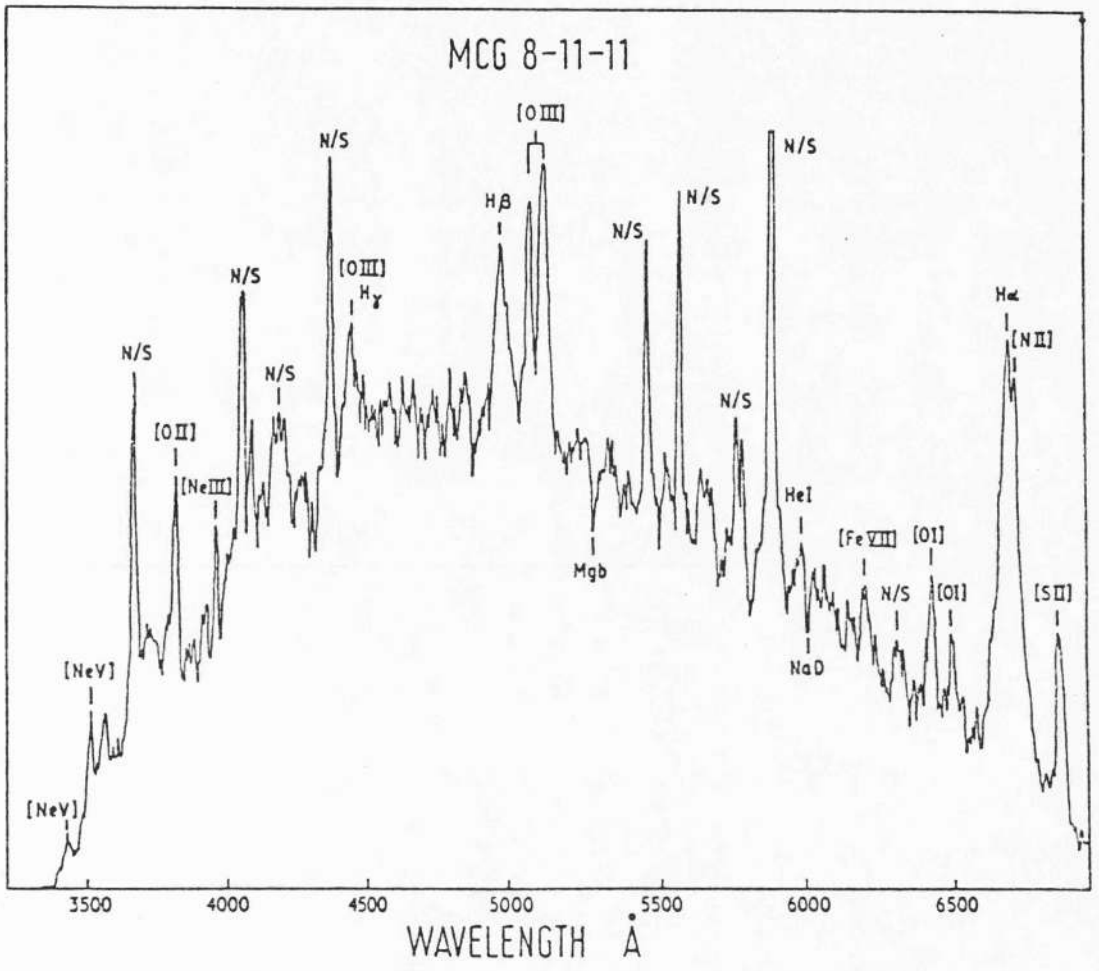

fig 3-5 SPECTRUM OF THE NUCLEUS OF MCG 8-11-11, taken with the Isaac Newton Telescope at an original dispersion of 210A mm^{-1}. The line identifications are indicated and the wavelength scale is as observed. Lines from the night sky are marked N/S. Plate saturation occurs for high intensity features (e.g. 4959,5007 OIII).

Table 3-1 Some properties of MCG 8-11-11

Position [a] (1950.0) α	$05^h\ 51^m\ 09^s.9$
δ	$+46^\circ\ 25'\ 55''$
Redshift, z	0.0205
m_v [b] (nucleus)	14.5
M_v (nucleus)	-21.5
$S_{2695\ MHz}$ [c] (mJy)	141
$P_{2695\ MHz}$ ($WHz^{-1}Ster^{-1}$)	1.9×10^{22}
Flux in 2 - 18 KeV [d] band, SSI counts s^{-1}	0.0 ± 0.2 to 1.6 ± 0.2
$L_{2-10\ KeV}$ (erg s^{-1})	5.2×10^{43} (3σ limit) to 1.4×10^{44}

a. Dressel and Condon (1976).

b. Estimated from our data by comparison with a spectrum of the nucleus of NGC4151 obtained on the same night and exposed to the same plate density at $\lambda 5500$ Å. Anderson's (1970) spectrophotometric observations of NGC4151, taken through a circular aperture of diameter 8 arc secs, were then used in deriving m_v for MCG 8-11-11.

c. Condon and Dressel (private communication). 1 mJy = 10^{-29} Wm^{-2} Hz^{-1} .

d. 1 SSI count s^{-1} = 5.1×10^{-11} erg cm^{-2} s^{-1}.

curve is shown in fig. 3-6. The χ^2 probability that the variations observed in our data are due merely to statistical fluctuations on a constant source intensity is 7.8×10^{-7}. To make this χ^2 probability consistent with a steady source at the 1% level (the 2A catalogue criterion) we would need to ignore four out of five $>3\sigma$ detections. Alternatively we must disregard the three most stringent upper limits. No clear pattern to the temporal behaviour of the source emerges from the data. The timescale for variability, however, must be at least as short as 32 days. This implies an upper limit to the size of the emitting region of 2.8×10^{-2} pc., comparable to the typical dimension calculated for the high density region in type 1 Seyfert galaxies from which the broad wings on the Balmer lines are emitted (see chapter 1-4).

Compared with NGC 3783 (previous section, 3-1) then, there is in this case not such good evidence for an x-ray continuum from optical emission lines although there is some support for this possibility. The optical spectrum is not good enough to reveal the very high exitation lines nor to search for the Bowen fluorescence lines. The identification is helped by two other facts. The variability in x-rays is on a timescale consistent with the sizes known to exist in Seyfert nuclei, which gives some clue as to the origin of the x-ray emission. Also the chance of finding a $14^m.0$ Seyfert galaxy in such a small area of the sky by chance must be of the order 10^{-3}. Such <u>post facto</u> calculations are always suspect, nevertheless, overall, it is highly plausible that MCG 8-11-11 is the identification of 2A0551+466. If so it becomes the first Seyfert galaxy to be discovered by means of its x-ray emission.

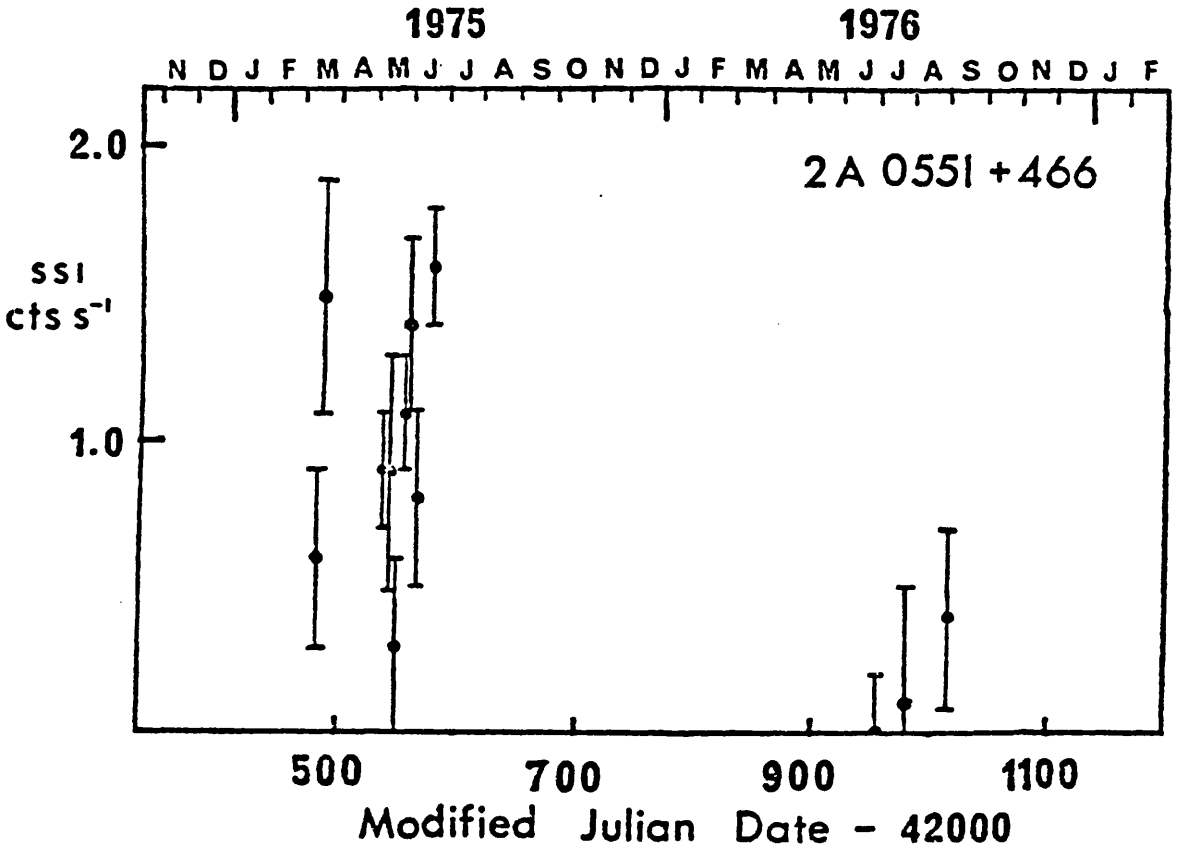

fig 3-6 SSI X-RAY LIGHT CURVE FOR 2A0551 +466.

3-3 Establishing Seyferts as a Class of x-ray emitter.

Special arguments such as those of the two previous sections could be continued for other individual cases as they occur. However, being particular they cannot establish, once and for all, that Seyfert galaxies are normally x-ray sources. Some, more systematic, overall approach is needed.

NGC 3783 and MCG 8-11-11 were identified before the complete 2A catalogue (Cooke et al., 1978, Appendix A) was ready. The completion of this catalogue allowed the statistical comparison of a list of Seyfert galaxies, independently compiled by Weedman (1977), with the 2A source list. The following arguments show that the great majority of the proposed identifications with Seyfert galaxies represent real identifications:

(1) There are 88 Seyfert galaxies in the list of Weedman (1977) while the total area of LOP error boxes in the 2A catalogue is 17.4 sq. deg. If there were no real relation between Seyfert galaxies and Ariel V x-ray sources, we would expect a total of

$$\frac{(\text{total area of LOP boxes})}{(\text{area of sky with } |b|>10^\circ)} \times 88 = 0.04$$

of the Seyfert galaxies listed by Weedman to lie inside the LOP error boxes by chance. The number actually observed is 7. Another two galaxies, NGC 4151 and NGC 5548, lie just outside the 90% confidence error boxes, but inside the 95% ones. A further two (MCG 8-11-11, ESO 141-G55) lie inside 90% confidence error boxes, but are not listed by Weedman. Clearly, chance coincidence cannot account for the number of detections.

A similar analysis may be applied to the PST sources. The PST has been applied to over 100 random points in the sky, detecting only one peak at 3σ. In contrast, application of the technique

to the 88 Seyferts listed by Weedman yielded 10 detections at $>5\sigma$, two of which were not detected as LOP sources. All, or almost all, of these detections must, therefore, represent a real association between the x-ray source and the Seyfert galaxy.

(2) A related method of discussing the statistics is to perform a covariance analysis. Fig. 3-7 is a histogram of ρ, the number density of Seyferts from the Weedman list lying in annuli of thickness 10 arc min and centred on 2A catalogue x-ray sources, as a function of θ, the angular radius of the annulus (solid line). As a comparison, the corresponding histogram for a set of random points (formed by adding 15° galactic longtitude to each 2A catalogue x-ray source position) is also shown (dashed line). Seyferts established only by the PST and those discovered as a result of optical searches of 2A catalogue x-ray source boxes are not included in this analysis. The density of chance coincidences, as defined by the plot at 1° - 2°, is some 100 times smaller than the value at the peak. The 'randomised' histogram shows no peak whatsoever. Although the number of sources involved is small, this is a highly significant excess.

(3) As discussed more fully in chapter 5-3, the galaxies detected as x-ray emitters tend to be the brightest optically of the Seyferts (see fig. 3-8). Clearly if the associations were due to chance the galaxies would be randomly scattered amongst all magnitudes. This result implies a correlation between optical and x-ray properties of the galaxies.

(4) The fact that two Seyfert galaxies (MCG 8-11-11, previous section, 3-2, and ESO 141-G55, next section, 3-4) have been discovered in error boxes of previously unidentified 2A sources strengthens our

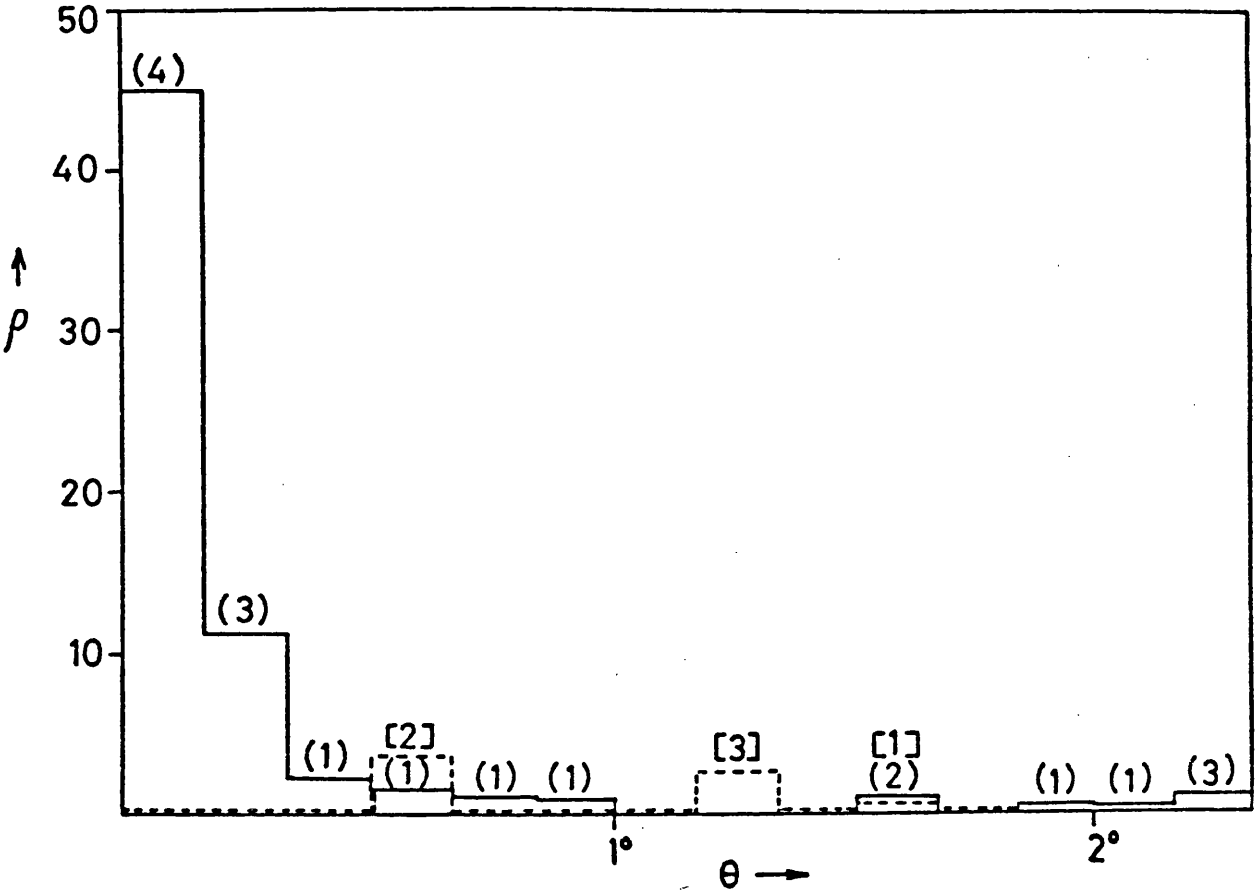

fig 3-7 HISTOGRAMS OF ρ, THE NUMBER DENSITY OF SEYFERTS FROM THE WEEDMAN LIST LYING IN ANNULI OF THICKNESS 10 ARC MIN AND CENTRED ON '2A' CATALOGUE SOURCES, AS A FUNCTION OF θ, THE ANGULAR RADIUS OF THE ANNULUS (solid line). The dashed line is the corresponding histogram for a set of random points, formed by adding 15° galactic longtitude to each '2A' catalogue position. The units of ρ are 0.0108 galaxies per square degree. The numbers in parentheses are the number of galaxies per annulus, () referring to the solid line and [] to the dashed line.

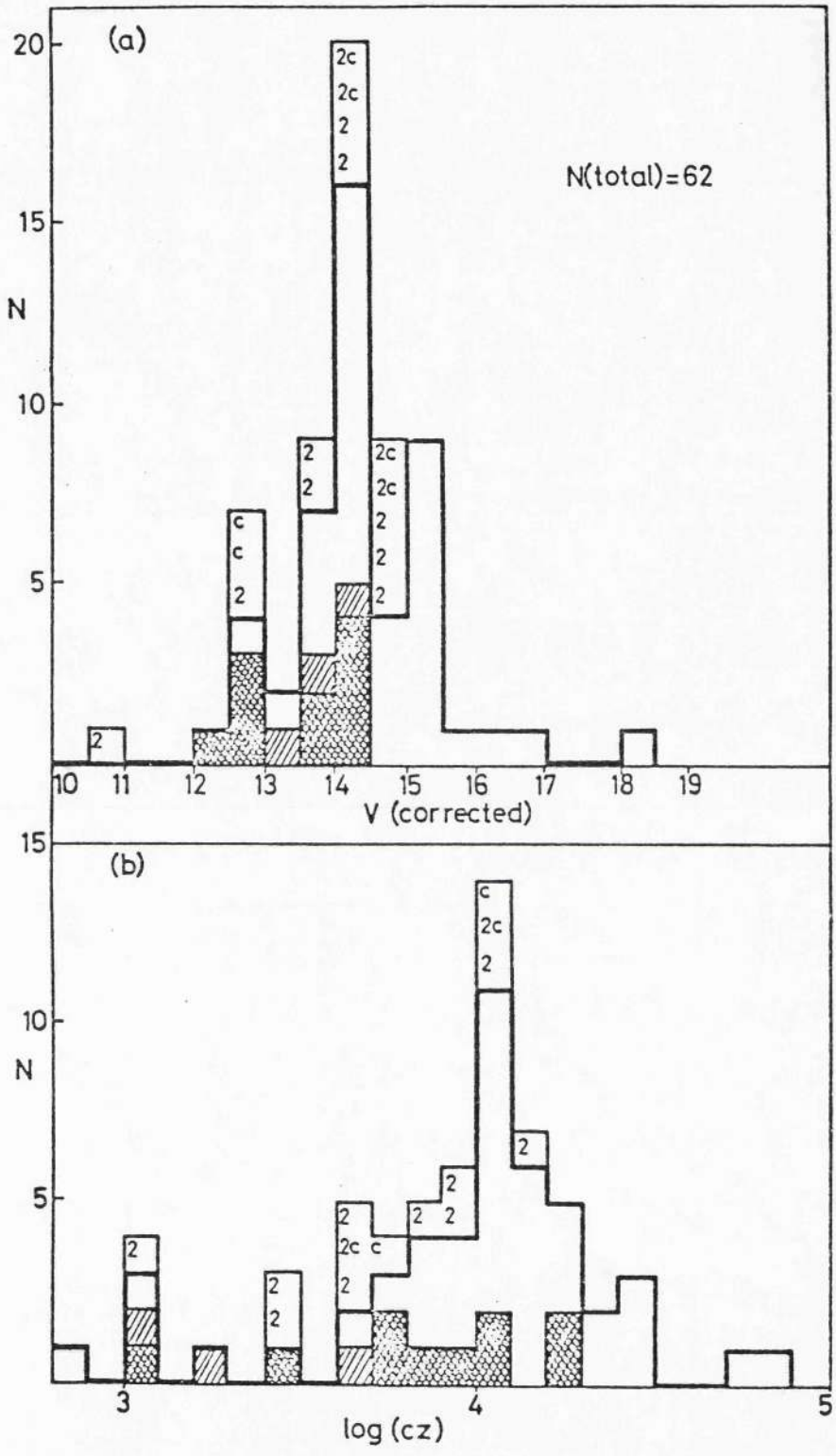

fig 3-8 HISTOGRAMS OF THE NUMBER OF SEYFERT GALAXIES AGAINST:

(a) APPARENT NUCLEAR MAGNITUDE (corrected for absorption within our own galaxy by A_v = 0.18 cosec b mag), and against

(b) LOG CZ , for direct comparison with (a).

In both diagrams the thin solid line represents the total number of Seyfert galaxies in Weedman's (1977) list for which a nuclear magnitude is available, while the thick solid line represents type 1 galaxies not confused in SSI data. Cross-hatched boxes are detections at x-ray wavelengths, while the boxes representing IC4329A, NGC3227 and NGC6814, whose identifications are less certain than the others,are shaded. The boxes marked C represent galaxies affected by confusion so that no x-ray data are available and boxes marked 2 are type 2 Seyfert galaxies.

confidence in the association of x-ray emission with Seyfert galaxies.

There is thus essentially no doubt that the great majority of these 2A identifications are correct and that Seyfert galaxies, as a class, contain many powerful x-ray emitters.

The absence of these Seyfert galaxies from the 3U catalogue (Giacconi et al., 1974) is readily understood. At 10 UHURU ct s^{-1} ($\approx$ 3.3 Ariel(SSI) ct s^{-1}) the 3U catalogue is 52% complete and at 2 - 3 UHURU ct s^{-1} only 24% complete (Murray, 1978). These figures include coverage with the 5^{o} x 5^{o} collimator which is heavily confused at these flux density levels so that the effective completeness figures are somewhat lower. In contrast, the PST survey of Seyfert galaxies from SSI data (see 3-4) is 80% complete at 2 UHURU ct s^{-1} (0.7 Ariel(SSI) ct s^{-1} ; fig 3-9). It is this greater completeness rather than an improved limiting sensitivity that has enabled the SSI to establish this class of extragalactic x-ray source.

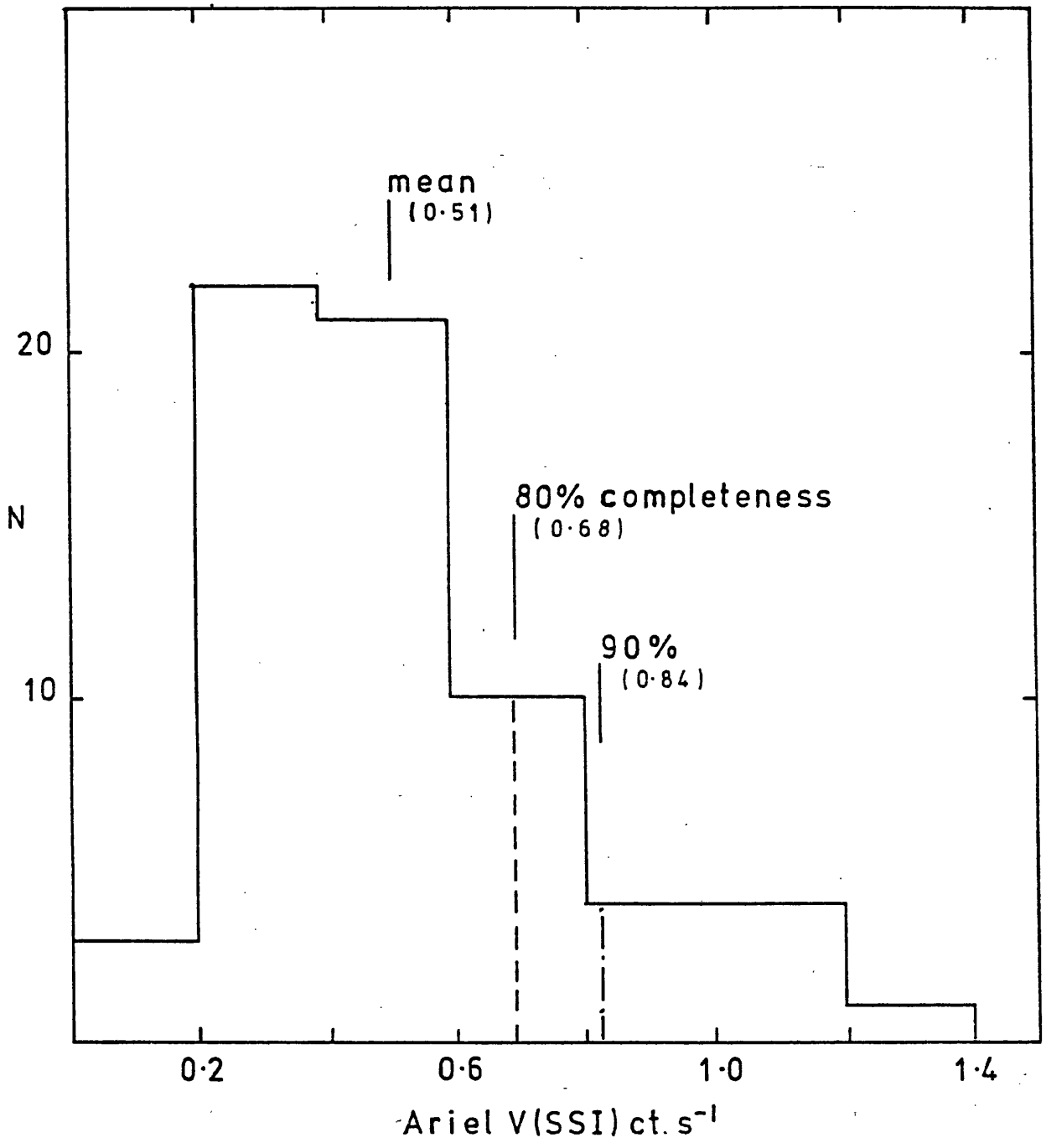

fig 3-9 HISTOGRAM OF THE NUMBER OF SEYFERTS PRODUCING GIVEN PST UPPER LIMITS (in SSI ct s^{-1}). The distribution can be used to estimate the completeness of coverage at different flux densities.

3-4 Discussion of individual sources

Table 3-2 lists all the known x-ray sources associated with Seyfert galaxies. Given in this table are the number of lines for each source detected by LOP, the significance of the PST detection (given for the LOP sources as well since the PST has also been applied to them), the area of the error box, the observed intensity in Ariel(SSI) ct s^{-1}, the luminosity in the 2 - 10 keV band and a note on whether variability in the x-ray flux has been observed. Included in Table 3-2 are two Seyfert galaxies (3C120 and 3C390.3) not seen by the SSI but detected by other observers (Schnopper et al., 1977; Charles et al., 1975). The detection criteria for the sources found only by the PST is $>5\sigma$, which is roughly equivalent in significance to that used for LOP sources.

For almost all the remaining known Seyfert galaxies (see Weedman, 1977) upper limits to their luminosities are given in Table 3-3, for the 2 - 10 keV band. (limits are given as 'apparent intensity' + 3σ). For some galaxies, indicated in Table 3-3 by a * , the flux density lay in the range 3 - 5σ. The distribution of PST sigmas shown in fig. 3-10 suggests that many of these will be real sources although they fall short of the reliability required for the 2A catalogue. Table 3-4 gives their fluxes and luminosities assuming them all to be real sources. In a few cases, confusion with nearby sources prevented application of the PST.

The analysis of the previous section (3-3) cannot convince us that any individual identification is correct. Each x-ray source error box has therefore been searched for plausible alternative identifications. Figs. 3-11 a-j show the relation of the error boxes to the Seyfert galaxies and to any other "interesting objects". We have searched the catalogues listed in Table 3-5 for such objects. The probability of finding a faint radio source inside a 2A box is quite high, so we have not considered them

Table 3-2 X-ray detected Seyfert galaxies.

Object	X-ray Name	N(lop)	PST σ	Error box area (Square°)	F_{lux} (SSI ct s^{-1}) (2-10 KeV)	Log_{10} (X-ray Luminosity) erg s^{-1}	X-ray variability ?
NGC 1275	2A0316+413	9	46	0.015	3.7 ± 0.4*	44.36*	
3C 120	0430+052	-	-	-	(1.1± 0.3)	44.39	
† MCG 8-11-11	2A0551+466	6	6	0.093	1.0 ± 0.1	43.93	YES
† MKN 376	2A0710+456	5	10	0.150	0.6 ± 0.1	44.58	
† MKN 79	2A0738+498	7	7	0.584	0.6 ± 0.1	43.77	
NGC 3227	A1021+198	-	6	1.460	0.6 ± 0.1	42.13	
† NGC 3783	2A1135-373	8	15	0.118	1.1 ± 0.1	43.28	
† NGC 4151	2A1207+397	38	52	0.011	3.2 ± 0.2	42.85	YES
IC 4329A	2A1347-300	8	11	0.100	1.7 ± 0.2	43.82	
† MKN 279	2A1348+700	6	11	0.275	0.9 ± 0.2	44.24	
NGC 5506	2A1410-029	5	5	0.207	1.3 ± 0.2	43.00	YES
† NGC 5548	2A1415+255	12	12	0.114	0.8 ± 0.1	43.65	
3C 390.3	3U1825+81	-	-	-	(0.9 ± 0.2)	44.77	YES
† ESO 141-G55	2A1914-589	3	5	0.292	0.4 ± 0.1	44.05	
NGC 6814	2A1938-105	-	7	2.240	0.7 ± 0.1	42.60	
† MKN 509	2A2040-115	5	8	0.398	0.9 ± 0.1	44.36	

* taking L_x (NGC1275) = 0.2 L_x (2A0316+413), see section 3.2.

† used in computing the bivariate x-ray/optical luminosity function

Table 3-3 PST upper limits for Seyfert galaxies.

	SEYFERT	X-RAY FLUX (2-10 KeV) SSI ct s^{-1}, 3σ limits.	LOG_{10} (X-ray luminosity) [2-10 KeV] erg s^{-1})
†	MKN 335	< 0.58	< 43.87
	III ZW 2	< 1.75	< 45.46
†	ZW 0039+40	< 0.65	< 45.15
	MKN 348	CONFUSED	-------
	I ZW 1	< 0.61	< 44.66
†	MKN 352	< 0.48	< 43.34
	T 109-38	< 0.25	< 42.79
	MKN 1	CONFUSED	-------
†	II ZW 1	< 0.54	< 44.51
†	AKN 42	< 1.07	< 44.45
†	MKN 358	< 1.00	< 44.59
	4C 29.6	< 0.78	< 45.28
* †	MKN 590	< 0.54	< 43.90
†	AKN 79	< 0.36	< 43.46
†	AKN 81	< 1.38	< 44.53
†	NGC 985	< 0.52	< 44.30
* †	NGC 1068	< 0.50	< 42.36
†	MKN 372	< 0.62	< 44.08
†	MKN 609	< 0.55	< 44.04
†	NGC 1566	< 0.28	< 41.93
†	III ZW 55	< 0.84	< 44.00
†	MKN 618	< 1.11	< 41.94
*	AKN 120	< 0.60	< 44.13
†	MKN 3	< 0.46	< 43.26
* †	MKN 6	< 0.54	< 43.63
†	MKN 374	< 0.38	< 44.18
†	MKN 9	< 0.33	< 44.04
†	MKN 78	< 0.48	< 44.23
†	MKN 10	< 0.38	< 43.85
†	MKN 382	< 0.37	< 43.94
†	MKN 110	< 0.37	< 43.99
†	ZW 0934+01	< 0.46	< 44.35
	3C 227	< 0.62	< 44.96
†	MKN 124	< 0.21	< 44.15
†	AKN 223	< 0.48	< 43.67
†	MKN 141	< 0.28	< 43.94
†	MKN 142	< 0.74	< 44.11
*	TON 524A	< 0.62	< 44.66
†	MKN 34	< 0.74	< 44.11
†	AKN 253	< 0.42	< 43.76
	NGC 3516	CONFUSED	-------
†	MKN 40	< 0.24	< 43.37
†	MKN 176	< 0.21	< 43.69
†	MKN 42	< 0.21	< 43.40
†	NGC 4051	< 0.24	< 41.43
	MKN 50	CONFUSED	-------
†	NGC 4507	< 0.67	< 43.26
†	MKN 231	< 0.18	< 43.79
	X COMAE	CONFUSED	-------
†	MKN 236	< 0.18	< 44.00
†	MKN 64	< 0.18	< 45.08
	3C 287.1	< 0.78	< 45.87
	MKN 268	CONFUSED	-------
†	MKN 270	< 0.36	< 42.77
†	MKN 69	< 0.71	< 44.92
†	MKN 463	< 0.30	< 44.19
†	MKN 464	< 0.60	< 44.51
†	MKN 474	< 0.69	< 44.38
†	MKN 478	< 0.30	< 44.58
	4C 35.37	< 0.34	< 44.62
†	MKN 290	< 0.44	< 43.95
	MKN 291	CONFUSED	-------
	MKN 298	CONFUSED	-------
*	MKN 486	< 0.46	< 44.16
†	MKN 504	< 0.84	< 44.34
* †	MKN 506	< 0.55	< 44.32
* †	3C 382	< 0.60	< 44.23
†	NGC 6764	< 0.27	< 42.54
	II ZW 136	< 0.69	< 44.72
†	MKN 304	< 0.46	< 44.61
@	NGC 7469	CONFUSED	-------
†	MKN 315	< 0.21	< 43.82
†	NGC 7603	< 0.79	< 44.14
	PKS 2349-01	< 0.42	< 45.41
†	MKN 541	< 0.45	< 44.20

Notes to Table 5-2

† used in computing the bivariate x-ray/optical luminosity function.

* objects for which the PST gave $3\sigma <$ flux density $< 5\sigma$.

@ this Seyfert was subsequently detected with a modified PST program that avoided the confusion problem in this case. It is listed as 2A2259+085 in the 2A catalogue with a flux of 1.1 ± 0.1 SSI ct s^{-1}. The error box is large (0.92 sq deg) so that the identification is not assured.

Table 3-4 Seyfert galaxies producing a PST significance just below the acceptance threshold (marked * in Table 2)

object	type	x-ray flux [2-10keV) SSI ct s^{-1}] ¶	PST	cz (km s^{-1})	log(L_x, erg s^{-1})
Mkn 590	1	0.3 ± 0.1	3.6	8100	43.65
NGC 1068	2	0.2 ± 0.1	4.0	1090	41.73
Akn 120	1	0.3 ± 0.1	4.5	9900	43.82
Mkn 6	1	0.3 ± 0.1	3.9	5290	43.28
Ton 524A	1	0.3 ± 0.1	3.8	18000	44.34
Mkn 486 (§)	1	0.4 ± 0.1	4.0	11700	44.10
Mkn 506	1	0.3 ± 0.1	4.5	12900	44.05
3C382	1	0.3 ± 0.1	3.8	17580	44.32

¶ rounding up errors reduce the apparent significance shown in this column.

§ a second PST run including more data gave 5.2 σ for this galaxy.

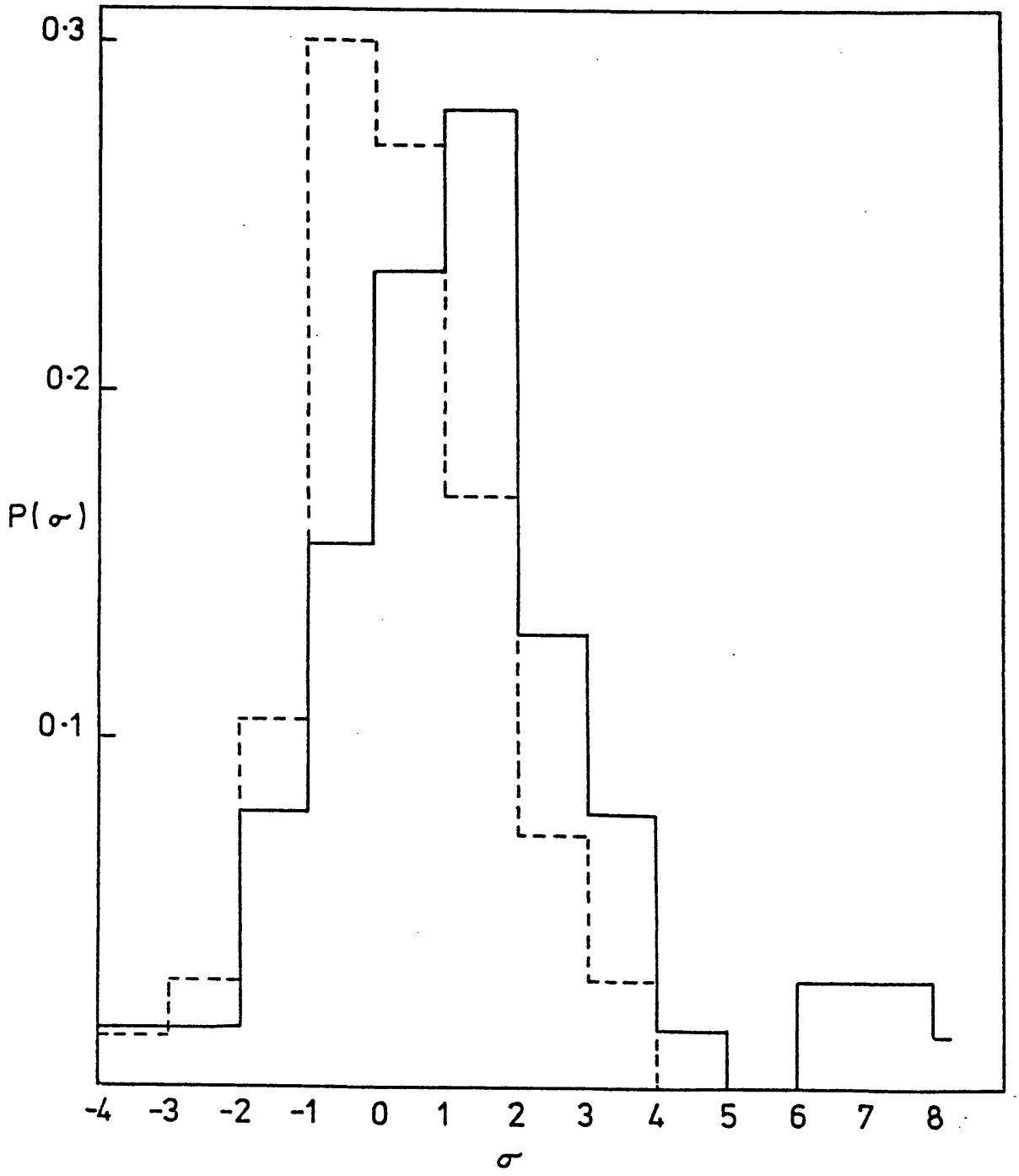

fig 3-10 HISTOGRAM OF FRACTION OF PST RUNS AT A GIVEN SIGNIFICANCE σ FOR

(a) SEYFERT GALAXIES (solid line)

(b) " random" positions (dotted line)

The distributions differ significantly at better than the 0.1% level.

Table 3-5 Catalogues searched for identification candidates

Clusters of Galaxies	: Abell (1958)
Galaxies	: Revised NGC catalogue (Sulentic and Tifft 1973)
	Uppsala General Catalogue of Galaxies (Nilson 1973)
Globular clusters	: Lang (1974)
	Hogg (1973)
BL Lac objects	: Stein, O'Dell and Strittmater (1976)
Active Galaxies	: Weedman (1977)
	Markarian lists I-VII
	Smith, Spinrad and Smith (1977)

as plausible identifications. Included in fig. 3-11 are the error boxes for all the proposed x-ray Seyferts except NGC 1275 and NGC 5506 (for which the 2A boxes are not a significant improvement over the 3U boxes), and NGC 3783 and MCG 8-11-11 (for which 2A boxes superimposed on optical photographs have been given in 3-2 and 3-3).

Notes on individual sources are given below:

NGC 1275 (3U0316-41 ; 2A0316+413)

The x-ray source 3U0316+41 is extended, with a radius of some 50 arc min (Wolff et al., 1976). It will not be possible to deduce the contribution of the nucleus of NGC 1275 until variability has been detected or a high resolution map becomes available. NGC 1275 has many features which are unusual for a Seyfert galaxy and is hard to classify in terms of normal Seyfert type 1 or 2. The galaxy has been classified as peculiar by de Vaucouleurs and de Vaucouleurs (1964) and as type KE2p by Morgan (1959). Associated with it are an extensive series of H_α emitting filaments (Lynds, 1970) and the complex radio source 3C 84 (Ryle and Windram, 1968).

3C 120 (0430+052)

X-ray emission from 3C 120 has been reported by Schnopper et al. (1977) from observations in 1975 November with the SAS-3 satellite. 3C 120 has not been detected by the SSI, our lowest (3σ) upper limit for its intensity being 0.9 Ariel(SSI) ct s^{-1}, consistent with the SAS-3 value. A deep plate published by Arp (1975) shows an inner disc with knots or jets surrounded by a much fainter outer envelope about 60 x 100 arc sec in extent. The structure of the nuclear radio source is discussed by Schillizzi et al. (1975).

MCG 8-11-11 (2A0551+466)

See chapter 3-3.

Mkn 376 (2A0710+456) Fig. 3-11 a.

Plates described by Adams (1977) show that Mkn 376 possesses an inner envelope along with probable outer spiral arms. No radio emission has been detected from it, the λ21cm flux density $\underline{S}_{21cm} < 10$ mJy (de Bruyn and Wilson, 1976). A group of faint galaxies lies within the box.

Mkn 79 (2A0738+498) Fig. 3-11 b.

Mkn 79 is a barred spiral, type SB(rs)c (Adams, 1977) and a weak radio emitter with $\underline{S}_{21cm} = 18.8$ mJy (de Bruyn and Wilson, 1976). A number of faint galaxies lies within the error box.

NGC 3227 (A1021+198) Fig. 3-11 c.

A source not in the 2A catalogue found in the PST survey of Seyferts mentioned above. Details of the error box are given in Table 3-6:

Table 3-6: PST Error Box Details for A1021+193

	R.A. (degrees 1950.0)	decl.
centre:	155.29	19.82
corners:	154.92	20.64
	155.81	20.44
	154.50	19.01
	155.40	18.81
Area of box:	1.46 sq. deg.	
Galactic co-ordinates of centre:	l = 217.54	b = 55.43

The PST flux density is consistent with the upper limit given by Ulmer and Murray (1976), which corresponds to 0.5 Ariel(SSI) ct s^{-1}. Optical spectra of the nucleus, obtained with the AAT, show it to be a type 1 Seyfert (FWZI Hβ = 4800 km s^{-1}), contrary to its classifications as

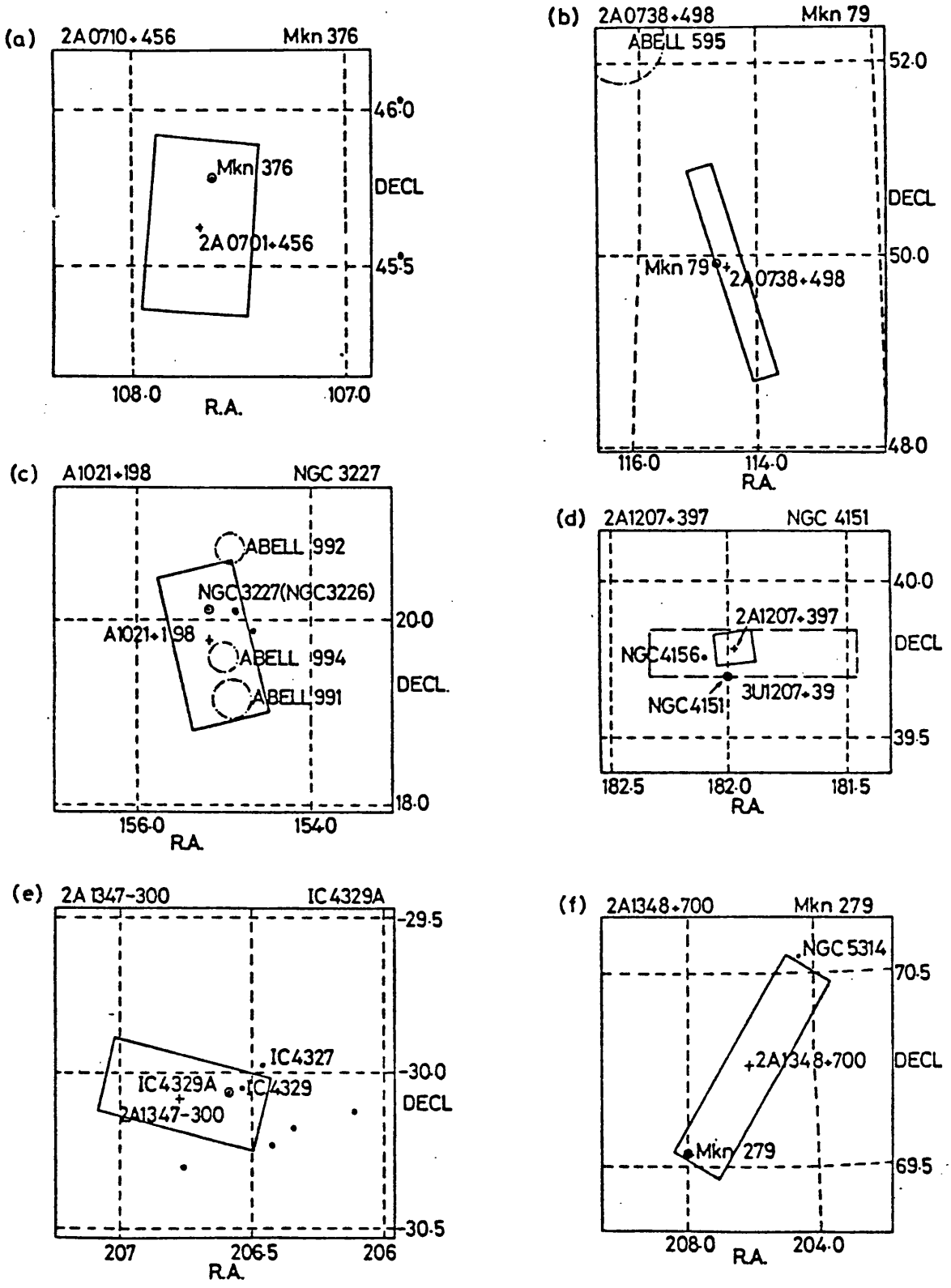

fig 3-1' RELATION OF THE SEYFERT GALAXIES AND OTHER "INTERESTING OBJECTS" TO THE ERROR BOXES OF THE 2A SURVEY. They are plotted on an equal area projection.+ marks the most probable position of the x-ray source. ⊕ marks the Seyfert galaxy. '·' marks bright (non-Seyfert) galaxies. Dashed circles represent the size (as given by Lang, 1974) of globular clusters. Dashed-dotted circles represents the extent, as defined by Abell (1958), of rich clusters of galaxies. In fig 2d the dashed rectangle is the error box of 3U1207+39. R.A. and Dec. are given as decimal degrees, epoch 1950.0.

type 2 given by Weedman (1977) (see also Anderson, 1970). The galaxy has been classified type SAB(s)ap by de Vaucouleurs and de Vaucouleurs (1968) and g?S4p by Morgan (1959). NGC 3227 shows two spiral arms, one of which extends to the elliptical companion NGC 3226. The nuclear radio source has been studied by de Bruyn and Willis (1974). Two distant Abell clusters lie inside the error box (A991, D=5, R=1 ; A994, D=6, R=1) and a third just outside. Although identification of A1021+198 with one of these clusters cannot be ruled out, NGC 3227 seems the most probable candidate because of its nearness and brightness.

NGC 3783 (2A1135-373)

See chapter 3-2.

NGC 4151 (3U1207+39 ; 2A1207+397) Fig. 3-11 d.

NGC 4151 lies just outside the 2A 90% confidence error box, whose area is a factor of 9 smaller than that of the 3U box. The galaxy does, however, lie inside the 2A box of 95% confidence. The x-ray source has been extensively studied. The best spectral data are from the Ariel V (MSSL) proportional counter spectrometer (see chapter 2-1) (1.5 - 15 keV; Ives et al., 1976) and the UCSD OSO-7 experiment (20 - 175 keV; Baity et al., 1975, Paciesas et al., 1977). These authors conclude that the spectrum is best represented by a power law with a low energy cut-off near 2.5 keV. Representing the spectrum by $\frac{dN}{dE} = A\, E^{-\alpha} \exp(-N_H \sigma)$, where is the absorption cross-section (e.g. Brown and Gould, 1970), the quoted parameters are:

Ives et al. : $\alpha = 1.62 \pm 0.2$, $N_H = 4.2 \times 10^{22} cm^2$ (1974 Nov)

$\alpha = 1.39 \pm 0.2$, $N_H = 5.2 \times 10^{22} cm^2$ (1976 Jan)

Paciesas et al. : $\alpha = 1.60 \pm 0.9$. (1975 Jan)

Such large column densities must be local to the source (Ives et al., 1976).

The x-ray flux density of NGC 4151 has changed by a factor 2 - 3 over 3 years (Ives et al., 1976), although there is, as yet, no evidence for variability in the spectral shape. The probable x-ray flare with a risetime of 3 day (see chapter 6-2) demonstrates that the size of the emitting region is $\lesssim 8 \times 10^{15}$cm. NGC4151 has been classified SAB(rs)ab by de Vaucouleurs and de Vaucouleurs (1968) and gRs4p by Morgan (1959). The flux density at λ 21 cm is S_{21cm} = 338 mJy (van der Kruit, 1971).

IC 4329A (2A1347-300) Fig. 3-11 e.

IC 4329A lies within a cluster of galaxies dominated by the giant elliptical IC 4329. The separation of these two galaxies is $\approx$ 3 arc min. Since x-ray variability has not been detected and no spectral information is available, it is not yet possible to determine the relative contributions of IC 4329A, IC4329 and the cluster to the observed x-ray emission. Disney (1973) refers to IC 4329A as an edge-on SA spiral. The nucleus is heavily reddened and the dereddened value of $M_v \approx -25$ is similar to that of quasars. IC 4329A contains a weak radio source with S_{21cm} = 24 mJy (M.J. Disney, reported in de Bruyn and Wilson, 1976).

Mkn 279 (2A1348+700) Fig. 3-11 f.

Adams (1977) describes Mkn 279 as possessing a dense nuclear region surrounded by a faint disc. Mkn 279 is a member of a small group of galaxies and is a weak radio source, S_{21cm} = 21.2 mJy (de Bruyn and Wilson, 1976).

NGC 5506 (3U1410-03 ; 2A1410-029)

This identification has been discussed by Bahcall et al. (1975) and Wilson et al. (1976). Although the optical spectrum of NGC 5506 is similar to that of a type 2 Seyfert, the emission lines are narrow, with widths of only $\approx$ 400 km s^{-1} (FWHM). Morphologically, NGC 5506 appears to be of type Irr II and closely resembles M 82 (Wilson et al., 1976). The

galaxy cannot be classified on the Khachikian and Weedman (1974) scheme. The nearby elliptical galaxy NGC 5507 does not show emission lines. The source is discussed more fully in chapter 7.

NGC 5548 (2A1415+255) Fig. 3-11 g.

NGC 5548 lies just outside the 90% confidence error box but inside that of 95% confidence. It has been classified (R')SA(s)0/a by de Vaucouleurs and de Vaucouleurs (1968) and g?S1pn by Morgan (1958). Radio emission is reported by van der Kruit (1971), S_{21cm} = 27 mJy.

3C 390.3 (3U1825+31)

This x-ray source has been detected by the UHURU (Giacconi et al., 1974) and the 'Copernicus' (Charles et al., 1975) satellites. Charles et al. considered the source to be variable, thus ruling out identification with the surrounding cluster of galaxies. Unfortunately 3C 390.3 lies in a 2A "confused region". Optically 3C 390.3 consists of an intense nucleus surrounded by very faint nebulosity (Penston and Penston, 1973). The radio structure is a classical powerful double source, with a flat spectral component coincident with the nucleus of the galaxy (Harris, 1972; Miley and van der Laan, 1973).

ESO 141-G55 (2A1914-589) Fig. 3-11 h.

A type 1 Seyfert galaxy discovered during the programme of optical spectroscopy of galaxies in the error boxes of unidentified x-ray sources. A spectrum obtained at our request by M.G. Smith and A. Boksenberg using the AAT shows very broad Balmer lines ($\approx$ 11,000 km s^{-1} FWZI) and broad Fe II emission. The highest excitation forbidden line is [Ne V] (IP=0.07 keV) λ3426 Å. Various other data are included in Table 5-1. The spectrum will be discussed in more detail in chapter 7. Observations with the Parkes 64 m radio telescope set a 3 σ upper limit of 15 mJy at 6 cm.

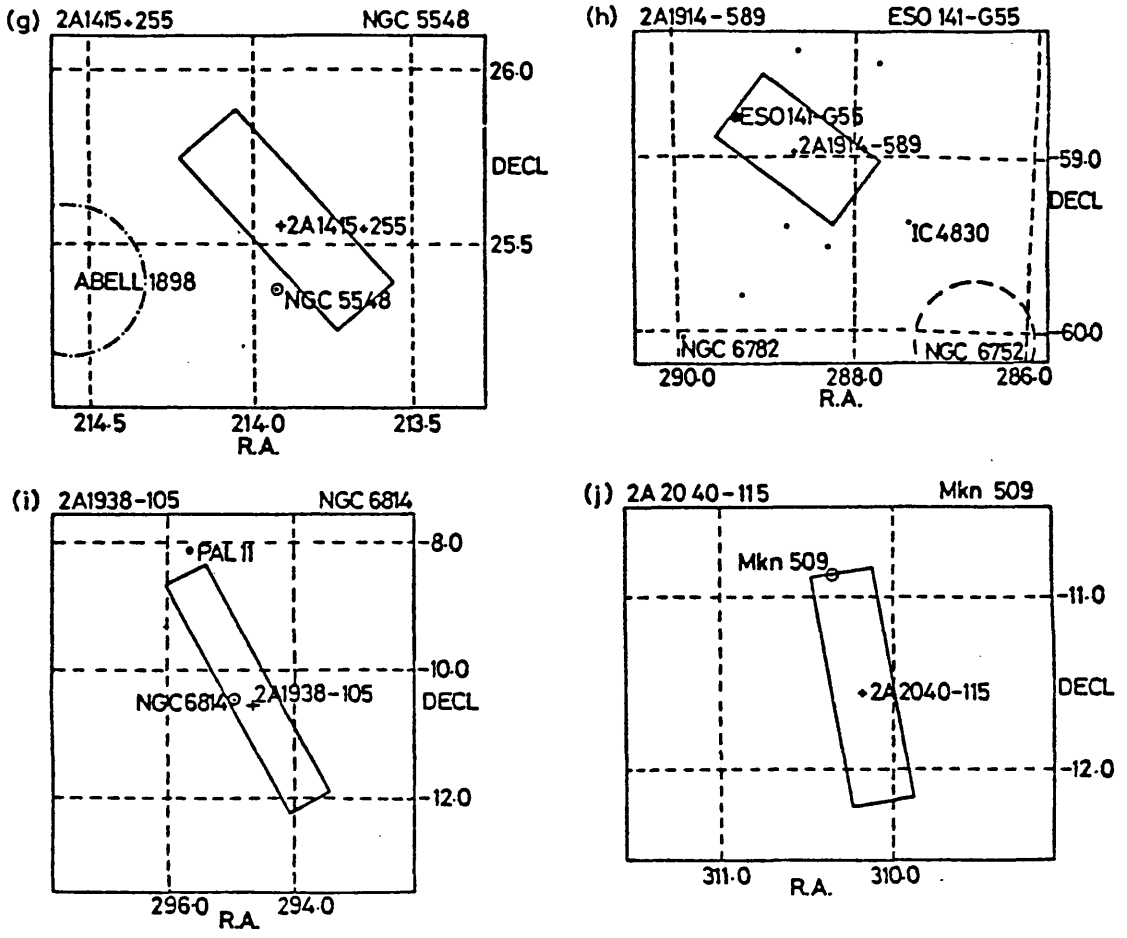

(fig 3-11 CONTINUED)

NGC 6814 (2A1938-105) Fig. 3-11 i.

A source detected only by the PST. Our flux density is well below the upper limit established by Ulmer and Murray (1976), which corresponds to 1.2 Ariel(SSI) ct s^{-1}. NGC 6814 has been classified type SAB(rs)bc by de Vaucouleurs and de Vaucouleurs (1968). No radio emission has been detected from it, $\underline{S}_{21cm}$ 5mJy (de Bruyn and Wilson, 1976). The globular cluster Pal 11 lies just outside the 90% confidence error box and may be considered a possible alternative identification. For a distance of 28.8 kpc (Lang, 1974), the luminosity would be $L_{2-10keV} = 3.5 \times 10^{36}$ erg s^{-1}.

Mkn 509 (2A2040-115) Fig. 3-11 j

Plates taken by Adams (1977) of this galaxy show a bright nucleus surrounded by a faint, apparently structureless, envelope. The galaxy has not been observed in the radio survey of Seyferts with the Westerbork telescope.

Of these identifications, three are more doubtful than the rest. The two sources detected only with the PST (NGC 3227 and NGC 6814) have large error boxes and permit plausible alternative identifications. IC 4329A lies in a cluster of galaxies which may well contribute to the x-ray emission. These reservations will be borne in mind in the following sections.

3-5 Completeness of Identifications with Seyfert galaxies

The total number of probable x-ray emitting Seyfert galaxies now stands at 15, including two (3C 120 and 3C 390.3) discovered by other workers but not seen by the SSI because of confusion with nearby sources and/or variability. In addition, there is the galaxy NGC 5506, the probable identification of 2A1410-029, which exhibits similarities to Seyfert galaxies in its optical spectrum.

In order to study the statistical properties of Seyfert galaxies at x-ray wavelengths, it is desirable to use a sample of Seyferts complete to a given x-ray flux density. Since optical catalogues of Seyferts are probably incomplete, all 'unidentified' 2A source error boxes are being searched for Seyfert galaxies. Although this is a continuing programme (see chapter 7) something can be said from the results so far.

Two approaches have been used:

(1) Slit spectroscopy of all bright galaxies in the error boxes using the Isaac Newton and Anglo-Australian Telescopes. One new Seyfert galaxy (MCG 8-11-11, see chapter 3-3) has been discovered in this manner.

(2) Objective Prism surveying with the UK SRC Schmidt telescope on Siding Spring mountain. At the time of writing, all 2A boxes in the region of sky $8^h < \alpha < 22^h$, $\delta < +22$ (39% of the area of sky covered by the 2A catalogue) have been surveyed. On these objective prism plates, candidates for Seyfert galaxies with $V < 17^m$ may easily be recognised through slit spectroscopy as in (1). Only one new Seyfert galaxy (ESO 141-G55, see chapter 3-4 and chapter 7) has been found in this manner.

The conclusion is that there are almost certainly no more than 2 or 3 x-ray emitting type 1 Seyferts with $V < 14^m.5$ in unidentified 2A source error boxes. Since we detect as LOP x-ray sources 11 out of the 31 type 1 galaxies with $V < 14^m.5$ which are listed by Weedman (1977), there are probably no more than 6 to 8 undiscovered type 1 Seyferts with $V < 14^m.5$.

chapter 4. SEYFERT GALAXY X-RAY LUMINOSITY FUNCTION - and contribution to the diffuse x-ray background.

4-1 The diffuse x-ray background.

A diffuse background radiation of cosmic x-rays was detected in the very first cosmic x-ray rocket flight (Giacconi et al., 1962) and has been intensively studied ever since. The radiation may be truly diffuse, as in the case of the 2.7 K microwave background. It is likely, however, that in the x-ray case at least a substantial fraction is due to the superposition of many faint unresolved sources. A study of the spatial fluctuations of the background can thus give information on the number of such faint sources which exist (at the level of about one per beam area), (Scheuer, 1974 ; Condon 1974).

Conversely the identified populations of x-ray sources can be analysed to estimate the contribution they are likely to make to this background. Now that a substantial sample of x-ray detected Seyfert galaxies exists this can be done with some degree of confidence. Previously such an accurate estimation had only been possible for the class of clusters of galaxies (e.g. McHardy, 1978a).

Schwartz and Gursky (1974) have collected together reliable measurements of the background intensity. Their resulting spectrum is shown in fig. 4-1. No single power-law can fit these observations. There seems to be a significant change in slope at about 20 keV. Below 2 keV the background spectrum steepens again in some parts of the sky. Above some hundreds of keV the background spectrum appears to flatten again. This complex shape suggests that more than one production mechanism may be at work.

The solid line in fig. 4-1 is fitted by Schwartz and Gursky

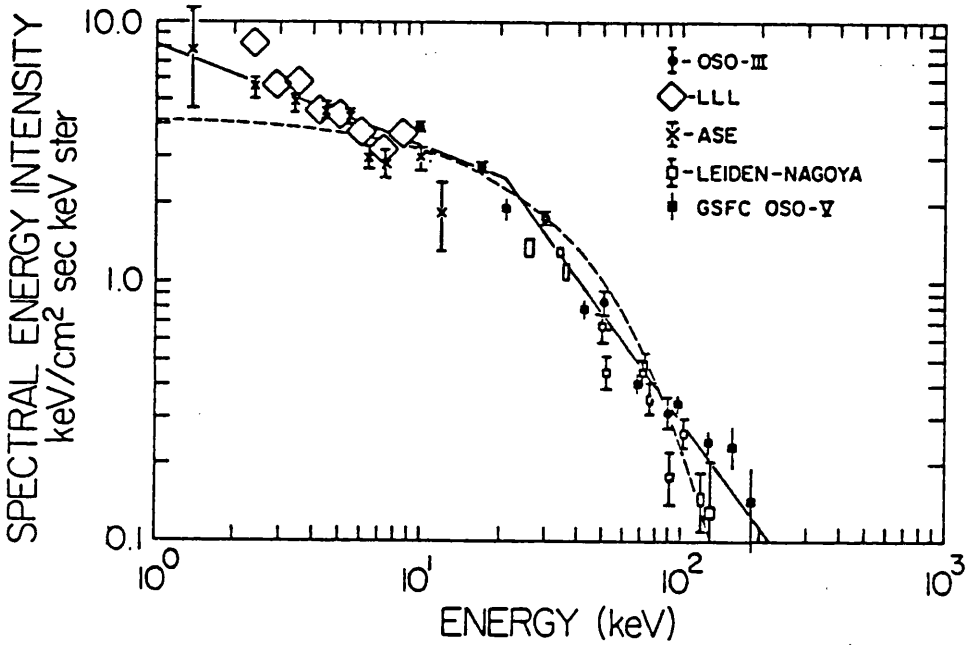

fig 4-1 MEASUREMENTS OF THE DIFFUSE X-RAY BACKGROUND ENERGY SPECTRUM (in keV $keV^{-1}cm^{-2}sr^{-1}s^{-1}$). Data were selected from published results according to the following criteria: (1) The experiment either spanned a wide range of geomagnetic conditions, or (2) included means of directly detecting and reducing effects of charged particles in the detector. Results reported only in the form of parameters for an assumed spectral shape are excluded. The data presented here have sufficient precision to reject the hypothesis that a single power law shape fits all the data between a few keV and a hundred keV. (from Schwartz and Gursky, 1974).

and represents

$$I(E) = 8.5E^{-0.40} \quad 1 < E < 21 \text{ keV}$$

$$167\ E^{-1.38} \quad E > 21 \text{ keV}$$

$$\text{keV } (\text{keV.cm}^2.\text{s}^1.\text{sr})^{-1}$$

The measured intensity of the background (I(E)) can be more easily compared with that expected from summations of point sources if it is converted into a volume emissivity at given energies, since this is a quantity easily determined from the luminosity function of classes of objects. If the emissivity (B(E)) is constant per unit volume, i.e. not evolving with cosmic time then (for Friedman cosmologies)

$$I(E) = \frac{1}{4\pi} \cdot \frac{C}{H_o} \cdot B(E_o) \int_o^{z_{max}} \frac{(1+z)^{-0.5}}{(1+z)^2 \sqrt{1+2q_o z}} \cdot dz$$

(Schwartz and Gursky, 1974, equation 10.8)

The integral varies in value from $\frac{1}{3}$ to $\frac{2}{3}$ depending on the value of the deceleration parameter, q_o, chosen and is not sensitive to the choice of cut-off redshift, z_{max}, for $z_{max} \gtrsim 3$.

Then, following Schwartz and Gursky,

$$B(E) = 1.2 \times 10^{-26} E^{-0.40} \text{ keV cm}^{-3} \text{ s}^{-1} \text{ keV}^{-1}$$

so, integrating over the standard SSI energy range of 2-10 keV,

$$\bar{B} = \int_2^{10} B(E)\, dE = \underline{2.3 \times 10^{39} \text{ erg s}^{-1} \text{ Mpc}^{-3}}$$

This is not the value found by Schwartz and Gursky, corrected to our Hubble constant (50 km s^{-1}Mpc^{-1}) since there is a numerical error at this last point in their derivation (Schwartz and Gursky, private communication). The fraction of this emission which is supplied by Seyfert galaxies must now be compared with this value.

4-2 Bivariate x-ray luminosity function

There are problems in determining the volume emissivity of Seyfert galaxies. The Seyfert galaxies in the 2A catalogue have luminosities in the range 10^{42}-10^{45} erg s^{-1} but are there Seyferts emitting outside this band, either nearby but too underluminous to be detected or superluminous but too distant? Also, there are around 25 unidentified sources in the 2A catalogue. If many of these turn out to be previously unknown Seyferts (like MCG 8-11-11 and ESO 141-G55) then the estimate of emissivity will have to be revised upwards.

Two methods of determining the volume emissivity are used here - the Bivariate x-ray/optical and the monovariate $1/V_{max}$ method, generalised. Each overcomes some problems but fails on others. Both methods determine the space density of Seyferts as a function of x-ray luminosity, i.e. they produce an x-ray luminosity function (XLF), from which an emissivity is easily found.

This section and the one following derive the two luminosity functions, and their relative merits are discussed.

BIVARIATE SAMPLE This method makes use of the derived SSI upper limits for the Seyfert galaxies. As a sample we consider all known Seyfert galaxies and use all those for which we could produce either a positive detection or an upper limit to the x-ray flux density, together with the redshift z and the apparent photographic magnitude m_p. We exclude from the sample a few objects with $z > 0.1$ to avoid possible cosmological effects, and also 5 3C objects with $z < 0.1$. The reason for the latter exclusion (3C84=NGC1275,3C120,3C227,3C382,3C390.3; three of them are detected as x-ray sources) is that at least 4 of the 5 galaxies are elliptical or N-type and all are strong radio sources. Although they have spectroscopic properties similar to those of optically selected Seyfert galaxies, the latter are mostly spirals and have typical radio powers only moderately

CONSTRUCTING A BIVARIATE X-RAY/OPTICAL LUMINOSITY FUNCTION

- take a given range of L_X:
- within this range,
  for each range of M_V, construct

$$f = \frac{\text{(number of Seyferts detected in x-rays)}}{\text{(number detectable with given sensitivity)}^*}$$

*using the PST upper limits to define the "number detectable"

- put these f_{ij} into an array:

	M_{P1}	M_{P2}	----	
L_{X1}	$f_{11} \times \rho_o(M_{P1})$	$f_{12} \times \rho_o(M_{P2})$	----	$\Sigma_j f_{ij} \cdot \rho_o(M_{Pj}) = \rho_x(L_{X1})$

- multiply by the optical space density, $\rho_o(M_{Pj})$, at M_{Pj}.

- these products, summed over M_{Pj}, are then the x-ray space density, $\rho_x(L_{X1})$, in L_{X1}.
- the set of $\rho_x(L_{Xi})$ form the x-ray luminosity function.

fig 4-2 THE METHOD OF CONSTRUCTING THE BIVARIATE X-RAY/OPTICAL LUMINOSITY FUNCTION.

stronger than is characteristic of normal spirals. It is possible, therefore, that the x-ray properties of the radio powerful Seyfert galaxies also differ from those of Seyfert galaxies selected purely on the basis of their optical properties. We shall not count as positive detections the three less certain identifications, NGC3227, NGC6814 and IC4329A, and also exclude NGC5506 because its classification as a Seyfert is in doubt (chapter 3-4). In all, the sample used to estimate the XLF (the objects are indicated in Tables 3-2 and 3-3) contains 63 Seyfert galaxies, 9 of which are detected.

THE BIVARIATE XLF The bivariate derivation of the XLF goes via the, known, optical luminosity function to the x-ray luminosity function using the fraction of detected out of detectable galaxies in each range of x-ray luminosity (L_x) and optical absolute magnitude (M_p). Fig 4-2 illustrates the process.

First each galaxy for which an x-ray detection or upper limit exists is sorted into an interval of L_x. For each interval of M_p within the interval of L_x the fraction f_{ij} (fig. 4-3) is calculated. The upper limits of Table 3-3 are used to find the denominator. Each interval of M_p has an associated space density, $\rho(M_{p_i})$, which can be taken from the optical luminosity function of Huchra and Sargent (1973; and see chapter 1-2, fig. 1-3). The product of f_{ij} and $\rho(M_{p_i})$ gives the space density of Seyferts in the M_{p_i} range and L_{x_j} range so summing over M_p gives the density in L_{x_j} alone – which is the required quantity for the luminosity function.

Table 4-1 shows the f_{ij} obtained. This table shows immediately that the number of upper limits or detections is substantial (> 10) only in the two intervals $-21>M_p>-22$ and $-22>M_p>-23$ for $L_x \geq 10^{43.5}$ erg s^{-1}. The estimate of f_{ij} can thus be considered reasonably good in this region of the (M,L) plane, while in all the other bins the estimates are obviously of much less significance.

Table 4-1 f_{ij} for the bivariate x-ray/optical luminosity function of Seyfert galaxies.

Log L_x	-19	-20	-21	-22	-23	-24	-25
45	0/3	0/6	0/18	0/29	0/7	0/0	
	0/3	0/6	0/18	1/28	0/6	0/0	
44	0/3	0/6	0/17	2/22	1/4	0/0	
	0/3	0/4	0/10	3/12	0/1	0/0	
43	0/3	0/3	1/6	0/3	0/0	0/0	
	0/2	1/1	0/2	0/2	0/0	0/0	
42	0/1	0/0	0/1	0/2	0/0	0/0	
	0/1	0/0	0/1	0/1	0/0	0/0	
41	0/1	0/0	0/0	0/0	0/0	0/0	

M_p

These f_{ij} deserve a further comment. While about 35% of the Seyfert galaxies with $-22>M_p>-23$ have $L_x>10^{43.5}$erg s^{-1}, less than 10% of the Seyfert galaxies with $-21>M_p>-22$ lie in the same range of x-ray power. This seems a rather significant indication that the brighter galaxies tend to be the more powerful x-ray emitters. This suggestion will be discussed more fully in chapter 5-3.

The f_{ij} are converted to values of $\rho(L_x)$ by multiplying them by the Huchra and Sargent (1973) space densities. Note that these space densities were calculated for Markarian Seyferts with $M_v < -20$. The resulting x-ray luminosity function is shown in fig. 4-3 a. The vertical error bars are calculated by applying Poissonian statistics to the small numbers of galaxies detected. It should be emphasised that these error bars are quite uncertain and do not take into account several other possible sources of error (e.g. the errors on the Huchra and Sargent luminosity function).

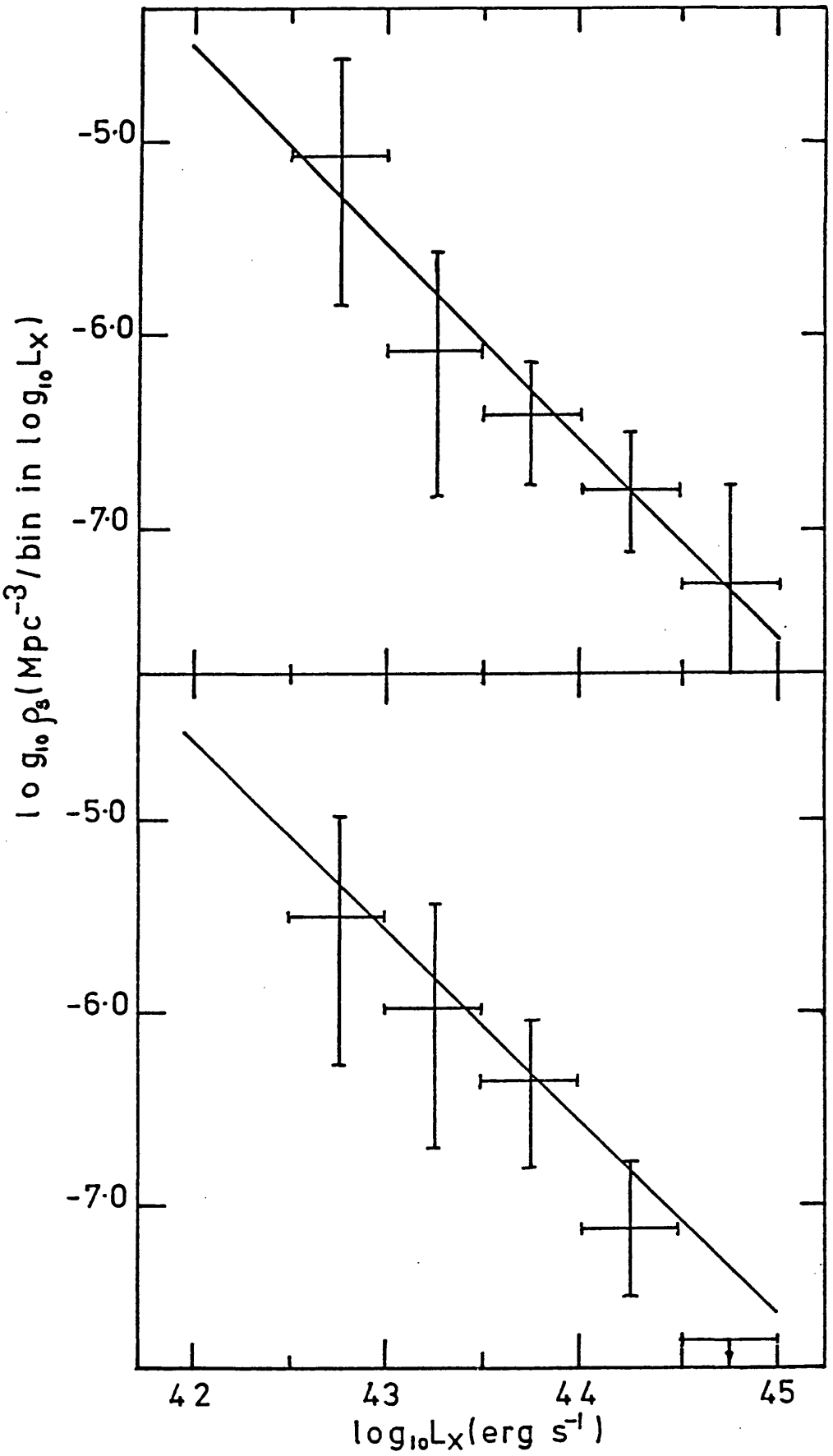

fig 4-3 (a) THE BIVARIATE X-RAY LUMINOSITY FUNCTION OF SEYFERT GALAXIES, derived as described in chapter 4-2. The straight line has a slope of -1 and corresponds to $\rho_s(L_x) = 2.0 \times 10^{37} L_x^{-2} Mpc^{-3}$ where the units of L_x are erg s^{-1}.

(b) THE MONOVARIATE X-RAY LUMINOSITY FUNCTION OF SEYFERT GALAXIES, derived as described in chapter 4-3. The straight line is identical to that in fig 4-3 a .

4-3 Generalised $^1/V_{max}$ XLF

A more direct approach to deriving the Seyfert XLF is to use the method introduced by Schmidt (1968) and deal solely with an x-ray selected sample. Each source emits a given luminosity, L (related to its true flux density S, as $L=4\pi r^2 S$). A source of this luminosity could be detected by the survey in question out to some maximum distance r_{max}. For a uniform survey over solid angle Ω the volume V throughout which the source could have been detected is just

$$V = \frac{\Omega}{3} r^3 = \frac{\Omega}{3} \left(\frac{L}{4\pi S_{lim}}\right)^{3/2} \qquad -(1)$$

The volume emissivity due to each source is just L/V and the total volume emissivity of the class being considered is then simply the $\Sigma_i L_i/V_i$ over all sources in the survey. This assumes that all the sources of the selected class in the survey have been identified.

In the case of x-ray surveys none has so far achieved uniform sky coverage. The 2A survey limit varies by at least a factor 2 (Cooke et al., 1978, fig. 3., Appendix A) which alters V_{max}, and hence the volume emissivity, by a factor ≈ 3. In assessing the contributions made to the diffuse x-ray background this could be a very significant error (100% becoming 33%). A correction for this varying limit is needed.

Warwick and Pye (1978) have calculated sky coverage corrections for the 2A catalogue, allowing for confusion and noise, by a Monte-Carlo method. Computing limitations prevented the method from being applied below 0.6 SSI ct s^{-1} which limits the sample slightly. Using this information it is possible to derive a luminosity function by varying the solid angle covered by the survey to that appropriate to each source luminosity.

If S_{lim} varies over the sky so that the fraction of the catalogue area over which the sensitivity limit lies in the range $S_{lim} \rightarrow S_{lim}+dS_{lim}$ is $\phi(S_{lim})dS_{lim}$ then equation (1) is replaced by

$$V_{max} = \int_0^{\infty} \frac{\Omega}{3} \left(\frac{L}{4\pi S_{lim}}\right)^{3/2} \cdot \phi(S_{lim}) \cdot dS_{lim}$$

$$= L^{3/2} \int_0^{\infty} \frac{\Omega}{3} \left(\frac{1}{4\pi}\right)^{3/2} \cdot \frac{\phi(S_{lim})}{S_{lim}^{3/2}} \cdot dS_{lim}$$

This integral can then be evaluated using the data of Warwick and Pye to give $\phi(S_{lim})$. If this is done in increments of S_{lim} sufficiently small that $S_{lim}^{3/2}$ does not vary significantly over the increment then

$$\int_0^{\infty} \frac{\phi(S_{lim})}{S_{lim}^{3/2}} \, dS_{lim} \approx \Sigma_i \frac{1}{\bar{S}^{3/2}} \, \theta(>S)\Big|_{S_i}^{S_{i+1}}, \text{ where } \bar{S} = \frac{S_i + S_{i+1}}{2}$$

There is a further problem with this method. A population of sources of true flux density S will give rise to a distribution of measured flux densities F, which will have a positive bias. This effect is due to noise and confusion. Warwick and Pye (1978) have derived these distributions for the 2A catalogue and their inverses. A source with measured F could have arisen from a range of S. If the probability distribution of these S is labelled $Q(F|S)dS$ then each source F contributes to each interval of S, and thus to the derived luminosity interval, with weighting $Q(F|S)$. i.e. probability of a source of measured intensity F hav ing a true intensity in the range $S_i - S_{i+1}$ is q where

$$q = \int_{S_i}^{S_{i+1}} Q(F|S) \, dS$$

Using this approach the luminosity function obtained is shown in fig. 4-3 b. The error bars are based on the effective number of sources in each bin (i.e. $\Sigma_i q_i(SdS)$ over all sources). The sample used here includes all of the 9 Seyferts with $F > 0.6$ SSI ct s^{-1} found as LOP sources in the 2A catalogue (including MCG2-58-22 and MR2251-178, see chapter 7-1) but excluding IC4329A and NGC1275 (they make a negligible

difference if included) and NGC5506 which should probably not be included as a Seyfert (see chapters 3-4, 7-1).

COMPARISON OF THE METHODS

The two luminosity functions (figs. 4-3 a,b) agree well with each other although arrived at by almost independent means. The bivariate approach is good in that it uses the more sensitive PST data, including the upper limits. However it is a somewhat circuitous method which may compound the errors involved. It also relies on an optical luminosity function for Markarian Seyferts which may not be applicable to all Seyferts. A last problem is that the Huchra and Sargent (1973) optical luminosity function suffers from differential absorption with galactic latitude (Kiang, 1976). This reduces V_{max} from the value assumed by Huchra and Sargent.

The $1/V_{max}$ method is by comparison direct and, as shown, can be generalised to accommodate the variable limiting flux density encountered in x-ray surveys. It does assume however that all the Seyfert galaxies in the 2A survey have already been found. In chapter 3-5 it was predicted that 2 or 3 Seyferts with $V < 14^m.5$ would have been detected in the remainder of the 2A survey. Two have since been found (ESO113-IG45 and MCG 2-58-22, see chapter 7-1). Since Seyferts with $V < 17^m$ would have been detected in the searches conducted so far without any having been found with $14.5 < V < 17$ it seems likely that essentially no more Seyferts are to be found in the 2A survey. (Such statements, as a rule, should be treated as tentative).

4-4 Contribution to the x-ray background radiation

It is convenient in the discussions that follow to use an analytical representation of the points. The full line drawn through the points in figs. 4-3 a,b represents

$$\rho_s(L_x) = 2.0 \times 10^{37} L_x^{-2} \ (\mathrm{Mpc}^{-3}) \qquad -(1)$$

(note that the slope (-1) of the line in fig. 4-4 differs from the exponent of L_x in this equation (-2) since the bins in L_x in fig. 4-4 are proportional to L_x.) The form (1) is only a reasonable representation of the points and not a rigorous fit. It is, of course, affected by large uncertainties which we shall take into account in the following discussion.

The XLF can now be used to estimate the contribution of the Seyfert galaxies to the number counts of x-ray sources and the x-ray background radiation. The total emissivity in the 2-10 keV band of Seyfert galaxies is just

$$B_s(2\text{-}10\mathrm{keV}) = \int_{L_{x_{min}}}^{L_{x_{max}}} \rho_s(L_x)\, L_x\, dL_x \qquad -(2)$$

LIMITS TO THE XLF Before the background contribution of Seyferts can be derived the limits $L_{x_{max}}$ and $L_{x_{min}}$ have to be estimated. Both limits must be specified since, for the slope of the XLF found here, each logarithmic interval of L_x gives an equal contribution to the x-ray background.

Using equation (1) the total density of Seyfert galaxies radiating in the range $L_{x_{min}} < L_x < L_{x_{max}}$ is :

$$\rho_s = \int_{L_{x_{min}}}^{L_{x_{max}}} \rho_s(L_x)\, dL_x \qquad -(3)$$

For $L_{x_{min}} = 10^{42.5}$ erg s^{-1}, equation (3) gives a value of ρ_s which already

corresponds to 33% of the total density of Seyfert galaxies with $M_p < -20$ ($\approx 2.4 \times 10^{-5}$ Mpc^{-3}) or 30% if the (M_p) of Huchra and Sargent is extrapolated to $M_p = -19$ (density $\approx 2.8 \times 10^{-5}$ Mpc^{-3}). The implication is that the XLF must flatten and turn down at about $10^{42.0}$ erg s^{-1}. This will be represented by a cut-off at this value in equation (1).

Using equation (1) with an upper limit of 10^{45}erg s^{-1} to Seyfert x-ray luminosity, it is found that the number of Seyfert galaxies with flux density above 1 SSI ct s^{-1} is $N_s(>1$ SSI ct s$^{-1}) = 0.95$ sr^{-1}. This value may be compared with the total number of x-ray sources $N_x(>1$ SSI ct s$^{-1}) = 3.2$ sr^{-1} in the 2A catalogue. From the above value of N_s, we expect about 7.5 Seyfert galaxies in the area of the Ariel V survey complete to SSI ct s^{-1} (7.9 sr), whilst 4 objects are actually found (MCG8-11-11, NGC3783, NGC4151, MCG2-58-22). The disagreement is not serious from a statistical point of view but indicates that, since

$$N_x(>S) \propto \int \rho_s(L_x) L_x^{3/2} \, dL_x,$$

the slope of the XLF is either somewhat larger than 2 or steepens beyond $L_x = 10^{44.0}$-$10^{44.5}$ erg s^{-1}.

BACKGROUND CONTRIBUTION Equation (2) can now be integrated to give the Seyfert volume emissivity. Using $L_{x_{min}} = 10^{42}$ erg s^{-1} and $L_{x_{max}} = 10^{45}$erg s^{-1},

$$B_s(2\text{-}10\text{keV}) = (1.7 \pm 0.8) \times 10^{38} \text{ erg s}^{-1}\text{Mpc}^{-3}.$$

This is a fraction 6% of the total volume emissivity of the diffuse x-ray background (see 4-1). The use of forms different from (1) but still reasonably compatible with the points in fig. 4-4 a,b, yields values for B_s within a factor 1.5 - 2 of the one above.

If there were a simple continuum of 'activity' in galaxies from Seyfert galaxies down to the 2×10^{39}erg s^{-1} of M31 the contribution from 'Seyfert and less active' galaxies could be twice the value found here for

Seyferts alone. This estimate relies on extrapolating the present XLF down to $L_x = 10^{39}$ erg s^{-1} without a change in slope. At this value of L_x however the density of x-ray emitters would exceed the density of field galaxies ($M_v < -20$) by an order of magnitude, implying that the XLF must flatten at lower luminosities.

The only Seyfert galaxy whose spectrum is well studied is NGC4151 for which (see chapter 3-4)

$$I(E) \propto E^{-(0.4 \pm 0.2)} \qquad 1.5 < E < 80 \text{ keV}.$$

If this spectrum is typical of many Seyferts, then Seyfert galaxies contribute about 15% of the diffuse background near 50 keV (much less than the estimate of Baity et al., 1975, which appears to contain a numerical error). It is clearly important to measure the high energy spectra of more Seyfert galaxies to make this estimate more certain.

EVOLUTION All these contributions are calculated assuming no cosmological evolution of Seyfert galaxies. By demanding that the contribution to the background intensity from the Seyfert galaxies be less than the total observed value, an upper limit to any evolution of the x-ray volume emissivity due to Seyfert galaxies may be obtained. If, following Rowan-Robinson and Fabian (1975), we let

$$B_s(\nu,z) = B_s(\nu,0)\exp(Q(1-(1+z)^{-1})) \qquad -(4)$$

where $B_s(\nu,z)$ is the volume emissivity of Seyfert galaxies per unit frequency range, then the background intensity is (c.f. Schwartz and Gursky, 1974, eqn. 10.8)

$$I_s(\nu) = \frac{c\, B_s(\nu,0)}{4\pi H_o} \int_o^\infty \frac{\exp\ Q[1-(1+z)^{-1}]}{(1+z)^3}\, dz \qquad -(5)$$

for an Einstein - de Sitter universe (deceleration parameter $q_o = \frac{1}{2}$,

curvature K=0). From (5)

$$I_s(\nu) = \frac{c\, B_s(\nu,0)}{4\pi H_o} \cdot \left(\frac{\exp(Q) - (1+Q)}{Q^2} \right) \qquad -(6)$$

From our value of B_s(2-10 keV) we find $B_s(\nu,0) = 3.5 \times 10^{-28}$keV $s^{-1}cm^{-3}keV^{-1}$. Since $I_s(\nu) < I_{obs}(\nu) = 4$ keV $cm^{-2}s^{-1}keV^{-1}sr^{-1}$ at 6 keV (Schwartz and Gursky, 1974), which is the energy of maximum efficiency of the SSI detector, equation (6) implies $Q < 5.5$.

For optically selected quasars and steep-radio-spectrum quasars $Q \approx 10$ (Schmidt, 1977). X-ray emission from Seyferts thus cannot evolve as strongly as these objects. The corrolary of this is that the entire diffuse x-ray background can be explained by Seyfert galaxies undergoing only moderate evolution.

chapter 5. CORRELATION OF X-RAY EMISSION WITH OTHER SEYFERT PROPERTIES

5-1 The Data

In chapter 3 it was established that Seyfert galaxies are, in general x-ray emitters. Chapter 4 derived their luminosity function and gave arguments to suggest that their x-ray luminosity was limited to the range 10^{42}-10^{45} erg s^{-1}. From the SSI x-ray flux density data alone one can go no further in understanding the mechanism that gives rise to this emission. In particular one cannot relate it to the standard model for Seyfert galaxies outlined in the first chapter.

Thus, as a preliminary to any discussion of the various possible mechanisms for x-ray production in Seyfert galaxies, it is necessary to search for correlations between the x-ray luminosity and properties in other wavebands. A summary of the more important properties in other wavebands of the galaxies detected as x-ray sources is given in Table 5-1. The less certain identifications (IC 4329A, NGC 3227 and NGC 6814) have not been included. The table includes many measurements made at the AAT by the optical astronomers engaged in the identification programme for 2A sources described in chapter 3.

These data can be used to plot x-ray luminosity against parameters characteristic of the three regions within a Seyfert nucleus described in chapter 1-4. First, however, another fact is striking - the Khachikian / Weedman type (ch 1-3) of the Seyfert is clearly important to the existence of strong x-ray emission (Table 5-1a,col.4). This is discussed below.

TABLE 5-1

Properties of Seyfert Galaxies Detected as X-ray Sources[a]

(a) Continuum Spectrum

Object	X-ray name	cz (km s^{-1})	Type (1)	Absolute Luminosities - Continuum						Colours	
				M_V[e]	M_K (2.2μ)	M_L (3.5μ)	$\log_{10} P_{10\mu m}$ (WHz^{-1}Ster^{-1})	$\log_{10} P_{1.4GHz}$ (WHz^{-1}Ster^{-1})	$\log_{10} L_{2-10keV}$ (erg s^{-1})	B-V	U-B
NGC1275	2A0316+413	5290(1)	?	-22.68 (6)	-25.82 (7)	-26.97 (6)	23.01 (8)	24.30 (9)	44.36[f](2)	0.64 (1)	-0.23 (1)
3C120	0430+05(10)	9900(1)	1	-22.61(14)	-26.36(14)	-27.29 (8)	22.94 (8)	24.30(15)	44.35 (10)	0.58 (1)	-0.75 (1)
MCG8-11-11	2A0551+466	6150(16)	1	-21.9 (16)	-	-	-	22.53[h](16)	43.93 (16)	-	-
Mkn 376	2A0710+456	16500 (1)	1	-23.47 (6)	-	-28.23 (6)	-	<22.04 (18)	44.58 (2)	0.55 (1)	-0.58 (1)
Mkn 79	2A0738+498	6580 (1)	1	-21.95(14)	-25.35(19)	-26.20 (6)	22.54 (8)	21.51 (18)	43.77 (2)	0.47 (1)	-0.74 (1)
NGC3783	2A1135-373	2740 (1)	1	-20.72(20)	-23.99(21)	>-24.89 (21)	21.83(22)	21.08[i](23)	43.28 (24)	0.56 (1)	-0.70 (1)
NGC4151	2A1207+397	990 (1)	1	-19.02 (6)	-23.08 (7)	-24.28 (6)	21.63 (8)	21.11 (27)	42.85 (2)	0.53 (1)	-0.72 (1)
Mkn 279	2A1348+700	9220 (1)	1	-22.12(14)	-	-	-	21.83 (18)	44.65 (2)	0.69 (1)	-0.45 (1)
NGC5506	2A1410-029	1820 (2)	2?	-16.79(29)	-23.50(30)	-	-	21.59 (18)	42.85 (2)	0.56[j](29)	-0.02[j](29)
NGC5548	2A1415+255	4990 (1)	1	-21.46(14)	-25.40 (7)	-26.00 (6)	22.21 (8)	21.48 (27)	43.65 (2)	0.46 (1)	-0.82 (1)
3C390.3	3C1825+31	17100 (1)	1	-23.6 (34)	-27.62 (2)	-	-	23.57[k](35)	44.77[l](36)	0.68 (1)	-0.69 (1)
ES0141-055 (31)	2A1914-589	11070 (2)	1	-22.6 (2)	-	-	-	-	44.05 (2)	-	-
Mkn509	2A2040-115	10650 (1)	1	-23.85 (6)	-27.00(19)	-28.24 (6)	<23.73(19)	-	44.36 (2)	0.23 (1)	-0.93 (1)

TABLE 5-1 continued

(b) Optical line spectrum

Object	X-ray name	Description: FeII	Description: Highest Excitation line	Description: Spectrum quality[b]	Optical spectrum - Line intensities[c]: $\log_{10}P(H\alpha)$ (erg s^{-1})	$\log_{10}P(H\beta)$	$\log_{10}P(HeII,\lambda4686)$ (erg s^{-1})	$\log_{10}P([OIII],\lambda5007)$	Optical spectrum - Line ratios: [SII] ratio 6717Å 6732	[OIII] ratio λ4363Å/(λ4959+λ5007)[d]	Hβ FWZI (km s^{-1})
NGC1275	2A0316+413	absent(2)	[NeIII](3)	3 (3)	42.25 (3)	41.22 (3)	<40.58 (3)	41.76 (4)	-	0.08 (5)	6000 (5)
3C120	0430+052	faint (11)	[FeX] (11)	2 (11)	43.05(12)	42.23(11)	41.55(11)	42.40(11)	0.91 (11)	0.04(11)	15000[e](13)
MCG8-11-11	2A0551+466	-	[FeVII](16)	3 (16)	-	-	-	-	-	-	8000(16)
Mkn376	2A0710+456	strong (17)	[OIII] (17)	2 (17)	43.07 (4)	42.51(17)	<41.51(17)	41.82 (4)	-	-	18100(13)
Mkn79	2A0738+498	faint (13)	[FeVII](13)	2 (13)	42.62 (4)	42.09(13)	41.24(13)	41.89 (4)	0.56 (13)	0.04(13)	12200(13)
NGC3783	2A1135-373	faint (2)	[FeX] (2)	1 (2)	42.00 (2)	41.57 (2)	40.95 (2)	41.41 (2)	0.8 (2)	0.09 (2)	9900 (2)
NGC4151	2A1207+397	faint (25)	[FeX] (26)	1 (25)	41.92 (4)	41.36(25)	40.41(25)	41.79 (4)	0.8 (25)	0.015 (25)	9000(25)
Mkn279	2A1348+700	faint (13)	[OIII] (13)	1 (13)	42.64 (4)	42.18(13)	41.30(13)	41.80 (4)	1.0 (13)	0.05 (13)	18500(13)
NGC5506	2A1410-029	absent(28)	[FeVII](28)	2 (28)	41.23(28)	40.40(28)	39.58(28)	41.30(28)	1.1 (28)	0.015 (28)	800(28)
NGC5548	2A1415+255	medium(13)	[FeVII](13)	2 (13)	42.54 (4)	41.92(13)	40.22(13)	41.87 (4)	1.0(13)	0.08 (13)	15400(13)
3C390.3	3U1825+81	faint (32)	[FeX] (33)	2 (32)	43.14(32)	42.35(32)	40.58(32)	42.35(32)	-	0.09 (32)	18000[e](32)
ESO141-055	2A1914-589	faint (2)	[NeV] (2)	2 (2)	-	≈42.5 (2)	≈41.4 (2)	41.8 (2)	-	0.019 (2)	11000 (2)
Mkn509	2A2040-115	faint (2)	[FeVII](2)	2 (2)	-	-	-	-	0.93 (13)	0.15 (2)	15100 (13)

TABLE 5-1 subtable

Reddening corrected parameters for NGC1275 and NGC5506

Object	A_V (mag)	$\log_{10}$ P(Hα) (erg s^{-1})	$\log_{10}$ P(Hβ) (erg s^{-1})	$\log_{10}$ P(HeII λ4686) (erg s^{-1})	$\log_{10}$ P([OIII] λ5007) (erg s^{-1})	M_V
NGC1275	2.0 (3)	42.39 (3)	42.15 (3)	<41.55 (3)	42.65 (4)	-24.68 (6)
NGC5506	1.0 (28)	41.84 (28)	41.28 (28)	40.50 (28)	42.15 (28)	-18.69 (29)

Notes to Table 5-1

a. IC4329A, whose identification is uncertain, and sources established by PST only (NGC3227 and NGC6814) have not been included.

b. The spectrum quality has been classified in terms of the ratio of the strength of the weakest line detected in the spectrum to the strength of Hα :

$$R_W > 0.10 = \text{Quality 3}$$
$$0.10 > R_W > 0.01 = \text{Quality 2}$$
$$0.01 > R_W = \text{Quality 1}$$

c. No correction for reddening has been applied since the intrinsic Balmer decrements of the type 1 Seyferts probably differ from case B values. For the narrow line galaxies (NGC1275 and NGC5506) the subtable gives values of A_V and dereddened values for optical magnitude and line intensities, presuming the intrinsic Balmer decrement to be described by case B conditions.

d. Corrected for reddening in the cases of NGC1275 and NGC5506.

e. Nuclear magnitude, corrected for absorption in our galaxy $A_w = 0.18$ cosec b mag.

f. Assumes $L_{x_{2\text{-}10\ keV}}$ (NGC1275) = 0.2 $L_{x_{2\text{-}10\ keV}}$ (2A0316+413).

g. Represents average FWZI of Hα and Hβ.

h. Derived by extrapolating spectrum from 2.7 GHz using $\alpha = -0.39$.

i. Derived from 5 GHz flux density assuming $\alpha = -0.8$.

j. UBV data for NGC5506 for an aperture 5.5 arc secs in diameter. In an aperture 88 arc secs in diameter: $M_V = 12.50$, B-V = 0.93, U-B = 0.32 (ref. 29).

k. Power from nucleus of galaxy.

l. In 2-6 keV band.

References for Table 5-1

1. Weedman, 1977
2. new AAT measurements (see text)
3. Shields and Oke, 1975.
4. Adams and Weedman, 1975.
5. Anderson, 1970.
6. Stein and Weedman, 1976.
7. Penston et al., 1974.
8. Rieke and Low, 1972.
9. Ryle and Windram, 1963.
10. Schnopper, H.W. et al., 1977.
11. Phillips and Osterbrock, 1975.
12. Shields et al., 1972.
13. Osterbrock, 1977a.
14. Weedman, 1973.
15. Pauliny-Toth and Kellermann, 1968.
16. chapter 3-2
17. Osterbrock, 1976.
18. de Bruyn and Wilson, 1976.
19. Allen, 1976
20. Osmer and Smith, 1974.
21. Glass, 1973.
22. Kleinmann and Wright, 1974.
23. Penston et al., 1977.
24. chapter 3-1
25. Boksenberg et al., 1975.
26. Oke and Sargent, 1963.
27. Van der Kruit, 1971.
28. Wilson et al., 1976.
29. Disney, 1976, private communication.
30. Allen, 1976b, private communication.
31. Holmberg et al., 1976.
32. Osterbrock et al., 1976.
33. Ward et al., 1977
34. Sandage, 1967.
35. Miley and Van der Laan, 1973.
36. Giacconi et al., 1974.

5-2 X-ray emission vs. Seyfert type

All the x-ray sources for which a Khachikian/Weedman type is not in doubt are of type 1. As already noted (chapter 3-4), NGC 1275 is a peculiar object and the classification of NGC 5506 as a Seyfert galaxy is uncertain. The lack of detection of type 2's is not due to a distance effect, since they are, on average, nearer than the type 1's. For the 71 type 1 Seyfert galaxies in Weedman's (1977) list (including NGC 3227 and Mkn 6 reclassified as type 1, see 3-2 and Neugebauer et al., 1976), the average recession velocity is 14260 km s^{-1} , while for the 16 type 2's this parameter is 7190 km s^{-1}. To discuss the probabilities of detection of the two types in a given volume of space, we note that there are 54 type 1 galaxies nearer than the most distant of the 16 type 2's ($cz \approx 15{,}300$ km s^{-1}) 8 of these 54 are detected as LOP x-ray sources and another 2 by the PST. Another two are detected by other satellites and 5 more are marginal ($3\text{-}5\sigma$) detections with the PST (see table 3-4). Of the 16 type 2 galaxies only NGC 1068 is even a marginal x-ray emitter . These considerations emphasise that type 1 Seyfert galaxies are more luminous in the 2-10 keV band than are type 2 Seyferts.

5-3 X-ray vs. Optical Continuum emission

In type 1 Seyferts the optical continuum is believed to be "non-thermal" emission from a central compact source (see 1-4). Such a compact region may well be the seat of the x-ray emission. In this case a correlation between the optical flux density and the x-ray flux density might be expected.

Histograms of the number of Seyfert galaxies against apparent nuclear magnitude V (corrected for absorption within our galaxy) and against $\log_{10}$ cz are shown in figs 5-1a and b. It is clear that the galaxies detected as x-ray sources tend to be the apparently brightest in V. There is also a weaker tendency for the more nearby objects to be detected. Referring to fig 5-1a one finds that all the 13 galaxies detected as x-ray sources have $V < 14^{m}.5$. However none of the 8 type 2's with $V < 14^{m}.5$ is detected although two lie in confused regions.

Fig 5-2 shows a plot of apparent nuclear magnitude V against the flux density in the 2-10 keV band. As seen previously in fig 5-1a, the Seyfert galaxies found to be x-ray emitters tend to be the optically brightest type 1's. For the detected galaxies, there is a weak correlation between V and $\log_{10} F_x$ at the 3% significance level. IC 4329A and sources detected by the PST (NGC 3227 and NGC 6814) have not been included in assessing this significance. If NGC 3227 and NGC 6814 are included the significance is also 3%. The evidence is, therefore, in favour of a correlation between optical and x-ray continuum brightness in type 1 Seyferts (see also chapter 4.). It is interesting to note that if the correlation between apparent optical and x-ray brightness also extends to quasars, their absence from current x-ray catalogues is readily understood.

In discussing this and subsequent correlations between intensities at two different wavebands, we have preferred to present

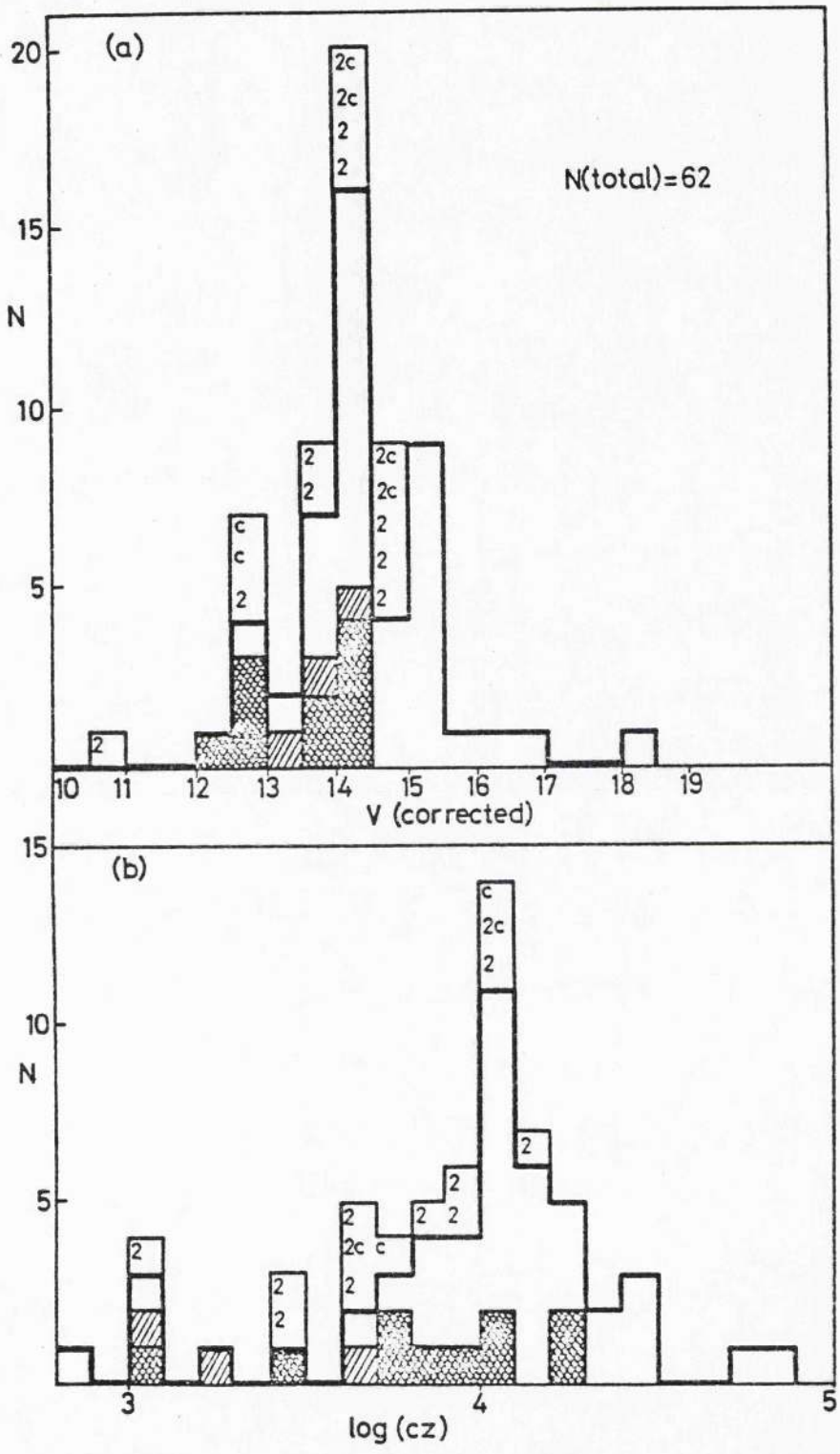

fig 5-1 HISTOGRAMS OF THE NUMBER OF SEYFERT GALAXIES AGAINST:

(a) APPARENT NUCLEAR MAGNITUDE (corrected for absorption within our own galaxy by A_v=0.18 cosec b mag), and against

(b) LOG CZ , for direct comparison with (a).

In both diagrams the thin solid line represents the total number of Seyfert galaxies in Weedman's (1977) list for which a nuclear magnitude is available, while the thick solid line represents type 1 galaxies not confused in SSI data. Cross-hatched boxes are detections at x-ray wavelengths, while the boxes representing IC4329A, NGC3227 and NGC6814, whose identifications are less certain than the others, are shaded. The boxes marked 'C' represent galaxies affected by confusion so that no x-ray data are available and boxes marked '2' are type 2 Seyfert galaxies.

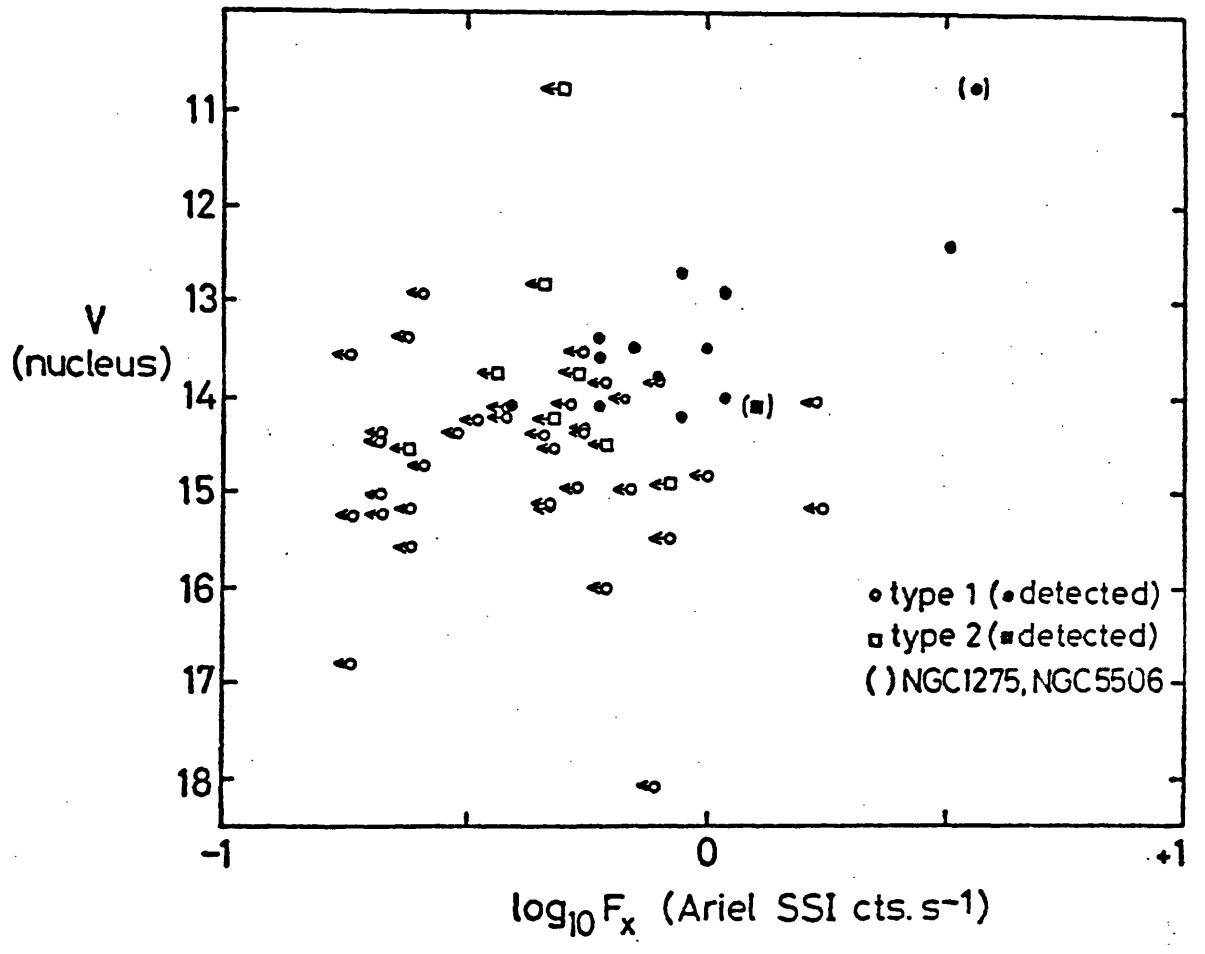

fig 5-2 A PLOT OF APPARENT NUCLEAR MAGNITUDE V (corrected for absorption within our own galaxy using A_v=0.18cosec b mag) AGAINST X-RAY FLUX DENSITY, F_x. The values of V for NGC1275 and NGC5506 have also been corrected for internal absorptions $A_v = 2^m.0$ and $1^m.9$ respectively (c.f. Table 5-1). (see also fig 7-1 a and chapter 7-1).

diagrams involving the flux density rather than the absolute luminosity for the following reason.

When a class of objects is detected over a small range of apparent brightness in both wavebands but with a large range of distance, a correlation will appear in a plot of absolute luminosities even when there is no correlation between the corresponding flux densities. The values of the x-ray and infrared flux densities and the flux density in Hα vary over only an order of magnitude or less. (see following sections). Although some of the other parameters considered exhibit a wider range of apparent brightness the corresponding diagrams are presented in each case for the sake of uniformity, except where the quantity involved does not scale with distance (colour and FWZI, chapter 5-6). Diagrams involving luminosities have also been constructed and their appearance is commented on in each case. A plot of M_v against the absolute luminosity in x-rays shows a very strong correlation which is largely a consequence of the above selection effect, (see also chapter 5-5 and fig. 5-5).

5-4 X-ray vs. Infrared and Radio emission

The short timescale variability seen in some type 1 Seyfert galaxies infrared emission (Penston et al., 1974) suggests that it arises with the optical continuum, in the inner region (1) (see chapter 1-4) of the nucleus. Penston et al. also believe the infrared colours indicate a continuation of the optical "power-law" continuum. This is supported by the correlated B and 2.2μm variability that they observe. In type 2 Seyferts the infrared emission is believed to be thermal re-radiation from dust associated with the forbidden line region,(3), since the emission at 10μm comes from a resolved region in NGC 1068 (Becklin et al.,1973).

Plots of the flux densities at λ3.5μm (m_L) and λ10μm against the x-ray flux density are given in figs 5-3a,b, for the galaxies detected as x-ray sources. Strong correlations exist between the λ10μm and 2-10 keV flux densities (better than 1% significance level) and between the λ3.5μm and 2-10 keV flux densities (≈ 1% significance). The 3.5μm plot,having a substantial number of points, is more convincing. Corresponding plots involving the powers also show strong correlations.

The radio emission from Seyferts (de Bruyn and Wilson,1977) is fairly unambiguously coming from the extended forbidden line region,(2). Fig 5-3c shows λ21cm flux density against x-ray flux density. Only weak correlations exist in either the radio/x-ray flux density or the radio/ x-ray power diagrams.

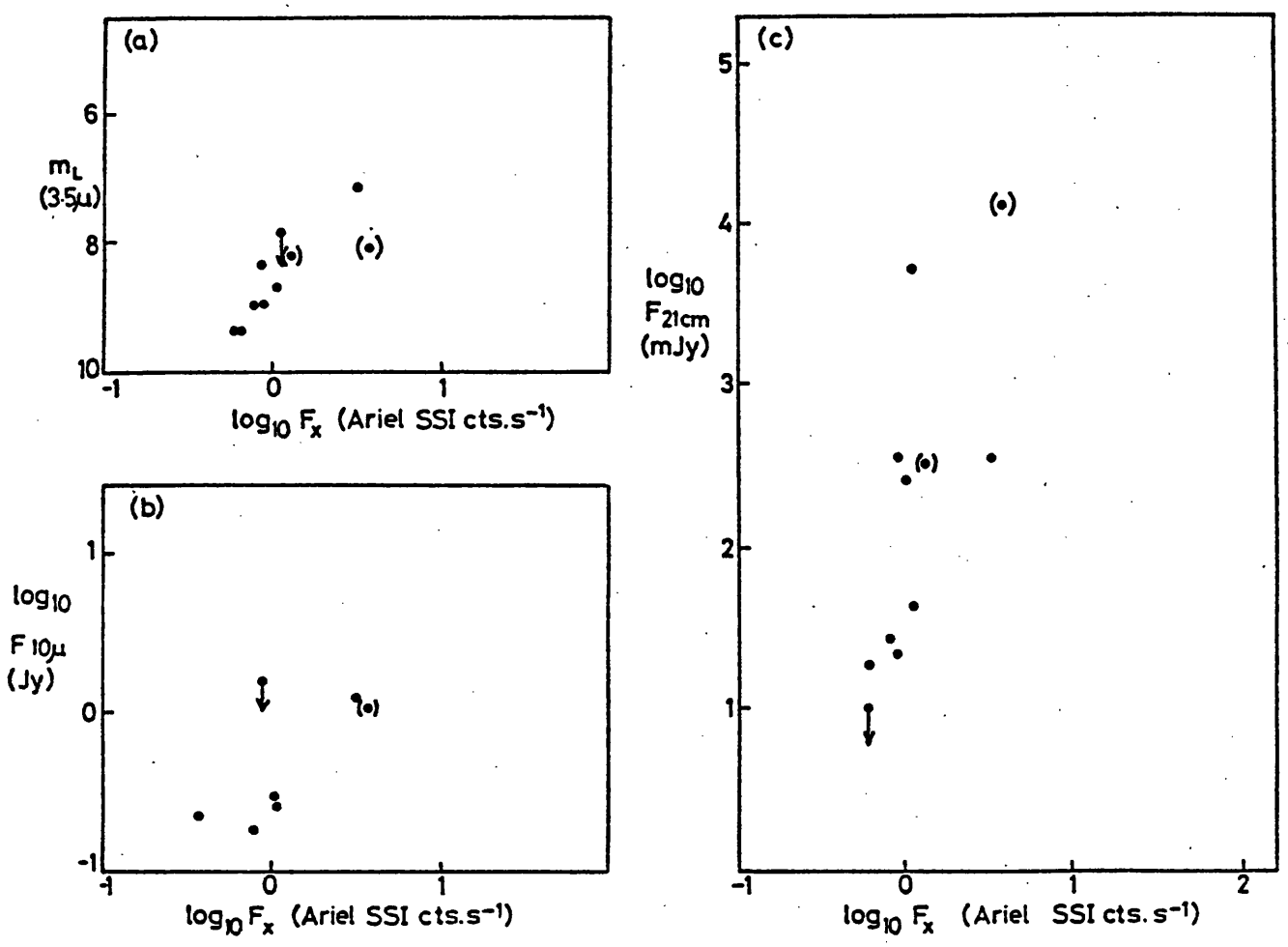

fig 5-3 PLOTS OF CONTINUUM EMISSION AT VARIOUS WAVELENGTHS VERSUS X-RAY FLUX DENSITY. Apparent intensities rather than absolute have been used for reasons explained in chapter 5-3. NGC1275 and NGC5506 are shown in brackets.

(a) Apparent magnitude at λ3.5μm.

(b) Flux density at λ10μm

(c) Flux density at λ21cm.

5-5 X-ray vs. Optical Emission Line intensities

Figs. 5-4 a-c give plots of the flux densities in Hα , He II λ4686 Å (a high excitation line) and [O III] λ5007 Å against 2-10 keV flux density. The only significant correlation involves the Hα vs. 2-10keV flux densities (fig. 5-3a) which are correlated at the 2% significance level. This relation also shows up in the corresponding diagram involving powers. A weak correlation may exist in the diagram L_{HeII} vs. L_x.

Since, in section 5-3, a relation between M_v and L_x was apparent and since Adams and Weedman (1975) find that $L_{H\alpha} \propto M_v$ over a wide range of M_v (fig. 5-5a) a similar relation would be expected between $L_{H\alpha}$ and L_x. Adams and Weedman suffer, to some extent, from the selection effect described in section 5-3. If one plots instead flux densities and apparent magnitudes, using their data, the relation is much less apparent (fig. 5-5b). A relation is nevertheless still present.

The $F(H\alpha)$ vs. F_x relation found here is slightly stronger than that found for m_v vs. F_x (chapter 5-3).

The strong forbidden line [O III] λ5007 Å seems to be uncorrelated with x-ray flux density, as was the λ21 cm radio flux. Both these quantities are characteristic of the outer, low density, region, (3).

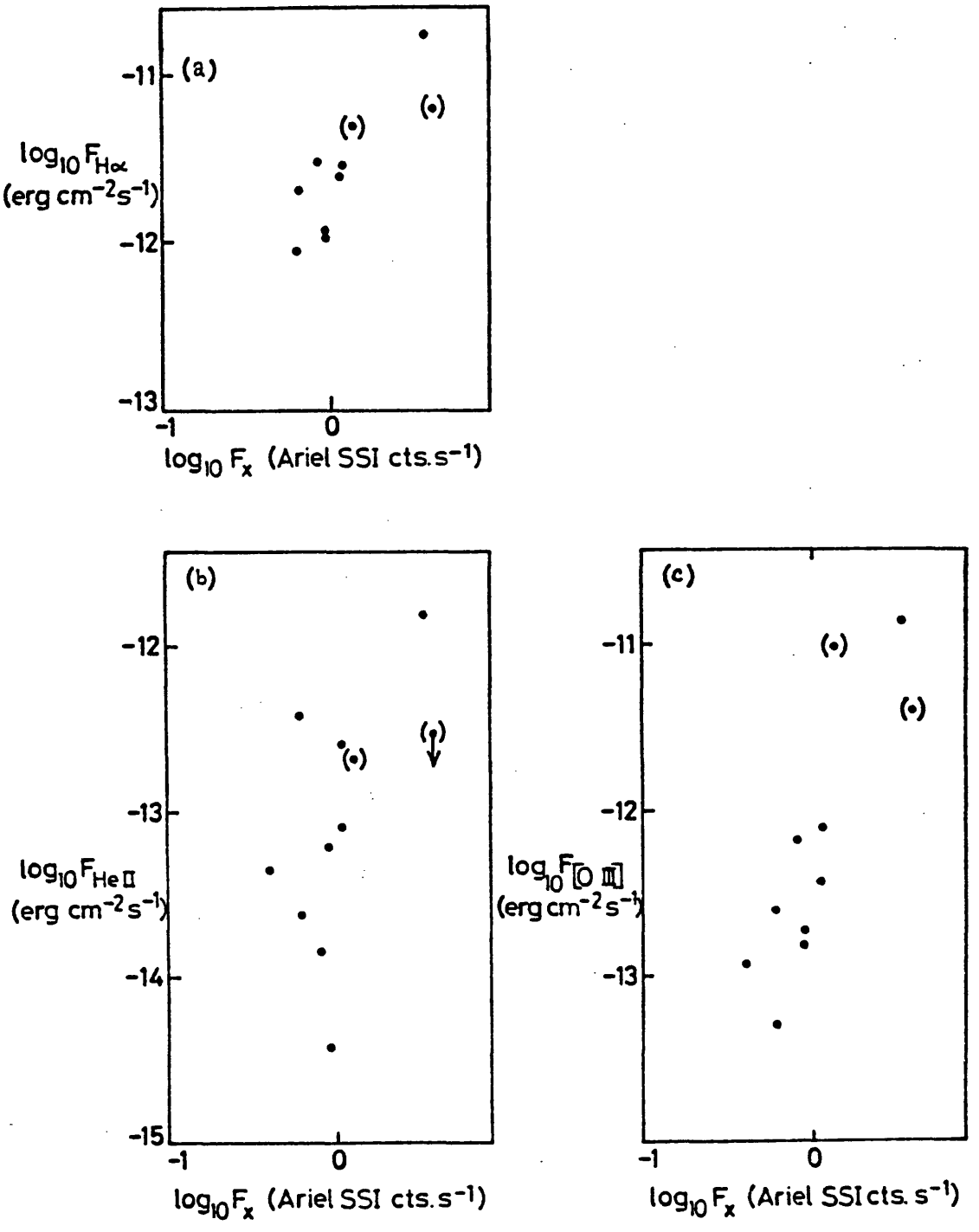

fig 5-4 PLOTS OF VARIOUS EMISSION LINE INTENSITIES VERSUS X-RAY FLUX DENSITY. Apparent intensities have been used rather than absolute for reasons explained in chapter 5-3. NGC1275 and NGC5506 are shown in brackets.

(a) Intensity of Hα .

(b) Intensity of HeII λ4686Å.

(c) Intensity of [OIII] λ5007Å.

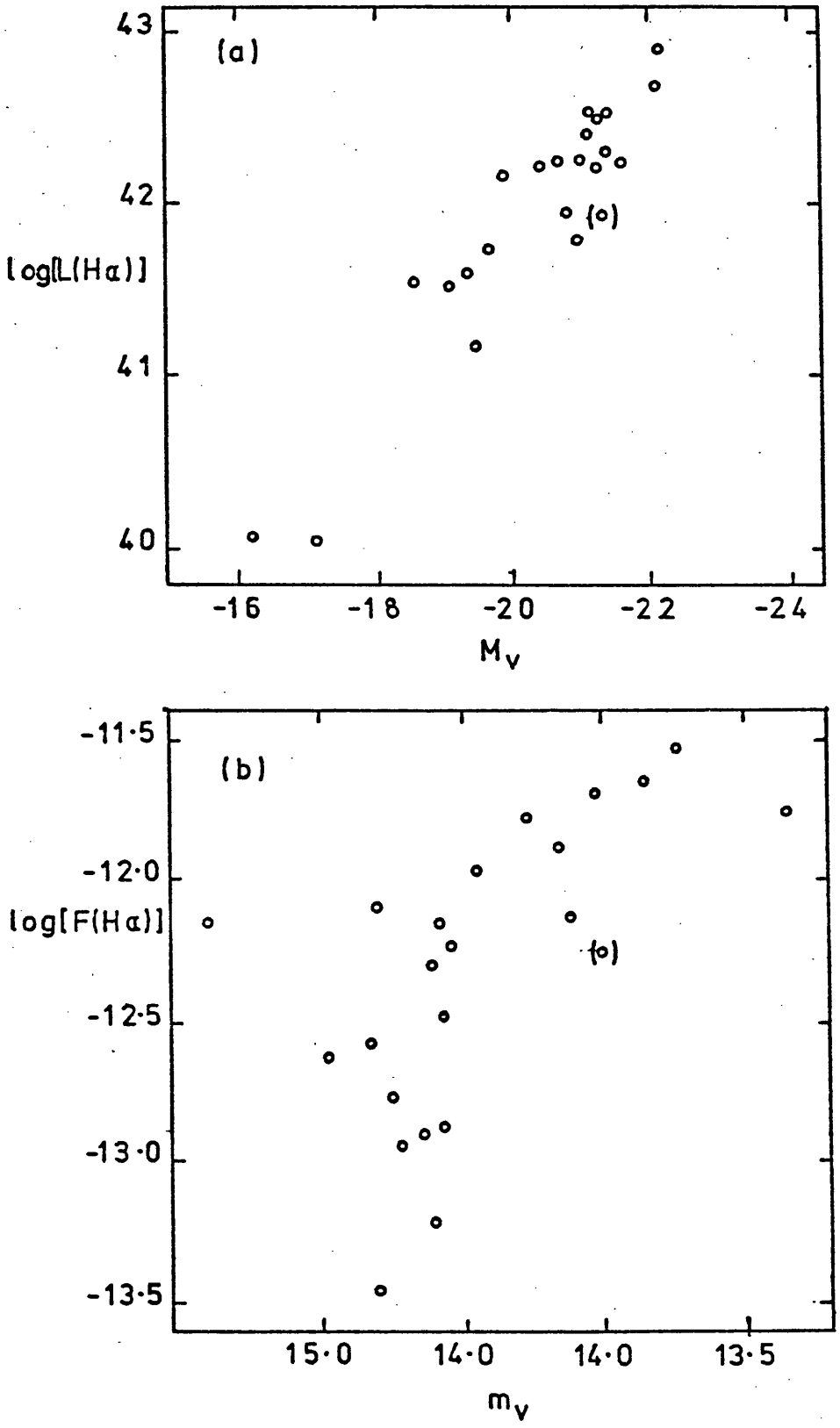

fig 5-5 PLOTS OF (a) LOG(POWER IN Hα) VERSUS ABSOLUTE V MAGNITUDE, and
(b) LOG(FLUX DENSITY IN Hα) VERSUS APPARENT V MAGNITUDE
for type 1 Seyfert gal axies using the data of Adams and Weedman (1975). NGC7603, which has highly variable Balmer line emission is shown in parentheses. Although the two parameters are correlated in (b) the relationship is clearly much less pronounced than it appears from (a) where the scaling with distance has produced a falsely strong correlation.

5-6 X-ray emission vs FWZI of Balmer lines, (B-V) and (U-B)

The quantities plotted against x-ray emission in this section do not scale with distance and so absolute luminosities must be used. The plots are shown in figs. 5-6b-c.

The blue colours of Seyfert galaxies mark them out from normal galaxies and were used by Markarian as his primary search criterion (chapter 1-2). The majority of the known Seyferts were discovered in this way. Consequently one might expect that uv-excess was some indicator of "activity" and would be correlated with x-ray luminosity. Type 1 Seyferts have a greater uv-excess than type 2 Seyferts (fig.1-5) and are also preferentially detected in our x-ray survey but figs. 5-6 a and c show no correlation with x-ray power and colour.

The Full Width at Zero Intensity (FWZI) of a line is a difficult quantity to measure. The broad Balmer wings often blend into the background smoothly so that the detectable width is a function of the signal-to-noise of the data. The widths for Hβ quoted in Table 5-1 and used in fig. 5-6a come, in some cases, from the Wampler image dissector scanner which has substantial instrumental wings on its response (see e.g. sky lines in plate I of Robinson and Wampler, 1972). These difficulties limit the usefulness of the FWZI.

It is, however, the natual measurement to make if one suggests that the x-rays in Seyfert nuclei might come from thermal shock heating (as in supernova remnants, see e.g. Gorenstein and Tucker, 1974) of two colliding, permitted line region, clouds. The temperature reached would be proportional to v^2, the relative velocity of the clouds. If the FWZI of the permitted lines is taken to be pure Doppler broadening then it should be roughly correlated with 2-10 keV emission. If NGC 5506 and NGC 1275 are not included, a weak correlation ($\approx$ 7% significance) may exist between L_x and FWZI.

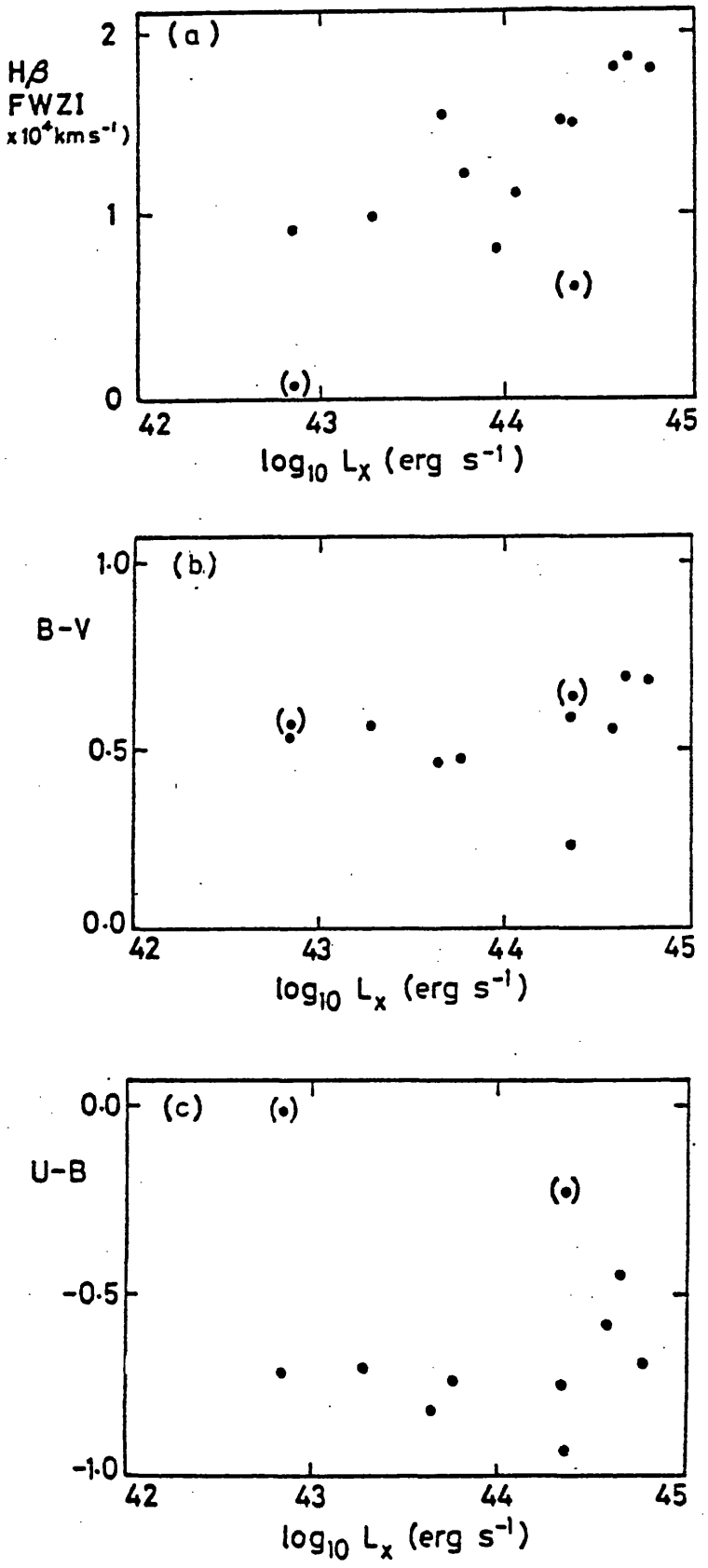

fig 5-6 PLOTS OF VARIOUS OPTICAL PARAMETERS VERSUS X-RAY FLUX DENSITY.

(a) Full width zero intensity (FWZI) of Hβ . (see also fig 7-1 b and chapter 7-1).

(b) Colour (B-V)

(c) Colour (U-B)

5-7 Location of the x-ray emission in Seyfert nuclei

The correlations noted in the previous sections give very strong evidence about the location of the x-ray emission in Seyfert nuclei. The lack of type 2 Seyferts in the list of detections is, in itself, important.

The most prominent differences between Seyfert galaxies of types 1 and 2 are the existence of broad wings on the permitted lines and a non-thermal infrared and optical continuum in Seyferts of type 1. Both of these components are believed to arise in a very compact region $\lesssim 0.1$ pc in extent (see chapter 1-4). It seems likely, therefore, that the x-ray emission is also associated with this "core" region peculiar to type 1 galaxies, rather than with the more extended region from which the forbidden lines are emitted, or from the galaxy as a whole. This conclusion is confirmed by the variability of the x-ray flux in at least three galaxies (chapter 3-4 and Table 3-2). The shortest timescales for variability are found in NGC 4151 (3 days, see chapter 6) and MCG 8-11-11 (32 days, see chapter 3-2). The x-ray emitting region in these Seyferts cannot then be larger than 3×10^{-3} pc and 3×10^{-2} pc respectively.

The strong preference for x-ray detection of type 1 galaxies contrasts with the results of radio continuum surveys in which type 2 galaxies are preferentially detected (de Bruyn and Wilson, 1976; chapter 1-3, fig. 1-7). de Bruyn and Wilson (1977) have recently argued that the radio sources, in contrast to the x-ray emission, in most Seyfert galaxies originate in a region some hundreds of parsecs in extent. Excluded from this last conclusion are objects like NGC 1275, 3C 120, 3C 390.3 and Mkn 348, which exhibit a flat spectrum, self-absorbed, very compact radio source.

For the rest, significant correlations exist between L_x and M_v, M_L, $P_{10\mu m}$ and $L_{H\alpha}$. It is important to emphasise that all four of these properties correlating with L_x are generally considered to be

associated with the "core" region ($\lesssim 0.1$ pc in extent) which is peculiar to type 1 Seyfert galaxies. Properties associated with the more extended forbidden line region, such as L([O III] λ5007 Å) and P(λ21cm) are not significantly correlated with x-ray power. Our conclusion that the x-ray emission is associated with the central "core" regions (1 and/or 2) is thus further strengthened.

chapter 6. X-RAY VARIABILITY OF SEYFERT AND RELATED GALAXIES

INTRODUCTION

Long-term x-ray variability has been reported in a small number of active galaxies. The most notable of these is Cen A (NGC 5128, 3U1322-42), which increased its flux by a factor of 1.6 ± 0.2 in only 6 day (Winkler and White, 1975). Such observations indicate that the x-ray emission from this class of active galaxy x-ray source arises in a region of extreme compactness (≈0.005 pc across). In chapter 5 it was shown that this is very probably the case for the Seyfert galaxies, independent of x-ray variability arguments.

Most previous studies of variability over a time base greater than a few weeks have been complicated by the need to compare fluxes taken from different experiments. The availability of data from the SSI covering 18 months of operation, provides an opportunity to study variability in the extragalactic x-ray sources free from these complications.

MCG 8-11-11 has already been seen to be variable from SSI data alone (chapter 3-2). In this case little could be said about the form of the variations. Three sources, however, have been particularly frequently observed by the SSI, NGC 4151, the Coma cluster and Cen A. From these observations and those of Mkn 421 (2A1102+384) some tentative generalisations can be made.

6-1 The Coma cluster (2A1257+283)

Before one can have confidence in claims to see variability in sources, particularly weak ones, with the SSI it is best to show that some similar, constant, source is clearly found to be steady using the instrument.

The pointing axis instruments on Ariel V (see chapter 2-1) control 80% of the observing time and tend to prefer observations in the galactic plane. The SSI is thus forced to scan the galactic poles very frequently. Fortunately the north galactic pole has both the Coma Cluster of galaxies and NGC 4151 near it.

Coma (3U1257+28) is known to be extended at x-ray frequencies from UHURU measurements. It is thus likely to make a good standard candle. Lea et al.(1973) determined a radius of 16 ± 3 arc min, assuming the now questionable isothermal gas sphere model (see e.g. Gull and Northover, 1975). This radius is of the same order of magnitude, however, as for the adiabatic model, and we would thus not expect variability on measurable timescales.

It should be noted, nevertheless, that limits to the flux of a possible compact central source in Coma are not stringent. The lowest available limit is 14%, in the 0.48 to 1.45 keV band using OAO Copernicus data (Griffiths et al.,1974). The strong low energy cut-offs found in many compact sources, e.g. NGC 4151 (Ives et al.,1976) make this energy range ineffective for the detection of such sources. Higher energy (1.4 - 4.6 keV) Copernicus data are compatible with a compact component as large as 30% ($\approx$4.5 UHURU ct s^{-1} in the central region of the x-ray source assuming a uniformly bright disc for the extended emission (Griffiths, private communication) . So a relatively bright compact source, possibly either of the two central cD galaxies, NGC 4874 and NGC 4889, is thus far allowed.

The observations are shown in fig 6-1 . Each flux measurement is the result of summing the orbits in a given Observing Slot (chapter 2-3), typically

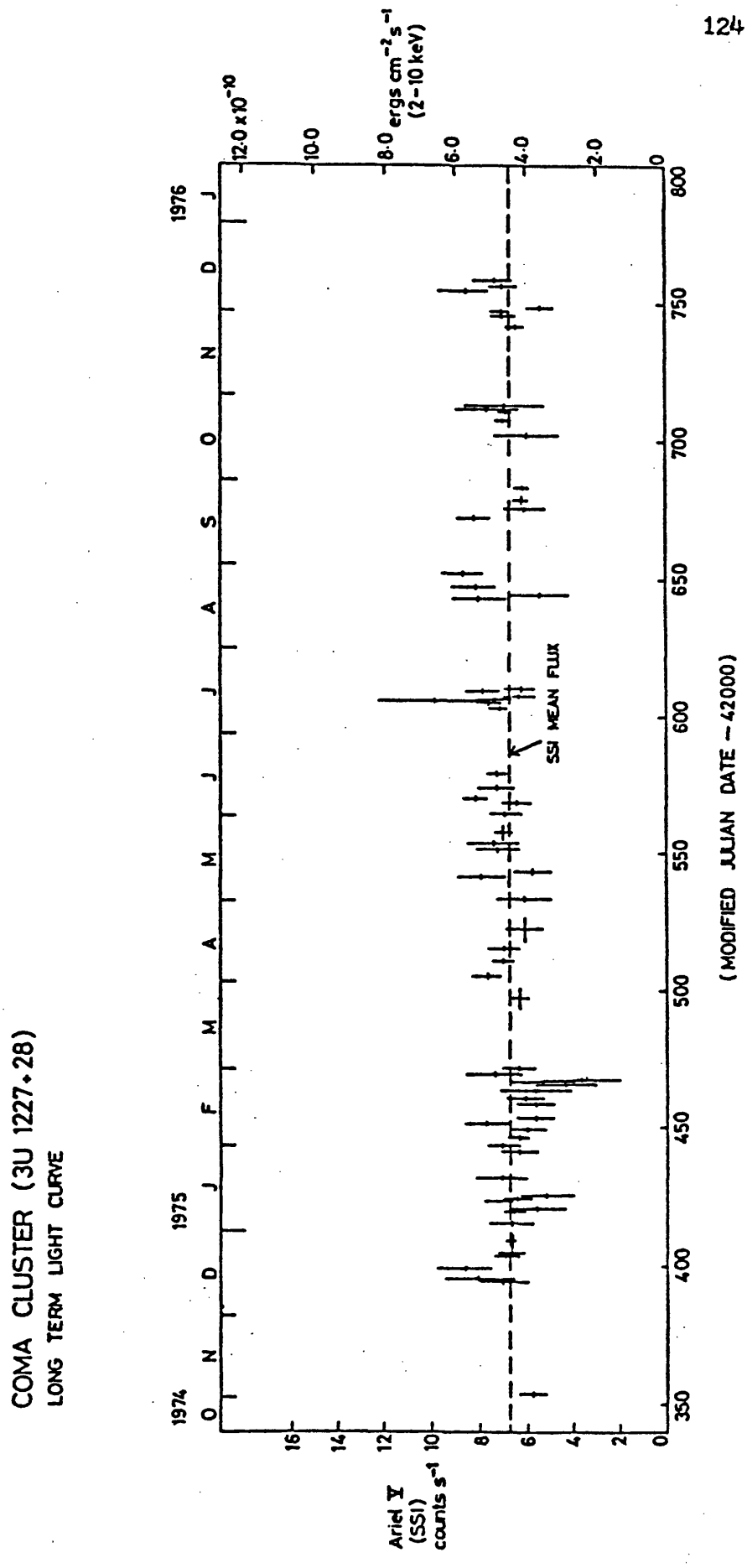

fig 6-1 ARIEL V SSI LIGHT CURVE FOR THE COMA CLUSTER.

3 day. Error bars are $\pm 1\sigma$ and apply to the Ariel V(SSI) ct s^{-1} scale. (An additional error of conversion must be allowed for on the flux density scale). All sightings of the source at a collimator transmission less than 0.45 were omitted to keep the effects of spacecraft attitude errors (estimated at 0°.2) negligible. Sightings of less than 3.0σ significance were omitted if the error on the intensity was larger than the largest error on a $>3\sigma$ sighting (see chapter 2-4). Points that were possibly affected by confusion with nearby sources were also omitted.

With the unreliable points eliminated it was then necessary to convert the instrument count rate into physical units. The spectrum of the Coma cluster as determined by the MSSL pointing axis experiment on Ariel V (Sanford and Ives, 1976). By folding this through our instrument response, and making allowance for the resolution of the SSI, the SSI count rate in terms of erg $cm^{-2}s^{-1}$ for a standard 2-10 keV range has been found. The weighted mean flux is given in Table 6-1. Allowance has been made for the errors involved in folding the data when quoting a flux in physical units.

The flux is consistent with the UHURU value (Giacconi et al, 1973).

The data was searched for variability in three ways:

(1) A simple weighted χ^2 test on the fit to a constant flux density gave a reduced χ^2 of 1.19 for 117 degrees of freedom. This is clearly consistent with a constant source. ($P(\chi^2)$, the probability of exceeding the value of χ^2 with random fluctuations on a constant source intensity, ≈ 0.15.)

(2) A weighted linear χ^2 fit was made to the data producing a linear regression coefficient of -0.17. The gradient was only 2.2σ from zero. Thus there is no evidence for a linear trend in the data. The slow gain change of the SSI over the 18 months observing time should cause a gradual change in count rate as the effective low energy cut-off is lowered. With the shape of the Coma spectrum

this implies that the count rate should increase with time. This effect has not been allowed for here since no secular change is in any case detectable at the 2σ level. At 95% confidence the upper limit to the annual rate of change is 6%.

(3) There are still some points some way from the mean count rate. If these were caused by a nearby, unnoticed, extra source, a plot of count rate against the position angle of the collimator would show them clustering at a particular value. Fig 6-2 a, shows such a plot. No such effect is seen.

It is difficult to set confidence limits for random variability on various timescales. The standard deviation of the data set is 0.57 ct s^{-1}. The mean separation of the data points in time is 6 day. Thus, roughly, at 2σ confidence Coma is not varying randomly by more than 20% on timescales from 6 day to 1 year.

Coma is thus a constant source within the limits of the data ($\lesssim$20% corresponds to $\lesssim 1.4 \times 10^{44}$ erg s^{-1} at 113 Mpc). If this is taken as an upper limit to any compact x-ray component within the cluster then such a component's absolute luminosity could still be large.

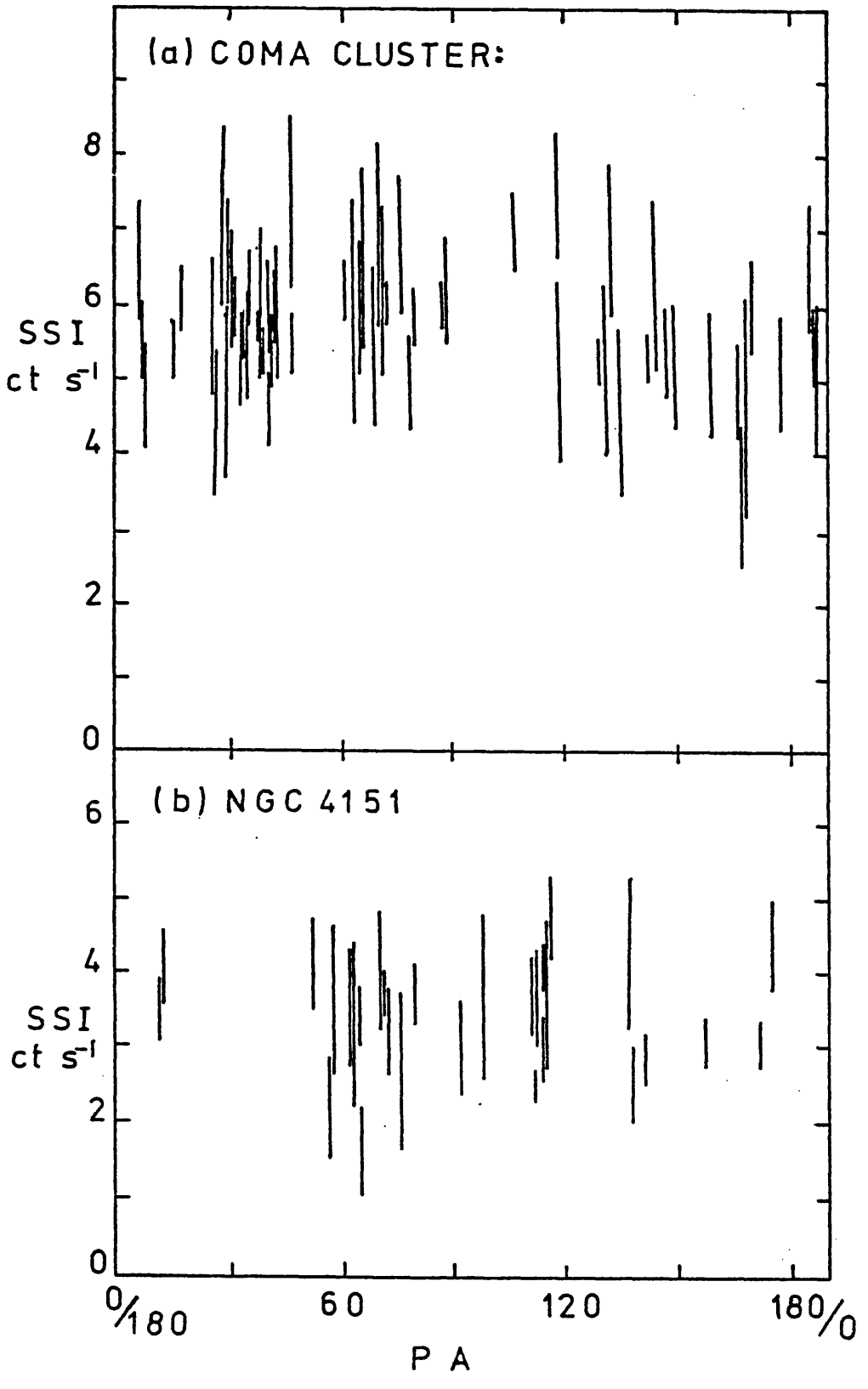

fig 6-2 SSI FLUX DENSITY AS A FUNCTION OF POSITION ANGLE FOR

(a) THE COMA CLUSTER.

(b) NGC4151.

Table 6-1 Weighted mean flux density levels for Coma and NGC4151.

Unit of flux density	Coma	NGC4151
Ariel V(SSI) ct s^{-1}:	6.74 ± 0.13	3.24 ± 0.18
photons $cm^{-2}s^{-1}$:	(8.1 ± 0.8) x 10^{-2}	(1.90 ± 0.20) x 10^{-2}
erg cm^{-2} s^{-1} :	(4.5 ± 0.5) x 10^{-10}	(1.54 ± 0.19) x 10^{-10}

6-2 NGC 4151 (2A1207+397

There is thus some justification for confidence in the reality of any variability seen by the SSI.

NGC 4151 (3U1207+39) is known to vary optically and in the infrared on timescales of 100 day (Penston et al., 1974). A change in the x-ray flux density has been reported between the 1971/2 UHURU observations (Gursky et al., 1971) and the 1974/5 Ariel V pointing experiment observations (Ives et al., 1976). The SSI data allow a search for shorter timescale changes.

The procedure followed in analysing the Coma data was applied to NGC 4151. The observations are shown in fig. 6-3.

The spectrum of Ives et al. (1976) has been used to calibrate our count rate, as before, and hence derive a mean value for the flux density about 30% below the MSSL value and ≈70% above the UHURU value. This indicates variability on a $\lesssim$100 day timescale (e.g. between point (a) and (b), fig. 6-3). However, caution should be exercised in assessing this result because of the uncertainties of conversion*.

The scatter on the SSI points is clearly greater than for the Coma cluster and repeating the χ^2 test confirms this, giving a reduced χ^2 of 3.19 for 36 degrees of freedom, which is very clearly inconsistent with a steady source ($P(\chi^2) = 0.4 \times 10^{-9}$). Dividing the data into two equal time bins (about the point "A" in fig. 6-2) and repeating the χ^2 test on each bin separately produces the result that the first time bin has a χ^2 of 1.29 for 12 degrees of freedom, whereas the second bin has a χ^2 of 3.13 for 17 degrees of freedom; thus for the first half of the observations the data is consistent with a steady source but for the second half it is inconsistent. The weighted mean count rate from this first, constant, half of the data is given in Table 6-1.

---

* The increase in cut-off found by Barr et al. (1977) reduces the (2-10) keV conversion factor for SSI ct s^{-1} by only 6%.

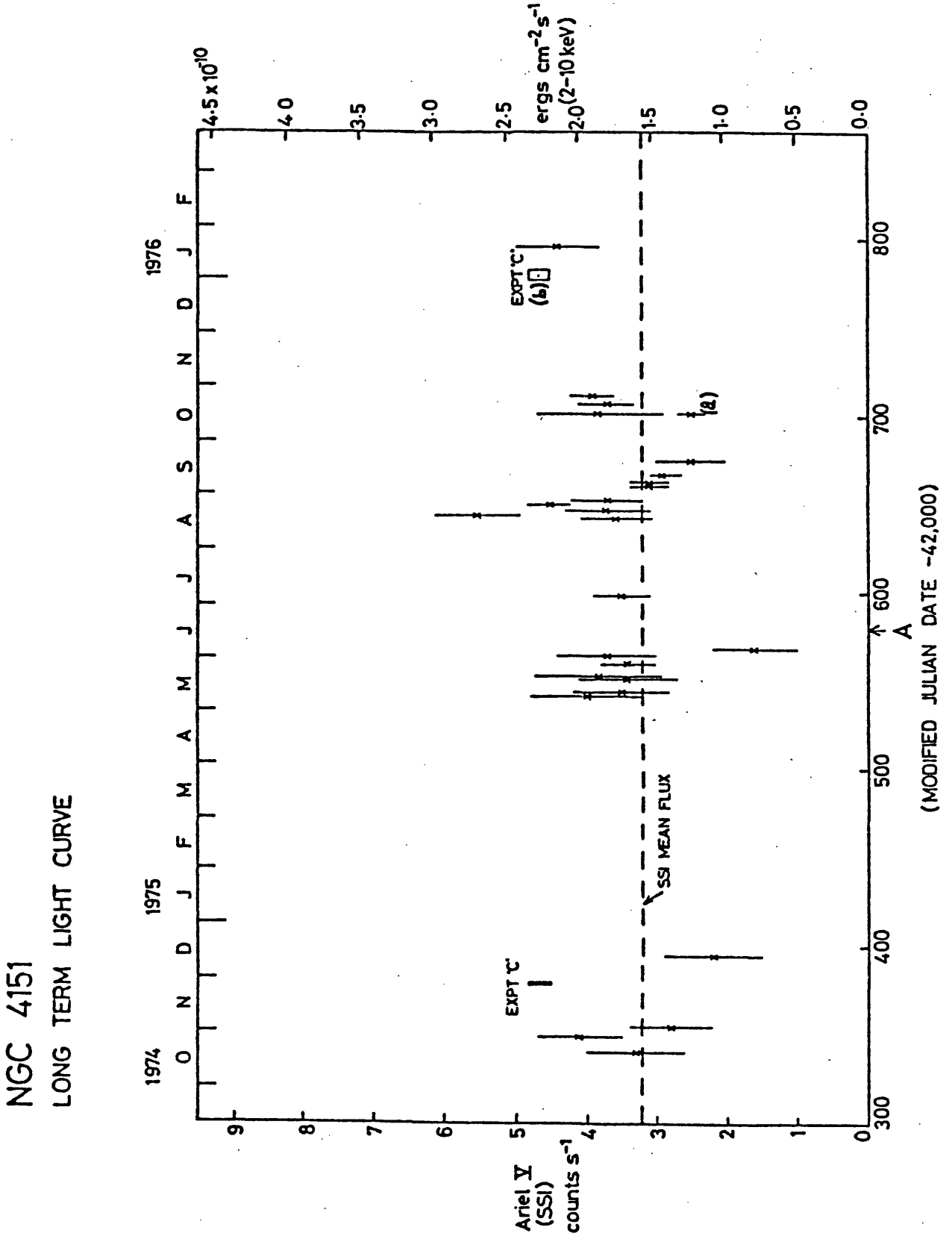

fig 6-3 ARIEL V SSI LIGHT CURVE FOR NGC4151. The boxes labelled 'EXPT C' are the measurements made with the MSSL pointing axis experiment on Ariel V (Ives et al., 1976).

Part of the second half of the data is plotted on an expanded scale in fig. 6-4. Although the number of data points is limited they clearly show evidence of a flare in August 1975, followed by a decay over the following 10 days. A careful search to find an instrumental cause for this feature gives confidence in the reality of the flare. The source increased its count rate by a factor of 1.7 ± 0.2 in a time no greater than 3 day. It is conceivable that a short-lived transient similar to 2A1102+384 (Ricketts et al., see also chapter 6-3) was confused with NGC 4151 in our detectors and caused this behaviour. The probability of such a source arising at just such a time as it would be perfectly aligned in our collimators with NGC 4151 and at no other time must be, however, extremely small. A plot of intensity vs. position angle for NGC 4151 (fig. 6-2 b), like that for Coma shows no grouping of high points.

The flare is not well-defined by our data. Nonetheless we can estimate from the light curve a lower limit on the amount of energy contained in the flare at 5×10^{47} ergs, taking a distance to NGC 4151 of 11 Mpc, and assuming that the spectrum of the flare is the same as that of the constant emission.

The maximum luminosity of the flare above the constant source level is $(1.5 \pm 0.2) \times 10^{42}$ erg s^{-1}.

The variability reported here for NGC 4151 is on a timescale two orders of magnitude shorter than implied by the previous UHURU/MSSL x-ray measurements. The data do not exclude the possibility that other flares occurred during the period covered up to ≈ 15 per year. If the flaring behaviour were this rapid it could account for the discrepency between the SSI and 'Expt.C' fluxes. At this rate the mean energy from flares over a year could reach 10% of the total energy released by NGC 4151 in x-rays over the same time.

The optical (U-band) data of Dibaiye (private communication, see fig. 1-1) shows fairly common variability on similar timescales to

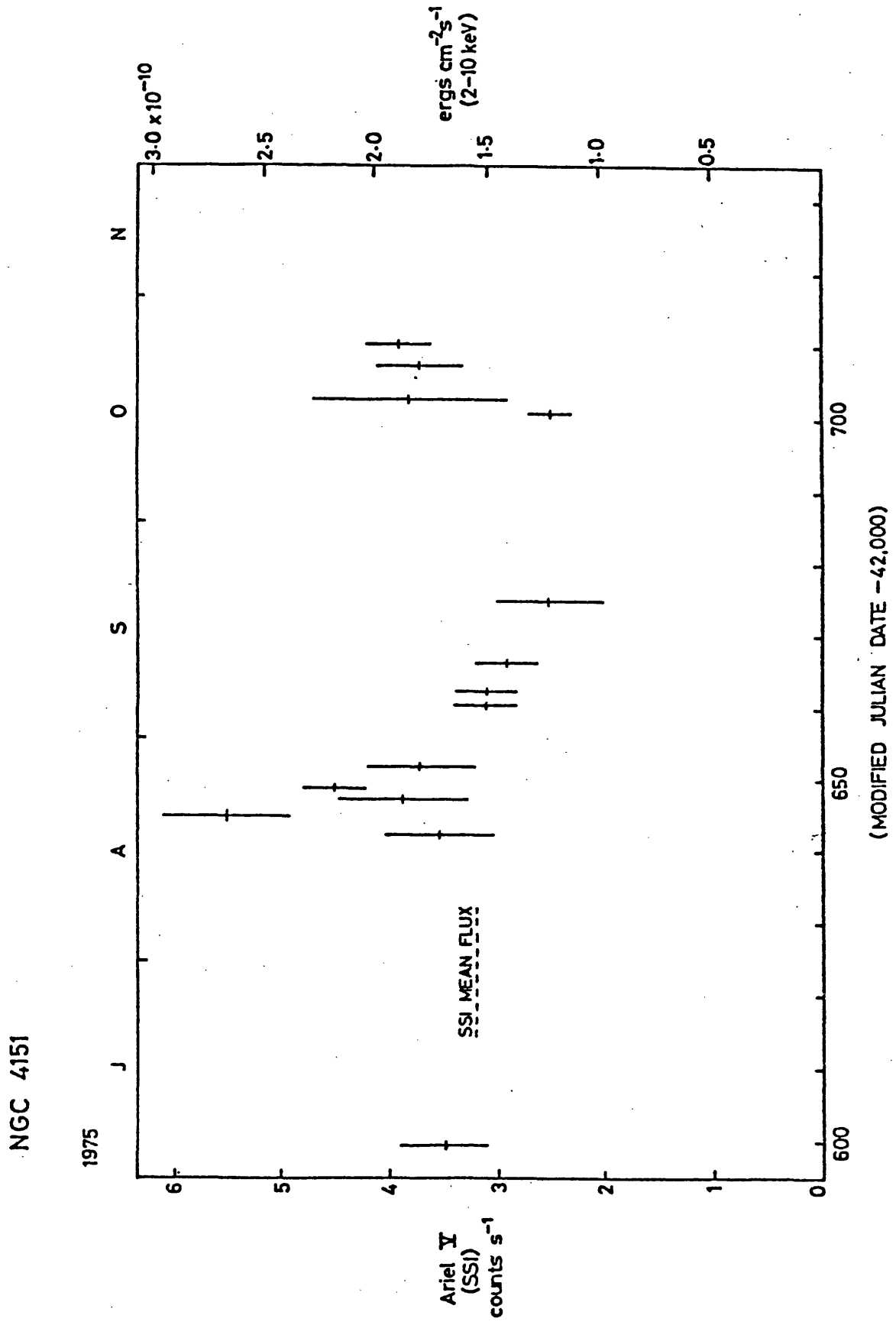

fig 6-4 A PORTION OF THE NGC4151 LIGHT CURVE OF FIG 6-3 SHOWING THE DETAIL OF THE OBSERVATIONS THAT INDICATE FLARING.

that found here. Both sets of observations can only just resolve such variations so that the comparability of the timescales could be a data artifact. Simultaneous observations will be needed to see if the two are physically connected.

We can infer from the rise time a size for the flaring region of $<8 \times 10^{15}$ cm. This is equivalent to the Schwarzschild radius for a mass of 3×10^{9} $M_{\odot}$ (see chapter 1-4). On models involving a single compact object this forms an upper limit to their mass.

Such short timescales are not easy to incorporate into models not involving a single central body. Certainly simple versions of the alternative, building block models employing supernova-formed pulsars (as in Kardashev, 1970) seem to be excluded by these observations. If one tries to identify the flare with the formation of a pulsar in a supernova then the upper limits placed on x-ray emission from observed supernovae (Canizares et al., 1974) prevent this being done. The flare in NGC 4151 produces more than 10 times too many x-rays for this model to hold. More complex building block models of the kind developed by Arons, Kulsrud and Ostriker (1975) incorporating co-operative effects within a cluster of pulsars are not excluded. The flare parameters found here are not extreme for their model.

6-3 Cen A (NGC 5128; 2A1322-427)

The nucleus of the active radio galaxy NGC 5128 (Cen A) has been detected from $\approx 10^9$ to $\approx 10^{26}$ Hz. More specifically it is known to be a source of radio, infrared, x- and γ-rays (see e.g. Grindlay, 1975, and references therein), the nucleus being obscured by dust at optical frequencies. Previous authors have shown the x-ray emission to be variable (Winkler and White, 1975, Stark et al., 1976).

Fig. 6-5 shows the earlier observations of Cen A as luminosities in the 2-6 keV band (assuming a distance of 5 Mpc, Burbidge and Burbidge, 1959). Where necessary the published fluxes have been converted to this uniform energy range using the spectral and calibration details quoted in each paper. These standardised values are in excellent agreement with those given by Grindlay et al. (1975). Even allowing for uncertainties in calibration between different instruments, the data show a clear upward trend by a factor ≈ 4 over the period 1971 to April 1973 (Fig. 6-5, points 2,3a,3b). A rapid increase by a factor 1.8 ± 0.2 over 6 days in April 1973 (fig. 6-5, points 3b,3c) (Winkler and White, 1975), implies a compact source of dimension $\lesssim 1.6 \times 10^{16}$ cm., supporting the implication of the low energy x-ray spectral cut-off (Tucker et al., 1973, Perola and Tarenghi, 1973), that the x-ray emission originates in the galactic nucleus. The positioning of the x-ray source to within 15 arc sec of the centre of the nucleus by the SAS-3 satellite (Schnopper and Delvaille, 1977) gives further support for this view.

Though there is no strong evidence for changes in the 2-10 keV spectrum with intensity variations (Winkler and White, 1975, Grindlay et al., 1975, Stark et al., 1976) the long-term intensity increase (1970-1973) appears to be greater at 10-50 keV (Winkler and White, 1975).

SSI LIGHT CURVE

The SSI measurements are also shown in fig. 6-5. They cover the period March 1975 to March 1977. The analysis procedure was the same as

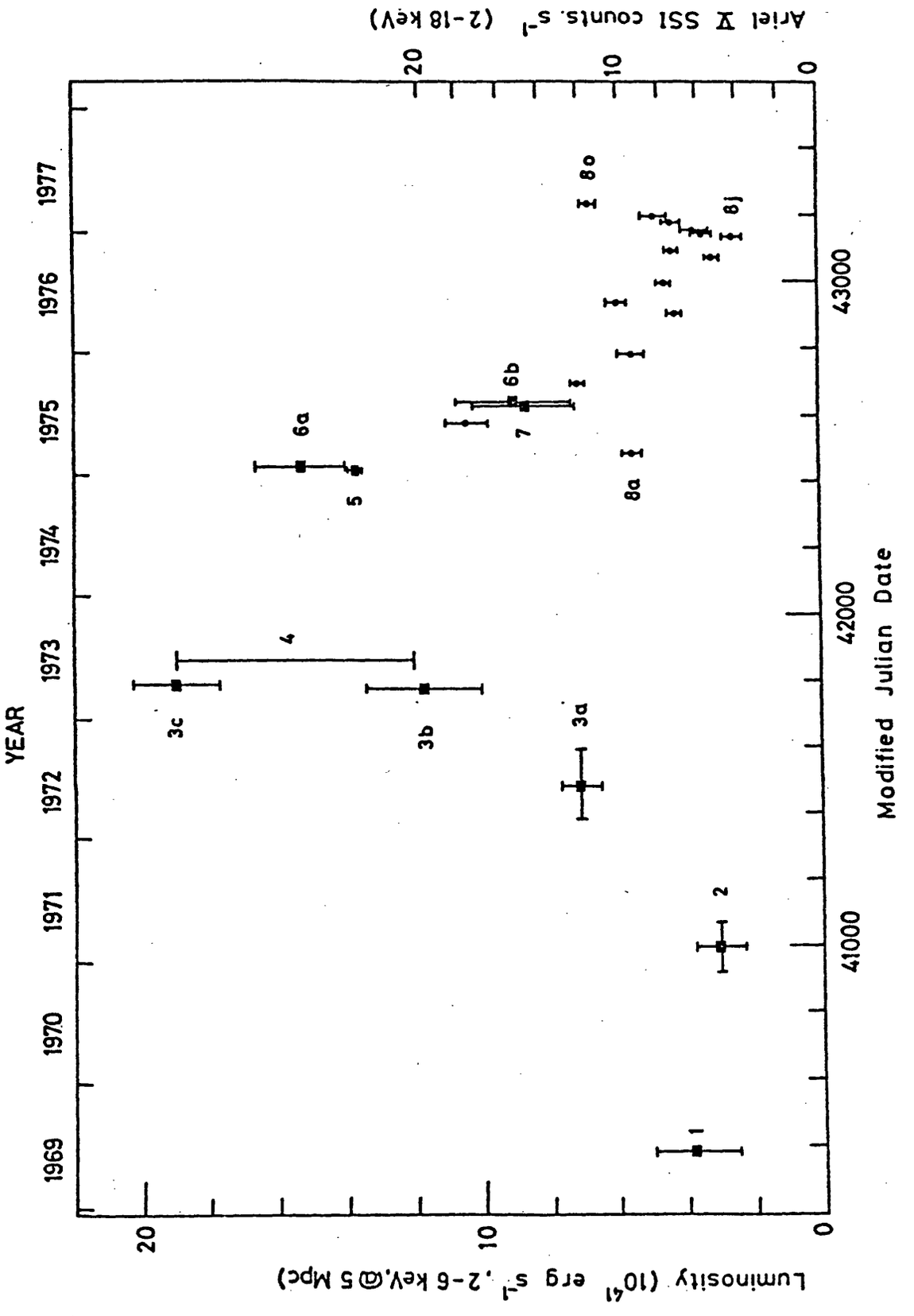

fig 6-5 LONG TERM LIGHT CURVE OF NGC5128. The filled circles (•), numbered &a-o, are SSI observations. The other numbered and lettered data points are from previous observations by many authors: (1)Bowyer et al.(1970, rocket); (2) Tucker et al.(1973, UHURU);(3) Winkler and White (1975,OSO-7); (4) Davison et al. (1975, Copernicus); (5) Stark et al. (1976, Ariel V Expt.C); (6) Grindlay et al. (1976, Copernicus).

for Coma (chapter 6-1) and NGC 4151 (chapter 6-2). Each plotted point is the result of a summation over an Observing Slot of 2 - 6 days and assumes that the position of the x-ray source is the nucleus of NGC 5128. Error bars are $\pm 1\sigma$, as for NGC 4151. The SSI counting rates are converted to luminosities according to the relation $L_{2\text{-}6keV}$ (erg s^{-1}) = 0.59 x 10^{41} x (Ariel V(SSI) ct s^{-1})$_{2\text{-}18keV}$, derived from the known spectral response of the SSI, the spectrum of Stark et al., and a distance of 5 Mpc to the source.

From the observations variability on several timescales is evident:

(1) A general downward trend, from $\approx 1 \times 10^{42}$ erg s^{-1} in mid-1975 (in good agreement with the nearby Copernicus point,7, and ANS point, 6b), to $\approx 3 \times 10^{41}$ erg s^{-1} in December 1976. This lower value being the discovery and UHURU level. The e-folding time for this decay is $\approx$ 1 year.

(2) Faster intensity variations on timescales of weeks to months, indicated by the scatter of points 8a-8o. Least squares fits of the data points 8b to 8i to a linear trend and an exponential trend yield χ^2 values of 96 and 83 respectively, with 6 degrees of freedom. The corresponding standard deviations of the data about the fitted trends are 2.2 and 1.8 Ariel(SSI) ct s^{-1}.

(3) An approximately linear intensity rise from 4.2 ± 0.5 Ariel V(SSI) ct s^{-1} on 18 December 1976 to 11.4 ± 0.4 Ariel V(SSI) ct s^{-1} on 26 March 1977 (points 8j to 8o). These data points are well fitted by a linear trend with slope 0.07 Ariel V(SSI) ct s^{-1} day^{-1}.

(4) To search for variability on still shorter timescales the SSI data has been subdivided in intervals of $\approx \frac{1}{2}$ day. For each data set (i.e. each SSI data point in fig. 6-5) a least squares fit of both a constant intensity and a linear intensity trend have been

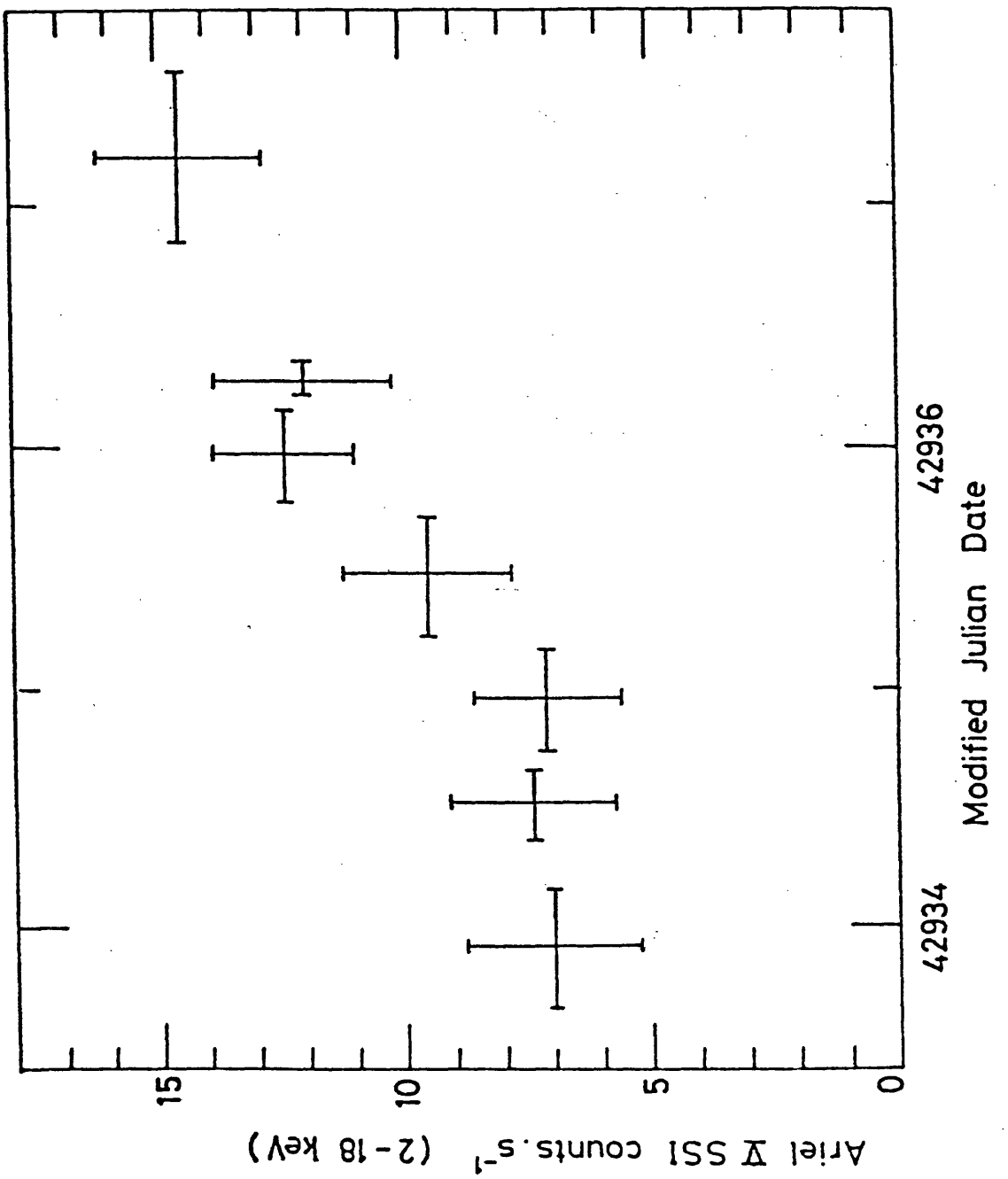

fig 6-6 ARIEL V LIGHT CURVE OF NGC5128 DURING THE CONTINUOUS OBSERVATION OF 4 to 8 June 1976, AVERAGED OVER ~0.5 DAY INTERVALS.

performed. After allowing for possible small systematic errors in intensity determination (e.g. small attitude drifts), a significant short-term variation is found during one observation (point 8f) taken from 4-8 June 1976 (i.e. MJD 42933.6 to 42937.6). This higher resolution plot is shown in fig. 6-6 and displays an intensity increase similar to that reported by Winkler and White, though on a slightly shorter timescale. Averaging over one day intervals centered on MJD 42934.06 and 42936.03 gives 'base' and 'peak' level intensities of 6.7 ± 1.2 and 12.1 ± 1.1 Ariel V(SSI) ct s^{-1} respectively, an increase of a factor 1.8 ± 0.4 in about 2 day. For the remaining data sets, intensity variations are $< 58\%$ (at about the 2σ limit, for timescales of 0.5 to 6 day). Since the intensity had decreased to 7.6 ± 0.3 Ariel V(SSI) ct s^{-1} by MJD 42990, it is evident that the whole 'flare' lasted $\gtrsim$ 2 day and $<$ 56 day. Since only one rapid increase is seen in a total of 46 day observation, we may estimate very roughly that such variations occur at a mean frequency $\lesssim 8$ per year.

INTERPRETATION

From the July 1975 Copernicus data, Stark et al. tentatively suggested that the x-ray flux from NGC 5128 might be returning to the pre-1972 level measured by UHURU (Tucker et al., 1973). The SSI observations clearly confirm this general fall and show that indeed the flux had declined to the pre-1972 state by the end of December 1976. This was followed by a general increase over the next 3 month (to the end of March 1977). In addition a second example of a rapid intensity increase on a timescale of a few days has been seen.

It is clearly of interest to attempt to establish any characteristic timescales from NGC 5128 over the period covered by fig. 6-5. The sparse data sampling limits the justification of any

speculation; however linear interpolation between the data points produces an unlikely step shape. The interpolation put forward here instead is of the form shown in fig. 6-7. That is, a 'slow outburst' with superimposed 'flares'. The light curve could be interpreted as a series of flares superimposed on a constant base level, the apparent envelope being a sampling accident. This seems unlikely given the trends (1) and (3) above, although a quantitative evaluation is difficult.

(1) Slow Outburst. The light curve exhibits an apparent envelope from point 2 through to point 8j (excluding point 3c) - a 'slow outburst' of total 'rise and fall' timescale T_{so}, $4 < T_{so} < 7$ year. The e-folding decay time is $\approx$ 1 year.

(2) Flaring Activity. Short rise times of the order 5 day are seen. That such short timescale activity is common is evidenced by the scatter of points 8a-8j. Unfortunately, no complete rise and fall is observed by one experiment. However, an idea of the total timescale involved, T_f, may be obtained by identifying points 5 - 6a - 8a with such a flare:

(a) Point 5 is 2 day long with no significant variability at 29% (3σ upper limit, Stark et al., 1976). Point 6a (Grindlay et al.) is consistent up to 11 day after this. If, then, point 5 was preceded by an intensity rise similar to that seen by Winkler and White or reported here then $T_f > 2 + 11 + 6 = 19$ day.

(b) Point 8a is 30 days after point 6a, so $T_f < 50$ day. Thus $19 < T_f < 50$ day if this flare is a typical example. The e-folding decay time is ≤ 40 day.

While flaring activity implied by the new SSI data is of smaller amplitude than examples in earlier observations, the increase relative to 'outburst level' is about the same ($\approx$ a factor 2). This could be due to

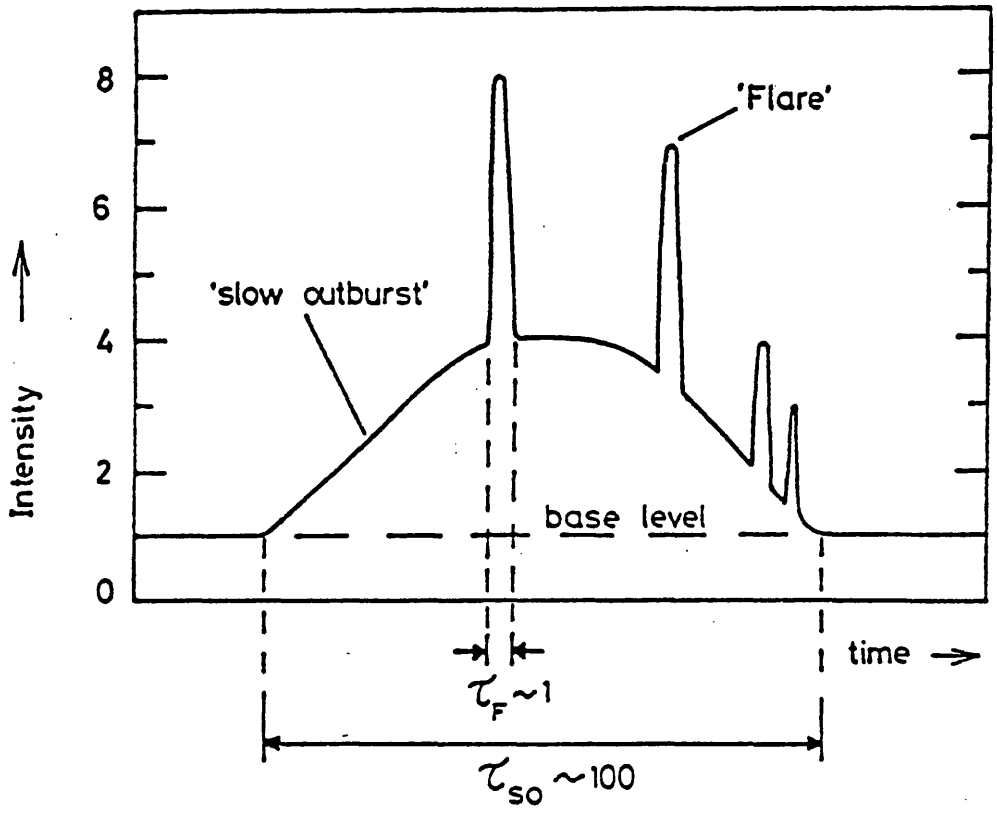

fig 6-7 SCHEMATIC LIGHT CURVE FOR NGC5128 X-RAY VARIABILITY.

observational selection, but if real, such a correlation would imply a physical association between the sources of the slow outburst and the flares. More sensitive and frequent observations over the next few years will be needed to determine whether flares occur only during a slow outburst, or are a normal feature of the source's behaviour.

It is instructive to speculate on the possible nature of the power source in the nucleus of NGC 5128. For example, if the 'slow outburst' were thought of as the result of a star being tidally disrupted and accreted by a massive black hole (see Hills, 1975), then the energy released as 2-10keV x-rays, assuming a star of one solar mass, would require a conversion efficiency of only 10^{-4} Because the x-ray spectrum is hard and extends at least up to 2 MeV (Hall et al., 1976, Grindlay, 1975) we should increase this estimate by a factor ≈ 5. Nevertheless, the mass required to be converted into energy to explain <u>all the emission</u> (slow outburst, flares, and base level) is still small.

6-4 Comparison of Variable Extragalactic x-ray sources

If fig. 6-7 is taken as a fair representation of the x-ray behaviour of NGC 5128 it may be instructive to make comparisons with other variable extragalactic x-ray sources. Of the 6 sources in active galaxies which are bright enough for variability to be observed with Ariel V and contemporary satellites, and which are not buried within extended x-ray clusters, only NGC 5506 has not yet been observed to vary. Given the sparseness of the data, this indicates that rapid variability is a characteristic of active galaxy x-ray sources. For 3C 390.3 (Charles et al., 1975) and 3C 273 (White et al., 1977) little more can be said than that they vary on a timescale of 1 - 2 years. For MCG 8-11-11 this timescale is $\approx$ 32 day.

For NGC 4151 (Ives et al., 1976 and chapter 6-2) and Mkn 421 (a BL Lac object, Ricketts et al., 1976) a more detailed comparison with NGC 5128 is possible.

NGC 4151 has been less well studied than NGC 5128 but it appears to fit the same general scheme, doubling its flux in the two years between the UHURU (Giacconi et al., 1974) and the Ariel V observations, during which it remained overall constant, and revealing at least one flare (see chapter 6-2), on a timescale of a few days. The mean level of the source may now have been seen to decay to its UHURU value (Barr et al., 1977).

A third source enables a closer comparison to be made. The identification of the BL Lac object Mkn 421 with the 'transient' x-ray source 2A1102+384 is strengthened by a new error box from the 2A catalogue (fig. 6-8). Its light-curve shows the same division into 'slow outburst' and 'flare' (fig. 6-9) that is seen for NGC 5128. There is some suggestion of a second flare in the decline of the slow outburst. For Mkn 421 both T_{so} and T_f are $\approx$ 1/100 of their values for NGC 5128.

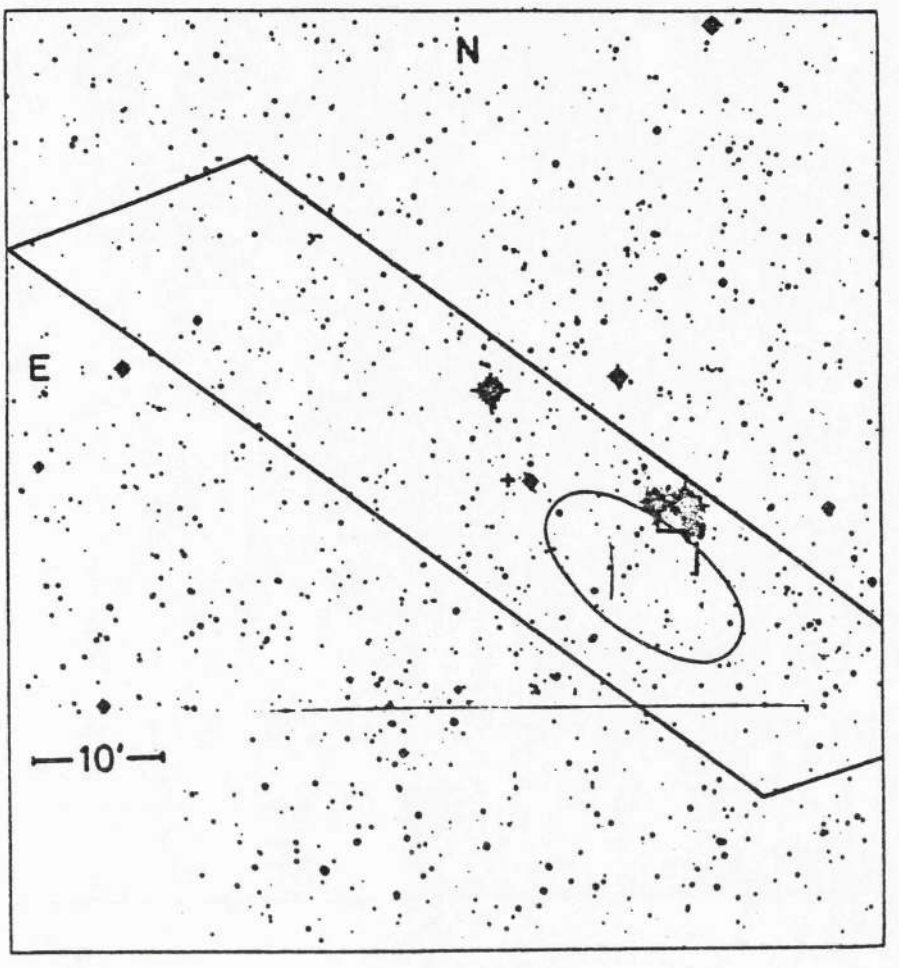

fig 6-8 DISCOVERY (Ricketts et al., 1976) AND '2A' ERROR BOXES FOR 2A1102+384. THE LACERTID MKN421 IS INDICATED (-,).

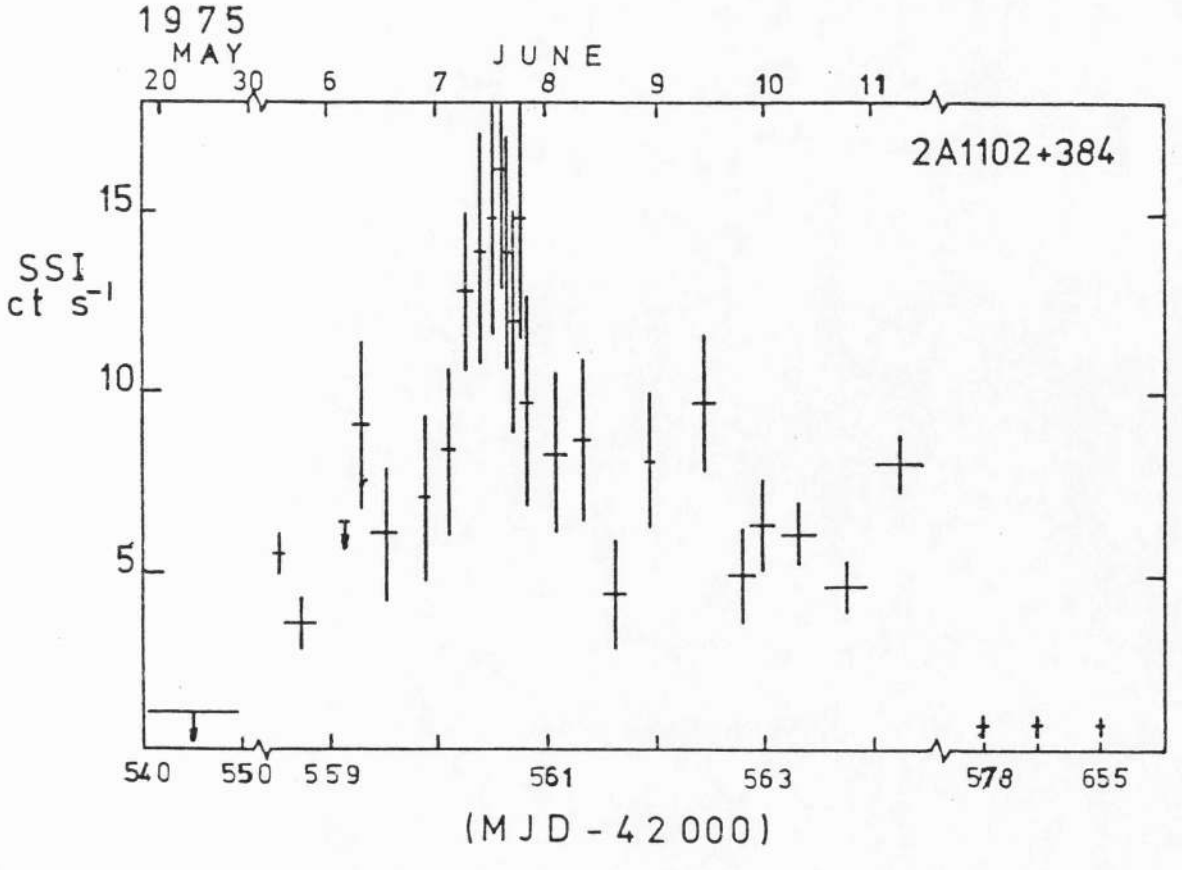

fig 6-9 SSI LIGHT CURVE FOR 2A1102+384 (= Mkn 421 ?).

Table 6-2 Comparison of variable extragalactic x-ray xources.

Source	timescale (days)		increase over 'normal' Flux			total energy (ergs)		
	"Slow outburst" τ_{SO}	"Flare" τ_F	"slow outburst"	"Flare"	total	"slow outburst"	"Flare"	
NGC5128	~ 2000	~ 20	4	1.6	7	3×10^{50}	1×10^{47}	Radio Galaxy
Mkn 421[a]	~ 30	1	6	2.5	16	2×10^{51}	3×10^{49}	BL Lac Object
NGC4151[b,c]	> 1400	~ 10	2	1.7	3.4	$> 10^{50}$	5×10^{47}	Seyfert Galaxy

References

(a) Ricketts et al. (1976)

(b) Elvis (1976)

(c) Ives et al. (1976)

Since an absorption line redshift from the underlying galaxy is available (Ulrich et al., 1975, Wills and Wills, 1974) the total energy in the slow outburst and flare can be estimated. These estimates are given in Table 6-2.

Table 6-2 also gives the values of these quantities for NGC 5128 and NGC 4151. The x-ray energy in the 1-day flare in Mkn 421 is some 300 times that in the ≈ 10-day flares in NGC 5128 and NGC4151. Thus for these sources the timescale and energy content of the x-ray flares appear inversely related.

These intercomparisons are obviously only a first attempt to bring order to the variability of x-ray active galaxies. It is interesting, but probably not significant, that Dibaiye has produced a schematic light curve identical to fig. 6-7 to characterize the long-term optical variability of Seyfert galaxies (e.g. fig. 1-1). There is no satellite under construction or in orbit which will be capable of recording the long term variability of these weak x-ray sources with improved quality. We must rely on the comparison of data from many different satellites to make these variations clear.

chapter 7. DEVELOPMENTS

7-1 Other relevant x-ray results

The sample of known x-ray Seyferts is not static. New identifications are made continually. The group of 15 used for the main body of work in this thesis has already (in less than a year) expanded to some 22. The conclusions established in the preceding chapters have not yet been invalidated by these new sources. The results have, rather, been extended.

This section describes the new work and its relation to that which went before.

NEW SEYFERT IDENTIFICATIONS

The six new x-ray Seyferts so far found have resulted from a variety of work.

The UHURU workers, prompted to some extent by the 2A results, have applied a version of the PST to their data and produced a list of Seyfert detections. This was largely possible due to their devising a method of analysing the UHURU spacecraft attitude for the large amount of data which lacked star sensor readings. This ability resulted in a "Fourth UHURU Catalogue of X-ray sources" (Forman et al., 1978) which possessed much improved completeness at low intensity levels. As expected (from the suggestion in chapter 3-3) many Seyfert galaxies were thus found.

The UHURU list of x-ray Seyferts (Tananbaum et al., 1978) contains sightings of 5 Seyferts seen by the SSI (NGC 3783,4151,5548,7469,* MCG 8-11-11), 2 Seyferts not seen by the SSI but already known as x-ray emitters (3C 120,390.3) and 2 Seyferts not previously seen at x-ray wavelengths (Mkn 335.541). Mkn 6 was reported in the 4U catalogue

---

* see footnote @ to Table 3-3.

(as 4U 0638+74) but failed to give a significant PST signal. It was thus dropped from the list of Tananbaum et al. although the lack of a PST peak may only indicate variability.

The rotation modulation collimator on board the SAS-3 satellite has produced ≈1 arcmin radius 90% confidence error circles for some weak 2A and 4U sources and has thus enabled the identification of 3 more Seyfert galaxies as x-ray sources. 3C 120 (Schnopper et al., 1977) was discovered before the 4U catalogue was produced. MR 2251-178 was found in the SSI error box of 2A2251-179 (Ricker et al., 1978a) and another Seyfert has been found in the box of 4U 0241+62 (Apparao et al., 1977). These last two may be quasars rather than Seyferts since high quality spectra and direct photography are not yet available. This uncertainty could be taken as a demonstration of the essential continuity between the two classes. (Such an inference could be misleading, see chapter 1-1).

Finally the joint Leicester/AAT identification program has continued to yield results. 2A0120-591 has been identified with ESO113-IG45 (Holmberg et al., 1975; = 'F-9', Fairall, 1977; Ward et al., 1978) and 2A2302-088 with MCG 2-58-22 (Vorontsov-Velyaminov, 1962; Ward et al., 1978).

These new identifications are listed in Table 7-1 which is as complete a list of x-ray Seyferts as can be compiled to date. (Table 7-2 lists all other active galaxy identifications to date.) All the Seyferts for which a Khachikian-Weedman type (see chapter 1-3) is certain are still type 1. The correlation of x-ray luminosity with optical continuum (V) magnitude (chapter 5-3) still holds good and the correlation with FWZI of Hβ (chapter 5-6) is strengthened, particularly by the addition of MCG 2-58-22 (fig. 7-1 b). Figs. 7-1 a,b, have also been modified to allow for:

(1) The variability in NGC 4151. The higher value should now be emphasised as it may reflect an unchanging, underlying flux which is modified by a varying N_H (Barr et al., 1977, see below).

(2) A reduction in the estimate of x-ray flux density originating from the nucleus of NGC 1275 to $\lesssim 6\%$ of 3U316+43 from measurements made by the scanning modulation collimater on HEAO-1 (Schwartz J. et al., 1977).

The detection of a Seyfert/quasar in the box of 4U0241+62 at a galactic latitude of $+2^{\circ}.4$ points up the fact that, based on the 2A source counts (Warwick and Pye, 1978) we expect some 33 extragalactic x-ray sources at $|b| < 10^{\circ}$ down to 1 UHURU ct s^{-1}. Without at least as good error boxes as those produced by the SAS-3 rmc a search for these elusive sources is likely to be extremely arduous.

One Seyfert at less than 10° from the galactic plane has been suggested as an identification for a 3U source, :- 3C 111. It lies at $b = -8^{\circ}.8$. Fig. 7-2 shows the 3U, 4U, and SSI error boxes in the region of 3C111. The SSI box is made up of 4 LOP (shown as dotted lines in fig. 7-2). Three of these are consistent with the source being at 3C111 but the fourth seems to rule this out. To base such a conclusion on one line alone is unwise but the orientation of the 4U box suggests the SSI position may well be correct. Mushotzky et al. (1977a) may have detected high energy x-rays (20-50 keV) from the 3C111 region using OSO-7.

The optical continuum flux density distributions for three of the new Seyferts in 2A boxes are shown in fig. 7-3. It is noticeable that they cannot be well fitted by a simple combination of power-law spectra, in contrast to the generally accepted belief for type 1 Seyferts (chapter 1-3). Such observations might favour models of accretion onto compact objects where the flow is irregular or turbulent, against those employing a steady accretion disc. Some type 1 Seyferts do possess, very clearly, power-law spectra, so that such an emphasis may be premature.

Table 7.1 All X-ray Seyferts (25/1/78)

Object	Status	X-ray name	cz(km s^{-1})	F_x(SSI ct s^{-1}) (2-10 KeV)	L_x*(erg s^{-1})	Var ?	Ref.
III Zw 2	S	S0000 +107	26,930	0.88 ±	1.5×10^{45}		[1]
Mkn 335	?E	4U0005 + 20	7,500	0.56 ± 0.19	7.8×10^{43}		[2]
ESO113-IG45		2A0120 - 591	13,970	0.5 ± 0.1	2.2×10^{44}		[3]
0241 + 61	?Q/S	4U0241+61	13,200	0.61 ±	2×10^{44}		[4]
NGC1275		2A0316 + 413	5,920	1.11 ±	7×10^{43}		[5]
3C120	S	4U0432 + 05	9,900	1.1 ±	2.3×10^{44}		[7,2]
MCG8-11-11		2A0551 + 466	6,150	1.0 ± 0.1	8.5×10^{43}	YES	[8]
Mkn 376		2A0710 + 451	16,800	0.6 ± 0.1	3.8×10^{44}		[6]
Mkn 79		2A0738 + 498	6,580	0.6 ± 0.1	5.9×10^{43}		[6]
NGC3227	?I	A1021 + 198	1,000	0.6 ± 0.1	1.3×10^{42}		[6]
NGC3783		2A1135-- 373	2,740	1.1 ± 0.1	1.9×10^{43}		[9]
NGC4151	S	2A1207 + 397	990	3.2 ± 0.1	7.1×10^{42}	YES	[10,11,2,12]
IC4329A	S	2A1347 - 300	4,140	1.7 ± 0.2	7.5×10^{43}		[6]
Mkn 279		2A1348 + 700	9,220	0.9 ± 0.2	1.7×10^{44}	YES	[2]
Mkn 541	S	4U2351 + 06	12,560	0.23 ± 0.09	8.3×10^{43}		[2]
NGC5548		2A1415 + 255	4,990	0.8 ± 0.1	4.5×10^{43}		[6]
3C390.3		4U1847 + 78	17,100	0.7 ± 0.1	5.9×10^{44}	YES	[13,2]
ESO141-G55		2A1914 - 589	11,070	0.4 ± 0.1	1.1×10^{44}		[3,6]
NGC6814	?I	2A1938 - 105	1,590	0.7 ± 0.1	4.0×10^{42}		[6]
Mkn 509		2A2040 - 115	10,650	0.9 ± 0.1	2.3×10^{44}		[6]
MR2251-178	?Q/S	2A2251 - 179	20,400	0.8 ± 0.1	5.0×10^{44}	YES	[14,15]
NGC7469	S	2A2259 + 085	5,020	1.1 ± 0.1	6.5×10^{43}		[6,15]
MCG2-58-22		2A2302 - 088	14,240	1.1 ± 0.1	5.0×10^{44}		[3]

Source existence in doubt ?E SAS-3 rmc (~ 2 arc min dia) error box S

Source identification in doubt ?I * H_0 = 50 km s^{-1} Mpc^{-1} Possibly a quasar ?Q

Table 7.2 Other Active Galaxy X-ray Sources (25/1/78)

Object	Status	X-ray name	cz(km s^{-1})	F_x(2-10 KeV) (SSI ct s^{-1})	L_x*(erg s^{-1})	Var ?	Type	Ref
NGC5506	S	2A1410-029	1820	1.3 ± 0.2	1.0×10^{43}	YES	hexelg	[1]
NGC2992		2A0948-140	2200	1.6 ± 0.1	1.8×10^{43}		hexelg	[2]
NGC7582		2A2315-428	1470	0.7 ± 0.1	3.5×10^{42}	YES	hexelg	[2]
NGC1365	?I	A0331-369	1571	0.3 ± 0.06	2.0×10^{42}		hexelg	[2]
M82	?I	2A0954+700	(150)	0.7 ± 0.1	2×10^{40}		? hexelg	[2]
3C273		2A1225+022	47,400	1.4 ± 0.2	8.0×10^{45}	POSS[3]	quasar	
Cen A(NGC5128)	S	2A1322-427	(250)	~ 5.0	$\sim 10^{42}$	VERY[4,5]	radio galaxy (lobes[7])	[6]
Mkn421	?I	2A1102+384	93,000(?)	~ 10	$\sim 2 \times 10^{46}$	VERY	Lacertid	[8]
Mkn501	?I	4U1651+39	10,200(?)	< 0.8	$\sim 2 \times 10^{44}$	POSS	Lacertid	

(* H_o = 50 Km s^{-1} Mpc^{-1})

'hexelg' = high excitation emission line galaxy

Lacertid = BL Lac type object

Source identification in doubt ?I

References for Table 7.1

1. Schnopper H.W. and Cash W. IAUC 3154.

2. Tananbaum H., Peters G., Forman W., Giacconi R., Jones C., Avni Y. submitted to Ap.J.Letters.

3. Ward, M.J., Wilson A.S., Penston M.V., Elvis M., Maccacaro T., Tritton K.P. submitted to Ap.J.Letters.

4. Apparae et al. IAUC 3150.

5. Schwartz J. et al. 1977 BAAS 9 no.4, part 2, p558, 03.03.10.

6. Elvis M., Maccacaro T., Wilson A.S., Ward M.J., Penston M.V., Fosbury R.A.E., Perola G.C., chapter 3, 1978, MNRAS, 182.

7. Schnopper H.W., Epstein A., Delvaille J.P., Tucker W., Doxsey R.E., and Jernigan G. Ap.J. 215, L7 (1977).

8. Ward M.J., Wilson A.S., Disney M.J., Elvis M., Maccacaro T., 1977, Astr. Ap., 59, L19, Cn 3.

9. Cooke B.A., Elvis M., Maccacaro, T., Ward M.J., Fosbury R.A.E., Penston M.V., 1976, MNRAS, 177, 121P.

10. Ives J.C., Sanford P.W., and Penston M.V., 1976, Ap.J.207, L159.

11. Elvis M., 1976, MNRAS, 177, 7P.

12. Barr P., White N.E., Sanford P.W., Ives J.C., 1977, 181, 43P.

13. Charles P.A., Longair M.S., Sanford P.W., 1975, MNRAS, 170, 17P.

14. Ricker G.R., Doxsey R.E., Dower R.G., Jernigan J.G., Delvaille J.P., MacAlpine G.M., Hjellming, P.M., 1978, Nature, 271, 35.

15. Cooke et al. : 2A catalogue (Appendix A), 1978, MNRAS, 182, 489.

References for Table 7.2

1. Ricker G.R., Dower R.G., Jernigan J.G., Doxsey R.E., Bradt H.V., Schnopper H.W., 1978, submitted to Ap.J.Letters.

2. Ward M.J., Wilson A.S., Penston M.V., Elvis M., Maccacaro T., Tritton, K.P., 1978, submitted to Ap.J.

3. White G.J. and Ricketts M.J.

4. Lawrence A., Pye J.P. and Elvis M., 1977, MNRAS 181, 93P.

5. Mushotzky R.E., Serlemitsos P.J., Becker R.H., Boldt E.A., Holt S.S., 1978, preprint.

6. Delvaille J.P., Epstein A., Schnopper H.W., 1978, Ap.J. 219, L81.

7. Cooke B.A., Lawrence A. and Perola G.C., 1978, MNRAS 182.

8. Ricketts M.J., Cooke B.A. and Pounds K.A., 1976, Nature 259, 546.

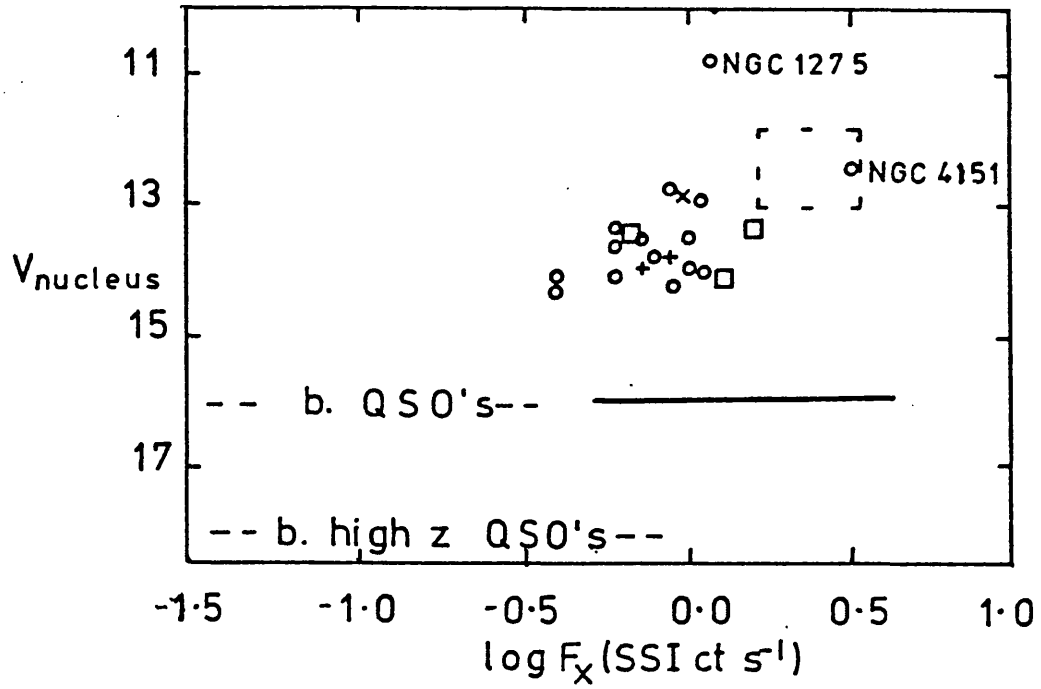

fig 7-1 (a) PLOT OF APPARENT V MAGNITUDE OF ACTIVE GALAXY NUCLEI VERSUS LOG(X-RAY FLUX DENSITY). Seyferts are marked o ; hexelgs □ ; Lacertids + ;quasars (3C273) x . The known range of variability of NGC4151 is indicated by the dashed rectangle. The solid horizontal line shows the depth to which the optical searches for emission line objects can be considered complete. '—b. QSO's—' indicates the m_v at which considerable numbers of bright quasars begin to be found. '— b. high z QSO's —' shows the corresponding m_v for z>2.5 quasars

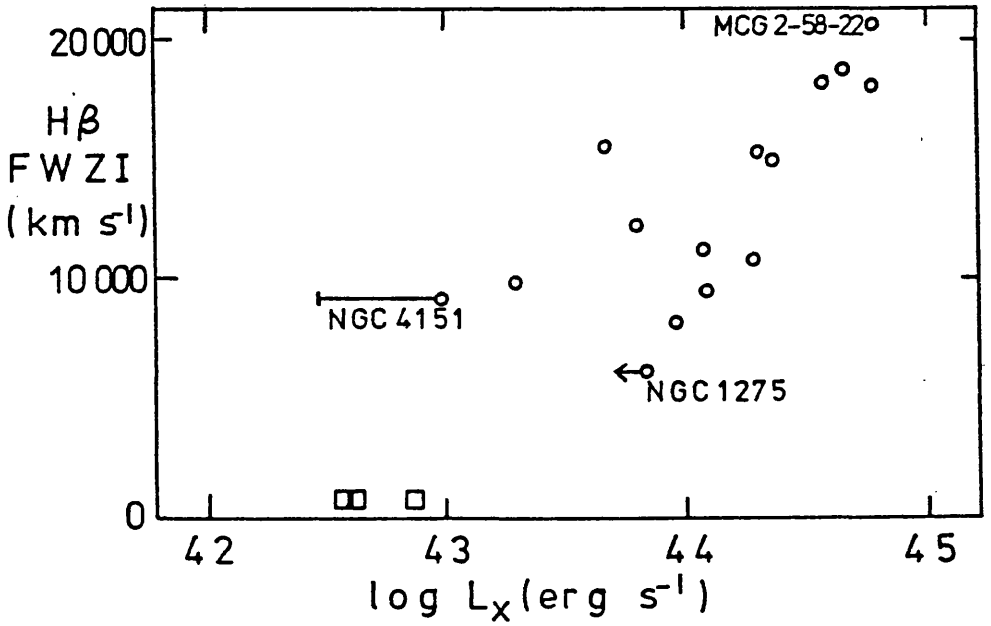

(b) PLOT OF Hβ FWZI AGAINST LOG(X-RAY LUMINOSITY). Seyferts are marked o ; hexelgs □. NGC4151's known range of x-ray variability is shown as ⊢——o, the upper end being probably more important (see text.) NGC1275 is shown as an upper limit from HEAO-1 obeervations (see text).

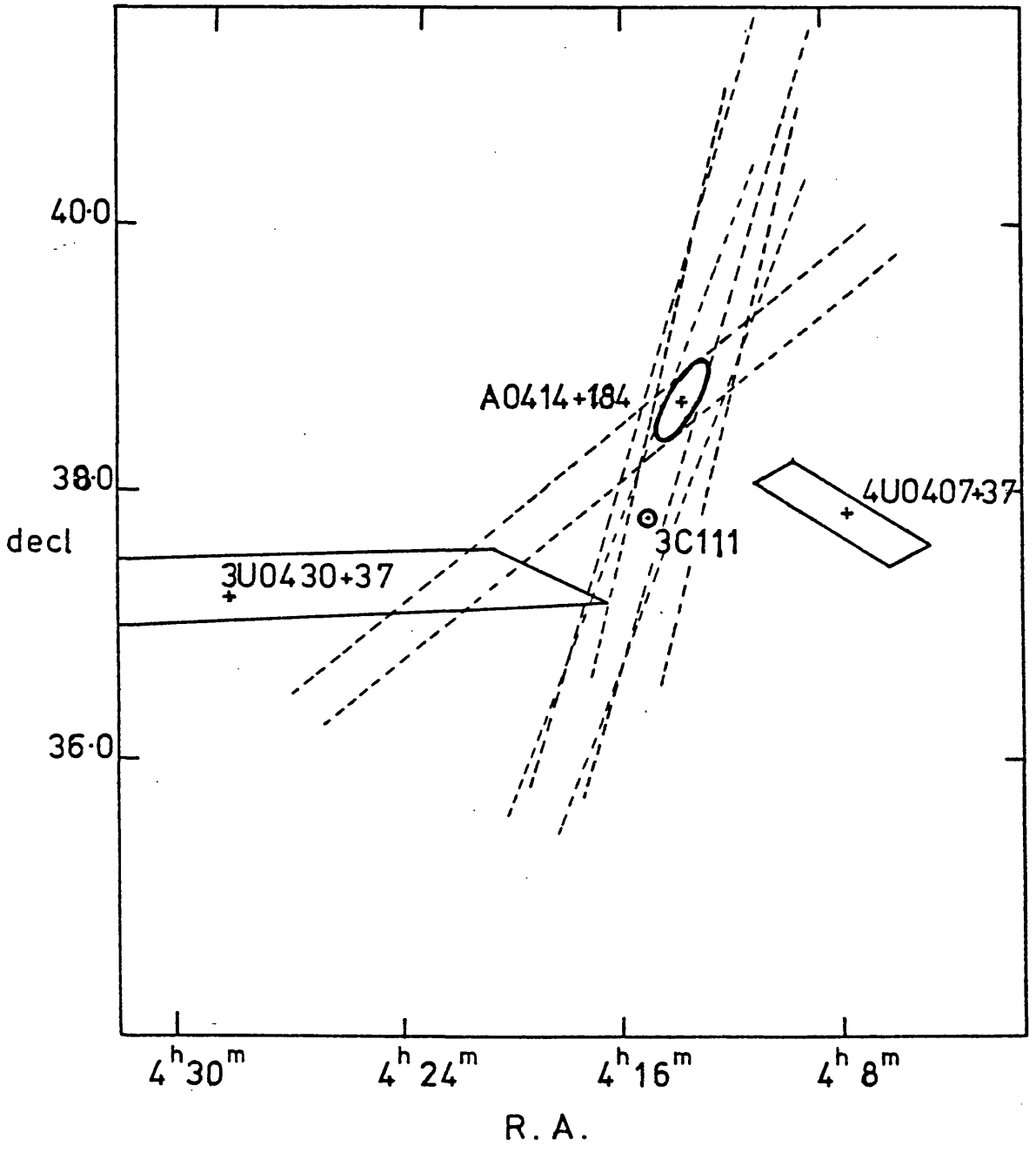

fig 7-2 X-RAY ERROR BOXES NEAR 3C111 (⊙). The dashed lines are the four LOP which make up the SSI error box.

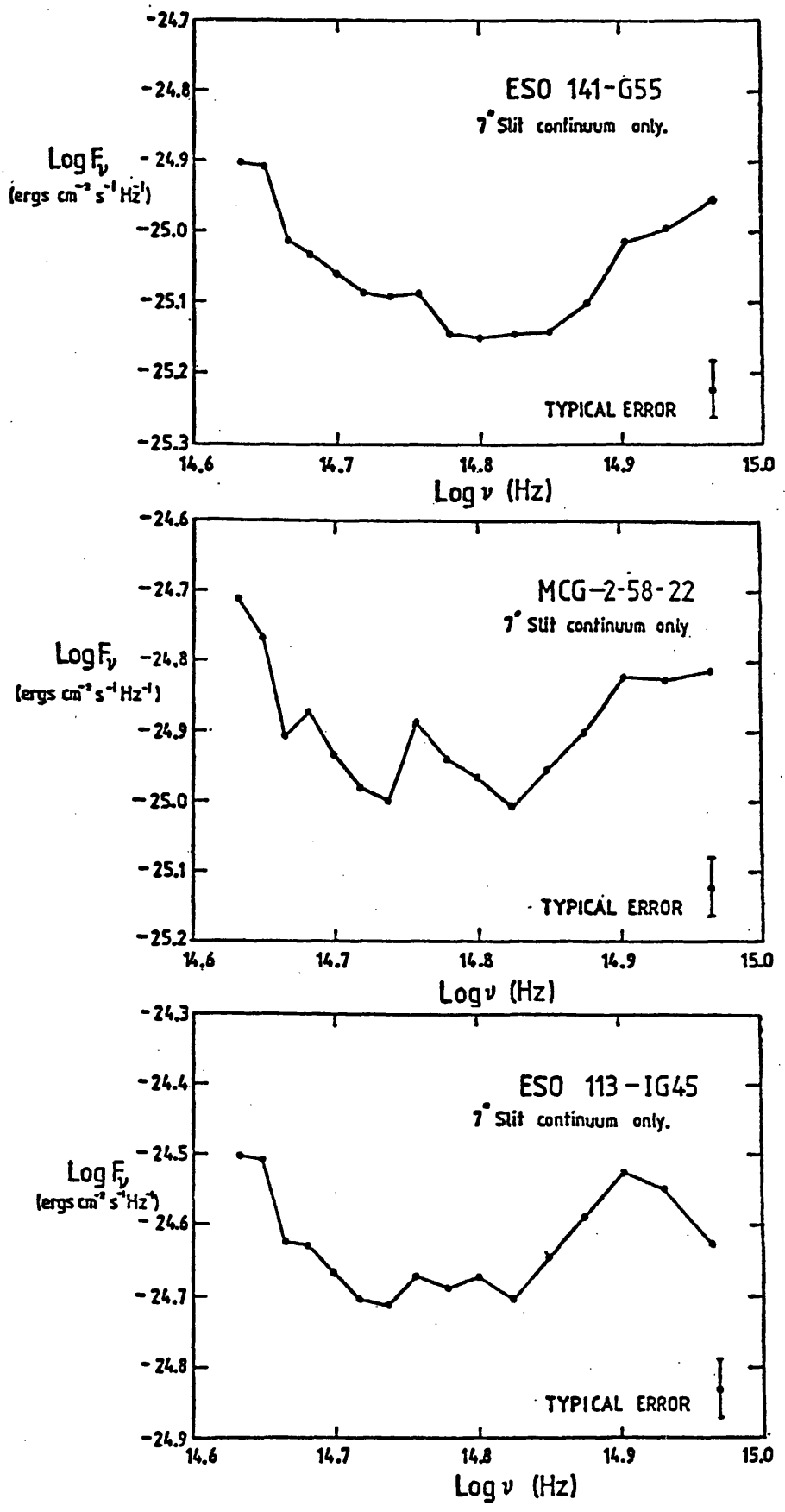

fig 7-3 OPTICAL CONTINUA FOR THREE OF THE NEWLY DISCOVERED SEYFERT GALAXIES.

VARIABILITY

Tananbaum et al. have shown that Mkn 279 is variable by intercomparing UHURU and 2A fluxes. 4U intensities cannot be used directly for this comparison as they are systematically overestimated. (The intensities were averaged over ($>3\sigma$) sightings not observations. 2A intensities are averaged, correctly, over observations, see chapter 2-4).

More remarkably, they appear to have detected variability in NGC 4151 on timescales ≈13 minutes, indicating emission from a region <2 AU ($<10^{-4}$ pc) radius. Naïvely converting this to a limiting mass via a Schwarzschild radius yields $M < 10^{6}$ $M_{\odot}$. Tananbaum et al. see this variability as 5 'flares' which approximately double the steady flux from NGC 4151 and which occur 1-2 times per day. They contain 10^{46-47} erg.

Such energies can be produced on such a short timescale by some models of x-ray emission from supernovae (e.g. Colgate, 1974) but a rate of flaring requiring 1 supernova per day would generate $>10^{46}$ erg s^{-1}, more than 20 times the total average electromagnetic radiation at all wavelengths seem from NGC 4151 (Stein and Weedman, 1976). This observation, if confirmed by more sensitive experiments, would seem to rule out multiple pulsar models.

Longer term variability of the spectrum of NGC 4151 has now been observed (Barr et al., 1977) with the MSSL proportional counter spectrometer on Ariel V (fig. 7-4). This variability appears to be due solely to variations in the absorbing column density. The observed change from an equivalent hydrogen column (using cosmic abundances) $N_H = 3.5 \times 10^{22}$ atom cm^{-2} to $N_H = 1.8 \times 10^{23}$ atom cm^{-2} is remarkably close to the change predicted by Mushotzky and Shields (1976, private communication). They modelled the properties of a forbidden line region cloud (region (3), chapter 1-4) from the forbidden line parameters. It is thus very reasonable

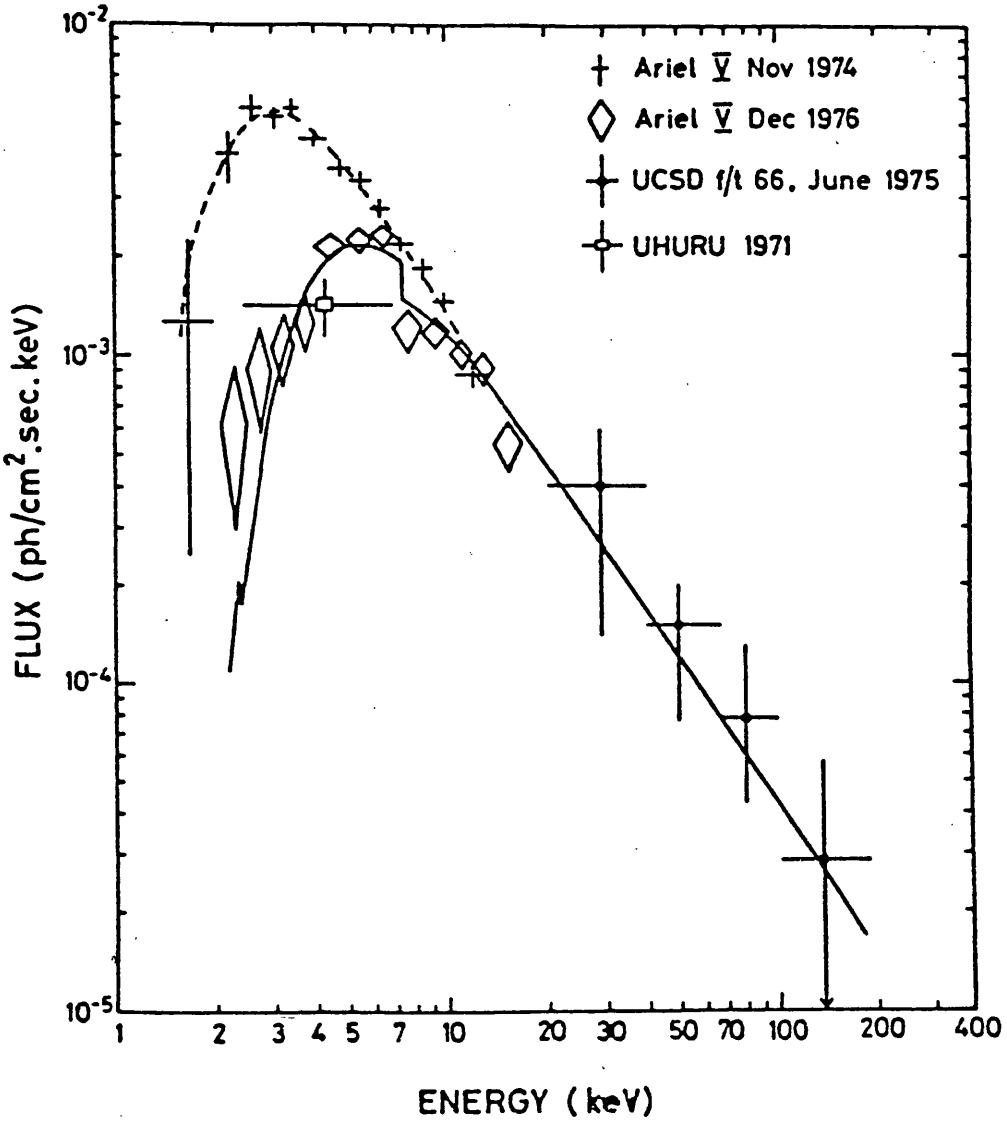

fig 7-4 THE PHOTON SPECTRUM OF NGC4151 (Barr et al.,1977). The solid and dotted lines are the best fit power-law spectra for the two Ariel V observations combined with the UCSD high energy data.

to explain this variable N_H in terms of such a cloud crossing the line of sight to the more compact central regions ((1) and (2), chapter 1-4). This is an independent confirmation ofthe conclusion of chapter 5-7 that the x-rays originate in this inner core. The x-ray spectrum during the shorter timescale variability in NGC 4151 is unknown. The faster moving permitted line region (2) clouds might produce variability down to 1/10 of that from forbidden line region clouds, assuming similar sized clouds. This could thus reach down to the 3-day level reported in chaper 6-2. Alternatively, such flares could be due to an intrinsic change in the central source intensity, as seems to be the case for the similar variability now reported from OSO-8 (Mushotsky et al., 1977b).

Other results from the MSSL experiment show that variability in NGC 5128 (see chapter 6-3) is due not to a changing column density but to an intrinsic change (Stark, Davison and Culhane, 1978, in preparation). Clearly then both kinds of variability are possible in active galaxy nuclei. With so few points on the light curves of NGC 4151 and NGC 5128 it is premature to say that they are different types of source but it also urges caution in accepting the suggestions of chaper 6-4 that a single, simple, light curve form could fit all such galaxies.

X-RAY SPECTRA

NGC 4151 is no longer the only Seyfert for which some spectral information exists. Stark et al. (1978) have produced rough spectra for NGC 5548, Mkn 279 and the peculiar NGC 5506 (fig. 7-5). The values of power-law photon index α (from $dN/dE = A\, E^{-\alpha} e^{-N_H \sigma}$) and N_H which they derive are quoted in Table 7-2 together with the same parameters for other active galaxy x-ray sources.

The 'best fit' spectra they derive are shown as solid lines in fig. 7-5. It seems clear from inspecting these figures that the 'best fits' are somewhat optimistic. It is probably not meaningful to fit 3 parameters to this data. If one fits just a spectral slope and normalization then NGC 5506 would have $\alpha \approx 1.0$ and Mkn 279 would have $\alpha \approx 0.4$. NGC 5548 shows a very suggestive bump at $\approx$7 keV reminiscent of the Iron feature in clusters of galaxies (Mitchell et al.,1976). It is clearly of too low a significance to be claimed as yet. It is worth noting though that the detection of such a line would show that at least some of the emission was thermal. Neither the non-detection of such a line nor the demonstration of a power-law x-ray spectrum over a wide range of energies can rule out such a mechanism. (A safely asymmetric position for supporters of thermal models. (but see chapter 7-2).)

Table 7-3 shows that the assumption used for the estimation of the Seyfert contribution to the high energy diffuse x-ray background (chapter 4-1) has, so far, been justified. 3C 273 is the only active galaxy with a significantly softer spectrum. Some galaxies are clearly much harder than NGC 4151. Mkn 279 appears to be about the hardest known x-ray source. NGC 5506 could also be much harder than NGC 4151. The hard x-ray contribution might thus be larger than previously expected.

Some authors have attempted to explain the entire γ-ray background with active galaxy emission (Strong et al., in preparation).

Table 7.3. X-ray Spectra of Active Galaxies

Power law fits to $dN/dE = AE^{-\alpha ph} e^{-N_H\sigma}$

Object	X-ray Name	αph	N_H(atom cm^{-2})	E_a(KeV), $=N_H\sigma$
NGC4151	2A1207+397	1.30±0.2	5.0×10^{22}	2.1[1,7,8] Variable N_H[1]
		1.74±0.3	1.8×10^{23}	4.0
3C273	2A1225+022	2.2 ±0.2	3.6×10^{22}	1.9 [2]
Cen A (nucleus)	2A1322-127	1.62	1.3×10^{23}	[3,4]
Mkn279	2A1348+700	* 0.7 (0.4	$\leq 1.2 \times 10^{23}$ -)	$\leq$ 3.8 [5] -
NGC5506	2A1410-029	* 1.6 (1.0	$\leq$ 8 x 10^{22} -)	$\leq$ 3.0 [5] -
NGC5548	2A1415+255	* 1.9 (1.9	$\leq$ 2 x 10^{22} -)	$\leq$ 2.0 [5] -
(c.f. (Crab Nebula	4U0531+21	2.1		[6])

* The spectral fits given in 5 are probably over ambitious. More credible, eyeball, fits to power law index alone are given in brackets.

References for Table 7.3

1. Barr P., White N.E., Sanford P.W., Ives J.C., 1977, MNRAS, 181, 43P.
2. Sanford P.W. and Ives J.C., 1976, Proc.R.Soc.Lond. A, 350, 491.
3. Mushotzky R.F., Serlemitsos P.J., Becker S.H., Boldt E.A., Holt S.S.
4. Stark J.P., Davison P.J.N., Culhane J.L., in preparation.
5. Stark J.P., Bell-Burnell J. and Culhane J.L., 1978, MNRAS, 182, 23P.
6. Toor A. and Seward F.D., 1974, A.J. 79, 995.
7. Paciesas W.S., Mushotzky R.F., Pelling R.M., 1977, MNRAS, 178, 23P.
8. di Cocco G., Boella G., Perotti F., Stiglitz R., Villa G., Baker R.E., Butler R.C., Dean A.J., Martin S.J. and Ramsden D., 1978, Nature 270, 319.

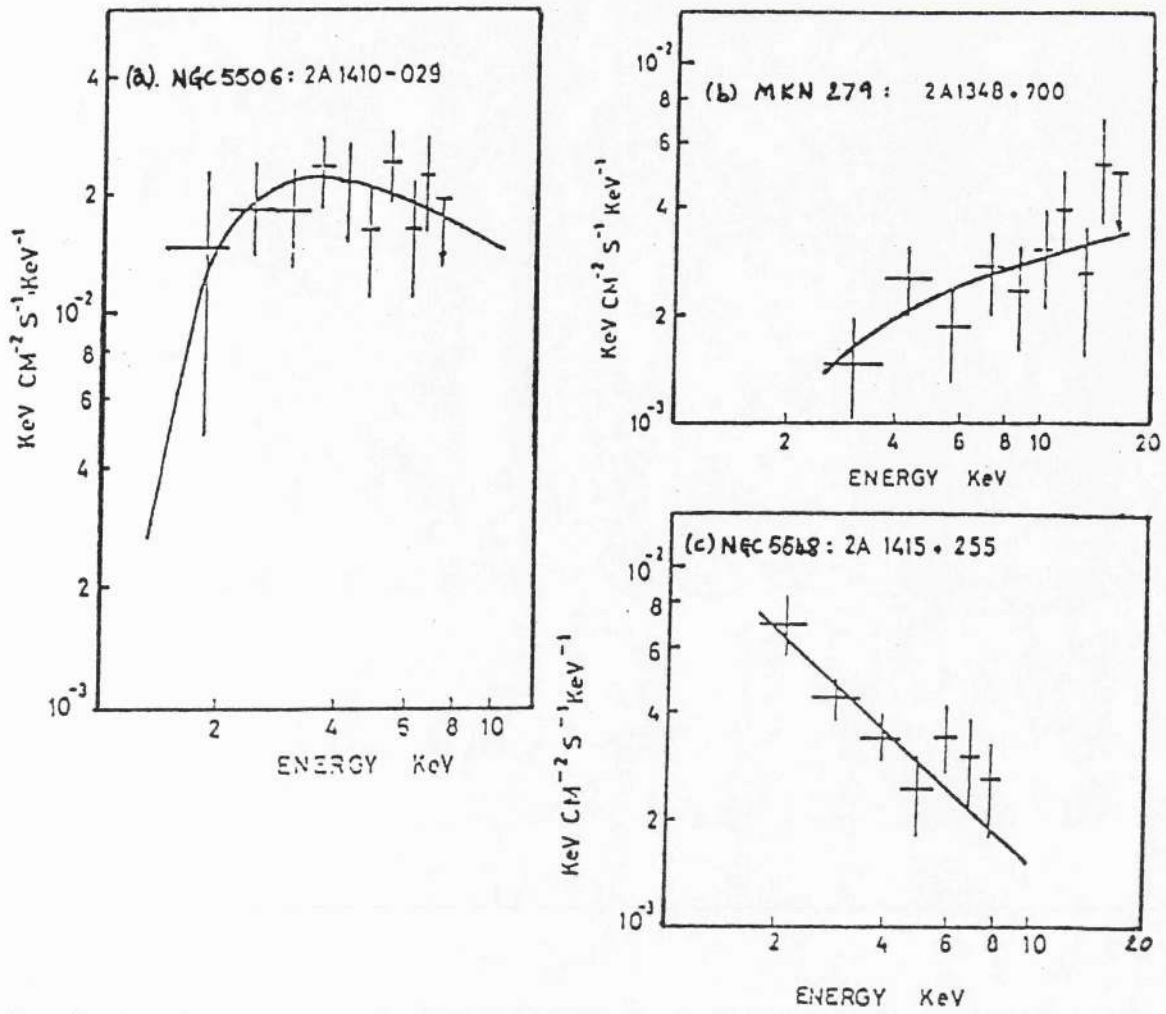

fig 7-5 ARIEL V (MSSL) SPECTRA FOR TWO SEYFERT GALAXIES AND NGC5506.(Stark et al.,1978). The solid lines are the formal best fit spectra derived by Stark et al.

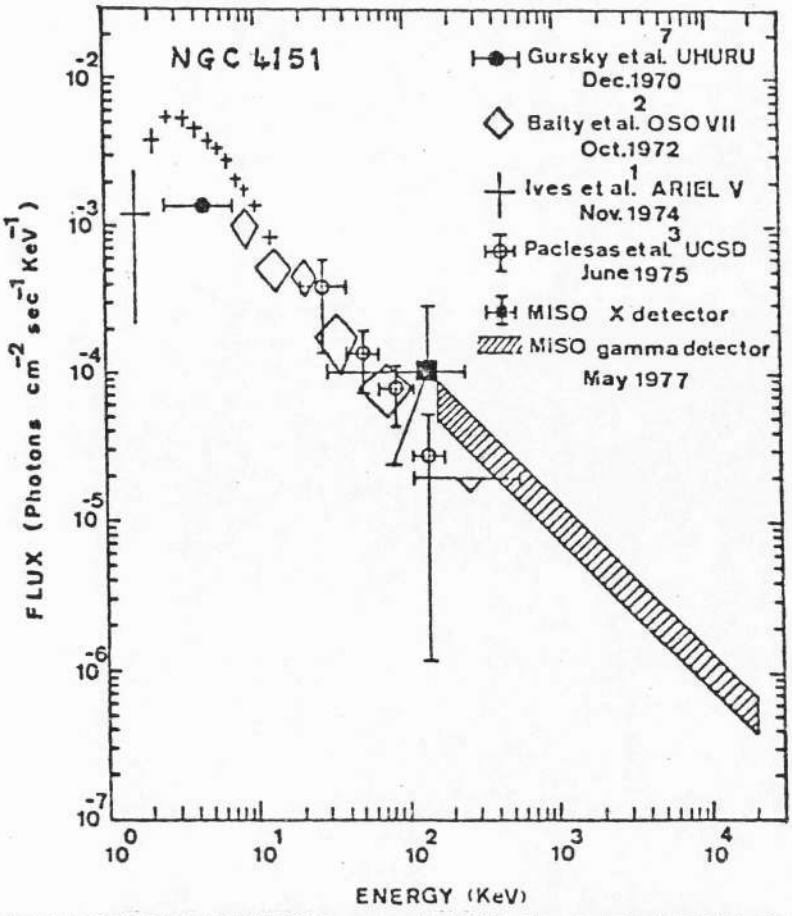

fig 7-6 THE EXTENSION OF THE NGC4151 SPECTRUM TO X-RAY ENERGIES (di Cocco et al.,1977). The spectral index has been assumed to agree with the x-ray data. Given this assumption the flux density found by di Cocco et al. normalises well with the x-ray data

The recent detection of NGC 4151 out to at least 1 MeV (di Cocco et al., 1977; fig. 7-6) together with the long-standing observation of Cen A at 1 MeV and probably at $\geq$ 300 GeV (Grindlay et al., 1975) have begun to support this suggestion observationally. That medium energy x-ray work shows other active galaxies may have harder spectra is extra positive evidence. This seems to be a promising new line of enquiry.

HIGH EXCITATION EMISSION LINE GALAXIES (HEXELGs)

The Leicester/AAT identification programme for 2A sources has produced another new class of x-ray emitting galaxy - High EXcitation Emission Line Galaxies (or 'Hexelgs' as they will be called here).

These galaxies possess forbidden line ionisation levels up to [Fe VII] (IP=0.10 keV) but the forbidden and permitted lines both have widths of only ≈400 km s^{-1} with no broad wings seen. They are thus too narrow to be classified as Seyfert types 1 or 2 and yet they seem to possess some 'non-thermal' ionising source. Perhaps the prototype of this kind of galaxy is NGC 5506 (Wilson et al., 1976). As seen in chapter 3-4 this galaxy has long been a candidate identification for the x-ray source 3U1410-03 (=2A1410-029),(Bahcall et al., 1975). This identification has now been confirmed by SAS-3 rotation modulation collimator observations (Ricker et al., 1978b) which produced a 1.1 arcmin radius error circle (90% confidence) centred only 12 arcsec north of the galaxy nucleus. Such galaxies are thus clearly capable of being x-ray emitters. The 2A identifications work shows that this may well be generally true of such hexelgs.

The two main identifications are of NGC 7582 with 2A2315-428 and of NGC 2992 with 2A0943-140 (Ward et al., 1978 discuss the identifications in detail). Table 7-4 gives some details of these galaxies. NGC 7582 shows excitation levels up to [Ne V] (IP=0.097 keV) and NGC 2992 has [Ne III] emission (IP=0.041 keV).

These successes prompted a PST search for x-rays from other bright emission line galaxies. 25 such galaxies were examined. (All those with $z < 0.01$ from Osmer, Smith and Weedman, 1974, Martin, 1976, and Penston et al., 1977). One, NGC 1365, gave a peak at $>5\sigma$ and was thus an acceptable source, with an intensity of 0.3 ± 0.06 Ariel (SSI) ct s^{-1}. Fig. 7-7 shows the error box produced for this source and Table 7-5 lists the co-ordinates of the best fitting rectangle.

Table 7-4 Properties of the 2 Emission Line Galaxies

	NGC 7582 (2A2315-428)	NGC 2992 (2A0943-140)
cz (Km s^{-1}) heliocentric	1500 ± 60	2450 ± 60
m_v (20 arc sec)	13.5†	13.27 (OSW)
M_v*	-19.06	-20.22
Hα/Hβ	10.9††	10.35 (OSW)
A_v(mag.)**	4.0	3.9
Lum Hβ ($erg\ s^{-1}$)	1.4×10^{40}	1.4×10^{40} (OSW)
Lum Hβ after correction for reddening ($erg\ s^{-1}$)	1.0×10^{42}	1.0×10^{42} (OSW)
FWZI Hα ($km\ s^{-1}$)	≈ 600	>1000 (OSW)
X-ray source error box size (sq. deg)	0.067	0.065
$\log_{10} L_x$ (2-10 KeV) ($erg\ s^{-1}$)	42.55	43.21

NOTE Data from Ward et al.(1978) except where referenced by OSW = Osmer, Smith and Weedman (1974b).

† Obtained from an observation with the Rodgers Scanner on the 74-inch Mount Stromlo telescope.

* H_o = 50 km s^{-1} Mpc^{-1}, corrected for extinction 0.18 cosec b^{II} mag.

†† Derived from AAT spectra calibrated by the Rodgers scanner observation on the 74-inch Mount Stromlo telescope (20 arc sec aperture).

** $A_v = 6.88 \log_{10} (H\alpha/2.8\ H\beta)$.

Finally the galaxy M 82 is morphologically very similar to NGC 5506 (Irr II, a very peculiar type, Wilson et al., 1976) and shows emission lines in places, although its nucleus is obscured by dust. The SSI error box of 2A0954+700 includes M 82 and makes it a good candidate for x-ray emission for the first time, the 3U and 4U boxes being very large.

There are thus 5 possible hexelgs emitting x-rays. The hard spectrum of NGC 5506 has already been noted (fig. 7-5 a). Comparison of the intensity of the MSSL Ariel V observation which produced this spectrum with the SSI data (fig. 7-8) shows that the source is clearly variable on a timescale of 134 day (at 6σ). It seems then that these hexelgs contain a compact region similar to that found in type 1 Seyferts but which is not apparent at optical wavelengths. Such galaxies are thus more closely linked with Seyfert galaxies and quasars than had been previously shown.

The x-ray luminosity of the hexelgs is 10^{42} - 10^{43} erg s^{-1} except for that of M 82 which is only 5×10^{40} erg s^{-1}. They thus occur at the lower end of the Seyfert galaxy range. The contribution that they make to the diffuse x-ray background is not known since no thorough survey of these objects yet exists. They probably could not exceed the 10% of all galaxies which are Markarian objects (chapter 1-2).

Certainly the discovery of compact x-ray sources in hexelg nuclei makes such compact 'quasar-like' regions a more common feature of galaxy structure than had been shown before.

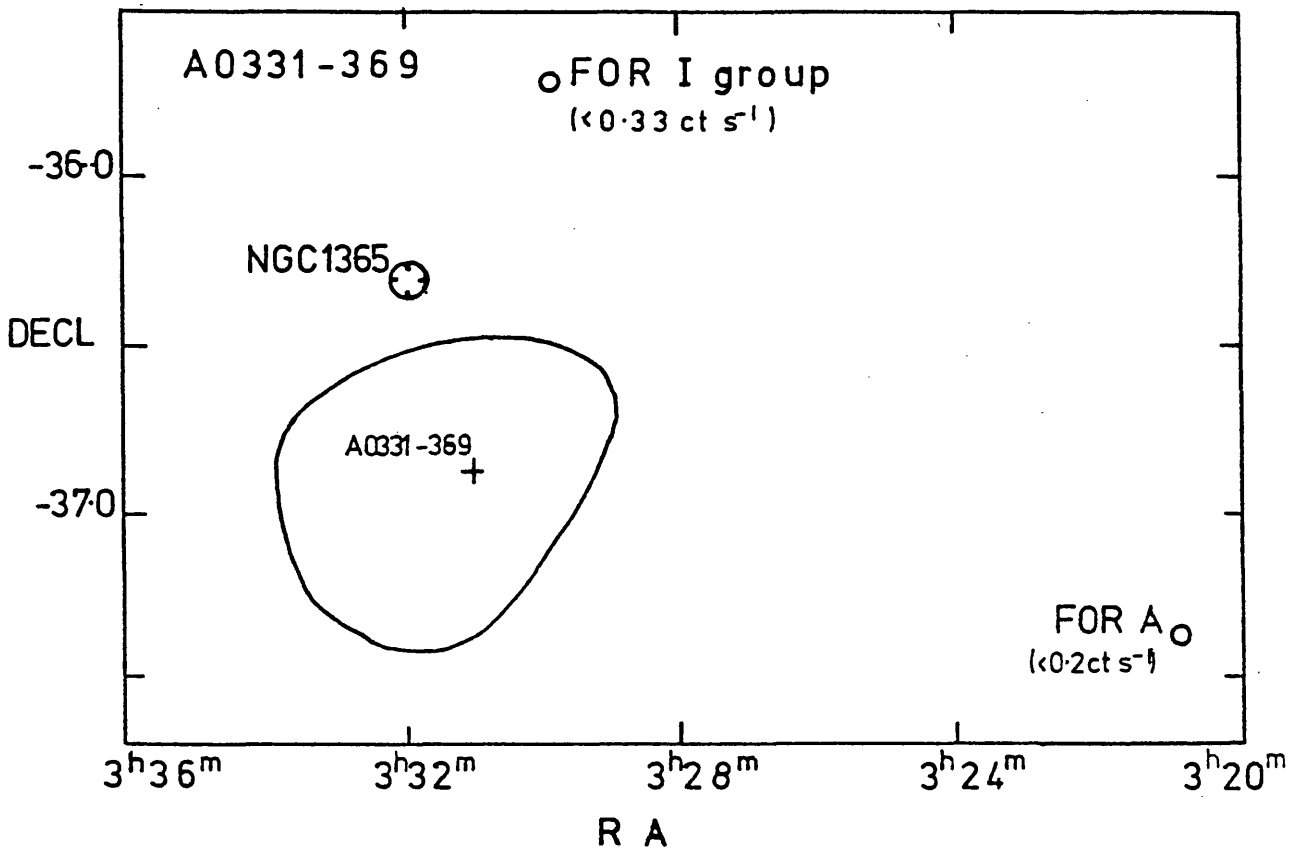

fig 7-7 THE SSI PST ERROR BOX (solid line) FOR A0331-369, found during a search of hexelgs with the PST. The position of NGC1365 is marked together with that of two possible alternative identifications (the For I group and the radio galaxy For A). Upper limits are given for these objects.

Table 7-5: PST Error Box Details for A0331-369

	R.A. (degrees 1950.0)	decl.
centre:	52.75	-36.90
corners	53.65	-36.79
	52.49	-36.29
	52.00	-37.03
	53.16	-37.05
area of box:	0.92 sq. deg.	
galactic co-ordinates of centre:	l = 239.0	b = -54.7

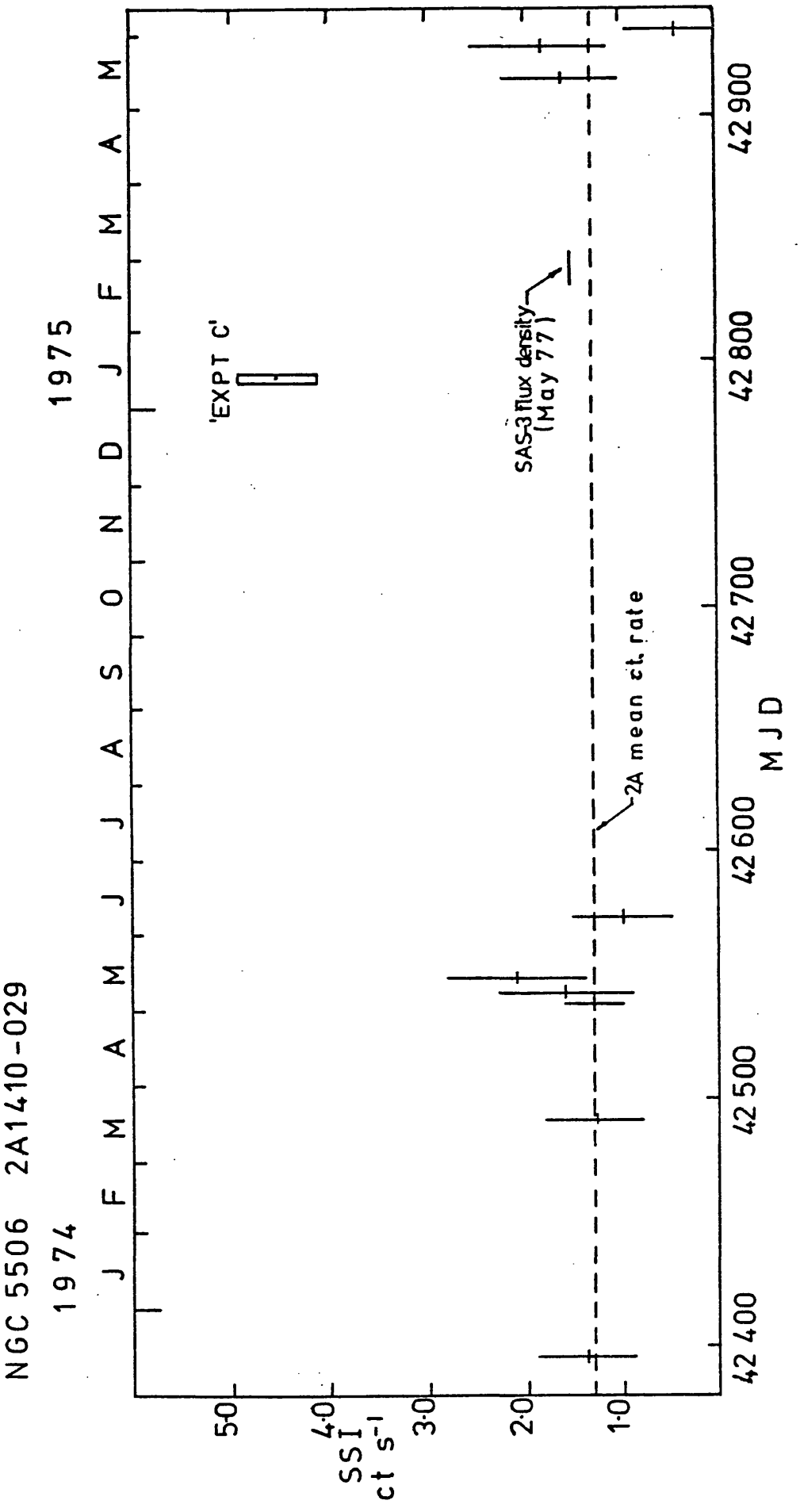

fig 7-8 ARIEL V LIGHT CURVE FOR NGC5506 (2A1410-029) using SSI and 'Expt C'(MSSL) data. MSSL data was converted to SSI ct s^{-1} using the standard conversion of 1 SSI ct s^{-1} = 5.1 x 10^{-11} erg $cm^{-2}s^{-1}$. The flux density found by SAS-3 in May 1977 is also shown using the same conversion factor.

7-2 Future Observations

The results described in this thesis are clearly only the initial stages in the investigation of active galaxy x-ray emission. New instrumentation on board satellites already under construction or in orbit will be able to provide greatly improved spectra from 0.1 to 100 keV, and possibly up to 10 MeV. The faintest detectable source will be some 1/1000th of the strength of the faintest source that the SSI can detect (at the lower end of the energy range). In this range the spatial resolution of x-ray telescopes will be better than 10 arcsec and isolated point sources may be positioned to 1-2 arcsec. With such improvements it is possible to imagine many measurements that will give useful results. Some of these are described below.

SEYFERT GALAXIES

Improved spectra for all the now well-established x-ray Seyferts are needed. Detection of Iron line emission, as noted in the previous section, would argue for some thermal emission. The medium energy (2-30 keV) experiments on UK-6 and EXOSAT will be well suited to this task. An Fe emission line may well have been detected in Cen A by OSO-8 at 6.4keV (Mushotzky et al., 1978), accompanied by an absorption edge at 7.1 keV. The authors explain this in terms of cold ($T < 2.5 \times 10^6$ K) iron absorbing and re-emitting the radiation from another, central, source. In this case thermal emission for the underlying source is avoided.

These Iron feature detections in Cen A coupled with the detection of an iron edge in NGC 4151 by Barr et al. (1977) show that abundance analyses of the clouds in the permitted and forbidden line regions are now possibilities. The detailed study of the low-energy cut-offs that are expected is possible with the solid state spectrometer on HEAO-B and will answer these questions. The spectral variability of Seyferts both optically

(Tohline and Osterbrock, 1976, chapter 1-1, fig. 1-2) and in the x-ray region (Barr et al., 1977) can be attributed to forbidden line region clouds crossing the line of sight to the photoionizing source. Thus the time variability of the low energy x-ray cut-off could give information on the density profile of such clouds. Correlated x-ray cut-off and Hα power variability would show that the disappearence of the Hα line was due to absorption and not intrinsic variability of the Balmer emission.

The x-ray data can give several such useful feedbacks to the optical observers. A measurement of x-ray cut-off will allow the normal argument predicting a cut-off from the observed reddening to be reversed. Since the reddening, found from the Balmer decrement, is not uniquely determined from the optical data because pure recombination conditions may well not apply, this is an important measurement. Optical depth effects will become separable from reddening for the first time.

Simultaneous measurements in the optical and x-ray are clearly going to be necessary with such rapid and large variability involved. Any real correlation of properties without such measurements is liable to be smeared out under such conditions. The demonstration of correlations in chapter 5 may thus indicate a limit to the extent of variability.

Given a good x-ray spectrum and careful measurements of high ionisation level forbidden lines it may be possible to determine the distance of individual clouds from the central ionising source, after the fashion of Tarter and Salpeter (1969 a,b) for galactic x-ray sources. Fe X can be produced by a flux of 0.235 keV x-rays. The number of photons required to produce a given line strength can be compared with the luminosity of the central source at this energy and the inverse square law used to calculate the separation of the cloud from the source.

The ability to image Seyfert galaxies at ≈5 arcsec resolution is unlikely to be useful beyond cz ≈ 5000 km s^{-1} at which point 1 kpc ≈ 2 arcsec. Nearer than cz ≈ 1000 km s^{-1}, 5 arcsec < 500 pc. Here the

forbidden line region may be resolved, if it emits x-rays. There are five Seyferts known with $cz \leq 1000$ km s^{-1} (NGC 1068,1566,3227,4051,4151). These should clearly be studied with the High Resolution Instrument (HRI) on HEAO-B. Some Seyferts seem to show disturbed structure, including jets (as in 3C 273 and M 87). These may give rise to x-ray emission which could be resolved. The 16 Seyferts known with $1000 < cz < 6000$ km s^{-1} (NGC 1275, 3516, 4507,5548,6764,6814,7469,IC 4329A, Mkn 1,3,6,270,352,438, Akn 79 and T0109-383) would be the obvious extension of the High Resolution Imaging programme for HEAO-B. The objects with suspected jets noted in Khachikian and Weedman (1974) should also be inspected. Extended x-ray structure $\approx$ 3 arcmin across may already have been detected in the nucleus of the radio galaxy Cen A (Delvaille et al., 1978).

QUASARS

To date 3C 273 is the only established x-ray quasar (=3U1224+02, 2A1225+022). The disappearance of 3U0138-01 from the 4U catalogue removes the possible x-ray quasar NAB0137-01 (Schreier et al., 1975). The source is not seen by the SSI either (White and Ricketts, 1977). White and Ricketts performed a PST survey of 65 quasars and produced one candidate at $>4\sigma$: PKS0349-14 (called A0349-14). If the identification is correct the quasar would have a luminosity of 2×10^{46} erg s^{-1}, very similar to that of 3C273 at $\approx 8 \times 10^{45}$ erg s^{-1}. Also 3C 351 is one of the candidates in the 1.6 square degree error box of 2A1705+609 (L_x, if correct, $= 2 \times 10^{46}$ erg s^{-1}). X-ray emission from quasars is thus in a similar position now to that of Seyfert galaxies before the 2A work reported in this thesis.

If the correlation of optical magnitude (m_v) and x-ray flux density found in chapter 5-3 (fig. 5-2) is correct and extends to quasars this state of affairs is to be expected. The replotting of fig. 5-2 as fig. 7-1a shows the optical magnitudes to be reached if the brightest quasars and the brightest, high redshift ($z > 2.5$), quasars are to be detected. Even choosing the least favourable m_v vs. F_x slope a factor 10 increase in x-ray sensitivity should show up many quasars as x-ray sources. A further factor 10 will reach out to the bright high-redshift quasars. It is possible from this graph that these $z > 2.5$ objects could be as bright as 1/10 UHURU ct s^{-1}. It is expected then that the HEAO-B grazing incidence optics instrumentation will produce an advance for quasars exceeding that produced for Seyferts by Ariel V. The K-corrections should be advantageous for the low-energy (≈ 0.1 - ≈ 3 keV) HEAO-B instruments in redshifting the low-energy cut-offs below the range of detection. A source with the same luminosity and emitted spectrum as 3C273 but at a redshift of 2.5 would produce a count rate as high as 1/3 that produced by the actual 3C273 in the Imaging Proportional Counter on HEAO-B.

BL LAC OBJECTS (LACERTIDS)

There are now two candidate x-ray emitters amongst the 30 or so BL Lac type objects known (Stein, O'Dell and Strittmatter, 1976): Mkn 421 (=2A1102+384 ?) and Mkn 501 (= 4U1651+39 ?).

BL Lac objects are characterised by their strong, highly variable radio emission associated with a starlike object which has a featureless 'non-thermal' optical continuum and is also variable. Since they have no emission or absorption features it is not normally possible to measure the redshift (and hence distance and luminosity) of these objects. In some cases a surrounding faint nebulosity yields an absorption redshift, or weak, transient, lines appear in the object itself. Where such a redshift is known (and it is known for Mkn 421 and 501) it is ≥ 0.05 giving Seyfert/ Quasar luminosities. Lacertids are thus usually assumed to be active galactic nuclei of some special kind.

If this is so then the lack of emission lines has to be explained. There are four present suggestions: (Stein, O'Dell and Strittmatter, 1976) -

(1) The lines are too broad to be distinguished from the continuum.
(2) The continuum is too bright with respect to the lines (small equivalent width)
(3) There are insufficient uv photons to produce enough ionisation.
(4) There is too little gas in the nucleus to produce detectable lines.

X-ray observations can attack possibilities (3) and (4) directly. The list of Stein O'Dell and Strittmatter (1976) shows that the two x-ray detected Lacertids are also (at least usually) the two brightest. They are plotted on fig. 7-1 a (as '+') and agree with the m_v vs. F_x relation. If this is true then all the remarks about detection of quasars apply to Lacertids. The faintest known Lacertid has $m_v \approx 19$. They may well all be visible to HEAO-B.

A certain identification of soft x-ray emission from a Lacertid would make (3) above a difficult position to maintain. Then again measurement of a large low-energy cut-off, particularly if variable, would indicate the presence of large amounts of gas in the nucleus, and if an x-ray emission line were seen then there would, very likely, have to be gas very close to the continuum source. The reason (4) above can thus be tested by x-ray measurements. Thus x-ray measurements could be of key importance in understanding these objects.

The identification of 2A1102+384 with Mkn 421 would be particularly interesting given its previous history (Ricketts et al., 1976 ; chapter 6-4, fig. 6-9). Since it was a transient source it is not obvious that it is correct to assume that the brightest or even the only source now found in its error box is the same source. Low level emission was seen from 2A1102+384 some months after its outburst so a 2 UHURU ct s^{-1} steady source may be always present.

HEXELGS

Confirming, extending and defining this probable new class of x-ray active galaxy are necessary first steps which mainly require improved sensitivity. To be sure of identifications will then also require improved spatial resolution. HEAO-B, once again, is the mission most suited to this task. Spectra and variability of the known x-ray hexelgs, following that undertaken for Seyferts can be performed by the UK-6 and EXOSAT missions.

HEAO-B, not being a sky survey instrument, will need to work from an optically produced list of high excitation emission line galaxies. The Cerro Tololo objective prism surveys (Smith, 1975) may yield such a list when the objects' optical spectra are examined in detail. The highest resolution of HEAO-B may well be more useful for hexelgs than for Seyferts. Because they are nearer than Seyferts finer scale structure can be examined. Their nuclei often contain several knots of emission for instance, and it is not clear which of these is producing the x-rays.

SUMMARY

These fairly brief notes show that the potential of x-ray astronomy to contribute to Seyfert and general Active Galaxy research can already be seen to be immense. It is good to know that the work done for this thesis has made a first contribution to this field, so clearly a subject just begun.

REFERENCES

Abbreviations

Ap.J.	Astrophysical Journal
Ap.J.Supp.	Astrophysical Journal Supplement Series
MNRAS	Monthly Notices of the Royal Astronomical Society
QJRAS	Quarterly Journal of the Royal Astronomical Society
A.J.	Astronomical Journal
A.& Ap.	Astronomy and Astrophysics
PASP	Publications of the Astronomical Society of the Pacific
BAAS	Bulletin of the American Astronomical Society

Abell G.O., 1958, Ap.J.Supp., 3, No.31, 211.

Adams T.F., 1977, Ap.J.Supp., 33, No.1, 19.

Adams T.F. and Weedman D.W., 1975, Ap.J., 199, 19.

Allen C.W., 1975, "Astrophysical Quantities", 3rd edition, Athlone Press, London.

Allen D.A., 1976, Ap.J., 207, 367.

Anderson K., 1970, Ap.J., 162, 743.

Anderson K.S., 1974, Ap.J., 189, 195.

Angel R., at NATO meeting on Quasars, Cambridge, England, 1977.

Apparao K. et al., IAU Circular 3150, 13 December 1977.

Arakelian M.A., 1975, Soubshch. Byurakan. Obs. 47, 3.

Arons J., Kulsrud R.M., Ostriker J.P., 1975, Ap.J., 198, 687.

Arp H., 1975, PASP, 87, 545.

Bahcall J.N., Bahcall N.A., Murray S.S. and Schmidt M., 1975, Ap.J., 199, L9.

Bahcall N.A., 1977a, Ap.J., 217, L77.

Bahcall N.A., 1977b, Ap.J., 218, L93.

Baity W.A., Jones T.W., Wheaton W.A. and Peterson L.E., 1975, Ap.J., 199, L5.

Barr P., White N.E., Sanford P.W., Ives J.C., 1977, MNRAS, 181, 43P.

Becklin E.E., Matthews K., Neugebauer G., Wynn-Williams C.G., 1973, Ap.J., 186, L69.

Boksenberg A., Shortridge K., Allen D.A., Fosbury R.A.E., Penston M.V. and Savage A., 1975, MNRAS, 173, 381.

Burbidge E.M. and Burbidge G.R., 1959, Ap.J., 129, 271.

Canizares C.R., Neighbours J.E., Matilsky T., 1974, Ap.J., 192, L61.

Carpenter G.F., Coe M.J., Engel A.R., Quenby J.J., 1976, Proc.R.Soc. Lond.A. 350, 521.

Charles P.A., Longair M.S. and Sanford P.W., 1975, MNRAS, 170, 17 p.

Colgate S.A., 1974, Ap.J., 187, 333.

Condon J.J., 1974, Ap.J., 188, 279.

Cooke B.A., Elvis M., Maccacaro T., Ward M.J., Fosbury R.A.E., Penston M.V., 1976, MNRAS, 177, 121P.

Cooke B.A., Ricketts M.J., Maccacaro T., Pye J.P., Elvis M., Watson M.G., Griffiths R.E., Pounds K.A., McHardy I., Maccagni D., Seward F.D., Page C.G., Turner M.J.L., 1978, MNRAS, 182, 489, (Appendix A)

de Bruyn A.G. and Willis A.G., 1974, A.& Ap., 33, 351.

de Bruyn A.G. and Wilson A.S., 1976, A.& Ap., 53, 93.

de Bruyn A.G. and Wilson A.S., 1978, A.& Ap., (submitted).

Delvaille J.P., Epstein A., Schnopper H.W., 1978, Ap.J., 219, L81.

de Vaucouleurs G. and de Vaucouleurs A., 1964, "Reference Catalogue of Bright Galaxies", Austin Texas: Univ. of Texas Press.

Dibaiye E.A., 1977, Sov. Astr. Lett. 3, (No.1), 1.

di Cocco G., Boella G., Perotti F., Stiglitz R., Villa G., Baker R.E., Butler R.C., Dean A.J., Martin S.J., Ransden D., 1978, Nature, 270,319.

Disney J.J., 1973, Ap.J., 181, L55.

Dressel L.L., Condon J.J., 1976, Ap.J. Supp., 31, 187.

Eggen O., 1976, QJRAS, 17, 325.

Elvis M., 1976, MNRAS, 177, 7 p.

Elvis M., Cooke B.A. and Pounds K.A., 1975, Nature, 257, 32.

Elvis M., Maccacaro T., Wilson A.S., Ward M.J., Penston M.C., Fosbury R.A.E., Perola G.C., 1978, MNRAS, 182, .

Fabian A.C., Zarnecki J.C., Culhane J.L., Hawkins F.J., Peacock A., Pounds K.A., Parkinson J.H., 1974, Ap.J., 189, L59.

Fairall A.P., 1977, MNRAS, 180, 391.

Forman W., Jones C., Cominsky L., Julien P., Murray S., Peters G., Tananbaum H., Giacconi R., 1978, Ap.J.Supp. (submitted).

Giacconi R., Gursky H., Paolini F.R. and Rossi B.B., 1962, Phys.Rev.Lett. 9, 439.

Giacconi R., Kellogg E., Gorenstein P., Gursky H., Tananbaum H., 1971, Ap.J., 165, L27.

Giacconi R., Murray S., Gursky H., Kellogg E., Schreier E., Matilsky T., Koch D. and Tananbaum H., 1974, Ap.J.Supp., 27, 37.

Glass I.S., 1973, MNRAS, 164, 155.

Gorenstein P. and Tucker W.H., 1974, ch.7 of "X-ray Astronomy" ed. Giacconi R. and Gursky H., (D. Reidel).

Griffiths R.E., Cooke B.A., Peacock A., Pounds K.A., Ricketts M.J., 1976, MNRAS, 175, 449.

Griffiths R., Peacock A., Davison P.J.N., Rosenberg F., Smart N.C., 1974, Nature, 250, 471.

Grindlay J.E., Schnopper H., Schreier E.J., Gursky H. and Parsignault D.R., 1975, Ap.J., 201, L133.

Grindlay J.E., 1975, Ap.J., 199, 49.

Gull S.F., Northover K.J.E., 1975, MNRAS, 173, 585.

Gursky H., Kellogg E.M., Leong C., Tananbaum H., Giacconi R., 1971, Ap.J., 165, L43.

Hall R.D.,Meegan C.H.,Walraven G.D.,Djuth F.T.,Haymes R.C., 1976, Ap.J., 210, 631.

Harris A., 1972, MNRAS, 158, 1.

Hills J.G., 1975, Nature, 254, 295.

Hogg H., 1973, Publ. D. Dunlap Obs., 3, no. 16.

Holmberg E.B., Lamberts A., Schuster H.-E., West R.M., 1976, A.& Ap. Supp. 22, 327.

Huchra J., Sargent W.L.W., 1973, Ap.J., 186, 433.

Ives J.C., Sanford P.W., Penston M.V., 1976, Ap.J., 207, L159.

Kaluzienski L.J., 1977, Ph.D. thesis, University of Maryland, GSFC preprint X-661-77-107.

Kardashev N.S., 1970, Sov. Astr. -AJ, 14, 375.

Kellogg E.E., 1974, ch. 9, pp 327-334, of 'X-Ray Astronomy' ed. Giacconi R. and Gursky H., (D. Reidel).

Khachikian E. Ye., Weedman D.W., 1974, Ap.J., 192, 581.

Kiang T., 1976, MNRAS, 174, 425.

KLeinman D.E., Wright E.L., 1974, Ap.J., 191, L19.

Kukarkin B.V., Kholopov P.N., Efremov Yu.N., Kukarina N.P., Kurochkin N.E., Medvedeva G.I., Perova N.B., Psorsky Yu.P., Fedorovich V.P., Frolov M.S., 'General Catalogue of Variable Stars', 1969, supplement 1971, (Moscow, Astron. Council Acad. Sci., USSR).

Lang K.R., 1974, 'Astrophysical Formulae',(Springer-Verlag, Berlin).

Liller M.H., Liller W., 1975, Ap.J., 199, L133.

Lynds C.R., 1970, Ap.J., 159, L151.

Markarian B.E., 1967, Astrofizika, 3, 55.

Markarian B.E., 1969 a, Astrofizika, 5, 443.

Markarian B.E., 1969 b, Astrofizika, 5, 581.

Markarian B.E., 1973, Astrofizika, 9, 5.

Markarian B.E.,Lipovetsky V.A., 1971, 7, 511.

Markarian B.E.,Lipovetsky V.A., 1972, 8, 155.

Markarian B.E.,Lipovetsky V.A., 1973, 9, 487.

Markarian B.E.,Lipovetsky V.A., 1974, 10, 307.

Martin W.L., 1974, MNRAS, 168, 109.

Martin W.L., 1976, MNRAS, 175, 633.

Matthews T.A.,Morgan W.W., Schmidt M., 1964, Ap.J., 140, 35.

Miley G.K., van der Laan H., 1973, A.& Ap., 28, 359.

Minkowski R., Wilson O.C., 1956, Ap.J., 123, 373.

Mitchell R.J., Culhane J.L., Davison P.J.N.,Ives J.C., 1976, MNRAS, 175, 29P.

Morgan W.W., 1959, PASP, 71, 394.

Morgan W.W., Kayser S., White R.A., 1975, Ap.J., 199, 545.

Murray S.S., 1978, Ap.J., in press.

Mushotzky R.F., Baity W.A., Wheaton Wm. A., Peterson L.E., 1976, Ap.J., 206, L45.

Mushotzky R.F., Baity W.A., Peterson L.E., 1977a,Ap.J., 212, 22.

Mushotzky R.F., Boldt E.A., Holt S.S., Serlemitsos P.J., 1977 b, BAAS, 9, 609, 27.01.09.

Mushotzky R.F., Serlemitsos P.J., Becker R.H., Boldt E.A., Holt S.S., 1978, Ap.J., in press.

McClintock J.E., Canizares C.R., Tarter C.B.,1975, Ap.J., 198, 641.

McHardy I.M., 1978 a, MNRAS, submitted.

McHardy I.M., 1978 b, in preparation.

Neugebauer G., Becklin E.E., Oke J.B., Searle L., 1976, Ap.J., 205, 29.

Nilson P., 1973, 'Uppsala General Catalogue of Galaxies', Nova Acta Regiae Societas Scientarum Upsaliensis, Ser.V, A, Vol.1 .

Oke J.B., Sargent W.L.W., 1968, Ap.J., 151, 807.

Osmer P., Smith M.G., 1974, Ap.J., 189, 187.

Osmer P., Smith M.G., Weedman D.W., 1974a,Ap.J., 189, 187.

Osmer P., Smith M.G., Weedman D.W., 1974 b, Ap.J., 192, 279.

Osterbrock D.E., 1974, 'Astrophysics of Gaseous Nebulae',(Freeman, San Fransisco.)

Osterbrock D.E., 1976, Ap.J.,203, 329.

Osterbrock D.E., 1977 a, Ap.J.,215, 733.

Osterbrock D.E., 1977 b, Lick Obs. Bull., no. 774, Physica Scripta (Sweden), in press.

Osterbrock D.E., Koski A.T., 1976, MNRAS, 176, 61P.

Osterbrock D.E., Koski A.T., Phillips M.M., 1976, Ap.J.,206, 898.

Osterbrock D.E., Miller J.S., 1975, Ap.J., 197,535.

Pacholczyk A.G., Weymann R.J., 1968, A.J., 73, 870.

Paciesas W.S., Mushotzky R.F., Pelling R.M., 1977, MNRAS, 178, 23P.

Pauliny-Toth I.I.K., Kellerman K.I., 1968, Ap.J., 152, L169.

Perola G.C., Tarenghi M., 1973, A.& Ap., 25, 461.

Penston M.V., Penston M.J., Selmes R.A., Becklin E.E., Neugebauer G., 1974, MNRAS, 169,357.

Penston M.V., Fosbury R.A.E., Ward M.J., Wilson A.S., 1977, MNRAS, 180, 19.

Penston M.V., and M.J., 1973, MNRAS, 162, 109.

Phillips M.M., Osterbrock D.E., 1975, PASP, 87, 949.

Pye J.P., Cooke B.A., Elvis M., 1976, 262, 195.

Pye J.P., Warwick R.S., 1978, in preparation.

Ricker G.R., Dower R.G., Jernigan J.G., Doxsey R.E., Bradt H.V., Schnopper H.W., 1978 b, Ap.J., submitted.

Ricker G.R., Doxsey R.E., Dower R.G., Jernigan J.G., Delvaille J.P., MacAlpine G.M., Hjellming R.M., 1978 a, Nature, 271, 35.

Ricketts M.J., Cooke B.A., Pounds K.A., 1976, Nature, 259, 546.

Rieke G.H., Low F.J., 1972, Ap.J., 176, L95.

Robinson L.B., Wampler E.J., 1972, PASP, 84, 161.

Rowan-Robinson M., Fabian A.C., 1975, MNRAS, 170, 199.

Ryle M., Windram M.D., 1968, MNRAS, 138, 1.

Sandage A.R., 1967, Ap.J., 150, L9.

Sanford P.W., Ives J.C., 1976, Proc. R. Soc. Lond., A, 350, 491.

Sargent W.L.W., 1970, Ap.J., 160, 405.

Schilizzi R.T., Cohen M.H., Romney J.D., Schaffer D.B., Kellerman K.I., Swenson G.W. Jr., Yen J.L., Rinehart R., 1975, Ap.J., 201, 263.

Scheuer P.A.G., 1974, MNRAS, 166, 329.

Schmidt M., 1968, 151, 393.

Schnidt M., 1977, IAU Symposium no.74, in press.

Schnopper H.W., Epstein A., Delvaille J.P., Tucker W.H., Doxsey R., Jernigan G., 1977, Ap.J., 215, L7.

Schreier E., Schnopper H.W., Gursky H., 1975, Ap.J., 201, L137.

Schwartz D., Gursky H., 1974, ch.10, p.371 of 'X-Ray Astronomy', ed. Giacconi R. and Gursky H., (D.Reidel).

Schwartz J., Johnson M., Doxsey R.E., Schwartz D.A., Gursky H., Bradt H., 1977, BAAS, 9, 558, 03.03.10 .

Seyfert C., 1943, Ap.J., 97, 28.

Shields G.A., Oke J.B., 1975, PASP, 87, 879.

Shields G.A., Oke J.B., Sargent W.L.W., 1972, Ap.J., 176, 75.

Smith H.E., Spinrad H., Smith E.O., 1976, PASP, 88, 621.

Smith J.F., and Courtier G.M., 1976, Proc. R. Soc. Lond., A, 350, 421.

Smith M.G., 1975, Ap.J., 202, 591.

Stark J.P., Bell-Burnell J., Culhane J.L., 1978, MNRAS, 182, 23P.

Stark J.P., Davison P.J.N., Culhane J.L., 1976, MNRAS, 174, 35P.

Strittmatter P.A., Williams R.E., 1976, Ann. Rev. Astr. & Ap., 14, 307.

Stein W.A., O'Dell S.L., Strittmater P.A., 1976, Ann. Rev. Astr. & Ap., 14, 173.

Stein W.A., Weedman D.W., 1976, Ap.J., 205, 44.

Sulentic J.W., Tifft W.G., 1973, 'The Revised New General Catalogue of Non-Stellar Astronomical Objects',(Univ. Arizona Press, Tucson).

Tananbaum H., Peters G., Forman W., Giacconi R., Jones C., Avni Y., 1978, Ap.J., submitted.

Tarter C.B., Salpeter E.E., 1969 b, Ap.J., 156, 943.

Tarter C.B., Tucker W.H., Salpeter E.E., 1969 a, Ap.J., 156, 943.

Tohline J.E., Osterbrock D.E., 1976, Ap.J., 210, L117.

Tucker W.H., Kellogg E., Gursky H., Giacconi R., Tananbaum H., 1973, Ap.J., 180, 715.

Ulmer M.P., Murray S.S., 1976, Ap.J., 207, 364.

Ulrich M-H., Kinman T.D., Lynds C.R., Rieke G.H., Ekers R.D., 1975, Ap.J., 198, 261.

van den Bergh S., 1975, JR astr Soc Canada, 69, 105.

van der Kruit P.C., 1971, A.& Ap., 15, 110.

van der Kruit P.C., 1973, A.& Ap., 29, 263.

Villa G., Page C.G., Turner M.J.L., Cooke B.A., Ricketts M.J., Pounds K.A., 1976, MNRAS, 176, 609.

Vorontsov-Velyaminov B., Krasnogorskaja, A., 1962, 'Morphological Catalogue of Galaxies', (Moscow, USSR).

Ward M.J., Wilson A.S., Disney M.J., Elvis M., Maccacaro T., 1977, A.&Ap., 56, L19.

Ward M.J., Penston M.V., Boksenberg A., Sargent W.L.W., 1978, in preparation.

Ward M.J., Wilson A.S., Penston M.V., Elvis M., Maccacaro T., Tritton K.P., 1978, Ap.J., submitted.

Walker M.F., 1968, Ap.J., 151, 71.

Warwick R.S., Pye J.P., 1978, MNRAS, submitted.

Weedman D.W., 1973, Ap.J., 183, 29.

Weedman D.W., 1977, Ann. Rev. Astr. and Ap., 15, 69.

White G.J., Ricketts M.J., 1977, MNRAS, 181, 435.

White G.J., Ricketts M.J., Lloyd C., 1978, in preparation.

Wolff R.S., Mitchell R.J., Charles P.A., Culhane J.L., 1976, Ap.J., 208, 1.

Wills D., Wills B.J., 1974, Ap.J., 190, 271.

Wilson A.M., 1977, M.Sc. thesis, University of Birmingham.

Wilson A.S., Penston M.V., Fosbury R.A.E., Boksenberg A., 1976, MNRAS, 177, 673.

Winkler P.F., White A.E., 1975, Ap.J., 199, L139.

Zwicky F., 1964, Ap.J., 140, 1467.

Zwicky F., Herzog E., 1963, 'Catalogue of Galaxies and Clusters of Galaxies', 2.

Zwicky F., Herzog E., 1966, 'Catalogue of Galaxies and Clusters of Galaxies', 3.

Zwicky F., Herzog E., 1968, 'Catalogue of Galaxies and Clusters of Galaxies', 4.

Zwicky F., Herzog E., Wild P., 1961,
'Catalogue of Galaxies and Clusters of Galaxies', 1.

Zwicky F., Karpowitz M., Kowal C., 1965,
'Catalogue of Galaxies and Clusters of Galaxies', 5.

Zwicky F., Kowal C., 1968, 'Catalogue of Galaxies and Clusters of Galaxies', 6.

THE *ARIEL V* (SSI) CATALOGUE OF HIGH GALACTIC LATITUDE ($|b| > 10°$) X-RAY SOURCES

B. A. Cooke, M. J. Ricketts, T. Maccacaro, J. P. Pye, M. Elvis, M. G. Watson, R. E. Griffiths, K. A. Pounds, I. McHardy, D. Maccagni, F. D. Seward, C. G. Page and M. J. L. Turner

REPRINTED FROM

Mon. Not. R. astr. Soc. (1978) **182**, 455–470

PUBLISHED BY

BLACKWELL SCIENTIFIC PUBLICATIONS

OXFORD LONDON EDINBURGH MELBOURNE

Mon. Not. R. astr. Soc. (1978) 182, 489–515

The *Ariel V* (SSI) catalogue of high galactic latitude ($|b| > 10^\circ$) X-ray sources

B. A. Cooke, M. J. Ricketts, T. Maccacaro*, J. P. Pye, M. Elvis, M. G. Watson, R. E. Griffiths†, K. A. Pounds, I. McHardy, D. Maccagni‡, F. D. Seward§, C. G. Page and M. J. L. Turner

X-ray Astronomy Group, Physics Department, University of Leicester, Leicester LE1 7RH

Received 1977 July 8; in original form 1977 April 1

Summary. The 2A catalogue is the result of 10 000 orbits of observation by the Leicester University Sky Survey Instrument on the *Ariel V* satellite and it contains 105 X-ray sources with $|b| > 10^\circ$. The procedures and criteria used in establishing these sources and measuring their intensities and positions are described. As a consequence of the comparatively small error boxes (0.1 to 0.5 square degree) and the sensitivity limit of the survey (90 per cent of the sky to better than 1.2 *Ariel* count/s ≈ 3.2 *Uhuru* count/s), new optical identifications are suggested.

1 Introduction

The Leicester Sky Survey Instrument (SSI) on *Ariel V* started observations of X-ray sources in 1974 October. Its principal aims were (i) to carry out a new and more complete sky survey in the 2–18 keV range (the 3U survey by Giacconi *et al.* 1974 was essentially complete over the whole sky only down to ~10 *Uhuru* count/s, with decreasing coverage down to ~2 *Uhuru* count/s), (ii) to take a detailed study of source variability, and (iii) to improve the positional accuracy of less well-defined 3U sources and aid their identification. As many of the sources seen by the SSI near the galactic plane have already been described (Villa *et al.* 1976; Seward *et al.* 1976a, b), this catalogue has been restricted to $|b| > 10^\circ$ in order to concentrate on X-ray sources which are potentially extragalactic. The data presented are the result of approximately two years of surveying, producing a sky coverage to a depth of approximately 1.2 *Ariel* count/s (≈ 3.2 *Uhuru* count/s) and a catalogue containing 105 sources.

* On leave from: Istituto di Fisica Dell'Università, Milano, Italy.
† Present address: Center for Astrophysics, 60 Garden Street, Cambridge, Massachusetts 02138, USA.
‡ On leave from: Laboratorio de Fisica Cosmica e Tecnologie Relative, CNR, Milano, Italy.
§ On leave from: Lawrence Livermore Laboratory, Livermore, California, USA.

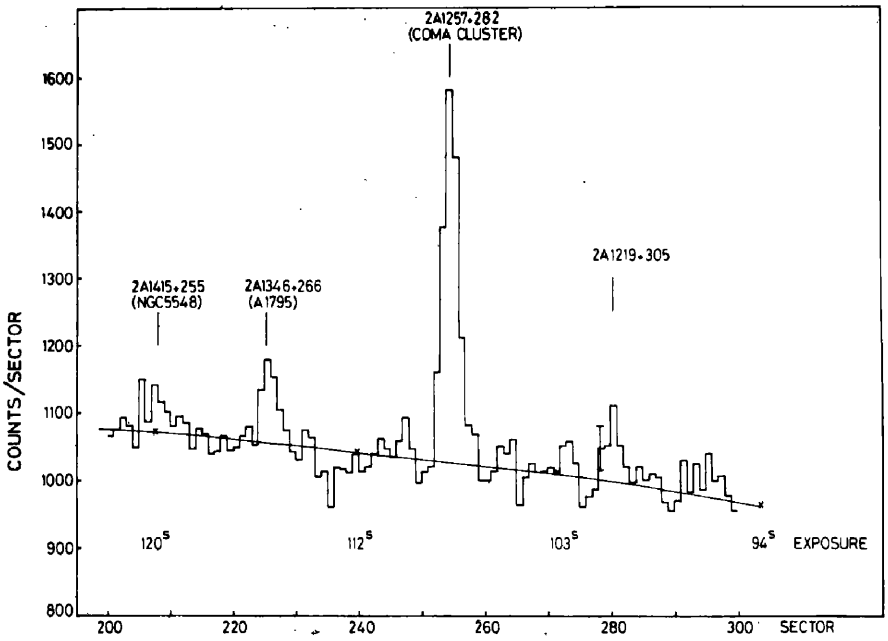

Figure 1. Part of a 51-orbit superimposed data set showing the Coma Cluster, 2A 1257 + 283, a source with improved position 2A 1346 + 266 (was 3U 1349 + 24), identified now with A1795 and two new *Ariel* sources 2A 1415 + 255 (identified with a Seyfert Galaxy NGC 5548) and 2A 1219 + 305. The best-fitting background and the sky exposure time (centre of collimator) are also shown.

2 Description of the instrument

A detailed description of the SSI has been published previously (Villa *et al.* 1976). Briefly it consists of a set of proportional counters viewing from the side of the spin-stabilized spacecraft and having a 'fan beam' field of view set by mechanical collimators. The field of view is $0°.75 \times 12°.0$ (FWHM) with the long axis inclined at 65° to the spin plane. As the satellite spins, the SSI therefore sweeps over a great circle of the sky, viewing a strip some 10° wide. Most of the survey data were taken in a mode where a 360° strip of sky, divided in 1024 spatial elements or sectors, is integrated for one orbit. No spectral resolution is used in this mode so that the data apply to the whole spectral range 2–18 keV. The sensitivity is such that in one orbit a source ~ 5 *Ariel* count/s at 100 per cent collimator transmission is visible at the 3σ level above a background of diffuse X-rays and cosmic rays. Typically *Ariel V* holds a given spin-axis position for several days, correcting the attitude drift as necessary, so that we are able to superimpose data from many orbits and improve the sensitivity. Fig. 1 shows part of an observation with the SSI at high galactic latitude, where 51 orbits have been superimposed. In general, observations of sources which are more than 6° from the centre of the collimator have not been used to estimate source positions, intensities or upper limits on intensities.

3 Data analysis

Sets of superimposed orbit data are scanned automatically, and the first task is to fit an acceptable background. The background level is only a slowly varying function of position since (a) the high-energy particle flux is spread evenly in all sectors by the axial rotation of the spacecraft, (b) the diffuse cosmic X-ray flux is apparently isotropic, and exposure time varies slowly with position, (c) fluorescent X-rays from the upper atmosphere of the Earth, which are detectable during solar outbursts, are spread over many sectors by the orbital motion of the spacecraft. The chance of background fluctuations giving rise to a significant peak with a shape like that of a source is very small, so that the probability of an inter-

section of three such lines is negligible. With the background subtracted, the data are searched for any peaks which, when fitted by the equivalent of a point-source response, exceed the local background by 2.5σ. The file of positions and heights is then matched against a catalogue of known sources, mainly 3U and MX (Markert *et al.* 1975), and peaks inconsistent with a position within the quoted error box are listed as new sources. Eventually all the 'matched' and 'new' peaks are plotted on an all-sky map as boxes (called 'lines of position' hereafter) of length 24° and angular width as defined in Section 5. Using this map, potential new sources are picked out by eye by searching for plausible intersections of at least three lines of position. Revised positions for sources already catalogued are determined in the same way, except that a minimum of five detections of 2.5σ or greater was required for any source which did not satisfy the three times 3σ criterion (see Section 5).

Before assigning a source to the 2A catalogue, the data from which each line of position was derived were checked for reasonableness of background fitting and peak shape, and the possibility that the peak was due to a distant sighting of a very strong galactic source, e.g. Sco X-1 or the Sun, was investigated. Supporting positional data of less statistical significance were also searched for.

4 Sky coverage

The concentration of the *Ariel V* spin-axis pointing directions in the galactic plane (influenced by the other, on-axis experiments) has produced a non-uniform sky coverage with highest density near the galactic poles. However, we have attempted to achieve, for all points in the sky, at least three data sets which are capable of yielding a 3σ signal from sources of intensity 1 *Ariel* count/s. Following the criterion of requiring three intersecting 3σ lines of position, the minimum source intensity detectable in a region of sky is that capable of producing a 3σ peak in the data set which is the third most sensitive for that region. Contours of this parameter on an azimuthal equal-area projection are shown in Fig. 2(a) and (b). The fraction of sky covered as a function of source intensity is shown in Fig. 3 (solid line). This method produces a small underestimate of the sky coverage which is discussed in Section 9.

5 Determination of source position

During the production of this catalogue, it became obvious that a number of 3U and MX sources were not detected by the SSI and therefore that at least some high-latitude X-ray sources are variable, but on unknown timescales. Criteria for source existence based on a consistent intensity could therefore be misleading and the 2A criteria are based on significance alone, namely that a source must have produced at least three sightings of 3σ or greater. In some cases, when the *Ariel V* pointing experiments have returned several times to a particular source, the three sightings could produce lines of position at very similar position angles. In such cases additional observations were arranged to produce a new line of position as nearly orthogonal as possible.

To produce a positional error box for a source, the line-of-position data were combined using a probability contouring program to give the 90 per cent iso-probability contour and the point of maximum probability density (see for example Davison 1973). The latter is the quoted source position (Table 1, column 4) and has been used for computation of the source intensity. To facilitate replotting a source error box (e.g. on star charts), the 90 per cent contours were fitted by ellipses and the corners of the circumscribing rectangle (in azimuthal equal-area projection) having sides parallel to the ellipse axes are quoted in Table 1, column 5.

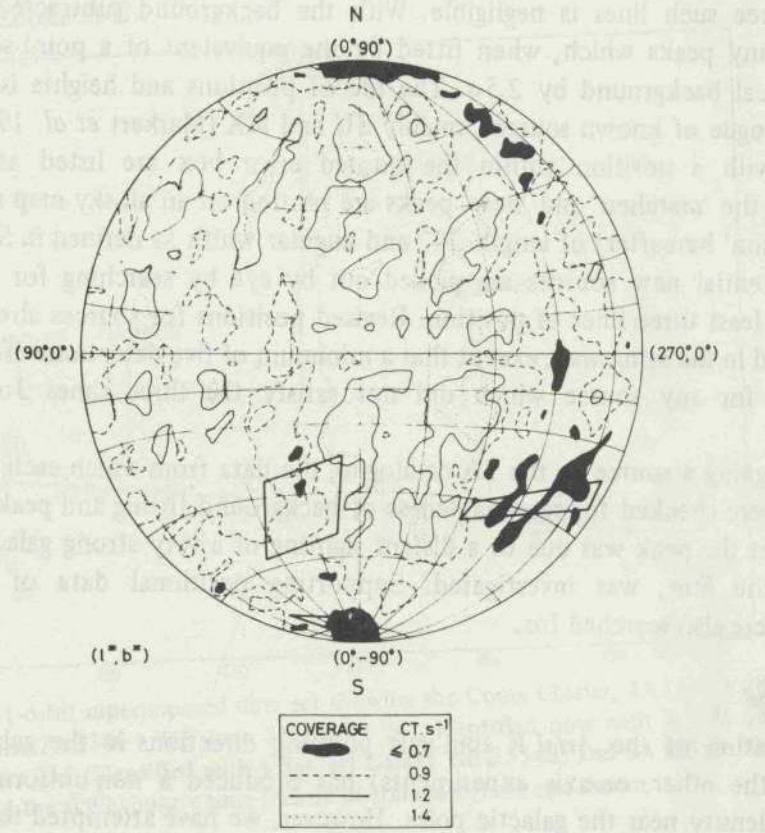

(a)

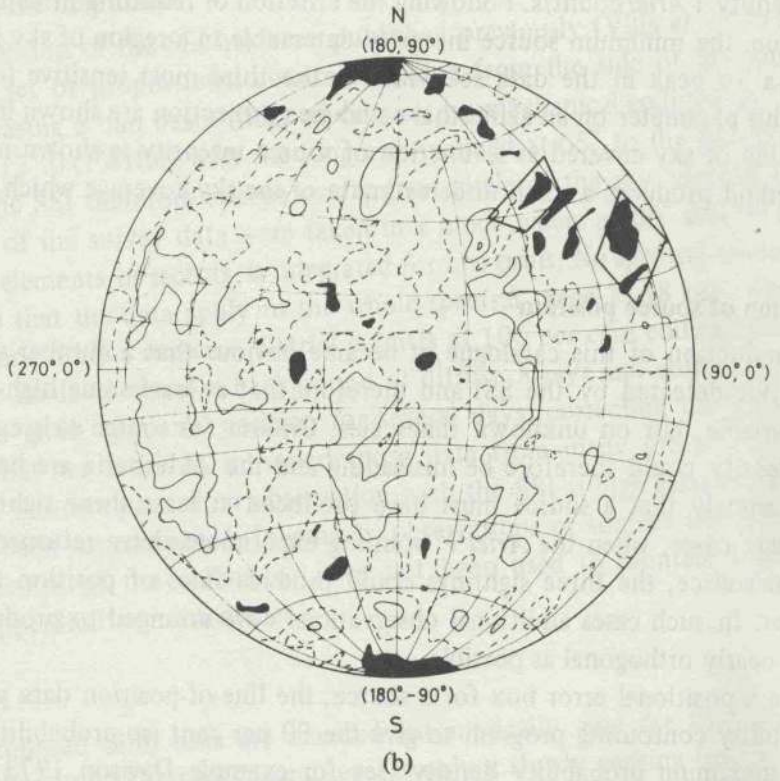

(b)

Figure 2. (a and b) Sky coverage maps showing minimum detectable (3σ) intensity for source discovery at each point in the sky. Intensity contours are: $\leqslant 0.7$ *Ariel* count/s = Black; 0.9 *Ariel* count/s = – – –; 1.2 *Ariel* count/s = ——; 1.4 *Ariel* count/s = ... The maps are equal-area azimuthal projections in l, b with grid lines at intervals of 20° with additional lines at $b = \pm 10°$. Fig. 2(a) has its centre at (0°, 0°) and (b) at (180°, 0°). The 'confused regions' described in Section 9 and Table 3 are enclosed with heavy lines.

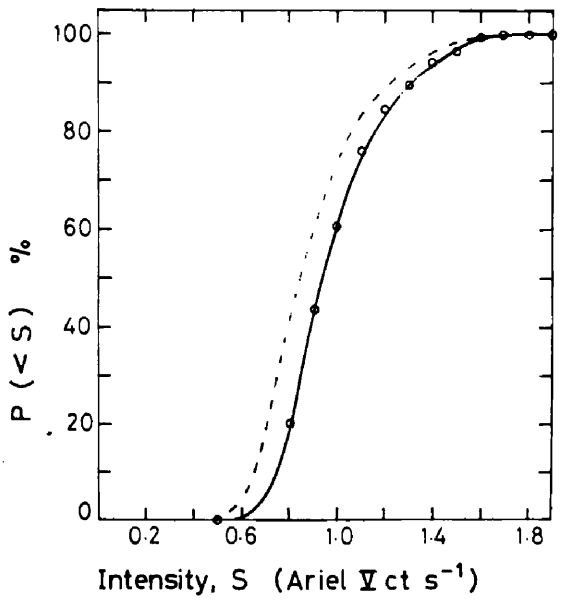

Figure 3. Percentage of the high-latitude sky ($|b| > 10°$) covered to a minimum detectable (3σ) intensity $< S$ *Ariel* count/s for source discovery, according to the criteria of (a) the minimum detectable intensity on the third most sensitive data set (solid line), and (b) the minimum detectable intensity for which the probable number of sightings, taking account of all useful data sets, is just three (dashed line).

Each input line of position to the contouring program was a one-dimensional Gaussian distribution, perpendicular to the major axis of the line of position, of standard deviation σ given by

$$\sigma^2 = (\mathrm{FWHM})^2/3\sigma_D^2 + A^2$$

where $\sigma_D = S/\sqrt{N}$, the signal-to-root-background counts of the peak detected in the data set, and A is an angle ($= 0°.07$) which represents a positional error arising from systematic errors in the spacecraft attitude and the mechanical alignment of the SSI, and is estimated by contouring sources with very precise positions (e.g. Cyg X-1, Crab Nebula). The accuracy of this distribution width was tested by using the routine analysis procedures on simulated randomized data. A comparison of the σ from the distribution of peak positions found in the simulation, with that calculated from the above formula with the simulated signal-to-noise ratio, shows that the formula is appropriate for $\sigma_D > 3$. For a relatively intense high-latitude X-ray source such as 2A 0316+413 (Perseus Cluster/NGC 1275), for which we have a large number of source detections, the resulting contour is essentially a test of the positional accuracy possible with the SSI. The contour, Fig. 4, is approximately circular of width $\sim 0°.1$ and agrees well with the error box for 3U 0316+41 and the actual position of NGC 1275.

As this is a catalogue of X-ray sources detected by the SSI, all the objects in Table 1 have a 2A name (the prefix 2 distinguishing sources from those previously reported from any of the *Ariel V* experiments which have a variety of detection and location criteria). To reflect the general improvement in source positions obtained with the SSI, the IAU notation has been adopted with an additional digit in the declination part of the source name. The distribution of error box sizes in the 2A and 3U catalogues is shown in Fig. 5. In the *Uhuru* catalogue the second peak and the largest error boxes presumably result from observations with the side 2 detector ($5° \times 5°$ collimator). Because of the size of some of the 3U error boxes it is difficult to know whether or not a nearby 2A source should be associated with it. Tentative associations are flagged with a question mark. Comparing the 2A and MX data,

Table 1

ARIEL NAME ST	OTHER NAMES	POSITION RA DEC / LII BII	ERROR BOX RA DEC	RA DEC	RA DEC	RA DEC	AREA	AV ERR	INTENSITY MIN ERR	MAX ERR	CODE	IDENT OBJECT CODE	OTHER INFORMATION
2A0039+411 IMP PST	3U0021+42	9.75 120.98 41.10 -21.46	10.90 40.90	9.25 41.87	8.67 41.22	10.27 40.38	1.150	.7 .2				M31 **	RPROB=0.026
2A0039-096 IMP	3U0026-09	9.94 115.57 -9.63 -72.10	9.73 -9.50	9.70 -9.69	10.16 -9.77	10.21 -9.58	.075	1.2 .1			S	A85[E] *	A89,WKB0039-096, FJ0038-09 ALSO NEAR
2A0042+323 CON	3U0042+32	10.72 121.50 32.35 -30.23	10.78 31.84	10.42 32.78	10.62 32.83	10.98 31.89	.137		.1 .1	14.0 2.0	T		RISETIME < 1 DAY
2A0054-015 NEW		13.73 126.39 -1.58 -64.14	14.18 -2.03	13.01 -1.46	13.17 -1.13	14.34 -1.69	.365	.8 .1			S	A119[E] **	3C29,4C-1.04 IN BOX L.F.RADIO [A]
2A0102-222 NEW		15.50 153.45 -22.24 -84.06	15.93 -21.90	14.90 -21.90	15.00 -22.60	16.00 -22.50	.700	.4 .1			S	A133 *	
2A0102-242 NEW PST	3U0057-23?	15.50 166.60 -24.25 -85.70	16.00 -23.75	14.90 -23.75	15.00 -24.75	16.00 -24.75	1.000	.3 .1				A140 *	A141 ON EDGE OF BOX RPROB=0.009
2A0116-737 CON	3U0115-73 SMC X-1	19.05 300.39 -73.78 -43.48	19.23 -73.83	18.74 -73.79	18.82 -73.71	19.31 -73.76	.009		.8 .2	23.0 2.0	P	SK160[B] ****	0.7S & 3.9D PERIODS, EXTENDED LOWS [C,D]
2A0120-591 NEW		20.16 295.38 -59.11 -57.82	20.78 -59.34	19.38 -59.24	19.49 -58.89	20.88 -59.99	.207	.5 .1			S		NGC484 OUTSIDE TO N.
2A0120-353 NEW		20.23 264.31 -35.32 -79.56	19.94 -35.33	20.41 -35.14	20.52 -35.30	20.05 -35.51	.063	.7 .1			S	GROUP *	CONTAINS NGC526,527
2A0207-746 NEW		31.90 296.15 -74.64 -41.70	32.89 -74.60	30.87 -74.94	30.40 -74.75	32.40 -74.41	.106		0.0 .2	11.8 2.9	T		

[A] : FELDMAN 1977,PRIVATE COMMUNICATION
[B] : WEBSTER ET AL.1972.
[C] : LUCKE ET AL.1976.
[D] : SCHREIER ET AL.1972.
[E] : MACCAGNI ET AL.1977.

ARIEL NAME ST	OTHER NAMES	POSITION RA DEC / LII BII	ERROR BOX RA DEC RA DEC RA DEC RA DEC	AREA	INTENSITY AV ERR / MIN ERR / MAX ERR	CODE	IDENT OBJECT CODE	OTHER INFORMATION
2A0235-526 NEW		38.77 -52.62 / 272.24 -57.99	39.04 -52.54 / 38.76 -52.84 / 38.37 -52.71 / 38.65 -52.40	.078	.5 .1	S		
2A0251+413 IMP	3U0227+43 MX0255+41	42.98 41.38 / 146.45 -15.57	42.75 41.18 / 42.84 41.61 / 43.17 41.57 / 43.08 41.14	.083	1.9 .1	S	NGC 1129 **	GROUP
2A0252+060 NEW		43.07 6.09 / 169.28 -45.18	43.02 5.72 / 42.75 6.31 / 43.10 6.47 / 43.37 5.88	.192	.5 .1	S		A400 ON EDGE OF BOX WHICH CONTAINS 3C75
2A0255+132 IMP	3U0254+13	43.87 13.23 / 164.12 -39.10	43.88 13.41 / 44.01 13.15 / 43.84 13.07 / 43.71 13.32	.041	1.5 .1	S	A401[E] *	BETWEEN A401 & A399 L.F.RADIO [A]
2A0311-227 NEW		47.91 -22.78 / 212.89 -57.49	48.11 -22.73 / 47.98 -22.98 / 47.69 -22.84 / 47.91 -22.59	.056	1.1 .1	S		
2A0316-443 NEW		49.05 -44.31 / 252.75 -56.12	48.57 -44.52 / 48.98 -43.92 / 49.49 -44.09 / 49.08 -44.70	.210	.5 .1	S	CLUSTER[E] *	PKS0316-44 IN BOX
2A0316+413 CON	3U0316+41	49.11 41.37 / 150.55 -13.23	48.98 41.31 / 49.08 41.46 / 49.22 41.40 / 49.12 41.26	.015	18.5 .4	S	PERSEUS CL ****	EXTENDED[B].CONTAINS PT.SOURCE NGC1275[C]
2A0335+096 NEW		53.83 9.63 / 176.29 -35.29	53.36 9.13 / 53.86 10.34 / 54.26 10.18 / 53.75 8.97	.414	.8 .1	S	GROUP *	LINE OF GALS. CONTAINING V.CLOSE PAIR
2A0343-536 IMP	3U0328-52	55.82 -53.63 / 264.68 -48.76	56.28 -53.64 / 55.61 -53.89 / 55.36 -53.64 / 56.03 -53.40	.110	.7 .1 / .1 .2 / 1.4 .3	I		CLUSTER CA0340-538 ON EDGE OF BOX [D]
2A0349-139 NEW		57.30 -13.94 / 204.58 -46.02	56.99 -14.30 / 57.04 -13.55 / 57.56 -13.59 / 57.50 -14.33	.296	.3 .1	S		QUASAR PKS0349-1403 NEARBY

[A] : FELDMAN 1977,PRIVATE COMMUNICATION
[B] : FORMAN ET AL.1972.
[C] : GORENSTEIN ET AL.1977.
[D] : PYE & COOKE 1976A.
[E] : MACCAGNI ET AL.1977.

Table 1 – *continued*

ARIEL NAME	ST	OTHER NAMES	POSITION RA DEC	LII BII	ERROR BOX RA DEC	RA DEC	RA DEC	RA DEC	AREA	INTENSITY AV ERR	MIN ERR	MAX ERR	CODE	IDENT OBJECT CODE	OTHER INFORMATION
2A0352+309	CON	3U0352+30	58.05 30.94	163.04 -17.11	58.02 30.85	57.97 30.99	58.09 31.02	58.14 30.89	.12	7.8 .1	6.6 .4	11.3 .9	I	X PER[A] ****	13.9M X-RAY/OPTICAL PERIOD [B,C]
2A0411+103	IMP	3U0405+10	62.81 10.39	182.49 -28.15	62.64 10.15	62.63 10.60	62.91 10.61	62.92 10.16	.100	1.2 .1			S	A478 **	[D]
2A0430-615	IMP	3U0426-63	67.74 -61.57	272.14 -40.10	68.27 -61.41	67.41 -61.84	67.16 -61.73	68.03 -61.30	.377	1.1 .1	.9 .1	2.0 .3	I		CLUSTER SERS 40/6 IN BOX[E,K]. PKS0429-61
2A0431-136	NEW		67.80 -13.61	209.85 -36.61	67.70 -13.81	67.67 -13.41	67.88 -13.39	67.91 -13.79	.067	.9 .1			S	A496 **	L.F.RADIO [F]
2A0456-449	IMP	3U0510-44	74.17 -44.93	250.17 -38.38	73.37 -45.80	73.87 -43.90	74.87 -44.02	74.41 -45.94	1.130	.7 .1			S		
2A0512-399	IMP	MX0513-40	78.15 -39.97	244.36 -34.99	78.25 -39.74	78.31 -40.19	78.03 -40.21	77.98 -39.76	.075	1.2 .1	.5 .4	3.0 .4	I	NGC1851 **	GLOBULAR CLUSTER [G,H,I]
2A0521-720	CON	3U0521-72 LMC X-2	80.32 -72.07	283.17 -32.68	80.34 -72.17	79.99 -72.07	80.30 -71.97	80.64 -72.07	.016	7.0 .5					IN LMC. CONFUSED REGION
2A0526-328	NEW		81.74 -32.85	236.74 -30.73	81.49 -33.11	81.51 -32.56	81.96 -32.57	81.94 -33.12	.160	.8 .1			S		
2A0532-664	CON	3U0532-66 LMC X-4	83.13 -66.43	276.37 -32.55	83.75 -66.78	82.06 -66.31	82.50 -66.07	84.18 -66.53	.200	2.0 .5					IN LMC. CONFUSED REGION
2A0532-056	IMP	3U0527-05	83.21 -5.65	209.23 -19.48	83.18 -5.89	83.08 -5.41	83.21 -5.38	83.31 -5.86	.053	1.9 .1			S	02 ORI *	ORION NEBULA. [J]

[A] : GIACCONI ET AL.1974.
[B] : WHITE ET AL.1976.
[C] : LILLER 1975.
[D] : ELVIS ET AL.1975A.
[E] : VIDAL 1975.
[F] : FELDMAN 1977,PRIVATE COMMUNICATION
[G] : CLARK ET AL.1975.
[H] : PYE & COOKE 1976B.
[I] : GRINDLAY 1976.
[J] : WHITE & RICKETTS 1977.
[K] : MACCAGNI ET AL.1977.

ARIEL NAME	ST	OTHER NAMES	POSITION RA DEC	LII BII	ERROR BOX RA DEC	RA DEC	RA DEC	RA DEC	AREA	INTENSITY AV ERR	MIN ERR	MAX ERR	CODE	IDENT OBJECT CODE	OTHER INFORMATION
2A0539-642	CON	3U0539-64 LMC X-3	84.94 -64.20	273.68 -31.96	84.63 -64.09	85.28 -64.15	85.20 -64.30	84.56 -64.24	.037	6.0 .5					IN LMC. CONFUSED REGION
2A0540-698	CON	3U0540-69 LMC X-1	85.21 -69.82	280.26 -31.45	85.54 -69.81	85.14 -69.93	84.87 -69.82	85.27 -69.70	.020	6.0 .5					IN LMC. CONFUSED REGION
2A0551+466	NEW	MX0600+46?	87.81 46.62	165.57 10.51	87.63 46.36	87.60 46.86	87.94 46.88	88.02 46.38	.093	1.0 .1	.1 .4	1.6 .2	I	MCG8-11-11 **	SEYFERT GALAXY [A]
2A0608+497	NEW	MX0600+46?	92.21 49.73	164.11 14.54	92.24 50.39	92.58 49.12	92.06 49.06	91.71 50.33	.344	.5 .1			S		
2A0626-541	IMP	3U0624-55	96.54 -54.17	262.95 -25.14	96.74 -53.87	96.88 -54.45	96.28 -54.50	96.15 -53.92	.162	.8 .1			S	CLUST[B,O] **	OTHER BRIGHT GALS. & FJ0635-54 NEARBY
2A0708-357	IMP PST	3U0657-35	107.00 -35.70	247.15 -12.05	107.00 -34.90	106.30 -35.90	107.20 -36.40	107.90 -35.30	1.070	.6 .1					RPROB=0.1
2A0710+456	NEW		107.69 45.63	172.05 22.82	107.47 45.34	107.41 45.89	107.90 45.92	107.96 45.36	.150	.6 .1			S	MKN376 **	SEYFERT GALAXY [C]
2A0738+498	NEW		114.31 49.89	168.62 28.26	113.70 48.78	114.74 50.95	115.15 50.87	114.09 48.70	.584	.6 .1			S	MKN79 *	SEYFERT GALAXY [C]
2A0815-075	NEW		123.80 -7.50	230.09 15.26	124.00 -7.20	123.40 -7.20	123.40 -8.00	124.00 -8.00	.450	.8 .1			S	A644 *	
2A0859+509	NEW PST		134.76 50.95	157.87 41.15	132.91 48.95	136.13 52.97	136.60 52.82	133.35 48.81	1.448	.3 .1					MCG+09-15-041 & -055 IN BOX. RPROB=0.085

[A] : WARD ET AL.1977.
[B] : VIDAL 1975.
[C] : WEEDMAN 1977.
[D] : MACCAGNI ET AL.1977.

Table 1 — *continued*

ARIEL NAME	ST	OTHER NAMES	POSITION RA DEC / LII BII	ERROR BOX RA DEC RA DEC RA DEC RA DEC	AREA	INTENSITY AV ERR	MIN ERR	MAX ERR	CODE	IDENT OBJECT CODE	OTHER INFORMATION
2A0906-095	IMP	3U0901-09	136.57 -9.54 / 239.33 24.67	136.48 -9.79 136.38 -9.36 136.63 -9.31 136.73 -9.74	.085	1.6 .1			S	A754 [A] **	WK80906-095 MSH09-002
2A0922-317	NEW		140.53 -31.71 / 259.72 13.06	140.51 -31.92 140.28 -31.60 140.53 -31.48 141.75 -31.80	.072	1.3 .1			S		[B]
2A0943-140	NEW		145.84 -14.03 / 249.66 28.84	145.76 -14.18 145.71 -13.86 145.98 -13.87 145.96 -14.19	.065	1.6 .1			S	NGC2992/3 *	POSSIBLE INTERACTING SYSTEM
2A0946-310	CON	3U0946-30	146.60 -31.02 / 263.11 17.14	146.39 -30.48 147.00 -31.42 146.76 -31.54 146.15 -30.59	.197	1.1 .1			S		NGC3001 ON EDGE, NGC2997 OUTSIDE
2A0954+700	IMP	3U0943+71	148.60 70.04 / 141.10 40.68	147.52 69.67 148.62 70.63 149.63 70.50 148.49 69.54	.311	.7 .1			S	M82 **	
2A1033-270	IMP	3U1044-30	158.38 -27.01 / 259.27 26.60	158.46 -27.39 157.97 -26.83 158.26 -26.63 158.75 -27.20	.182	.7 .1			S	A1060 **	
2A1058-226	NEW		164.66 -22.67 / 272.26 33.28	164.77 -23.32 164.15 -22.17 164.51 -22.01 165.13 -23.16	.377	.5 .1			S	A1146[C] *	NGC3511,3513 JUST OUTSIDE BOX
2A1102+384	NEW		165.50 38.42 / 179.92 65.11	165.28 38.38 165.62 38.58 165.73 38.46 165.39 38.26	.036	.8 .2	18.9 2.0		F	MKN421 **	BL LAC OBJECT [D]
2A1135-373	NEW		173.94 -37.36 / 287.26 23.00	174.17 -37.65 173.53 -37.24 173.71 -37.06 174.35 -37.47	.118	1.1 .1			S	NGC3783 **	SEYFERT GALAXY [E]
2A1141+199	CON PST	3U1144+19	175.34 19.95 / 235.09 72.84	175.32 21.34 174.48 21.06 175.28 18.88 176.10 19.14	1.950	.6 .2				A1367 *	3C264 IN CLUSTER RPROB=0.017

[A] : PYE ET AL.1976.
[B] : SEWARD ET AL.1976A.
[C] : MACCAGNI ET AL.1977.
[D] : RICKETTS ET AL.1976.
[E] : COOKE ET AL.1976.

ARIEL NAME	ST	OTHER NAMES	POSITION RA DEC	LII BII	ERROR BOX RA DEC	RA DEC	RA DEC	RA DEC	AREA	INTENSITY AV ERR	MIN ERR	MAX ERR	CODE	IDENT OBJECT CODE	OTHER INFORMATION
2A1150+720	NEW		177.52 72.08	129.31 44.59	176.57 72.20	178.30 72.19	178.27 71.95	176.56 71.97	.101	.8 .1					CONFUSED REGION
2A1207+397	CON	3U1207+39	181.97 39.79	154.91 74.96	182.05 39.72	181.88 39.74	181.90 39.84	182.06 39.83	.011	3.2 .2		5.5 .8	F	NGC4151 ***	SEYFERT GALAXY. LIGHT CURVE [A]
2A1219+305	NEW		184.82 30.51	185.67 82.80	185.10 30.61	184.72 30.23	184.51 30.39	184.88 30.77	.095	.9 .1	.1 .3	2.8 .6	I		NGC4314,4308 NEARBY
2A1225+022	CON	3U1224+02	186.49 2.21	289.67 64.21	186.69 2.22	186.42 2.00	186.26 2.19	186.53 2.41	.070	1.4 .2	.4 .3	2.1 .3	I	3C273 ***	QUASAR [B,E]
2A1228+125	CON	3U1228+12	187.23 12.58	284.42 74.45	187.16 12.70	187.37 12.58	187.28 12.44	187.08 12.56	.029	7.8 .3			S	VIRGO CL. ****	EXTENDED[B].CONTAINS POINT SOURCE M87[C]
2A1246-410	CON	3U1247-41	191.57 -41.05	302.45 21.55	191.97 -41.27	191.03 -40.97	191.10 -40.83	192.05 -41.13	.094	2.4 .1			S	CEN. CL. ***	FJ1245-41
2A1251-290	CON	3U1252-28	192.99 -29.01	303.78 33.59	193.43 -29.13	192.62 -29.28	192.53 -28.88	193.33 -28.74	.228	1.8 .1			S	CLUSTER **	MSH12-212
2A1257+283	CON	3U1257+28	134.36 28.30	59.24 87.93	194.42 28.33	194.35 28.24	194.29 28.27	194.36 28.36	.005	6.7 .1			S	COMA CL. ****	EXTENDED [D]. LIGHT CURVE [A]
2A1306-012	NEW		196.53 -1.28	311.86 61.03	196.92 -1.12	196.35 -1.71	196.11 -1.48	196.67 -.88	.210	1.1 .1			S		PKS1305-01 NEARBY
2A1322-427	CON	3U1322-42	200.74 -42.71	309.61 19.46	200.88 -42.75	200.63 -42.80	200.58 -42.66	200.83 -42.61	.021	8.8 .1	4.2 .5	17.5 1.0	F	NGC5128 ****	CEN A. LIGHT CURVE [F]

[A] : ELVIS 1976.
[B] : KELLOGG ET AL.1971.
[C] : GORENSTEIN ET AL.1976.
[D] : GURSKY ET AL.1971.
[E] : WHITE & RICKETTS 1977,IN PREP.
[F] : LAWRENCE ET AL.1977,IN PREPARATION

Table 1 – *continued*

ARIEL NAME	ST	OTHER NAMES	POSITION RA DEC	LII BII	ERROR BOX RA DEC	RA DEC	RA DEC	RA DEC	AREA	INTENSITY AV ERR	MIN ERR	MAX ERR	CODE	IDENT OBJECT CODE	OTHER INFORMATION
2A1326-311	IMP	MX1329-31	201.71 -31.16	312.42 30.75	201.33 -30.82	202.20 -31.02	202.05 -31.51	201.17 -31.31	.314	1.2 .1	0.0 0.0	0.0 0.0	S	CLUSTER **	PKS1327-31
2A1344-325	IMP	MX1347-32	206.20 -32.55	316.38 28.60	206.85 -32.42	206.53 -32.45	206.52 -32.68	205.84 -32.65	.101	2.8 .2	0.0 0.0	0.0 0.0	S	CLUSTER **	
2A1346+266	IMP	3U1349+2-	206.70 26.68	33.11 77.12	206.46 26.49	206.71 26.97	206.91 26.88	206.66 26.41	.078	1.1 .1	0.0 0.0	0.0 0.0	S	A1795 **	4C26.42
2A1347-300	NEW		206.78 -30.08	317.65 30.87	206.43 -30.02	207.03 -29.89	207.09 -30.13	206.49 -30.25	.100	1.7 .2	0.0 0.0	0.0 0.0	S	SEE INFO *	CLUSTER CONTAINS SEYFERT IC4329A [A]
2A1348+700	NEW		207.04 70.03	115.72 46.53	207.50 69.43	205.76 70.45	206.48 70.59	208.20 69.57	.275	.9 .2	0.0 0.0	0.0 0.0	S	MKN279 **	SEYFERT GALAXY [A]
2A1410-029	CON	3U1410-03	212.59 -2.92	339.09 53.89	212.18 -2.85	212.84 -2.64	212.96 -3.00	212.30 -3.21	.207	1.3 .2	0.0 0.0	0.0 0.0	S	NGC5506 *	EMISSION LINE GAL[B] NGC5507 ALSO IN BOX
2A1415+255	NEW		213.91 25.56	32.32 70.35	214.23 25.74	213.74 25.25	213.56 25.39	214.06 25.39	.114	.8 .1	0.0 0.0	0.0 0.0	S	NGC5548 *	SEYFERT GALAXY [A]
2A1418+485	NEW		214.67 48.54	89.65 62.66	214.47 48.13	214.30 48.88	214.85 48.93	215.00 48.20	.223	.4 .1	0.0 0.0	0.0 0.0	S	A1904 **	CLUSTER CENTRE JUST OUTSIDE BOX
2A1508+062	NEW	MX1514+06?	227.19 6.22	6.91 50.66	227.41 6.10	227.00 6.03	226.95 6.32	227.36 6.39	.094	1.4 .2	0.0 0.0	0.0 0.0	S	A2029 *	A2033 ALSO NEAR
2A1518+274	NEW PST		229.50 27.40	41.62 57.06	229.75 28.58	227.77 26.12	228.53 25.61	230.56 28.05	2.700	.5 .1	0.0 0.0	0.0 0.0			A2065 & B2 1515+26 IN BOX. RPROB<0.001

[A] : WEEDMAN 1977.

[B] : WILSON ET AL.1976.

ARIEL NAME	ST	OTHER NAMES	POSITION RA / DEC	LII / BII	ERROR BOX RA / DEC	RA / DEC	RA / DEC	RA / DEC	AREA	INTENSITY AV / ERR	MIN / ERR	MAX / ERR	CODE	IDENT OBJECT CODE	OTHER INFORMATION
2A1519+062	NEW	MX1514+06?	229.75 8.20	11.71 49.71	230.37 8.47	229.29 7.70	229.13 7.92	230.20 8.70	.282	1.3 .1	0.0 0.0	0.0 0.0	S	NGC5920 *	3C318.1
2A1556-756	CON	3U1544-75	239.02 -75.66	313.89 -17.17	233.82 -75.84	243.67 -75.12	244.06 -75.37	234.04 -76.11	.662	.9 .1	0.0 0.0	0.0 0.0	S		2 FAINT NEBULAE JUST OUTSIDE BOX.
2A1556+274	IMP	3U1555+27	239.22 27.47	44.41 48.57	238.96 27.35	239.31 27.72	239.48 27.60	239.13 27.23	.072	1.4 .1	0.0 0.0	0.0 0.0	S	A2142 **	[E]
2A1600+164	IMP	3U1551+15	240.10 16.42	29.36 44.55	239.63 16.20	240.30 16.99	240.56 16.66	239.88 15.97	.250	.8 .1	0.0 0.0	0.0 0.0	S	A2147/52 **	[A]
2A1616-155	CON	3U1617-15 SCO X-1	244.20 -15.56	353.01 23.81	244.09 -15.59	244.27 -15.46	244.31 -15.53	244.14 -15.66	.013	3620.0 3.0	2800.0 100.0	6500.0 100.0	I	V818 SCO ****	0.790 RAD.VEL.PERIOD RADIO SOURCE [B,C]
2A1626+396	IMP	3U1639+40	246.69 39.62	62.88 43.72	246.16 39.48	247.08 39.99	247.26 39.80	246.35 39.28	.168	1.2 .1	0.0 0.0	0.0 0.0	S	A2199[E] **	L.F.RADIO [D].
2A1627-673	CON	3U1626-67	246.87 -67.36	321.80 -13.11	246.98 -67.46	246.54 -67.40	246.67 -67.26	247.12 -67.33	.021	8.2 .2	0.0 0.0	0.0 0.0	S		
2A1630+057	IMP PST	3U1623+05	247.50 5.70	21.06 33.32	249.24 7.00	246.37 5.42	246.74 4.77	249.53 6.56	2.100	.3 .1	0.0 0.0	0.0 0.0			A2204 & A2210 IN BOX RPROB=0.1
2A1631-644	IMP	3U1632-64	247.87 -64.41	324.33 -11.45	247.82 -64.66	247.35 -64.29	247.80 -64.18	248.27 -64.55	.072	3.3 .2	0.0 0.0	0.0 0.0	S		
2A1655+353	CON	3U1653+35 HER X-1	253.90 35.39	58.10 37.60	253.77 35.36	253.97 35.49	254.04 35.42	253.83 35.30	.014	0.0 0.0	1.0 .4	65.0 5.0	P	HZ HER[F] ****	1.2S & 1.7D OPT/XRAY PERIODS,35D CY.[F,G]

[A] : COOKE ET AL.1977.
[B] : GIACCONI & GURSKY 1974.
[C] : COWLEY & CRAMPTON 1975.
[D] : FELDMAN 1977,PRIVATE COMMUNICATION
[E] : COOKE & MACCAGNI 1976.
[F] : GIACCONI & GURSKY 1974.
[G] : GURSKY ET AL.1972.

Table 1 – *continued*

ARIEL NAME	ST	OTHER NAMES	POSITION RA / DEC	LII / BII	ERROR BOX RA	RA	RA	RA	AREA	INTENSITY AV ERR	MIN ERR	MAX ERR	CODE	IDENT OBJECT CODE	OTHER INFORMATION
2A1659+337	IMP	3U1706+32	254.82 33.73	56.22 36.56	253.33 33.21	255.84 34.52	256.09 34.18	253.58 32.87	.763	.6 .1			S		A2244/2245 NEARBY
2A1704+241	NEW		256.02 24.15	45.24 33.12	256.04 23.86	255.67 24.19	255.95 24.45	256.32 24.13	.137	.6 .1	0.0 .2	2.8 .3	I		GROUP TO NW JUST OUTSIDE BOX.
2A1705+609	NEW PST		256.30 60.90	90.17 35.23	255.63 61.77	254.61 59.74	256.12 59.55	257.25 61.57	1.620	.4 .1					3C351,NGC6292,6306/7 IN BOX. RPROB=0.024
2A1705+786	CON	3U1706+78	256.42 78.62	110.93 31.84	255.82 78.48	255.93 78.76	256.94 78.74	256.81 78.46	.044	1.2 .1				A2256 **	CONFUSED REGION. NB78.26
2A1815+500	IMP	3U1809+50	273.81 50.00	78.04 25.87	274.00 50.03	273.78 49.86	273.60 49.95	273.82 50.12	.025	2.1 .1			S	AN HER[A] ****	3.1H PERIOD IN SOFT X-RAYS & OPT. [A,B]
2A1822-371	IMP	3U1822-37 SGR X-7	275.55 -37.12	355.85 -11.25	275.42 -37.10	275.63 -37.04	275.67 -37.14	275.46 -37.19	.014	8.9 .2	5.6 .7	10.2 .4	I		
2A1854+683	IMP	3U1843+67	283.59 68.35	99.02 24.84	280.93 67.50	286.48 69.75	287.07 69.55	281.51 67.32	.640	.6 .2				A2312 *	CONFUSED REGION
2A1914-589	NEW		288.67 -58.95	337.92 -26.45	287.72 -59.03	289.01 -58.53	289.54 -58.89	288.24 -59.40	.292	.4 .1			S	UGC141-G55 *	[C]. SEYFERT GALAXY
2A1919+438	IMP	3U1921+43	289.85 43.89	75.71 13.56	289.42 43.73	289.93 44.18	290.18 44.03	289.67 43.58	.101	2.6 .1			S	A2319 **	
2A1938-105	NEW PST		294.67 -10.52	29.14 -15.77	293.47 -11.92	295.42 -8.35	296.05 -8.68	294.12 -12.27	2.240	.7 .1				NGC6814 *	SEYFERT GALAXY [D]. RPROB=0.001

[A] : SZKODY & BROWNLEE 1977. [B] : HEARN & RICHARDSON 1976. [C] : HOLMBERG ET AL.1975.
[D] : WEEDMAN 1977.

ARIEL NAME	ST	OTHER NAMES	POSITION RA / DEC	POSITION LII / BII	ERROR BOX RA	ERROR BOX DEC	ERROR BOX RA	ERROR BOX DEC	AREA	INTENSITY AV / ERR	INTENSITY MIN / ERR	INTENSITY MAX / ERR	CODE	IDENT OBJECT / CODE	OTHER INFORMATION
2A2009-569	NEW		302.28 -56.95	340.90 -33.48	302.71 -56.89	302.06 -57.18	301.83 -57.02	302.47 -56.73	.072	1.2 .1			S	CLUSTER **	CLUSTER ELONGATED NW-SE
2A2040-115	NEW		310.19 -11.56	35.21 -29.98	309.88 -12.17	310.14 -10.83	310.50 -10.90	310.24 -12.23	.398	.9 .1			S	MKN509 *	SEYFERT GALAXY [A]
2A2127+120	IMP	3U2131+11	321.84 12.08	65.09 -27.19	321.65 12.07	321.94 12.21	322.01 12.08	321.72 11.93	.035	2.2 .1	1.4 .3	4.3 .7	I	NGC7078 ***	GLOBULAR CLUSTER [B,C,D]
2A2142+381	CON	3U2142+38 CYG X-2	325.68 38.14	87.38 -11.29	325.78 38.19	325.06 38.19	325.07 38.10	325.78 38.10	.011	132.0 .3	90.0 5.0	300.0 10.0	I	STAR [E] ****	0.860 RAD.VEL.PERIOD RADIO SOURCE [E,F]
2A2151-316	NEW		327.95 -31.67	15.64 -51.48	327.34 -32.02	328.30 -31.13	328.53 -31.31	327.57 -32.20	.254	.9 .1					CONFUSED REGION.3 V. DIST. GROUPS IN BOX
2A2155-609	NEW	MX2140-60?	328.85 -60.98	331.49 -45.67	327.92 -61.58	328.82 -60.24	329.67 -60.38	328.80 -61.72	.515	.8 .2			S		
2A2220-022	NEW		335.11 -2.22	61.84 -46.47	334.84 -2.48	335.07 -1.84	335.37 -1.95	335.15 -2.59	.174	1.0 .1			S	A2440 *	
2A2237-256	NEW	MX2244-24?	339.33 -25.62	28.85 -60.57	338.64 -26.06	339.63 -24.93	339.94 -25.15	338.94 -26.28	.408	.5 .1			S		MCG-04-53-026 IN BOX MCG-04-53-018 NEARBY
2A2251-179	NEW		342.79 -17.97	45.91 -61.32	342.25 -18.19	343.09 -17.55	343.25 -17.74	342.41 -18.38	.187	.8 .1	.2 .2	1.7 .4	I	GROUP *	
2A2259+085	NEW PST		344.88 8.50	82.66 -45.38	343.69 8.61	343.87 7.99	345.62 8.49	345.45 9.11	.920	1.1 .1				NGC7469 *	SEYFERT GALAXY [A] RPROB<0.001

[A] : WEEDMAN 1977.
[B] : GIACCONI ET AL.1974.
[C] : PYE & COOKE 1976B.
[D] : GRINDLAY 1976.
[E] : GIACCONI & GURSKY 1974.
[F] : CRAMPTON & COWLEY 1976.

Table 1 – *continued*

ARIEL NAME ST	OTHER NAMES	POSITION RA DEC	LII BII	ERROR BOX RA DEC	RA DEC	RA DEC	PA DEC	AREA	INTENSITY AV ERR	MIN ERR	MAX ERR	CODE	IDENT OBJECT CODE	OTHER INFORMATION
2A2302-088 NEW		345.55 -8.89	54.21 -58.73	345.32 -8.82	345.62 -8.67	345.75 -8.94	345.45 -9.09	.080	1.1 .1			S		MCG-02-58-022 IN BOX
2A2315-428 NEW		348.83 -42.81	347.81 -65.56	349.11 -42.73	348.78 -43.02	348.54 -42.87	348.87 -42.59	.067	.7 .1	.3 .2	1.4 .2	I	NGC7582 *	GRUS QUARTET. FAINT CLUSTERS NEARBY
2A2318-272 NEW	MX2321-23?	349.61 -27.20	28.32 -69.91	348.92 -27.82	349.87 -26.37	350.30 -26.59	349.35 -28.05	.558	.4 .1			S		
2A2322+166 NEW		350.54 16.68	94.93 -41.15	350.79 16.52	350.30 16.47	350.26 16.82	350.75 16.87	.129	.5 .1			S	A2589 **	
2A2344-285 NEW		356.21 -28.58	24.49 -75.80	356.45 -28.24	356.20 -28.98	355.95 -28.92	356.20 -28.17	.142	.7 .1			S	K 44 [A] **	FJ2345-28

[A] : MACCACARO ET AL.1977.

Notes on Table 1:

Column 1, *ARIEL NAME:* A 2A designation implies a source from this catalogue. This name supersedes all previous designations. The name is truncated to minutes of RA and the first decimal place in declination.

Column 2, *STATUS:* NEW = New source
IMP = Source with improved position
CON = Confirmed source
PST = Source established by Point Summation Technique only (see Section 8).

Column 3, *OTHER NAMES:* Designation in other catalogues if considered to be counterpart of 2A source (see Section 5). Any common name also given here.

Column 4, *POSITION:* Position of maximum probability in degrees of RA, dec (1950) and l, b rounded to two decimal places.

Column 5, *ERROR BOX:* RA and dec (1950) of the corners of a rectangle enclosing the 90 per cent confidence ellipse (see Section 5).

Column 6, *AREA:* Area of the 90 per cent confidence ellipse in square degrees.

Column 7, *INTENSITY AND VARIABILITY CODE:* The intensity values and the variability codes are assigned as follows:

Variability Code	*Intensity Quotation*
S = Steady source	Weighted mean of *all* observations of intensity $\pm 1\sigma$ error.
I = Irregular source	Weighted mean of *all* observations of intensity $\pm 1\sigma$ error; maximum intensity $\pm 1\sigma$ error; minimum intensity $\pm 1\sigma$ error (maximum and minimum intensity defined as observations most significantly above and below the mean).
P = Periodic source	Typical maximum intensity $\pm 1\sigma$ error; typical minimum intensity $\pm 1\sigma$ error.
F = Flaring source	Weighted mean of *all* steady observations $\pm 1\sigma$ error; maximum flare point $\pm 1\sigma$ error; other relevant data, e.g. timescale, in Column 10.
T = Transient source	PST upper limit (3σ plus 'measured' intensity) for non-detections; maximum intensity $\pm 1\sigma$ error; other relevant data in Column 10.

All intensities are given in *Ariel* count/s (see Section 6).

Column 9, *IDENT:* Suggested identifications obtained as described in Section 10 and previous identifications as referenced. The star identification code expresses confidence in the identification as follows:

**** = Almost certain: the object is inside a small (< 0.1 square degree) X-ray error box. There is substantial supporting evidence from other X-ray, optical, etc. observations.
*** = Very likely: as above but with weaker supporting evidence.
** = Probable: the object is just outside a small X-ray error box or inside a larger one and has supporting evidence.
* = Possible: positional coincidence only.

Column 10, *OTHER INFORMATION:* Other relevant data on the X-ray source, including references to previous identification, supporting evidence in other wavebands, timescales for periodic or transient sources, etc. For PST sources the probability P of the source arising by chance in the total sky area surveyed is given by RPROB = P (see Section 8).

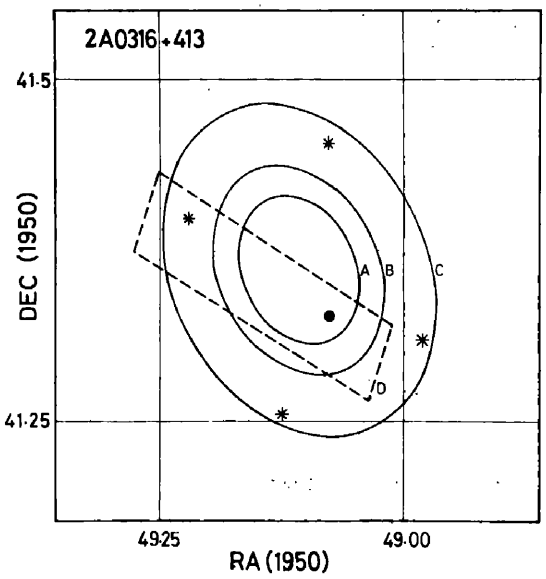

Figure 4. SSI error contours for 2A 0316 + 413 which contains NGC 1275. The isoprobability contours are at 68 (A), 90 (B) and 99.8 per cent (C). D is the quoted box for 3U 0316 + 41 and the four stars are the corners of the rectangle circumscribing the best-fitting ellipse to B. The solid circle is the position of NGC 1275.

we find two cases (MX 0600+46 and MX 1514+06) where a single MX source has been resolved into two separate 2A sources.

6 Determination of source intensities

We have summarized the intensity behaviour of a source in the 2A catalogue by a variability code and by intensities depending on that code. Light curves of sources of specific interest have been, or will be, published separately (e.g. for NGC 4151, Elvis 1976; and for NGC 5128, Lawrence *et al.*, 1977).

To obtain the variability code, the observed intensity values for a source (i.e. *all* observations of intensity with the source within 6° of the centre of the collimator) were first tested

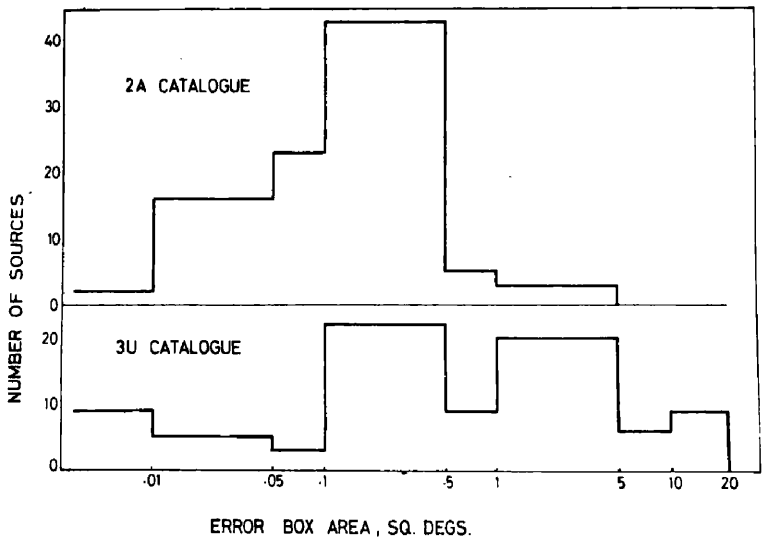

Figure 5. Frequency distributions of error box areas for the 2A catalogue (non-PST error boxes only) and the 3U catalogue.

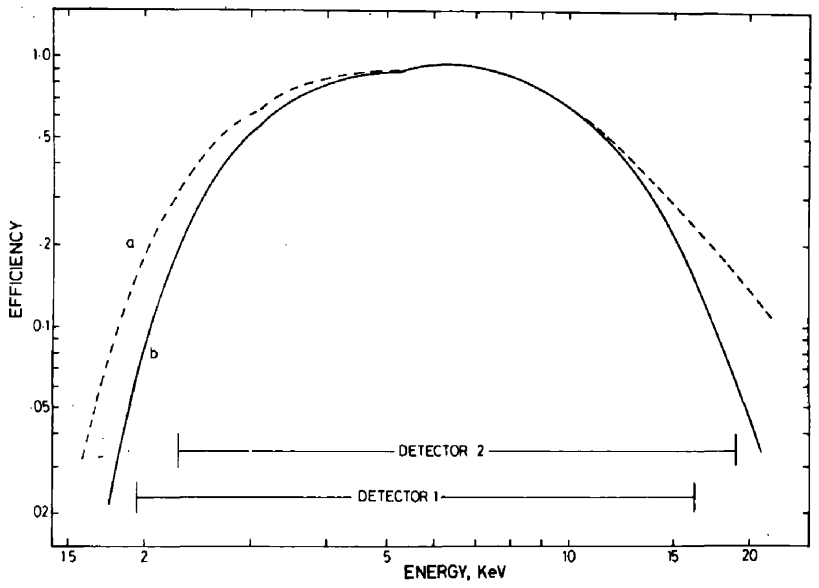

Figure 6. The SSI detector efficiency. Curve (a) shows the intrinsic efficiency while (b) includes the effects of detector energy resolution and pulse-height windows. The energy ranges of the two detector units of the SSI are indicated.

for consistency with a constant source intensity. This hypothesis was rejected if the formal probability associated with the χ^2 value was less than 1 per cent. If non-constant, the light curve was examined and assigned a variability code and appropriate intensities. The notes to Table 1 explain how the intensities and their errors were derived. For few of the sources assigned the variability code 'I' was the probability very much less than 1 per cent. Therefore the maximum and minimum intensity values quoted for these sources are not dramatically different from the average value.

Conversion of *Ariel* counts into an X-ray luminosity, or into other units, requires knowledge of the source spectrum, which has been measured in only a few cases. The conversion factor obtained from measurements of the Crab spectrum from Toor & Seward (1974) is 5.1×10^{-11} erg cm^{-2} s^{-1} (2–10 keV) per *Ariel* count/s. Varying the photon number index from 1 to 3 varies this value by a factor from 0.94 to 1.03. For a thermal spectrum with temperature varying between 2 and 16 keV, the factor is between 0.98 and 1.02. The general conversion factors for comparison with previous catalogues are

1 *Ariel* count/s $\approx$ 2.7 *Uhuru* count/s (2 ~ 6 keV)
$\approx$ 0.2 *OSO-7* count/s (3 ~ 10 keV).

To aid intensity comparisons of heavily cut-off sources, the SSI efficiency against energy is given in Fig. 6.

7 Angular sizes of sources

The main limitation on angular size measurements is that the collimator width, projected along the direction of the scan, is about 50 arcmin. Drifts in attitude during the period of data collection (one orbit), and the redistribution of counts needed to compensate for larger drifts in the analysis of sums of orbits, together broaden the effective response by about one sector (21 arcmin), so that a point source produces significant counts in five or six sectors. Provided that the signal-to-noise ratio is large enough, it is possible to get estimates, or at least upper limits, of source angular diameters by least-squares fits of suitably broadened collimator functions to the observed data. Since most sources are very much less than 1°

across, we do not expect to be able to improve on current estimates (Kellogg & Murray 1974) in these cases, although little effort has been applied to this problem so far.

8 Point-Summation Technique (PST)

In addition to source detection by the intersection of 3σ lines of position (see Section 3), we have searched for X-ray emission from selected astronomical objects by a Point-Summation Technique (PST) applied to the total data. A similar technique was used on the *Uhuru* data to provide upper limits for some active galaxies and globular clusters (Ulmer & Murray 1976; Ulmer *et al.* 1976). Given the position of the object, all suitable scan data are summed by using the position as a datum and ignoring the direction of the scan path. Data are excluded if affected by nearby catalogued X-ray sources or other forms of interference.

The summation is repeated for a $4^\circ \times 4^\circ$ grid of points around the object, and each time the collimator response function is fitted to give the signal-to-noise ratio (SNR). The criteria for the existence of a PST source are that near the object the SNR be above an adequate threshold and that the contours of SNR be consistent with a point source, since any excess in the superimposed data must be of the shape of the collimator response.

In order to determine the required threshold, the PST procedure was applied to over 200 positions, of which 70 per cent were chosen randomly over the sky and the remainder were in three areas of ~40 square degree each (not necessarily remote from known sources). Examination of the correlation of SNR's of pairs of points in the same grid as a function of spacing showed that, for points 1° apart, the correlation observed could occur by chance with a probability of 0.8 per cent, while for points $1^\circ.25$ apart the probability was 7.8 per cent. Thus the maximum density of essentially independent samples is ~1 per square degree. The area of sky searched with the technique, including objects of various classes and 3U X-ray source error boxes, totalled ~850 square degrees. The distribution of the SNR's at the ~200 positions was found to have a standard deviation of 1.14 and a mean value of 0.33, the difference from zero being accountable by the method of fitting the background to the data. From the distribution, the SNR values for each PST source have been used to calculate the probability of chance occurrence in the area searched. A threshold value for SNR of 4.6 has been used, which in the area sampled should only be exceeded by chance with a probability of 0.1. For most of the PST sources the actual chance probability was much lower than this, the values being given in Table 1, column 10. The positional error box quoted for PST sources is a quadrilateral (in azimuthal equal-area projection) which just encloses the contour ($SNR_{pk}-1$); simulations show that this contour is a reasonable approximation to the 90 per cent confidence region for the source location. The quoted source position is that of SNR_{pk} and the intensity is that found at this point.

Lists of objects which have been examined have yielded mostly upper limits in the range 0.15–0.5 *Ariel* count/s. These are given in Table 2. Some objects, notably some Seyfert galaxies, have given data satisfying the above source-detection criteria and these sources are included in the catalogue and flagged 'PST' in column 2 of Table 1. In addition there are some sources which, although not eventually satisfying the catalogue criteria described in Section 3, nevertheless had sufficient supporting data at lower significance to be made secure on the basis of the PST. These are also flagged PST in column 2. *Since only a small amount of sky has been examined by the PST, these sources should not be used in any statistical analysis of source occurrence.*

No upper limits are included in the catalogue unless they relate to a previously catalogued source for which we did not obtain data satisfying the catalogue criteria in Section 3. (In

Table 2. SSI upper limits on unconfirmed 3U, MX and other sources obtained by Point Summation Technique (PST).

Source	SSI* upper limit	Reported† intensity	Intensity† error	Source	SSI* upper limit	Reported† intensity	Intensity† error
3U 0001 – 31	0.63	1.19	0.15	3U 0917 – 63	0.50	1.48	0.19
0012 – 05	0.43	1.81	0.74	1169 + 59	0.56	0.89	0.15
0032 + 24	0.74	2.52	0.52	1144 – 74	0.32	1.59	0.30
0055 – 79	0.60	0.81	0.22	1231 + 07	1.20‡	2.48	0.52
0138 – 01	0.34	2.30	0.63	1237 – 07	1.07	0.48	0.15
0151 + 36	0.73	0.89	0.15	1439 – 39	0.42	1.22	0.15
0302 – 47	0.28	1.22	0.30	1443 + 43	0.36	1.11	0.26
0400 – 59	0.35	1.41	0.22	1645 + 21	0.82	2.26	0.67
0431 – 10	0.80	1.11	0.11	1736 + 43	1.40	4.00	0.89
0440 + 06	1.19	2.07	0.33	1849 – 77	0.45	1.11	0.19
0449 + 66	0.73	3.00	0.85	1904 + 67	0.45	1.85	0.37
0530 – 37	0.90	0.93	0.11	1956 + 65	0.45	1.74	0.15
0545 – 32	0.75	1.19	0.15	1959 – 69	0.38	1.04	0.15
0705 – 55	0.60	1.19	0.15	2041 + 75	0.45	1.26	0.26
0750 – 49	0.30	3.48	0.85	2128 + 81	0.55	0.56	0.11
0804 – 53	1.40‡	1.33	0.19	2346 + 26	0.63	2.59	0.44
				A2255§	0.42	0.59	0.20

Notes:

* Measured intensity plus 3σ error in *Ariel* count/s (present work).
† Reported intensity and 1σ error corrected to *Ariel* count/s according to conversions given in Section 6.
‡ Upper limit from most sensitive data set only.
§ From Cooke & Maccagni 1976.

fact none of the sources in Table 2 produced even $3 \times 2.5\sigma$ lines of position.) In this case the upper limits given in Table 2 have been obtained by surveying the whole quoted error box with the PST and quoting an upper limit derived from the peak intensity found. Some 3U and MX sources not detected in the main (lines of position) survey were located by this means and are included in Table 1. In each case we have assumed the source to be steady.

Subsequent papers will be concerned with clusters of galaxies (Ricketts *et al.*, in preparation), Seyfert galaxies (Elvis *et al.* 1978) and QSO's (White & Ricketts 1977b) investigated with the PST.

9 Completeness of the Sky Survey, and source confusion

In addition to the three most sensitive data sets which cross a point in the sky, there may be additional data sets which are almost as sensitive with respect to source detection. Because of counting statistics (and possibly because of source variability, should it exist), there is a certain probability that a source with an intensity below that calculated for a 3σ detection on the third most sensitive data set will be detected on that set, or even on less sensitive ones. This probability increases with the number and sensitivity of these additional data sets.

The result is that the fractional sky coverage at any intensity will always be underestimated. We have investigated, at most of the non-PST source positions in the catalogue, the relation between the minimum source intensity (I) which would yield a 3σ peak on the third most sensitive data set, and the intensity (I') for which the probable number of

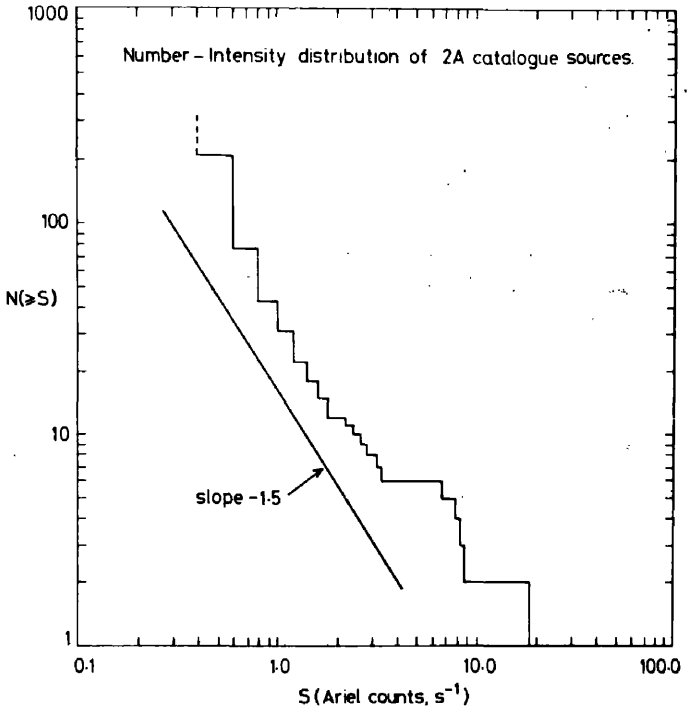

Figure 7. Log N/log S plot for 2A catalogue sources. Number of sources N ($|b| > 10°$) of intensity $\geq S$, is plotted against intensity S. N is corrected for sky coverage. Known galactic sources, PST sources and sources in confused regions have been excluded, together with the transient 2A 0042 + 323. 2A 1322 – 427 (NGC 5128) has been included at its 'average' intensity. A straight line of slope –1.5 is shown for comparison.

detections is just 3, taking into account all useful data sets. We find that the relation may be represented by $I = I' + (0.1 \pm 0.05)$ *Ariel* count/s. Hence at a typical point in the sky the coverage is to a strength ~ 0.1 *Ariel* count/s below that estimated from the third most sensitive data set. The effect on the sky coverage as a function of source intensity is shown in Fig. 3.

We have used the 2A sources (excluding PST established sources, sources in confused regions, known galactic sources, and the transient source 2A 0042+323) and sky coverage (corrected as above and in Section 4) to produce the integral source number/intensity (log N/log S) distribution shown in Fig. 7 (where N is referred to the area of sky $|b| > 10°$). For comparison with the measured distribution, Fig. 7 also shows a line of slope – 1.5. To examine the latitude distribution of sources we have repeated the above procedure for $|b| > 10°$ in five equal-area latitude bands in each hemisphere, thus obtaining $N(S > 0.8$ *Ariel* count/s) for each band. These numbers were then tested for consistency with there being an equal number of sources in each band. The resulting χ^2 value was 4.3 with 9 degrees of freedom, and was therefore quite consistent with an isotropic latitude distribution of sources. A more detailed analysis of the log N/log S and spatial distributions is in preparation (Warwick & Pye 1978).

Other effects can produce spurious X-ray sources. These are (a) conjunctions of spurious 3σ lines of position occurring because of random fluctuations in the data stream, and (b) sources arising by fluctuations in X-ray sky brightness, i.e. chance groupings of weak sources (probably not far below the Survey limit) which, together, have the intensity of a stronger source. We have estimated the importance of these effects as follows:

(1) The 2A catalogue is compiled from some 10000 orbits contained in about 350 data sets, and with our collimator FWHM we expect ~ 0.5 peaks at 3σ per data set due to

counting statistics (analysis of a sky area of ~ 0.9 Sr actually produced 11 unmatched lines of position, with SNR > 3, arising from the equivalent of nine data sets across the area). This leads to a probability of $\sim 10^{-5}$ of a single point crossing of three lines of position being generated from such random peaks.

(2) The source-confusion problem is the converse of the problem concerning the extent to which the diffuse X-ray background results from the combined contribution of discrete X-ray sources. This can be investigated by studying the point-to-point fluctuations in counting rate in X-ray detectors in which the X-ray background dominates over the particle background (e.g. Fabian 1975). The background due to sources may be considered as noise with a standard deviation σ_s which is a function of the effective instrumental beamshape of the X-ray detector. Then, as long as we take the minimum source strength in the catalogue as $> 3\sigma_s$, we can be sure that there is a suitably small chance that any source is merely a giant fluctuation (Cavaliere & Setti 1976). We have calculated σ_s from the integral

$$\sigma_s^2 = R\int_{S=0}^{S=S_u} S^2 dN(S),$$

where $dN(S)$ is the average number of sources in the range S to $S + dS$, and R is the ratio between the solid angle of our detector collimator and the total solid angle of sky outside $|b| = 10°$. We have truncated the integral at $S_u = 3.33$ *Ariel* count/s (≡10 *Uhuru* count/s), the limit to which the *Uhuru* catalogue was essentially complete for the whole sky. As a source distribution we have used

$$N(>S) = 33S^{-1.5},$$

where S is an *Ariel* count/s and $N(>S)$ refers to sources outside $|b| = 10°$. This distribution is consistent with our $\log N - \log S$ plot (Fig. 7), and with the distribution suggested as an upper limit by analysis of fluctuations in the X-ray diffuse background (Fabian 1975). The calculation yields a limiting strength for the 2A catalogue of $S = 0.63$ *Ariel* count/s above which we have ~ 60 'beam-areas' per source.

We are confident, however, in adding to the catalogue sources which are less intense than this limit, since the approach above makes no allowance for the discrimination against confusion which must result from the requirement that a source is established by three independent lines of position with significantly different position angles on the sky. The overlapping area of three typical lines of position is only a small fraction (0.07) of the area of an individual line so that the three lines are almost independent samples of sky brightness.

The SSI collimator isolates an element of the sky and integrates the X-ray sources (plus diffuse emission) in that element, via the collimator transmission function. We have simulated this build-up of X-ray sky brightness in the SSI by randomly filling such an element with sources from the distribution above. We find that the probability of the element displaying a strength greater than 1 *Ariel* count/s above the average element brightness is only 8.4×10^{-3}. From the arguments above, the probability of three typical lines of position producing a spurious source, due to confusion, is approximately the cube of this.

Because of the large number of scans at different position angles included by the PST, the effective beam area will tend to the common overlap area. This is confirmed by the low correlation between points ~ 1° apart (see Section 8), and justifies the higher sensitivity of this technique.

A remaining confusion problem arises when trying to separate a close group of sources with intensities greater than the survey limit. We recognise several such 'confused regions', and their approximate boundaries are given in Table 3 and marked on the sky-coverage map.

Table 3. Coordinates defining approximately the areas of sky containing further possible sources and called 'confused regions' (see Section 9).

(RA, dec, deg., 1950.0 and *l b*, deg.)

Region	RA dec	*l* *b*	RA dec	*l* *b*	RA dec	*l* *b*	RA dec	*l* *b*	Sources contained	
1	280	90	320	107	300	118	250	96	2A 1705+786	2A 1854+683
	60	25	70	14	85	26	65	38	3U 1825+81	3U 1904+67
									3U 1956+65	3U 2041+75
									3U 2128+81	
2	300	6	315	34	340	49	330	10	2A 2151−316	
	−35	−29	−15	−36	−15	−58	−35	−53		
3	140	149	140	138	200	120	200	118	2A 0954+700	
	65	40	75	36	75	42	65	52	2A 1151+720	
4	15	204	358	32	358	73	13	128	2A 0101−242	
	−27	−88	−27	−77	−15	−72	−20	−83		
5	333	317	340	320	82	272	98	274	3U 0055−79	A 0501−66*
	−73	−40	−67	−46	−63	−33	−64	−26	3U 0521−72	MX 0528−68*
									3U 0532−66	3U 0539−64
									3U 0540−69	

* See Griffiths & Seward (1977).

We are at present obtaining additional data for these regions and their analysis will be included in a subsequent paper. Meanwhile the presence of undetermined sources in these confused regions can produce some spuriously high points in the light curves of known sources in or near the regions. Those sources which would have been assigned any other variability code than *S*(= steady) have been given no code but have an average intensity calculated as for a steady source.

10 Source identification

Historically the identification of cosmic X-ray sources has been an iterative procedure guided by a knowledge of the classes of objects already associated with X-ray sources. New associations must have a suitably low probability of occurring by chance and be consistent with a reasonable X-ray luminosity from the object. The *Ariel V* SSI 90 per cent error boxes are typically of area 0.1 to 0.5 square degree, and usually the ratio between the axes is less than 3. The potential for associating a source with some astronomical object is thus much higher than for many of the weak 3U sources, for which the boxes were large.

Since this catalogue of X-ray sources at high galactic latitudes is consistent with an isotropic spatial distribution (see Section 9), we anticipate identifications either with extragalactic objects or with galactic objects which are either nearby or far out in the galactic halo. All new identifications proposed in the catalogue (Table 1, column 9) are with extragalactic objects such as clusters (CLUSTER) and groups (GROUP) of galaxies and active galaxies. To obtain these identifications we have examined many of the error boxes and their close surroundings for coincidences with optical and radio objects from the catalogues listed in Table 4. In addition, we searched the corresponding areas on prints from the

Table 4. Catalogues and lists of interesting objects searched for possible coincidences with 2A error boxes.

Abell 1958
Dixon's Master list of Radio Sources (RA40 version)
Finlay & Jones 1973
Klemola 1969
Markarian 1972
Markarian 1973
Sersic 1974
Sulentic & Tifft 1973
Vidal 1975

Palomar Observatory Sky Survey and its southern extension, the ESO 'Quick-Blue' Survey and the UK Schmidt IIIa J-plate Survey. Since the probability of finding a faint radio source in a 2A error box is quite high, we have not considered these to be plausible identifications unless there is supporting evidence.

The scarcity of identifications of X-ray sources with high-latitude galactic objects may be partly due to a current lack of knowledge (or even relative absence) of faint halo sources or of nearby sources of low luminosity. However, we can be confident that none of the unidentified 2A sources are associated with luminous galactic sources similar to Her X-1 or Cen X-3 ($L_x \sim 10^{37}$ erg/s), since the low intensities observed (< 5 SSI count/s) give extreme scale-heights above the galactic plane at the implied distances of 10–20 kpc. A number of objects, at high latitudes, have been detected in the soft X-ray region ($E \leqslant 0.28$ keV) and associated with normal stars (Mewe *et al.* 1975; Schnopper *et al.* 1976), flare stars (Heise *et al.* 1975), a hot white dwarf (Hearn *et al.* 1976) and U Geminorum systems (Rappaport *et al.* 1974; Hearn, Richardson & Clark 1976). However, for only one system, AM Her, which may be in the last class, is the source visible in the energy range of the SSI. We have searched for coincidences of 2A sources against lists of U Gem objects and of globular clusters without further success, but have not attempted to identify new 2A sources with any other type of stellar object. The earlier identifications of the brighter high-latitude X-ray sources with galactic objects were accomplished mainly by simultaneous observations of variability and, in particular, of periodicity (e.g. Her X-1). Such observations with X-ray telescopes of higher sensitivity in the future should assist in confirming or rejecting suggested associations of faint sources with galactic objects.

11 High-latitude transient sources

As well as very bright X-ray transients in the galactic plane (e.g. Elvis *et al.* 1975b), the SSI has also detected a number of faint transients at high galactic latitudes. Some of these have been described elsewhere (Ricketts, Cooke & Pounds 1976; Cooke 1976) and have a wide range of characteristic timescales. No firm definition has yet been reached on what is to be called a 'transient' and what a 'sporadically variable X-ray source'. Single sightings of transients, yielding only one (but highly significant) line of position, have not been included in the catalogue.

Acknowledgments

It is a pleasure to acknowledge the invaluable assistance and advice we have had from other members of the Leicester X-ray Astronomy Group and of the University. In particular we

thank Mr J. Lee for computer operations, Mrs C. Mehta for assistance in compiling the catalogue and Mr A. Riley of the University Computer Laboratory for skilful handling of the data base. Expert handling of *Ariel V* and transmission of the SSI data to Leicester by the team at Appleton Laboratory, Slough, contributed to this catalogue.

The *Ariel V* project is funded by the SRC, which also provided financial support for many of the authors. TM thanks the Italian foundation 'Angelo Della Riccia' for a fellowship.

References

Abell, G. O., 1958. *Astrophys. J. Suppl.*, 3, 211.
Cavaliere, A. & Setti, G., 1976. *Astr. Astrophys.*, **46**, 81.
Clark, G. W., Markert, T. H. & Li, F. K., 1975. *Astrophys. J.*, **199**, L97.
Cooke, B. A., 1976. *Nature*, **262**, 195.
Cooke, B. A. & Maccagni, D., 1976. *Mon. Not. R. astr. Soc.*, **175**, 65P.
Cooke, B. A., Elvis, M., Maccacaro, T., Ward, M. J., Fosbury, R. A. E. & Penston, M. V., 1976. *Mon. Not. R. astr. Soc.*, **177**, 121P.
Cooke, B. A., Maccacaro, T., Perola, G. C., Terenghi, M., Valentjin, E. A., 1977. *Astr. Astrophys.*, **58**, L17.
Cowley, A. P. & Crampton, D., 1975. *Astrophys. J.*, **201**, L65.
Crampton, D. & Cowley, A. P., 1976. *Astrophys. J.*, **207**, L171.
Davison, P. J. N., 1973. *Nature*, **246**, 90.
Elvis, M., 1976. *Mon. Not. R. astr. Soc.*, **177**, 7P.
Elvis, M., Cooke, B. A., Pounds, K. A. & Turner, M. J. L., 1975a. *Nature*, **257**, 33.
Elvis, M., Page, C. G., Pounds, K. A., Ricketts, M. J. & Turner, M. J. L., 1975b. *Nature*, **257**, 656.
Elvis, M., Maccacaro, T., Wilson, A. S., Ward, M. J., Penston, M. V., Fosbury, R. A. E. & Perola, G. C., 1978. *Mon. Not. R. astr. Soc.*, in press.
Fabian, A. C., 1975. *Mon. Not. R. astr. Soc.*, **172**, 149.
Finlay, E. A. & Jones, B. B., 1973. *Aust. J. Phys.*, **26**, 389.
Forman, W., Kellogg, E., Gursky, H., Tananbaum, H. & Giacconi, R., 1972. *Astrophys. J.*, **178**, L309.
Giacconi, R. & Gursky, H. (eds), 1974. *X-ray astronomy*, Astrophysics and Space Science Library, D. Reidel Publ. Co.
Giacconi, R., Murray, S., Gursky, H., Kellogg, E., Schreier, E., Matilsky, T., Koch, D. & Tananbaum, H., 1974. *Astrophys. J. Suppl.*, **237**, 37.
Gorenstein, P., Topha, K., Fabricant, D. & Harndon, F. R., 1976. *Bull. Am. astr. Soc.*, **8**, 553.
Gorenstein, P. *et al.*, reported in Gursky, H. & Schwartz, D., 1977. *A. Rev. Astr. Astrophys.*, **15**,
Griffiths, R. E. & Seward, F. D., 1977. *Mon. Not. R. astr. Soc.*, **180**, 75P.
Grindlay, J. E., 1976. *Highlights of astronomy*, Vol. 4.
Gursky, H., Kellogg, E. M., Murray, S., Leong, C., Tananbaum, H. & Giacconi, R., 1971. *Astrophys. J.*, **167**, L81.
Gursky, H., Kellogg, E. M., Levinson, R., Schreier, E. & Giacconi, R., 1972. *Astrophys. J.*, **174**, L143.
Hearn, D. R. & Richardson, J. A., 1976. *Preprint CSR-P-76-36.*
Hearn, D. R., Richardson, J. A. & Clark, G. W., 1976. *Astrophys. J.*, **210**, L23.
Hearn, D. R., Richardson, J. A., Bradt, H. V. D., Clark, G. W., Lewin, W. H. G., Mayer, W. F., McClintock, J. E., Primini, F. A. & Rappaport, S. A., 1976. *Astrophys. J.*, **203**, L21.
Heise, J., Brinkman, A. C., Schrijver, J., Mewe, R., Gronenschild, E., Den Boggende, A. & Grindlay, J., 1975. *Astrophys. J.*, **202**, L73.
Holmberg, E. B., Lauberts, A., Schuster, H.-E. & West, R. M., 1975. *Astr. Astrophys. Suppl.*, **22**, 327.
Kellogg, E., Gursky, H., Leong, C., Schreier, E., Tananbaum, H. & Giacconi, R., 1971. *Astrophys. J.*, **165**, L49.
Kellogg, E. & Murray, S., 1974. *Astrophys. J.*, **183**, L57.
Klemola, A. R., 1969. *Astr. J.*, **74**, 804.
Lawrence, A., Pye, J. P. & Elvis, M., 1977. *Mon. Not. R. astr. Soc.*, **181**, 93P.
Liller, W., 1975. *IAU Circ. 2888.*
Lucke, R., Yentis, D., Friedman, H., Fritz, G. & Shulman, S., 1976. *Astrophys. J.*, **206**, L25.
Maccacaro, T., Cooke, B. A., Ward, M. J., Penston, M. V. & Haynes, R. F., 1977. *Mon. Not. R. astr. Soc.*, **180**, 465.

Maccagni, D., Tarenghi, M., Cooke, B. A., Maccacaro, T., Pye, J. P., Ricketts, M. J. & Chincarini, G., 1977. *Astr. Astrophys.*, in press.
Markarian, B. Ye., 1972. *Astrofiz.*, **8**, 165.
Markarian, B. Ye., 1973. *Astrofiz.*, **9**, 5.
Markert, T. H., Clark, G. W., Lewin, W. H. G., Li, F. R., Schnopper, H. W., Sprott, G. F. & Wargo, G. F., 1975. *IAU Circ. 2765.*
Mewe, R., Heise, J., Gronenschild, E., Brinkman, A. C., Schrijver, J. & Den Boggende, A. J. F., 1975. *Astrophys. J.*, **202**, L67.
Pye, J. P. & Cooke, B. A., 1976a. *Mon. Not. R. astr. Soc.*, **177**, 21P.
Pye, J. P., & Cooke, B. A., 1976b. *Nature*, **260**, 410.
Pye, J. P., Cooke, B. A. & Elvis, M., 1976. *Nature*, **262**, 195.
Rappaport, S., Cash, W., Doxsey, R., McClintock, J. & Moore, G., 1974. *Astrophys. J.*, **187**, L5.
Ricketts, M. J., Cooke, B. A. & Pounds, K. A., 1976. *Nature*, **259**, 546.
Schnopper, H. W., Delvaille, J. P., Epstein, A., Helmken, H., Murray, S. S., Clark, G., Jernigan, G. & Doxsey, R., 1976. *Astrophys. J.*, **210**, L75.
Schreier, E., Giacconi, R., Gursky, H., Kellogg, E. & Tananbaum, H., 1972. *Astrophys. J.*, **178**, L71.
Sersic, J. L., 1974. *Astrophys. Space Sci.*, **28**, 365.
Seward, F. D., Page, C. G., Turner, M. J. L. & Pounds, K. A., 1976a. *Mon. Not. R. astr. Soc.*, **175**, 39P.
Seward, F. D., Page, C. G., Turner, M. J. L. & Pounds, K. A., 1976b. *Mon. Not. R. astr. Soc.*, **177**, 13P.
Sulentic, J. W. & Tifft, W. G., 1973. *The revised New General Catalogue of non-stellar astronomical objects*, University of Arizona Press.
Szkody, P. & Brownlee, D. E., 1977. *Astrophys. J.*, **212**, L113.
Toor, A. & Seward, F. D., 1974. *Astr. J.*, **79**, 995.
Ulmer, M. P. & Murray, S. S., 1976. *Astrophys. J.*, **207**, 364.
Ulmer, M. P., Murray, S. S., Gursky, H. & Bahcall, J. N., 1976. *Astrophys. J.*, **208**, 47.
Vidal, N. V., 1975. *Publ. astr. Soc. Pacific*, **87**, 625.
Villa, G., Page, C. G., Turner, M. J. L., Cooke, B. A., Ricketts, M. J. & Pounds, K. A., 1976. *Mon. Not. R. astr. Soc.*, **176**, 609.
Ward, M. J., Wilson, A. S., Disney, M. J., Elvis, M. & Maccacaro, T., 1977. *Astr. Astrophys.*, **59**, L19.
Warwick, R. S. & Pye, J. P., 1978. *Mon. Not. R. astr. Soc.*, in press.
Webster, B. L., Martin, W. L., Feast, M. W. & Andrews, P. J., 1972. *Nature Phys. Sci.*, **240**, 183.
Weedman, D. W., 1977. *A. Rev. Astr. Astrophys.*, **15**, in press.
White, G. J. & Ricketts, M. J., 1977. *Astrophys. Lett.*, **18**, 79.
White, G. J. & Ricketts, M. J., 1977b. *Mon. Not. R. astr. Soc.*, **181**, 435.
White, N. E., Mason, K. O., Sanford, P. W. & Murdin, P., 1976. *Mon. Not. R. astr. Soc.*, **176**, 201.
Wilson, A. S., Penston, M. V., Fosbury, R. A. E. & Boksenberg, A., 1976. *Mon. Not. R. astr. Soc.*, **176**, 673.

PRINTED IN ENGLAND BY
ADLARD AND SON LTD, DORKING

list of publications and preprints

Pounds, K.A., Cooke, B.A., Ricketts, M.J., Turner, M.J. and Elvis, M., 1975.
An extended observation of Cen X-3 with the Ariel V Sky Survey.
Mon.Not.R.astr.Soc. 172, 473.

Elvis, M., Cooke, B.A., Pounds, K.A. and Turner, M.J., 1975.
Ariel V Sky Survey: Identification of Abell 478 with the x-ray source 3U 0405+10.
Nature 257, 33.

Holt, S.S., Boldt, E.A., Serlemitsos, P.J., Kaluzienski, L.J., Pravdo, S.H., Peacock, A., Elvis, M., Watson, M.G. and Pounds, K.A., 1976.
Evidence for a 17d periodicity from Cyg X-3.
Nature 260, 592.

Elvis, M., Page, C.G., Pounds, K.A., Ricketts, M.J. and Turner, M.J.L., 1975.
Discovery of a powerful transient x-ray source (A0620-00) with the Ariel V Sky Survey Experiment.
Nature 257, 656.

Pye, J.P., Cooke, B.A. and Elvis, Martin, 1976.
Ariel V Sky Survey: Identification of Abell Cluster 754 with the X-ray Source 3U0901-09.
Nature, 262, 195.

Cooke, B.A., Elvis, M., Maccacaro, T., Ward, M.J., Penston, M.V. and Fosbury, R.A.E., 1976.
NGC 3783: A possible x-ray emitting Seyfert galaxy.
Mon.Not.R.astr.Soc., 177 Pt 3.

Elvis, M., 1976.
Ariel V Sky Survey: Long term monitoring of the x-ray emission from the Coma Cluster and NGC 4151.
Mon.Not.R.astr.Soc., 177, 7P.

Ward, M.J., Wilson, A.S., Disney, M.J., Elvis, M. and Maccacaro, T., 1977.
MCG 8-11-11 A Seyfert galaxy in an x-ray source error box.
Astron.Astrophys., 59, L19.

Cooke, B.A., Ricketts, M.J., Maccacaro, T., Pye, J.P., Elvis, M., Watson, M.G., Griffiths, R.E., Pounds, K.A., McHardy, I., Maccagni, D., Seward, F.D., Page, C.G. and Turner, M.J.L., 1977.
The Ariel V (SSI) Catalogue of high galactic latitude ($|b^{II}| > 10^{o}$) x-ray sources.
Mon.Not.R.astr.Soc.

Lawrence, A., Pye, J.P. and Elvis, M., 1977.
X-ray variability of NGC 5128.
Mon.Not.R.astr.Soc. 181, 93P

Elvis, M., Maccacaro, T., Wilson, A.S., Ward, M.J., Penston, M.V.
and Fosbury, R.A.E., 1977.
Seyfert galaxies as x-ray sources.
Mon.Not.R.astr.Soc.

Ward, M.J., Wilson, A.S., Penston, M.V., Elvis Martin and Maccacaro T,
Tritton, K.P.
Optical Identification of Extragalactic X-ray Sources
Ap.J.

M,ELVIS Ph.D. THESIS 1978

Martin Elvis, 1978.
Ph.D. thesis

SEYFERT GALAXIES AS X-RAY SOURCES.

ABSTRACT

Using data from the Leicester University Ariel V Sky Survey Instrument (SSI) the work reported in this thesis establishes that Seyfert galaxies form a class of extragalactic x-ray source.

The properties of Seyfert galaxies are reviewed and it is shown how standard arguments lead to a model of the structure of Seyfert galaxy nuclei containing three regions characterised by three types of emission: forbidden line, permitted line and 'non-thermal' continuum. Radio, infrared and optical parameters believed to derive from these three regions are then compared with x-ray flux densities from the SSI in an attempt to locate the source of x-ray emission. It is found that x-ray flux density correlates only with parameters describing the permitted line and continuum regions. Standard arguments presented earlier show that these regions are very small ($\approx$0.01 - 1pc diameter). Observable x-ray variability is thus possible and is indeed seen. The variability of x-ray emission from x-ray active galaxies is described using, in the main, SSI observations. Some suggestive similarities in their light curves are noted.

An x-ray luminosity function for Seyfert galaxies is constructed by two methods whose results agree well. Using this luminosity function the Seyfert galaxies are found to contribute $\approx$ 6% to the diffuse x-ray background, without evolution. They can account for the entire background if only moderate evolution is allowed.

Finally, recent developments in the field are noted: the discovery of more Seyfert galaxies as x-ray sources, variability, and some first x-ray spectra are reviewed. An extension to the class of 'x-ray active galaxies' in the form of high excitation emission line galaxies is reported. The great possibilities for future research in the area of x-ray active galaxies provided by new x-ray observatories in flight or under construction are explored briefly. It is clear that this is a subject just begun.